2.4.6 Probable Maximum Tsunami Hazards

This subsection examines the tsunamigenic sources and identifies the probable maximum tsunami (PMT) that could affect the safety-related facilities of Units 6 & 7. It evaluates potential tsunamigenic source mechanisms, source parameters, and resulting tsunami propagation from published studies, and estimates tsunami water levels at the site based on site-specific numerical model simulation results. Historical tsunami events recorded along the Florida coast are reviewed to support the PMT assessment. The approach taken is aligned with the PMT evaluation methodology proposed in NUREG/CR-6966 (Reference 201).

Units 6 & 7 are adjacent to the Biscayne Bay shore approximately 8 miles west of Elliott Key Barrier Island on the coast of the Atlantic Ocean, as shown on Figure 2.4.1-201. The grade elevations at the Units 6 & 7 plant area vary from approximately 19.0 feet to 25.5 feet NAVD 88. The entrance floor elevation of all safety-related structures (also referred to as the design plant grade elevation, which is 100 feet, or 30.48 meters, for the AP1000 reference datum) is at elevation 26 feet NAVD 88. The plant area is protected by a retaining wall structure with top elevation of 20.0 feet to 21.5 feet NAVD 88. As the grade is relatively high, tsunami events are not expected to pose any hazard to safety-related structures, systems, and components (SSCs) of Units 6 & 7, as described in the subsections below.

2.4.6.1 Probable Maximum Tsunami

The Atlantic and Gulf of Mexico Tsunami Hazards Assessment Group (AGMTHAG) evaluated potential tsunamigenic source mechanisms that may generate destructive tsunamis and affect the U.S. Atlantic and Gulf of Mexico coasts (Reference 202). The major tsunamigenic sources that may affect the southeastern U.S. coasts can be summarized as follows: submarine landslides along the U.S. Atlantic margin, submarine landslides in the Gulf of Mexico, far-field submarine landslide sources, earthquakes in the Azores-Gibraltar plate boundary, and earthquakes in the north Caribbean subduction zones (referred to as the Caribbean-North American plate boundary in Subsection 2.5.1).

Based on the below descriptions of the different source mechanisms, transoceanic tsunamis as a result of earthquakes in the Azores-Gibraltar (east Atlantic) plate boundary and tsunamis generated in the northeastern Caribbean region are identified as the primary candidates of the PMT generation that could affect Units 6 & 7.

2.4.6.1.1 Submarine Landslides along the U.S. Atlantic Margin

Submarine landslide zones along the U.S. Atlantic margin are concentrated along the New England and Long Island, New York sections of the margin, outward of major ancient rivers in the mid-Atlantic region, and in the salt dome province offshore of North and South Carolinas, as shown in Figure 2.4.6-201 (Reference 202). Although submarine landslides along the U.S. Atlantic margin, from Georges Bank offshore of the New England coast to Blake Spur south of the Carolina Trough, have the potential to cause devastating tsunamis locally, the presence of a wide continental shelf is expected to reduce their impact at the shoreline near the landslides (Reference 202).

AGMTHAG mapped a total of 48 landslide affected areas based on data compiled from bathymetry, GLORIA (Geological Long-Range Inclined Asdic) sidescan sonar imagery, seismic reflection profiles, and sediment core data (Reference 202). The general characteristics of the mapped landslides are summarized in Table 2.4.6-201. The distribution of landslide locations identified along the U.S. Atlantic margin from the Georges Bank to the Carolina Trough is shown in Figure 2.4.6-202. The largest submarine landslide area near Units 6 & 7 is the Cape Fear Slide complex, identified in an area south of Cape Hatteras, off the Carolina Trough. The Cape Fear Slide headwall is described as an amphitheater-shaped scarp centered on a lower slope at a depth of approximately 2300 to 2600

meters (7545.9 to 8530.2 feet), 50 kilometers (31.1 miles) long, and approximately 120 meters (393.7 feet) high. Within the headwall's failure area, two large salt diapirs project above the sea floor. A complex of slumps extends more than 40 kilometers (24.9 miles) upslope from the major headwall scarp, and mass-movement deposits are traceable for more than 400 kilometers (248.5 miles) downslope to a water depth of over 5.4 kilometers (3.35 miles) on the Hatteras Abyssal Plain (References 202, 223, 225, 226 and 227). Longitudinal lines in the 1987 GLORIA side-scan sonar image, Figure 2.4.6-238, (reproduced from Figure 4 in Reference 225), are interpreted as evidence of mass movement. The longitudinal lines represent both debris chutes between the salt diapirs at the head of the landslide area indicated by the Label A in Figure 2.4.6-238, and debris flow paths further downslope indicated by the Label B (Reference 225). In the proximal area of the landslide, Label C in Figure 2.4.6-238, an area of irregular, hummocky topography on the sea floor provides evidence of mass movement. At the distal portion of the slide, the landslide material extends across an older slope failure, the Cape Lookout Slide (Reference 225).

Multibeam swath bathymetric data from the SeaBeam 2100/12 system and single channel Chirp data using a Knudsen 320B/R echosounder acquired in 2007 (Reference 223), provide the basis for a new interpretation of the Cape Fear slide. The multibeam bathymetric images combined with the Chirp data revealed at least five major escarpments (labeled S1 through S5 in Figure 2 of Reference 223). The S1 scarp is the westward and shallowest of the scarps, at approximately 890 meters below sea level, and with a crown-shaped headwall that extends 40 kilometers (24.9 miles) downslope of both sides of the slide scar. The S1 scarp crosscuts the S4 and S5 scarps and extends upslope of the main headwall (S4 and S5 headwalls). The S2 and S3 scarps are located within the S1 debris field. The S2 scarp is an approximately 20-kilometer (12.4-mile)-long and approximately 3-kilometer (1.9-mile)-wide chute that abruptly widens downslope. The approximate headwall height for the S2 scarp is at least 30 meters. The S3 scarp is associated with the smallest disrupted area and has a height of at least 20 meters above the rupture surface. The main headwall scarp, S4, is likely the largest slide in the complex with an approximately 120-meter high headwall that extends over approximately 50 kilometers (31.1 miles). The S5 scarp intersects the northern flank of the S4 scarp and is a secondary slide. It extends approximately 10 kilometers (6.2 miles) north of the S4 slide and has a headwall height of approximately 30 meters. In addition to collecting data on the S1 through S5 scarps, the bathymetric data showed a north-south linear depression running subparallel to the continental slope break at the extreme southern end of the S4 escarpment. The Chirp data suggests, "this ~40 kilometers (24.9 miles) long feature represents the scarp of a previously unrecognized, seafloor breaking normal fault" (Reference 223).

Based on radiocarbon (C-14) analyses of core samples from within 50 kilometers (31.1 miles) of the slide's headwall, the age of the slide is estimated as between 9 to 14.5 thousands of years (References 228 and 229). However, an unconformity occurs between 0.5 and 2 meters depths within the Cape Fear Slide complex. The ages of the samples collected from the cores below the unconformity are older than 29 thousands of years. An interpretation of these data indicated a hiatus on the sole of the slide that separated the sediments that are younger than 14.5 thousands of years from those that are older than 29 thousands of years and that the slide was active during that time (Reference 228). This period of slide activity most likely occurred at the transition between the end of the last glaciation (Wisconsinan Stage) and the present interglacial age. This age bracket appears to be associated with the Pleistocene sea-level lowstand that occurred between approximately 12,000 and 28,000 years ago during the last glacial maximum (References 202, 223, 227, 228, 229, 230, 231 and 232). The possible triggering mechanisms for the slide activity are salt movement, driven by sediment loading, with salt diapirism causing over steepening of the seabed slope followed by failure and potential sediment instability due to gas hydrate decomposition (References 202, 223, 230, 231 and 232).

Units 6 & 7 are located approximately 400 miles (640 kilometers) southwest of Blake Spur with a wide and shallow continental slope and shelf in between (Figure 2.4.6-201). Details of the Atlantic continental shelf near the site are described in Subsection 2.5.1.1.1.1. Additionally, the landslide

zones are oriented in a manner that Units 6 & 7 would be away from the main axis of submarine landslide-generated tsunamis. The impact of any submarine landslide-generated tsunami on the continental slope and shelf north of Blake Spur would be considerably reduced before reaching Units 6 & 7. For example, Hornbach et al. (Reference 223) simulated a tsunami generated by the largest landslide from the Cape Fear Slide complex. The model results include contours of tsunami amplitudes 30 minutes after initiation of the landslide (see Figure 2.4.6-227). The major tsunami waves propagate along the axis of the landslide, both toward the coast and seaward. Geometrical spreading of the tsunami wave is prominent along the direction perpendicular to the axis of slide and toward the Straits of Florida. Based on the model results, the tsunami wave amplitude 30 minutes after slide initiation and about 200 kilometers (124 miles) along the Units 6 & 7 direction is approximately 1.5 meters (4.9 feet). In contrast, the tsunami amplitude off Miami, Florida, at a water depth of 783 meters (2569 feet) for the 1755 Lisbon Earthquake tsunami (which corresponds to the PMT) is 2.0 meters (6.6 feet) (Reference 209). The distance between the Cape Fear Slide complex and the off-Miami site at a water depth of 783 meters (2569 feet) is more than 800 kilometers (497 miles). Therefore, the tsunami maximum water level at the Units 6 & 7 site due to the Cape Fear Slide complex landslide would be lower than that from the 1755 Lisbon Earthquake tsunami.

To provide additional support to the conclusion based on the results of Hornbach et al (Reference 223) and to assess independently how a tsunami generated by a submarine slope failure at Cape Fear would affect PMT water levels at the Units 6 & 7 site, numerical models were used to estimate the wave that would be generated by such a failure and simulate its propagation towards the site, as described in Subsection 2.4.6.4.2.

Twichell et al. studied submarine erosion and characterized morphologic provinces for the Blake Escarpment (Figure 2.4.6-203) northeast of Units 6 & 7 (Reference 203). The Blake Escarpment, extending approximately 450 kilometers (280 miles) to the south from Blake Spur, is one of the largest cliffs in the ocean with a relief of about 4000 meters (13,120 feet) (Reference 203). Near the southern edge of the escarpment, it crosses with the Jacksonville fracture zone, which underlies the Blake plateau at the location of Abaco Canyon. The escarpment was isolated from the continent-derived sediments since late Cretaceous, first by the currents in the Suwannee Straits and later by the Gulf Stream, and erosion of the escarpment is evident over the period (Reference 203).

Twichell et al. identified three morphologic provinces along the Blake Escarpment with varying erosional behavior (Reference 203). These are (1) valleys with tributary gullies, (2) box canyons, and (3) strait terraces. Valleys with tributary gullies are in the northern part of the escarpment near Blake Spur that have undergone no or very little erosion over time. Box canyons are formed by the differential settlement of base rock probably over a long period and are identified south of the Jacksonville fracture zone. The overlying carbonate strata in box canyons are fragmented with continued erosion. The middle reach of the escarpment has straight terraces formed by differential erosion of lithologic differences in the strata exposed along the cliff faces and has lower erosion potential than box canyons (Reference 203). The study by Twichell et al. identified evidence of debris accumulation at the base of the escarpment; however, it did not characterize any tsunamigenic source in the escarpment (Reference 203). Units 6 & 7 are sheltered by the islands of the Bahamas from tsunamis, if any, generated in the region, thus protecting Units 6 & 7 from being affected by large tsunamis.

The Ocean Drilling Program (ODP) provides stratigraphic information on the Bahama platform and the Straits of Florida from borehole and seismic reflection survey results. The ODP data suggest evidence of significant submarine debris flows and turbidite deposits during a four million year interval in the middle Miocene (Reference 217). However, no stratigraphic evidence could be established to relate these Miocene gravity flows to any tsunami deposit or tsunami-like event along the southern Florida coasts. After the Miocene, no debris flow or turbidite deposit could be identified in this region, possibly due to the erosional effects of the Gulf Loop Current that was first established in the Pliocene. It is hypothesized that the debris flow and turbidite deposit resulted from materials

that had accumulated atop the carbonate banks at a marine high stand, which became unstable as sea level fell (Reference 217). Such debris flows are not expected to occur in the recent geological environment of eustatic sea level rise. Therefore, submarine landslide in the Straits of Florida and Bahamas regions is precluded as a PMT source candidate for the Units 6 & 7 site. Details of stratigraphic information in the Bahamas and the Straits of Florida are provided in Subsection 2.5.1.1.1.2. Potential geological hazards near the site region are described in Subsection 2.5.1.1.5.

Information on submarine landslide along the northern coast of Cuba is very scarce. Iturralde-Vinent (Reference 218) summarizes the current understanding of tsunami hazards in Cuba, details of which are provided in Subsection 2.5.1.1.5. Iturralde-Vinent identifies potential tsunami hazards for the Cuban north coast region based on large carbonate boulders found on marine terraces; however, no submarine landslide zones were identified in this region. Consequently, a submarine landslide along the north coast of Cuba was not included as a candidate PMT source for the Units 6 & 7 site.

Units 6 & 7, therefore, would not be impacted by significant submarine landslide-generated tsunamis from the U.S. Atlantic margin, the straits of Florida, Bahamas, or Cuba regions.

2.4.6.1.2 Submarine Landslides in the Gulf of Mexico

Within the Gulf of Mexico, evidences of submarine landslides are recorded in all three geological provinces (Carbonate, Salt, and Canyon/Fan) (Reference 202). The geological provinces within the Gulf of Mexico are shown in Figure 2.4.6-204. The largest submarine failures are found in the Canyon/Fan Province within the Mississippi Fan that was probably active 7500 years ago. The largest failure in the Salt Province is identified offshore of the Rio Grande River. Landslide evidences in the Carbonate Province are identified in the West Florida and Campeche Escarpments along the eastern and southern Gulf of Mexico, respectively (Reference 202).

Significant landslides on the West Florida Slope above the Florida Escarpment (Figure 2.4.6-205) are sourced in Tertiary and Quaternary carbonate deposit. This landslide zone, which is located approximately 300 miles (480 kilometers) west of Units 6 & 7, is hypothesized to be a composite of at least three generations of failures (Reference 202).

Based on the mapping of landslide zones in the Gulf of Mexico, AGMTHAG identified four likely landslide zones and characterized tsunamigenic source parameters that could be used to calculate corresponding tsunami amplitudes (Reference 202).

The West Florida Escarpment is the major marine geomorphic feature on the west coast of Florida. It has undergone significant erosion since its initial formation during the Cretaceous as part of a reef complex, with as much as 8 kilometers (5.0 miles) of erosional retreat of its base (Reference 203). In general, the slope on the West Florida Escarpment increases below 1750 meters (5741.5 feet) depth and frequently exceeds 40 degrees. The front of the escarpment is composed of Lower and Middle Cretaceous platform-interior bedded lagoonal limestones and dolostones. Accumulations of younger Pliocene and Pleistocene sediments associated with the Mississippi Fan (submarine deltaic deposits from the Mississippi Embayment) onlaps at the base of the escarpment (References 202 and 247).

A study was conducted in 1985 using SeaBeam bathymetric data and GLORIA (Geologic LOng-Range Inclined Asdic) side-scan sonar data collected by the USGS and the Institute of Oceanographic Sciences of the United Kingdom to examine the submarine mass failures in the West Florida Escarpment. The GLORIA images covered a broad area about 220 kilometers (136.7) in length along the escarpment between 25°N and 27°N. This study concluded that erosion has occurred since the initial formation of the escarpment and that erosional processes changed its morphology at different rates (Reference 250).

In the area north of 27°N, the escarpment is a relatively linear landform with slope gradients of less than 28 degrees and is dissected by numerous valleys spaced 1 to 5 kilometers (3.1 miles) apart with tributary gullies feeding into them (Reference 203, Figure 6-2). The Cenozoic sediments in this area have not been exposed to extensive erosion due to the presence of the thin discontinuous Cenozoic sediment cover as well as possible undisturbed reef structures in the underlying Cretaceous section. The slope above this part of the escarpment is smooth and is interrupted by only a few mass wasting scarps. Below the escarpment are aprons (as seen in GLORIA imagery and SeaBeam bathymetry [Reference 203, Figure 6-2]), which are inferred to be carbonate debris material that have been eroded and transported off the escarpment and interfinger with late Pleistocene-age fan deposits (Reference 203).

South of 27°N, part of the escarpment is also relatively linear but is terraced, and parts are deeply incised by large canyons. On the straight part of the escarpment, which occurs between 25.5°N and 26.5°N, the lower part of the escarpment is terraced, whereas the upper part is steeper and unterraced (Reference 203, Figure 6-3). The terraces have gradients of 10 degrees to 20 degrees, while the terrace risers and the upper part of the escarpment have gradients of 30 degrees to 42 degrees. The canyons incise the edge of the Florida platform by as much as 15 kilometers (9.3 miles). The canyon heads are 1 to 3 kilometers (0.6 to 1.9 miles) wide, and the mouths are 3 to 7 kilometers (1.9 to 4.3 miles) wide (Reference 203, Figure 6-4). The canyon's floors are flat and at the same depth as the abyssal plain floor except immediately below. The canyon's headwalls where the depressions occur are as much as 80 meters (262.5 feet) deeper than the abyssal plain floor. Talus deposits that have been eroded from the headwalls are seen in the GLORIA image (Reference 203, Figure 6-4). The headwalls have gradients that exceed 40 degrees and do not have terraces; however, the sidewalls are not as steep and do have discontinuous terraces. These canyons are called box canyons and are concentrated in two groups along the southern part of the escarpment. One group occurs between 26.5°N and 27°N and the second between 24.3°N and 25.6°N (Reference 203).

The area that is postulated to be the site for a maximum credible submarine landslide is identified along the southern part of the West Florida Slope as delineated in Figure 2.4.6-263 (Reference 239). Doyle and Holmes (Reference 249) and Twichell et al. (Reference 250) have stated that this area has undergone collapse. The area is described as characterized by "scarps [that] are still exposed on the seafloor and have 50-150 meters relief and are 10-70 kilometers in length" (Reference 239). According to ten Brink et al. (Reference 239), "some of the mass movement deposits are on the slope above the Florida Escarpment, but it is unknown how much of the failed material was transported farther and deposited at the base of the Florida Escarpment." These landslides from the West Florida Slope are composed of several smaller failure events as seen in the crosscutting relationships of the headwall scarps in the GLORIA imagery (Reference 250). The age of these failures is not known, but it is suggested by Mullins et al. (Reference 248) and Doyle and Holmes (Reference 249) that periods of increased mass wasting are associated with periods of higher sedimentation rates. Therefore, it is possible that the landslides along the southern part of the West Florida Slope are likely early Holocene (4500-10,000 years before the present) or older in age (Reference 251). The runout distance of the existing slope failure is uncertain, as landslide deposits at the base of the West Florida Escarpment are buried under younger Mississippi Fan deposits (Reference 239).

Because Units 6 & 7 are located on the eastern side of the Florida peninsula opposite of the Gulf of Mexico shoreline and a very wide continental shelf exists along the Gulf Coast of Florida, tsunamis generated within the Gulf of Mexico would likely be dissipated before reaching Units 6 & 7. Therefore, it was concluded that landslide-generated tsunamis from the Gulf of Mexico sources would not affect the safety-related facilities of Units 6 & 7 that have a design plant grade elevation of 7.92 meters (26 feet) NAVD 88. To provide additional support to this conclusion and to assess how a tsunami generated by a submarine slope failure at the Florida Escarpment would affect PMT water levels at

the Units 6 & 7 site, numerical models were used to estimate the wave that would be generated by such a failure and simulate its propagation toward the site as described in Subsection 2.4.6.3.

2.4.6.1.3 Landslide Sources along the Great Bahama Bank

A number of publications examined the various aspects of sediment deposits and sedimentary/geomorphic processes on and affecting the Great Bahama Bank (GBB), its western margin and the Straits of Florida. A review of this literature indicates that different investigators (References 253, 254, 255, 256, 257, 258, and 259) have proposed multiple hypotheses to explain the distribution of the cyclical successions of deposits as displayed in boring data obtained in the region (such as ODP Site 626, Clino borehole, and the Great Isaac Well, etc.) and interpreted from seismic reflection surveys as described below.

Mullins and Neumann (Reference 255) studied the carbonate deposits in the Bahamas using high-frequency; high-resolution seismic reflection profiles and bottom grab samples. They determine that, in general, the leeward deep bank margins are steeper, narrower, more dissected, and contain significantly greater amounts of coarse grained sediments than their windward margin counterparts. According to Mullins and Neumann (Reference 255), the processes that are responsible for the development of deep carbonate bank margins include: basement faulting, direction and magnitude of off-bank sediment transport, oceanic circulation, gravity and pelagic sedimentation, submarine cementation; and biological buildups. “Of these, basement faulting is primarily responsible for the initiation of carbonate platform edges. Off bank sediment transport is controlled by the physical energy flux such as winds, waves, storms at the sea surface and controls the availability of shallow water sediment for transport to the deep flanks” (Reference 255, p. 165).

Fulthorpe and Melillo (Reference 253) interpret the carbonate sediment cored at ODP Site 626 in the Straits of Florida to have been deposited by gravity flows having the characteristics of debris flows and high-density turbidity currents. These gravity flows could have been caused by gravitational instability that was the result of sediment loading of a carbonate platform slope during a period of rising sea level, triggering of slope failure by a decrease in sea level, or triggering by tectonics and earthquake activity during the middle Miocene.

Kuhn and Meischner (Reference 256) interpret the carbonate sediment from ODP Leg 101 Sites 628 (Little Bahama Bank), 632 (Exuma Sound), and 635 (Northeast Providence Channel) to have been deposited downslope during the initial stage of falling sea level. Gravity flows may occur along the entire slope, flowing downslope in a regional canyon system that is less prominent than on a steeper slope. Therefore, the gravity flows erode and entrain large amounts of fine-grained slope sediment (Reference 256).

By examining the seismic data and limited well data from the northwestern GBB, Eberli et al. (Reference 257) interpret that the deposits developed as a result of pulses of prograding sediments generated by fluctuations in sea level and that an aggradation phase on the marginal slope preceded progradation. The timing, amount, and mode of progradation and the geometries of the prograding units are controlled by several factors such as sea level, subsidence, carbonate production and accumulation, direction of wave energy, and angle of repose. Eberli et al. (Reference 257, p. 1002) state that the “sea level changes are responsible for the pulsed mode of progradation, and the sequences seen on seismic lines.”

Betzler et al. (Reference 258) interpret deposits of the Miocene-Lower Pliocene Bahamian carbonate ramp from core, geophysical logging, and high-resolution seismic reflection data from ODP Leg 166 (in the western margin of the GBB south of ODP Site 626 in the Straits of Florida). The deposits consist of cyclic alternations of light and dark grey wackestones/packstones with interbedded calciturbidite packages and minor slumps. These deposits are interpreted by Reference 258 to be the result of high-frequency sea level changes. Betzler et al. (Reference 258) propose two models to

explain the cycle generation. The first model applies the principle of highstand shedding and correlates the dark grey layers to low sea level (i.e., lowstands). The second model assumes that the dark grey layers formed as condensed sections during sea level rises (i.e., highstands). Betzler et al. (Reference 258, pp. 1141-1142) favor the second model "because the shallow water carbonate production area was not reduced significantly during sea level lowstands . . . the dark-grey/light-grey cyclicity is linked to the Miocene ramp geometry. . . it disappeared during the Early Pliocene, as the ramp began to change into a flat-topped platform." In addition to high-frequency sea level changes, Betzler et al. (Reference 258) interpret the depocenter shifts of Miocene gravity flows from an outer ramp position during the Early and Middle Miocene to a basin floor position during the Late Miocene and Early Pliocene (i.e., depocenter shifted from east to west) to be the result of increasing strength of bottom currents during the Late Miocene.

Betzler et al. (Reference 259) studied the shedding pattern along the slope and toe of slope deposits of the carbonate ramp of the western margin of the GBB using seismic lines, logging data, and quantitative petrographic data from ODP Leg 166. Betzler et al. (Reference 259) interpret two types of turbidite sequences. The first sequence is characterized by aggradation to weak progradation of the inner ramp that leads to gradual uphole increases in shallow water components within individual depositional sequences, whereas the second type formed during sea level falls and are characterized as fan depositional systems, which are laterally discontinuous. The first type of turbidite sequence on a large to medium seismic stratigraphy scale is laterally continuous over longer distances. The second type of turbidite sequence is characterized by a mixture of shallow water particles and other components with each turbidite package consisting of a distinct composition with no large scale compositional trends (Reference 259). Betzler et al. (Reference 259) interpret the shedding pattern to have recorded five orders of sea level changes with the turbidite packages reflecting the Middle Miocene sea level fall.

Considering the uncertainty in the actual mechanism of deposition of the sediments encountered at ODP sites near the GBB, and evidences of seabed instabilities as cited by some investigators, the potential of submarine slope failures along the western margin of the GBB and the associated tsunami flooding hazard at the Turkey Point Units 6 & 7 site warrants further evaluation.

Several areas that exhibit mass gravity flow deposits (Reference 264) occur on the western margin of the GBB. The western margin, which contains several areas of past and potential future slope failures, has been studied by References 256, 260, 263, 265, and 266 for various purposes. The data provided by References 264, 265, and 266 comprise part of the ODP Legs 101 and 166; scientific investigations and proceedings. Paleontological, biostratigraphic, geochemical, geophysical (seismic reflection survey), and sedimentological data were collected from ODP Legs 101 and 166. Data documented in Reference 263 consists of high-resolution seismic reflection profiles with submersible reconnaissance and bottom sediment samples. More recently, Mulder et al. (Reference 260) (supported by the French Institut National des Sciences de l' Univers program "Action Marges") acquired new high-quality multibeam bathymetry, high-resolution seismic profiles, and 17 gravity cores. The seismic reflection profiles (i.e., ODP Legs 101 and 166, and Reference 263) and multibeam bathymetry (i.e., Reference 260) contain features interpreted as the result of slope failure and mass gravity flow deposits (Figure 2.4.6-294). The seismic profiles (Figures 2 and 3 of Reference 263) are defined by a bank edge, a steep upper rocky slope interval or wall and a lower slope. The slopes observed on the seismic profiles are interpreted to be relatively young; possibly Holocene in age. The data supporting this evaluation is comprised of the clean, sharp slope profiles in Figures 2 and 3 of Reference 263. In addition, the bathymetric images on Figure 1 of Reference 260, Figure 1 of Reference 261, and Figure 8 of Reference 267 depict what appear to be relatively steep slopes that do not indicate significant modification. In addition, uranium/thorium dating methods give dates of approximately 810 to 10,120 years before the present on cored sediments from the slope (Reference 263). These data support a Holocene age for the slope failures. While these deposits may have formed as a result of downslope (east to west) transport of sediment formed on the Bahama's bank top, Mulder et al. (Reference 260, p. 605) interpret the mass gravity

flow deposits as a result of slope failures and state, “due to their large size, mass transport complexes can be tsunamigenic and have to be considered in the assessment of natural hazards.” Therefore, it is conservatively assumed that a future failure in the slope instability areas on the western margin of the GBB can generate a tsunami. The two areas on the western margin of the GBB that have a potential for a probable maximum tsunami (PMT) to the Turkey Point Units 6 & 7 site are the southern site and the northern site.

Southern Site

High-resolution multi-beam bathymetric and seismic reflection data collected recently have provided the basis for understanding the morphology of the western margin of the GBB and the adjacent seafloor of the Straits of Florida (References 260 and 261). These data display evidence of slope instabilities starting at a water depth of approximately 450 to 550 meters. Scars from slope failures are typically approximately 1 kilometer wide. These scars “evolve longitudinally toward a fan-lobe system in which erosional processes dominate over depositional systems. Tongue-shape patches of blind echo-facies are observed locally and could result from debris flow transport of reworked coarse sediment originating from the bank, or from deep-water coral mounds. The most impressive morphological feature is a large sediment failure and its associated mass transport complex” (Reference 260) (Figure 2.4.6-295). This mass gravity flow feature includes three failure scarps, spanning an area approximately 9 kilometers wide and ranging in height from 80 to 110 meters. Downslope of the scars, the seafloor is hummocky in nature (i.e., debris field). The debris field extends westward over 20 kilometers. The surface of the entire deformed area is approximately 300 square kilometers (Reference 260). This area, referred to as the southern site as shown in Figure 2.4.6-295, is located at approximately 24.9534°N, 79.2358°W and is approximately 90 kilometers west of the Great Bahama Island, approximately 90 kilometers south of the Bimini Islands and 125 kilometers from the Turkey Point Units 6 & 7 site. Figure 2.4.6-296 shows a profile of the bathymetry (Reference 260) at this location. As shown in Figure 2.4.6-296, the length of the steeper slope (>1.5 degrees) along this profile is approximately 3 kilometers with the upper third of the profile having a slope of < 5.8 degrees, while the middle third of the profile has a slope of < 3.8 degrees. Figure 2.4.6-293, which is reproduced from Reference 260, shows these scars and suggests that a larger area that encompasses these scars and some smaller adjacent scars is approximately 14 to 15 kilometers wide, which is consistent with the 13-kilometer width stated in Mulder et al. (Reference 260). The large- and small-scale morphologies in this area “include bypass areas, channel-levee lobe systems, gullied slopes, and products of slope instabilities at various scales, including long slump scars at the lower slope and mass transport complexes that extend approximately 30 kilometers into the adjacent basin floor” (Reference 260).

Northern Site

The northern site is located at approximately 25.6134°N, 79.3213°W, approximately 104 kilometers east of the site. This location is the closest potential slope failure area to the Turkey Point Units 6 & 7 site. This area is discussed in detail in Reference 263 and is briefly summarized here. It is described as consisting of a bank edge, a lithified accretionary slope (steep rocky slope interval or wall and thinned Holocene sequence), and a lower slope. The bank edge consists of vertical (1-5 meters) steps, separated by gently sloping, sediment covered terraces in water depths of less than 10 meters. The lower part of this interval is smooth or hummocky with a surface of thin (10-30 centimeters) hardgrounds (i.e., cementation by either aragonite or Mg-calcite) (References 263 and 268). A monotonous and generally smooth lithified accretionary slope with a gradient of approximately 15 to 20 degrees is located west and downslope of the bank edge. The water depth at its upper, shallow end occurs at depths between 15 and 65 meters. The deeper part of the slope occurs in water depths of 65 to 150 meters. The 1-5 meter wide ledges in the upper portion of the slope appear to act as steps for cascading sand from above. However, near Bimini and Riding Rocks, approximately 104 kilometers east of the Turkey Point Units 6 & 7 site, the accretionary slope is described as a vertical wall (>45 degrees) that is locally undercut between 35 and 80 meters. Below this wall, the slope gradients decrease from 30 to 35 degrees at 100 meters to 15 degrees at

300 meters. The slope is concave and lithified throughout the lower interval (References 263 and 268). Seaward of this location, a trough and “dump bump” topography marks the beginning of the lower slope. The lower slope west of and below the “dump bump” is a very low energy environment, found in water depths greater than 150 meters.

Figure 2.4.6-299 shows the bathymetry of the northern site near the Bimini Islands which exhibits failure scars, “Fs” (Reference 260). Figure 2.4.6-297 shows the location of several seismic reflection profiles presented in Reference 263. The seismic reflection profile along Line 5 in the study area near Bimini Island is shown in Figure 2.4.6-298. Near the top of the profile of Line 5, the steepest slope is approximately 20 degrees. Within approximately 1 kilometer, the slope decreases to approximately 17 degrees and further west (downslope) to 5 degrees along the profile. The slope of the face of the scarp at the northern site, based on the profile shown in Figure 2.4.6-300 is approximately 7 degrees. Different seismic profiles presented in Reference 263 suggest that low angle slopes to 20 degrees slope could be subject to failure.

Therefore, among slope failures of similar size, the impact on the Turkey Point Units 6 & 7 site would depend on the proximity of the tsunami source, the direction of the wave, and the bathymetry along the path of its propagation. The northern site location is referred to henceforth as the Postulated Slide Location. Based on this consideration, the Postulated Slide Location shown in Figures 2.4.6-295 and 2.4.6-297 was identified as being the most likely to generate a tsunami that would produce the maximum wave height at the Turkey Point Units 6 & 7 site. The Postulated Slide Location is approximately 13 kilometers southwest of South Bimini Island. At a distance of approximately 104 kilometers, the Postulated Slide Location at this point along the western margin of the GBB is the closest to the Turkey Point Units 6 & 7 site with the direction of a potential failure pointing directly towards the site.

The conservative approach to the GBB tsunami flooding evaluation is to incorporate source characteristics from both the hypothetical slide areas described above. The northern site, at approximately 25.6134° N, 79.3213° W, is therefore selected as the source location of the postulated slide for the tsunami modeling because of its proximity and direct path of tsunami wave propagation to the Turkey Point Units 6 & 7 site.

2.4.6.1.4 Far-Field Submarine Landslide Sources

Ward and Day (Reference 204) postulated a mega-tsunami scenario as a result of a possible catastrophic flank failure of the Cumbre Vieja volcano at La Palma of Canary Islands. They estimated that a future volcanic eruption of Cumbre Vieja could slide up to 500 cubic kilometers (120 cubic miles) of rock volume into the ocean running westward 60 kilometers (37.3 miles) offshore at a speed of 100 meters per second (328 feet per second) resulting in a tsunami amplitude of 20–25 meters (66-82 feet) at the Florida Atlantic coast. However, Mader pointed out that the assumption of linear propagation of shallow water wave, as used in Ward and Day’s analysis, only described geometrical spreading of waves and ignored the effects of short period wave dispersion (Reference 205). Such an assumption would overpredict the tsunami amplitude. Using the SWAN computer code, Mader computed a maximum tsunami amplitude less than 3.0 meters (10.0 feet) along the U.S. Atlantic coast and less than 1.0 meter (3.3 feet) near Miami, Florida (Reference 205). Mader adopted the initial tsunami amplitude as obtained from the physical model study of the Cumbre Vieja volcano flank failure performed at the Swiss Federal Institute of Technology (Reference 205). The Swiss Federal Institute of Technology experiment considered the failure as a single monolithic block (Reference 205). Pararas-Carayannis also disputed the claim by Ward and Day that a collapse of the Cumbre Vieja volcano is imminent (Reference 206).

More recent modeling efforts by Gisler et al. of the Cumbre Vieja volcano flank failure also showed significant wave dispersion (Reference 207). From the model simulation results, Gisler et al. demonstrated that the tsunami amplitude decay is proportional to $r^{-1.85}$ and $r^{-1.0}$, where r is the

distance from tsunami source, for the two- and three-dimensional models, respectively. The simulated tsunami amplitude varied between 1 and 77 centimeters (0.4 and 30 inches) along the Florida Coast (Reference 207). Gisler et al. used smaller slide volume but much higher slide speed compared to those used in Ward and Day (Reference 202). The amplitude in Ward and Day model scales proportionally with rock volume times slide speed. Hence, the much smaller predicted amplitude of Gisler et al. for the Florida coast cannot be attributed to the smaller slide volume (Reference 202). AGMTHAG concluded that a tsunami from this source is not expected to cause a devastating tsunami along the east coast of the United States (Reference 202).

The other notable far-field submarine landslide tsunami sources are located along the glaciated margins of northern Europe and Canada (Reference 202). The Storegga landslide in northern European margin is identified as a composite of seven slides over the past one-half million years with the largest and most recent landslide dated at 8150 years before present. The resulting tsunamis affected the coasts of Norway, Faeroes islands, Shetland islands, Scotland and northern England. The impacted areas were all within 600 kilometers (375 miles) of the slide (Reference 202).

The Grand Banks landslide in the Scotian margin near Newfoundland, Canada generated a devastating tsunami locally in 1929 (References 202 and 208). AGMTHAG indicated that increased deposition and slope failure on the Scotian margin was due to glacial advance that reached close to the shelf edge about one-half million years before present. However, deposition rate decreased significantly about 8000 years ago as deglaciation ended (Reference 202). The 1929 Grand Banks landslide is one of the only two landslide occurrences in the Scotian margin postdated to the Holocene. Units 6 & 7 would not be affected by teletsunamis from these landslide sources because the tsunamis would be dissipated before reaching them.

2.4.6.1.5 Earthquakes in the Azores-Gibraltar Plate Boundary

Tsunamigenic earthquake sources that may affect the Florida Atlantic Coast are located west of Gibraltar in the Azores-Gibraltar plate boundary near Portugal in the East Atlantic Ocean (at the Africa-Eurasia plate boundary) and in the northeastern Caribbean Basin (Caribbean-North American plate boundary). The Azores-Gibraltar plate boundary separates the African and Eurasian plates, as shown in Figure 2.4.6-206, and has been identified as the source of the largest earthquakes and tsunamis in the north Atlantic basin (Reference 202). AGMTHAG summarized six large tsunamigenic earthquakes that had occurred in this region over the past 300 years—in 1722, 1755, 1761, 1941, 1969 and 1975 (Reference 202). The 1755 Great Lisbon Earthquake, which was estimated in earthquake moment magnitude (M_W) to be 8.5–9.0, had the largest documented felt area of any shallow water earthquake in Europe, and was the largest natural disaster to have affected Europe in the past 500 years (Reference 202). The earthquake motion and ensuing submarine landslide contributed to tsunami waves of 5 to 15 meters (16.4 to 49.2 feet) that devastated the coasts of southwest Iberia and northwest Morocco and were reported as far north as Cornwall, England (Reference 202). Figure 2.4.6-206 shows the general tectonic setting and bathymetry of the eastern segment of the Azores-Gibraltar plate boundary.

The large tsunami waves also travelled across the Atlantic reaching as far north as Newfoundland, Canada and as far south as Brazil, and caused widespread damage in the eastern Lesser Antilles (Reference 202). However, there is no record of tsunami run-up on the U.S. east coast from this event, although several populated cities existed along the U.S. Atlantic coast in 1755 (Reference 202). Computer simulations by Mader (Reference 209) indicated that the maximum tsunami amplitude including run-up in the U.S. east coast was approximately 3.0 meters (10.0 feet). AGMTHAG simulated the 1755 earthquake tsunami with the source location varying within the Azores-Gibraltar region. The maximum tsunami amplitude in the deep water along the U.S. Atlantic margin was obtained as approximately 0.6 meter (2.0 feet) for a tsunami source location east of the Madeira Tore Rise (Figure 5-8, Reference 202). Further discussion of the 1755 earthquake-generated tsunami is provided in Subsections 2.4.6.2 and 2.4.6.3.

2.4.6.1.6 Earthquakes in the North Caribbean Subduction Zones

The Caribbean region is characterized by high seismic activities and is associated with a large number of past tsunamis (References 210 and 211). Tsunami sources in the northeastern Caribbean Basin that may affect the Florida Atlantic coast include the Puerto Rico and Hispaniola trenches, as shown in Figure 2.4.6-207. AGMTHAG simulated the distribution of peak offshore tsunami amplitude along the Gulf of Mexico and Atlantic Coasts from a postulated earthquake in the Puerto Rico trench. The simulation, which used a linear long-wave model for the deepwater regions and did not include frictional effects, predicted the maximum tsunami amplitude to be no more than 0.1 meter (0.3 foot) at a water depth of 250 meters (820 feet) near the longitude of approximately 80.2° W (longitude position estimated from Figure 8-2c of Reference 202). This longitude position represents generally the location within the Straits of Florida, which is south-southwest of Units 6 & 7. The maximum deepwater tsunami amplitudes along the U.S. Atlantic coast, however, were much higher, close to 5 meters (16.4 feet) near latitude 40° N (latitude position represents generally a location offshore of the New York/New Jersey coast) and approximately 3 meters (10 feet) near latitude 33.2° N (offshore of the South Carolina coast). The model simulated a maximum deepwater tsunami amplitude of about 3.5 meters (11.5 feet) near 28° N (offshore of Palm Bay, Florida) (Figure 8-3c of Reference 202). The relatively small tsunami amplitude near Units 6 & 7 is primarily a result of the presence of the Bahama platform to the east, as shown in Figure 2.4.6-208 and Figure 2.4.6-228. AGMTHAG did not model the propagation of tsunami waves across the continental shelf (water depth less than 250 meters or 820 feet) and run-up (Reference 202).

A similar tsunami model study was also performed by the West Coast and Alaska Tsunami Warning Center using a two-dimensional hydrodynamic model developed at the University of Alaska, Fairbanks (Reference 211). Four hypothetical worst-case scenarios with tsunami sources located in the Gulf of Mexico and the Caribbean regions were simulated using the West Coast and Alaska Tsunami Warning Center model. The simulations predicted the peak tsunami amplitude near Virginia Key, Florida, to be approximately 15 centimeters (0.5 foot) for an earthquake magnitude M_W of 9.0 in the Puerto Rico Trench. The simulated earthquake is larger in magnitude than any recorded earthquake in this region. The maximum recorded earthquake magnitude in this region is 8.3 (unknown earthquake scale) that struck the Guadeloupe Island in Lesser Antilles, as obtained from the National Geophysical Data Center (NGDC) earthquake database (Reference 212). Also tabulated in the NGDC earthquake database are two events with earthquake surface wave magnitude (M_S) of 8.1 that occurred near Haiti in 1842 and the Dominican Republic in 1946.

2.4.6.1.7 Other Sources

An extensive literature search did not return any information of seismically induced seiche in Biscayne Bay. In addition, because of low and flat topography near Units 6 & 7, the possibility of any subaerial slope failure that would generate tsunamis affecting Units 6 & 7 is precluded.

Earthquakes within the Gulf of Mexico are also recorded with epicenters located within the North American plate boundaries. Such “midplate” earthquakes are less common than earthquakes occurring on faults near plate boundaries and are unlikely to produce any destructive tsunami (Reference 213).

A significant tsunami generated directly by an earthquake only occurs if the earthquake is large (magnitude, with few exceptions, greater than about 6.5) and if the fault slip associated with the earthquake has a significant vertical seafloor displacement (thrust or normal faults). There is no record of surface fault rupture and significant seismic wave displacement at the seafloor associated with any historical earthquake in the central and eastern United States including the 1886 Charleston, South Carolina event of about magnitude 7, the largest historical earthquake in the U.S. Atlantic coastal region. Consequently, the conditions for tsunamigenesis by seafloor displacement associated with an earthquake do not appear to exist along the U.S. Atlantic margin; Units 6 & 7, therefore,

would not be impacted by significant tsunamis as a result of vertical seafloor displacement associated with the U.S. Atlantic margin earthquakes.

Although the north Caribbean subduction zone is noted for several seismically-generated tsunamis in recent times, as described in Subsection 2.4.6.1.6, potential submarine landslides of the carbonate platform edge north of Puerto Rico are capable of producing large tsunamis locally (see Subsections 2.4.6.2 and 2.5.1.1.5 for detailed discussions). However, because the Units 6 & 7 site is sheltered by the Bahamas Islands, such landslide-generated tsunamis are not expected to affect the site. This sheltering effect can be seen from the results of a tsunami model simulation caused by an earthquake in the Puerto Rico Trench (North Puerto Rico/Lesser Antilles subduction zone). Figure 2.4.6-228, taken from Reference 202, shows contours of tsunami amplitudes and the associated regional tsunami propagation pattern due to an earthquake at the Puerto Rico Trench. As indicated in the figure, the southeast Florida coast is sheltered by the Bahamas from tsunami waves generated in the area north of Puerto Rico. Although the mechanism of tsunami generation by earthquakes and landslides is different, the regional tsunami propagation pattern between the two is expected to be similar for the Puerto Rico Trench area. As Figure 2.4.6-228 indicates, the apparent earthquake tsunami beaming is along an azimuth perpendicular to the strike, i.e., in the north direction. For a landslide tsunami that may originate in the Puerto Rico Trench, the direction of the seaward tsunami propagation would also be in the north direction, and the tsunami amplitude would be relatively lower at far-field. This is because landslide tsunamis are greatly attenuated at far-field due to non-linear and dispersive effects compared to earthquake tsunamis (Reference 202). Therefore, a landslide in the carbonate platform north of Puerto Rico is not considered as a PMT source for the Units 6 & 7 site.

2.4.6.1.8 Summary of Potential Sources for PMT at Units 6 & 7

Units 6 & 7 are not located in the immediate vicinity of any tsunamigenic source. The landslide zone nearest to Units 6 & 7 is located on the west Florida slopes within the Gulf of Mexico, separated by a very wide and shallow continental shelf and the entire width of the Florida peninsula. There is no historical evidence of any tsunami from landslides in the Gulf of Mexico. Landslides in the U.S. Atlantic margin may potentially generate local destructive tsunamis. However, because Units 6 & 7 are located far away from any such sources, is mostly sheltered by the Bahama platform, and is protected by a retaining wall structure with top elevation of 20.0 feet to 21.5 feet NAVD 88, such tsunamis are not expected to cause any flooding concern to the safety-related facilities of Units 6 & 7. The orientation of the Puerto Rico trench and the presence of the Bahama platform prevents any destructive tsunami to impact Units 6 & 7 from this source. Therefore, it is concluded that the PMT would likely be caused by earthquake-generated transoceanic tsunamis from the Azores-Gibraltar plate boundary. Characteristics of tsunami source generators for both Azores-Gibraltar plate boundary and Caribbean region are presented in Subsection 2.4.6.3.

2.4.6.2 Historical Tsunami Record

Records of historical tsunami run-up events along the U.S. Atlantic coast near Units 6 & 7 are obtained from the NGDC tsunami database (Reference 214). The NGDC database contains information on source events and run-up elevations for tsunamis worldwide from approximately 2000 B.C. to the present time (Reference 214). A search of the NGDC tsunami database returned 11 historical tsunamis that have affected the U.S. and Canada east coast, as indicated in Table 2.4.6-202.

Three events in the record are the result of a combination of earthquakes and submarine landslides in the Nova Scotia margin off the coast of Newfoundland, Canada, and in the Labrador Sea off Newfoundland, Canada. The most recent and most severe tsunami from this area was that from the M_W = 7.2 earthquake and associated submarine landslide in the Nova Scotia margin in 1929. The ensuing tsunami, with a maximum run-up of approximately 7 meters (23 feet) at Taylor's Bay,

Newfoundland, Canada, was recorded as far south as Charleston, South Carolina (12 centimeters or 4.7 inches).

Three earthquakes in the Caribbean region generated tsunamis that were recorded in the U.S. east coast. The strongest earthquake was the M_s = 8.1 earthquake of August 4, 1946, with an epicenter northeast of the Dominican Republic, which was followed by the August 8, 1946 aftershock (magnitude 7.9 of unknown scale). The maximum tsunami run-ups from the two events were 5.0 meters (16.4 feet) and 0.6 meter (2.0 feet) at the coasts of Dominican Republic and Puerto Rico, respectively, for the August 4 and August 8 events. No run-up data is available from these events on the Florida Atlantic coast. The other tsunami event was caused by the earthquake of 1918 (M_w = 7.3) in Mona passage, located northwest of Puerto Rico, resulting from the displacement of four segments of a normal fault (Reference 214). A recent study hypothesized a combined earthquake- and landslide-generated tsunami for this event (Reference 215). The NGDC database indicates a tsunami amplitude of 6 centimeters (2.4 inches) near Atlantic City, New Jersey. However, no run-up was reported on the Florida Atlantic coast from this event. The maximum tsunami amplitude from this event reported along the western and northern Puerto Rico was 6.1 meters (20.0 feet).

The NGDC database also includes three tsunami events generated in the U.S. Atlantic margin with the Charleston, South Carolina, earthquake-generated (M_w = 7.7) tsunami of 1886 being the only confirmed tsunami. An earthquake event was also reported at Jacksonville, Florida, on the same day approximately an hour before the Charleston, South Carolina, earthquake. It has not been established if the two events were related (Reference 214). The resulting tsunami waves were reported in Jacksonville and Mayport, Florida, although no run-up information is available. The two other tsunami events are reported as probable in the NGDC database. The first tsunami event was the result of an earthquake in High Bridge, New Jersey (magnitude computed from the felt area, Mfa = 4.4) that produced a tsunami-like wave in Long Island, New York, in 1895. The second event was a possible landslide- or explosion-generated tsunami near Long Island, New York, that produced a maximum tsunami amplitude of 0.28 meter (0.9 foot) at Plum Island, New York, in 1964. No tsunami wave from the two events was reported in the Florida Atlantic coast.

The remaining two records in the NGDC database are transoceanic tsunami events: the Great Lisbon Earthquake tsunami of 1755 off the Portugal coast and the Boxing Day tsunami of 2004 off the west Sumatra coast, Indonesia. The earthquake west of Sumatra (M_w = 9.0) generated a tsunami that was recorded nearly worldwide and killed more people than any other tsunami in recorded history (Reference 214). A tsunami amplitude of 0.17 meter (0.6 foot) was recorded at Trident Pier on the Florida Atlantic coast. The Great Lisbon Earthquake that destroyed the city of Lisbon stuck at approximately 9:40 a.m. on November 1, 1755. Mader reported an estimated magnitude (M_w) of approximately 8.75–9.0 for the earthquake that was felt over an area of a million square miles (Reference 209). The earthquake generated a tsunami, which arrived at Lisbon between 40 minutes and 1 hour after the earthquake as a withdrawing wave, that emptied the Lisbon Oeiras Bay (Reference 209). The following tsunami wave arrived with an amplitude of approximately 20 meters (65.6 feet) followed by two more waves approximately an hour apart (Reference 209). The tsunami wave had amplitudes of 4 meters (13.1 feet) along the English coast, and 7 meters (23 feet) at Saba, Netherland Antilles, in the Caribbean after approximately 7 hours of travel (Reference 209). Lockridge et al. also reported tsunami arrival in the harbor at Cape Bonavista, Newfoundland, Canada, with a retreating wave and a subsequent returning wave approximately 10 minutes later (Reference 208). Model simulation by Mader showed that the tsunami wave arrived at the Florida Atlantic coast approximately 8 hours after the earthquake (Reference 209). The deepwater tsunami amplitude off the coast of Miami, Florida, was simulated to be approximately 2 meters (6.6 feet) with a period between 1.25 and 1.5 hours. Mader suggested a maximum tsunami amplitude of approximately 3.0 meters (10 feet) including wave run-up along the U.S. east coast (Reference 209).

Lockridge et al. reported tsunamis and tsunami-like events in the U.S. east coast in addition to the events reported in the NGDC database (Reference 208). Most of these additional events originated

along the New York, New Jersey, and Delaware coasts, and the Florida Atlantic coast remained unaffected. No seismically-induced paleotsunami deposits have been positively identified in available scientific literature within the 200-mile radius of the Turkey Point site, as described in Subsection 2.5.1.1.5. Distinguishing characteristics of tsunami versus storm deposits are also described in Subsection 2.5.1.1.5. Turkey Point site boring log data interpretation and relevance to paleotsunami deposits is described in Subsection 2.5.1.2.2.

2.4.6.3 Source Generator Characteristics

There is no tsunamigenic source present in the immediate vicinity of Units 6 & 7. The submarine landslide zones in the U.S. Atlantic margin and along the Gulf of Mexico coast are located far away from Units 6 & 7 and are separated by a wide and shallow continental slope and shelf, which would reduce the impact of any landslide-generated tsunamis at Units 6 & 7. The north Caribbean subduction zone and Azores-Gibraltar plate boundary are identified as the primary tsunamigenic earthquake sources that could affect the site. Model simulation results indicate that the shallow Bahama platform shields Units 6 & 7 from tsunamis generated in the northern Caribbean region (Reference 211). Therefore, the PMT for Units 6 & 7 would likely be transoceanic tsunamis from the Azores-Gibraltar region. The most recent major earthquake in the region occurred in 1969 (M_w = 7.8) and generated a small tsunami amplitude locally (Reference 202).

2.4.6.3.1 Azores-Gibraltar Plate Boundary

The Azores-Gibraltar plate boundary separates the African and Eurasian plates and extends from Azores in the west at the junction of North American, African, and Eurasian plates to east of Gibraltar strait, the area southwest of the Iberian Peninsula (see Figure 2.4.6-206). Based on literature on plate kinematic models and focal mechanisms, AGMTHAG indicated that the motion between the two plates is slow, changing along the boundary from divergent extension in the Azores to compression towards the east end that includes the Gorringe Bank and the Gibraltar Arc (Figure 2.4.6-206). The location of plate boundary in the east near Iberia is uncertain where a diffuse compression zone exists over a 200–330 kilometers (124–205 miles) width. The dominant active structures in the region are the Gorringe Bank Fault (GBF), the Marqués de Pombal Fault (MPF), the St. Vincente Fault (SVF), and the Horseshoe Fault (HSF) (Figure 2.4.6-206) (Reference 202).

The source location of the 1755 earthquake is still the subject of research in the scientific community. AGMTHAG summarizes the three major views on fault solution for the 1755 earthquake (Reference 202). First, in 1996, Johnson (also in 2007, Grandin et al.) suggested a northeast-southwest trending thrust fault, possibly outcropping at the base of the northwest flank of the Gorringe Bank (GBF). Second, Zitellini et al. in 2001 (also Grácia et al. in 2003) suggested active thrusting along the MPF as the source located approximately 80 kilometers (50 miles) west of Cape Sao Vincente. Third, Gutscher et al. in 2002 and 2006 (also Thiebot and Gutscher in 2006) proposed a fault plane in the western Gulf of Cádiz (Gulf of Cádiz Fault, GCF), possibly as part of an African plate subduction beneath Gibraltar (Reference 202).

AGMTHAG used the same set of fault parameters as proposed by Johnson to investigate constraints on the 1755 Lisbon earthquake epicenter, and potential tsunami hazard to the U.S. East Coast from possible future earthquake sources located in the east Atlantic region (Reference 202). The parameters are (Reference 202):

Source depth at the top of the fault plane = 5 kilometers (3.1 miles)
Length = 200 kilometers (124 miles)
Width = 80 kilometers (50 miles)
Dip = 40 degrees
Strike = 60 degrees
Average slip = 13.1 meters (43 feet)

The strike orientation as proposed for MPF and GCF sources differs considerably from the description for the GBF source proposed by Johnston. AGMTHAG investigated the effects of the variation in the location of earthquake epicenter and strike orientation on near-field and far-field tsunami amplitudes. Based on a comparison of model simulation results with reported tsunami amplitudes, AGMTHAG concluded that the 1755 earthquake was likely generated by a northwest-southeast trending fault located in the center of the Horseshoe plain south of Gorringe Bank (Reference 202).

2.4.6.3.2 Hispaniola-Puerto Rico-Lesser Antilles Subduction Zone

The Hispaniola-Puerto Rico-Lesser Antilles subduction zone was formed as the North American plate was subducting southwesterly beneath the Caribbean plate (Figure 2.4.6-207) (Reference 202). Relative plate movement changed to a more easterly direction resulting in a more oblique subduction beginning at 49 million years ago, which remained fairly stable afterwards as evidenced by the opening of the Cayman Trough between Cuba and Honduras (Reference 202). AGMTHAG describes the present subduction at the Puerto Rico trench as an old oceanic crust of 90–110 million years in age, subducting under Puerto Rico and Virgin Islands and at the Hispaniola trench as a thick crust of an unknown origin, which underlies the Bahama platform (Reference 202).

Although there are geometric similarities between the Puerto Rico trench and Sumatra-Andaman trench where the devastating 2004 Indian Ocean tsunami originated, AGMTHAG pointed out that the slip during the earthquake in the Puerto Rico trench is highly oblique and nearly parallel to the convergence direction unlike the Sumatra-Andaman trench (Reference 202). This difference in the slip angles indicates the potential for only small deformations of the overlying Caribbean plate.

In contrast to the Puerto Rico trench, slip on the Hispaniola trench is sub-perpendicular to the trench. Therefore, a large vertical motion is expected for a given magnitude of slip. Unlike the Puerto Rico trench, where a normal thickness oceanic crust is subducting, the crust entering the Hispaniola trench is very thick and would likely allow more stress to accumulate resulting in large earthquakes to occur (Reference 202).

The rupture parameters for the Puerto Rico and Hispaniola trenches, as proposed by AGMTHAG, are listed below (Reference 202):

Puerto Rico Trench (single rupture)

Length = 675 kilometers along the trench between 68° W and 62° W
Depth = 5 to 40 kilometers (3.1 to 25 miles)
Dip = 20 degrees
Strike = 70 degrees
Slip = 10 meters (32.8 feet)
Slip direction = 60 degrees
Shear modulus = 3×10^{10} Pa (6.3×10^{8} pounds/square feet)
Earthquake magnitude, M_w = 8.85

Hispaniola Trench

Length = 525 kilometers (326 miles) along the trench between 73° W and 68° W
Depth = 0 to 40 kilometers (0 to 25 miles)
Dip = approximately 20 degrees
Strike = 95–102 degrees
Slip = 10 meters (32.8 feet) assuming complete rupture of the Hispaniola trench
Slip direction = 23 degrees
Earthquake magnitude, M_w = 8.81

The magnitude of the earthquake-generated tsunami is related to the slip vector. The direction of slip vector is given by the slip angle, or rake, which is measured in the plane of the fault from the strike direction to the slip vector showing the motion of the hanging wall relative to the footwall. The slip (rake) angle of the fault is often estimated from analysis of focal mechanisms. In those cases where the slip angle cannot be directly measured, the assessment of the sense of slip could be based on an integration of direct observations of the fault and tectonic indicators (Reference 216). Based on dislocation theory, the amplitude of seafloor displacement is linearly proportional to the magnitude and direction of the slip vector, which vary for the dip-slip and strike-slip faults. The vertical displacement of an oblique-slip fault is estimated as the sum of the displacement fields derived from the dip-slip and strike-slip components.

AGMTHAG modeled three different source segments for the northern Puerto Rico/Lesser Antilles subduction zone, including the Puerto Rico and Hispaniola trenches (Reference 202). Tsunami propagation from these sources was modeled by linear long-wave theory, as described in AGMTHAG (Reference 202). The source parameters for the Puerto Rico and Hispaniola faults used in the model are slightly different than the source parameters described above and result in an earthquake moment magnitude ranging between 9.11 and 9.15. A summary of the tsunami source parameters including the expected range of magnitude and average slip angles for each tsunamigenic fault in Caribbean region is given in Table 8-1 of AGMTHAG (Reference 202).

2.4.6.4 Tsunami Analysis

The maximum tsunami water level at Units 6 & 7 is obtained for the postulated PMT generated by earthquake in the Azores-Gibraltar fracture zone. Tsunami propagation and the effects of near shore bathymetric variation at the Florida Atlantic coast are simulated in a two-dimensional computer model, the development of which is summarized in the following subsections. Detailed water level records near Units 6 & 7 are not available for tsunamis generated by past earthquakes in the Azores-Gibraltar fracture zone or in the Caribbean subduction zone for the listed earthquake magnitudes. In order to establish the model boundary condition, the resulting water levels in deep waters in the computer simulations by Mader (Reference 202) and Knight (Reference 211) for tsunamis generated from the Azores-Gibraltar and Caribbean sources are used as guidance for the PMT model. The PMT simulation for Units 6 & 7 uses the computer code Delft3D-Flow, which is a multi-dimensional modeling system that is capable of simulating the hydrodynamics and transport processes for fluvial, estuarine, and coastal environments (Reference 219). The analysis of the postulated PMT is described in Subsection 2.4.6.4.1.

In addition the generation and propagation of a tsunami caused by the Cape Fear slide was simulated to examine the water levels it produces at the site and to confirm that they are smaller than those produced by the postulated PMT. The simulation of the Cape Fear tsunami for Units 6 & 7 uses the model FUNWAVE-TVD (Reference 234). The analysis of the Cape Fear tsunami is described in Subsection 2.4.6.4.2.

In addition, the generation and propagation of tsunamis caused by postulated submarine slides near Cape Fear, the west Florida Escarpment, and the western margin of the GBB were simulated to examine the water levels they would produce at the site and to confirm that they are smaller than those produced by the postulated PMT. The simulation of these tsunamis for Units 6 & 7 uses the model FUNWAVE-TVD (Reference 234). The analyses are described in Subsections 2.4.6.4.2, 2.4.6.4.3, and 2.4.6.4.4.

2.4.6.4.1 Analysis of the PMT (Azores-Gilbraltar Fracture Zone Earthquake Tsunami)

2.4.6.4.1.1 Numeric Modeling Approach and Conceptualization

Subsection 2.4.6.1 establishes the Azores-Gibraltar fracture zone (specifically the 1755 Lisbon Earthquake source) as the candidate PMT source for Units 6 & 7. It is postulated that the earthquake-generated transoceanic tsunami from this source would propagate across the Atlantic Ocean and would be modified at the Bahama platform before reaching the site. Tsunami generation and transoceanic propagation from this source were studied previously using numerical model simulations (References 202 and 209). However, tsunami wave modification on the shallow Bahama platform and wave run-up onshore near Units 6 & 7 have not been reported in any literature. The primary objectives in developing the numerical model for Units 6 & 7 therefore are to account for the effects of near shore bathymetric variation on tsunami wave modification and tsunami run-up onshore.

Delft3D-FLOW, the flow module of the Delft3D modeling system, simulates two- or three-dimensional unsteady flow problems from tide or meteorological forcing. The FLOW module provides hydrodynamic solutions for which the horizontal length and time scales are significantly larger than the vertical scales (Reference 219) representing the shallow water conditions. Delft3D-FLOW has the capability of invoking the FLOOD solver, which employs a numerical technique (Reference 220) that can be applied to problems involving rapidly varied flows, for example, in hydraulic jumps and bores, and sudden flow transitions including rapid flooding and drying of land. The FLOOD scheme is suitable for simulating the tsunami waves, embankment breaches, hydraulic jumps, and flows over obstructions (Reference 219). Consequently, in the present analysis, the Delft3D-FLOW module along with the FLOOD solution scheme is applied to simulate tsunami propagation and run-up at Units 6 & 7.

Delft3D-FLOW assumes hydrostatic pressure distribution and therefore ignores frequency dispersion. As a result, model simulation results on tsunami propagation generally show steeper wave fronts with larger wave amplitudes compared to analytical solutions or benchmark laboratory test results (Reference 221). The shallow water conditions adopted in Delft3D-FLOW therefore are capable of resolving the tsunami wave propagation where the frequency dispersion is not significant and would be conservative in simulating the near shore tsunami amplitude.

2.4.6.4.1.2 Model Setup

AGMTHAG and Mader reported modeling of the 1755 Lisbon Earthquake tsunami and included most of the Atlantic Ocean in the model domain (References 202 and 209). The PMT model for Units 6 & 7, on the other hand, a portion of the Atlantic Ocean and the Gulf of Mexico are considered in the model setup, as described below.

Model Domain and Grids

To be able to investigate nearshore tsunami wave modification and onshore run-up, the tsunami model domain is selected to include detailed bathymetric variations in the area bounded by the Atlantic continental shelf, the Florida platform, Cuba, Dominican Republic, and the Blake-Bahama basin (as shown in Figure 2.4.6-209). In light of the uncertainties in defining the 1755 Lisbon Earthquake source in the Azores-Gibraltar region (References 202 and 209), tsunami generation at the source was not included in the model. Instead, the model (open) boundary in the Atlantic Ocean is established based on tsunami propagation patterns reported in existing literature, as described in Subsection 2.4.6.4.1.3.

The selected model domain is shown on Figure 2.4.6-210. The east model boundary in deep waters generally follows the simulated propagation of tsunami wave front after 6.5 hours of travel in Mader's analysis (Reference 209). The 6.5 hour wave front is selected to maximize the coverage of the ocean

in the model and also allow the model to be defined by one open sea boundary with a uniform boundary condition. This open boundary extends from Havelock, North Carolina to north east of the Dominican Republic. The north and west model boundaries follow mostly the coastlines of the southeastern United States. The south model boundary is set along the northern coastlines of the Dominican Republic, Haiti, and Cuba. The small passage between Haiti and Cuba is conservatively assumed to be blocked. Southwest of the site, the model includes a portion of the Straits of Florida, the area protruding past the Florida Keys, to allow the tsunami wave to travel farther into the Gulf of Mexico so that the effect of this boundary on the site is minimized. Extending the model farther into the Gulf of Mexico is not necessary, as the maximum tsunami water level at the site would occur before the effect of this boundary is reflected back at the site. Consequently, the model boundary in the Gulf of Mexico is simulated as a closed boundary.

The model uses curvilinear orthogonal grids that are generated with RGFGRID, the Delft3D module for grid generation and processing. The curvilinear option allows fitting grids cells along coastlines and contours of changing bathymetry. In addition, curvilinear grids could be oriented in relation to anticipated flow direction or wave propagation, thereby improving model accuracy.

A nested grid system with three different grid resolutions is developed using the domain decomposition tool within RGFGRID to appropriately resolve tsunami wave modification near the site. The three grid subdomains are shown on Figure 2.4.6-210. The first subdomain, SITE, covers the area near the site including the Biscayne Bay and the adjacent Straits of Florida, and has the finest grid resolution. The second subdomain, ISLANDS, includes most of the Bahamas with intermediate grid resolution. The third subdomain, DEEP, covers the rest of the model domain with a coarse grid resolution, which is mostly deep waters and is farther away from SITE and ISLANDS subdomains. At the interfaces between the subdomains, every third point in the finer grid is aligned with successive grid points in the coarser grid. Subdomain grid resolutions, represented by the square root of grid cell area, and grid spacings in the two orthogonal directions are given in Table 2.4.6-203. Figures 2.4.6-211 through 2.4.6-213 show the grids of the three subdomains.

Model Bathymetry

Tsunami model bathymetric and topographic data are obtained from the following public sources:

- Biscayne Bay sounding data from NOAA estuarine bathymetric database
- LiDAR (Light Detection And Ranging) data from NOAA Coastal Ocean Service database
- Coastal Relief data from NOAA National Geophysical Data Center (NGDC)
- ETOPO1 data from NOAA NGDC

The last two sources include both bathymetric and topographic (land) data, whereas the first source includes only bathymetric data, and the second source includes only topographic data. The four data sets have different horizontal and vertical resolutions. The Biscayne Bay sounding and LiDAR data have high vertical and horizontal resolutions compared to the Coastal Relief and ETOPO1 data. Therefore, they were given high priority and used first in populating the model depth data. The Coastal Relief data has higher horizontal resolution compared to the ETOPO1 data and therefore was given priority in populating the remaining model domain. A summary of resolution of available data is given in Table 2.4.6-204.

Bathymetric data from all sources are projected to the Azimuthal Equidistant map projection centered at Unit 6 & 7 for a uniform horizontal datum description. The Azimuthal Equidistant map projection is used to minimize distortion in both distance and direction from the site. All bathymetric and topographic elevations are converted relative to mean sea level (MSL) from their original source

datum. Conversion relationships between MSL and various vertical datums are selected based on NOAA's Virginia Key, Florida station.

The bathymetric and topographic elevations for the tsunami model are developed by using the Delft3D-QUICKIN module. Elevations at the grid points are determined by interpolating from the source data surrounding the grid points. Model bathymetric elevations at grid points with seabed located below the MSL are specified as positive, whereas, all grid points on land are given negative bathymetric (topographic) values. The developed model bathymetric map is shown on Figure 2.4.6-214.

Bed Roughness Condition

Bed roughness conditions in the tsunami model are specified through Manning's n roughness coefficient. For the initial tsunami model that is used to validate the open boundary condition where incoming tsunami waves are specified, a constant Manning's roughness coefficient of 0.025 (a typical value appropriate for the site) is used for the entire model domain, which represents natural channels in good condition (Reference 222). However, a Manning's *n* of 0.02 is used conservatively in the final analysis because the Manning's *n* sensitivity analysis results indicate that lower values give higher maximum tsunami water level at the site. This Manning's n value represents roughness conditions similar to a smooth earth surface (Reference 222). Water levels in deep areas, such as off Miami at water depth of 783 meters (2569 feet), would not be sensitive to Manning's *n* values because of very small flow velocities associated with deep areas. Water levels in shallow areas are sensitive to Manning's *n* values because of relatively higher velocities.

Initial Condition

The antecedent water level including the 10 percent exceedance high spring tide, initial rise, and long-term sea level rise, as specified in Subsection 2.4.5.2.2.1, is used as the initial water level for the tsunami model. The initial water level in the tsunami model, after conversion to MSL, is 1.36 meters (4.46 feet) MSL.

Time Step and Simulation Time

The tsunami model is run with a time step of 0.2 minute (12 seconds). The model simulations are continued for a period of 9 hours, although the travel time from the open boundary to the site is about 2.5 hours and the maximum tsunami water level at the site is reached after about 4.5 hours from the start of simulation. Therefore, simulation period of 9 hours is sufficient to capture the maximum water level at the site. The start and end time for model simulations are selected arbitrarily.

2.4.6.4.1.3 Selection and Validation of Open Boundary Condition

The model requires time history of incoming tsunami water level as the boundary condition along the eastern open boundary. However, no measured water level data from the 1755 Lisbon Earthquake tsunami is available at the model boundary location. Consequently, a synthetic time history of tsunami water level assuming a sinusoidal tsunami waveform is used to establish the model boundary condition.

Tsunami water level on the Atlantic coast near Miami, Florida, is obtained from the model simulation results performed by Mader for the 1755 Lisbon Earthquake tsunami (Reference 209). Because the source location and characteristics for the 1755 Lisbon Earthquake are not precisely known, Mader developed tsunami source parameters in such a way that the model reproduces tsunami amplitude and arrival time within reasonable accuracy at near- and far-field locations where these are known. Mader assumed the source location to be close to Gorringe Bank in the Azores-Gibraltar region, near the source location of the 1969 earthquake (1969 earthquake location is shown on Figure 2.4.6-206). To produce a tsunami amplitude of 20 meters (65.6 feet) with a 1-hour wave period that arrives at Lisbon, Portugal, 40 minutes after the earthquake, Mader considered fracture in a 300 kilometers

(186.4 miles) arc-fault with a slip of 30 meters (98.4 feet). Although Mader did not provide information on the strike angle or location, the curved fault structure resembles closely to the composite fault zone assumed by Gutscher et al. in 2002, 2006 and discussed in AGMTHAG (Reference 202). In addition, the slip magnitude assumed by Mader is higher than that listed in Subsection 2.4.6.3.

AGMTHAG also performed numerical model simulations of the 1755 Lisbon Earthquake tsunami to evaluate the potential tsunami impact on the U.S. east coast. AGMTHAG first investigated the constraints on the earthquake epicenter from far field simulations. AGMTHAG modeled three different source segments for the northern Puerto Rico/Lesser Antilles subduction zone including the Hispaniola, Puerto Rico and Virgin Island faults. The earthquake moment magnitude from the selected source parameters ranges between 9.11 and 9.15. Using a linear long-wave model, AGMTHAG obtained a maximum tsunami amplitude near the site of no more than 0.1 meter (0.3 foot), as described in Subsection 2.4.6.1.6. AGMTHAG simulated tsunami propagation for 16 such potential source locations as shown in Figure 2.4.6-215. Based on model simulation results, AGMTHAG concluded that the variation in local seafloor bathymetry significantly controls tsunami propagation across the Atlantic Ocean. The Gorringe Bank and the Madeira Tore Rise (see Figure 2.4.6-206 for locations) act as near source barriers protecting most of the U.S. east coast. For sources located east of Madeira Tore Rise and south of Gorringe Bank, Florida might be at risk if sufficient wave energy passes through the Bahamas (Reference 202). AGMTHAG did not simulate tsunami wave run-up in the near shore region and considered relative amplitude evaluation only (Reference 202). Because the simulated deepwater tsunami amplitude in the southeastern U.S. coast from AGMTHAG is smaller than the tsunami amplitude reported in Mader (References 202 and 209), the present analysis adopted tsunami amplitude from Mader in developing the boundary condition in the tsunami model.

Mader performed numerical modeling of the tsunami wave using the SWAN nonlinear shallow water wave code including the Coriolis and friction effects. The model domain extended from 20° N to 65° N and 100° W to 0° W with a 10-minute grid resolution. Model bathymetry information was generated from the 2-minute Mercator Global Marine Gravity topography of Sandwell and Smith of the Scripps Institute of Oceanography (Reference 209). A model time step of 10 seconds was used for the simulation. Mader obtained tsunami amplitude of 20 meters (65.6 feet) at 953 meters (3127 feet) water depth off Lisbon, Portugal, and 5 meters (16.4 feet) at 825 meters (2707 feet) water depth east of Saba, Netherlands Antilles in the Caribbean. Mader argued that with a run-up amplification of the wave, the maximum near-shore wave amplitude would be two to three times the deepwater tsunami amplitude. However, he also pointed out that some of the run-up effects were probably included in the simulation for water depths less than 1000 meters (3281 feet). This assumption would provide a maximum tsunami water level above 20 meters (65.6 feet) at Lisbon and above 7 meters (23 feet) at Saba, higher than the tsunami amplitudes reported by Lockridge et al. (Reference 208). Consequently, simulated water levels obtained by Mader along the U.S. east coast would likely be conservative. Mader obtained tsunami amplitude of 2 meters (6.6 feet) at 783 meters (2569 feet) water depth east of Miami, Florida with a tsunami period of 1.5 hours, and suggested a maximum tsunami wave amplitude, including run-up, of approximately 10 feet (3 meters) along the U.S. east coast (Reference 209).

The synthetic tsunami marigram at the model boundary is selected such that the maximum tsunami wave amplitude and drawdown off Miami, Florida at a water depth of 783 meters (2569 feet) are comparable or conservative compared to Mader's results for the same location. Mader estimated the maximum wave amplitude and drawdown of 2.0 meters (6.6 feet) and -3.5 meters (-11.5 feet), respectively, from the initial water level at MSL (Reference 209). To generate the tsunami marigram at the model boundary, three different sinusoidal wave patterns are considered, each with 2.0 meter (6.6 feet) amplitude and 1.5 hours wave period. The first case considers a single wave, the second case considers a continuous wave train, and the third case considers only two consecutive waves. Figure 2.4.6-216 shows the marigrams for the three cases.

Figure 2.4.6-217 shows the simulated tsunami water levels for the three selected cases at the 783 meters (2569 feet) water depth off Miami, Florida. Similar to Mader, model simulations for the three cases consider the initial water level to be at MSL. Continuous wave train at the boundary generates the maximum tsunami amplitude and drawdown of about 5.5 meters (18 feet) and -6.5 meters (-21.3 feet), respectively, with respect to the MSL. These amplitude and drawdown are much higher than what is indicated in Mader's analysis, and therefore model input conditions with continuous wave train are not considered to be realistic. The single wave boundary condition produced the maximum wave amplitude and drawdown of about 2 meters (6.6 feet) and -3.5 meters (-11.5 feet), respectively, which are in very good agreement with Mader's results. However, because more than one wave was reported to have impacted the Portuguese and Canadian coasts (References 208 and 209), the single wave boundary condition is not considered in the present analysis. The boundary condition with two consecutive waves generates the maximum wave amplitude and drawdown of 4.5 meters (14.8 feet) and -5.3 meters (-17.4 feet), respectively. Although these values are much higher compared to Mader's results, they are conservatively adopted for this analysis. This tsunami amplitude is also much higher than the tsunami amplitudes reported in AGMTHAG for many different earthquake source locations and orientations in the Azores-Gibraltar fracture zone and for the Caribbean sources (Reference 202).

2.4.6.4.1.4 Sensitivity of Model Parameters and Conditions

Model sensitivity analysis is conducted for the following parameters and conditions: grid size, time step, Manning's n value, tsunami wave period, Coriolis effects, non-reflective boundaries, and tsunami wave form and steepness.

Grid Size

Model grid configuration is selected based on bathymetric data resolution, computational economy, etc. A finer mesh model grid is developed as part of grid size sensitivity analysis to demonstrate that the selected grid sizes resolves the required flow problems reasonably well. In the finer mesh model, grid sizes for the ISLANDS and SITE subdomains are refined by a factor of 5/3 (1.67), whereas the grid sizes in subdomain DEEP remained unchanged because of computational economy. Additionally, because the DEEP subdomain is located farther away from the site and in high water depths, a finer grid resolution in this area is not expected to produce any significant variation in tsunami water level at the site. The difference in tsunami water levels at the site from the two grid descriptions is very small, as shown in Figure 2.4.6-218. The selected coarser grid configuration therefore is considered adequate.

Time Step

Model simulations are performed with a computational time step of 0.2 minute (12 seconds). However, to demonstrate time step independence, a model simulation with 0.1 minute (6 seconds) time step is performed. Because the water levels at the site from the two simulations are nearly identical, the use of 12 seconds time step is considered acceptable.

Manning's n value

Model simulations are performed for two additional Manning's *n* values of 0.02 and 0.03. The results indicate that a lower Manning's *n* value produces a higher water level at the site. For this analysis a Manning's *n* of 0.02 is selected conservatively, which represents a smooth earth surface (Reference 222).

Tsunami Wave Period

Mader indicated that for the 1755 Lisbon Earthquake tsunami, the eastern U.S. coast, and the Caribbean would experience tsunami wave periods varying between 1.25 and 1.5 hours (Reference 209). Results from an additional model simulation with a tsunami wave period of 1.25

hours show that the maximum water level at the site is lower than maximum water level from the selected wave period of 1.5 hours. Therefore, the selected wave period is adopted in this analysis.

Coriolis Effects

Coriolis forces depend on the latitude and angular velocity of earth's rotation on its own axis. Model simulation results with and without Coriolis forces indicate that the effect of Coriolis force on the maximum water level at the site is insignificant. Coriolis forces therefore are not considered in model simulations.

Non-Reflective Boundaries

A sensitivity analysis is performed to assess the effect of non-reflective boundary conditions on the maximum tsunami water level at the site. The two open boundaries of the model, i.e., the forcing boundary where the incoming tsunami waves are specified and the southwest boundary where no-flow boundary conditions were specified, are made non-reflective by utilizing the Riemann type boundary condition (Riemann BC) of Delft3D (Reference 219). This type of boundary allows waves approaching the boundary from within the modeling domain to leave the boundary without reflecting back into the modeling domain.

The sensitivity analysis results indicate that the maximum tsunami water level at the site is not that sensitive to the non-reflective boundary condition. The tsunami water level time history at the site with and without Riemann BCs is shown in Figure 2.4.6-229. As indicated in the figure, the maximum water level at the site for the case without Riemann BC is slightly higher by 0.1 meters (0.3 feet), compared to the case with Riemann BCs. This demonstrates that the impact of Riemann BC on the maximum water level, the use of the Riemann BC results in a slightly larger difference in the predicted water level as indicated in Figure 2.4.6-229.

Tsunami Wave Form and Steepness

To test the effect of steeper tsunami waves on the maximum water level at the site, two wave forms with steeper wave fronts at the forcing boundary were considered: (1) isosceles N-wave (same crest and trough wave amplitude) and (2) steeper sinusoidal wave. Details are given below.

The first wave form is isosceles N-wave that was formulated based on Reference 224 as given below.

$$\zeta(t) = \alpha \frac{3\sqrt{3}}{2} A \cosh^{-2}(k'(t - t_n)) \tanh(k'(t - t_n)) \quad (1)$$

where ζ is water level with respect to still water level, α is wave height adjustment factor, t is time, A is wave amplitude, k' is a factor that determines the shape of the wave, and t_n is time associated with the location of the center of the wave.

The following isosceles N-wave parameters were selected so that the approximate wave period and wave height of the isosceles N-wave matches that of a sinusoidal wave: $\alpha = \frac{2}{3\sqrt{3}}$ k' = 0.077/min., and t_n = 45 min.

Figure 2.4.6-230 shows the wave form of the isosceles N-wave and sine-wave.

The second wave form tested is a combination of two sinusoidal wave forms such that the rising portion of the wave form is steeper than a regular sinusoidal wave. To accomplish this, the wave period of the rising portion was reduced by a factor of three (from 90 to 30 min.), and the wave period

of the falling portion was increased by a factor of 1.67 (from 90 to 150 min.) so that the overall period is the same as the regular sinusoidal wave (90 min.). The formulation used is provided below:

For t = 0 to 7.5 min. (first rising portion): $$\zeta(t) = A\sin\left(3\frac{2\pi}{90}t\right) \quad (2a)$$

For t = 7.5 min. to 82.5 min. (falling portion): $$\zeta(t) = A\sin\left(\frac{2\pi(t+30)}{2(90-2*7.5)}\right) \quad (2b)$$

For t = 82.5 min. to 90 min. (end rising portion): $$\zeta(t) = A\sin\left(3\frac{2\pi}{90}(t-(90-4*7.5))\right) \quad (2c)$$

Where t is time in min.

Figure 2.4.6-231 shows the wave form of the regular and steep sine-waves.

Figures 2.4.6-232 to 2.4.6-234 compare the water levels between the case that did not include steepening of the wave form and the sensitivity test case with steepened sine-wave at the forcing boundary, off Miami at 783 meters (2569 feet) depth, and at the site, respectively. Figures 2.4.6-235 to 2.4.6-237 compare the water levels between the case that did not include steepening of the wave form and the sensitivity test case with isosceles N-wave at the forcing boundary, off Miami at 783 meters (2569 feet) depth, and at the site, respectively. As shown on Figures 2.4.6-234 and 2.4.6-237, the results indicate that wave steepening does not increase the maximum tsunami water level at the site. One of the reasons is that the steepened wave forms have less wave volume compared to the non-steepened sinusoidal wave form in that the amount of wave energy available to produce run-up is less, especially in regard to the isosceles N-wave.

2.4.6.4.1.5 Model Simulation Results

As described in Subsections 2.4.6.4.1.2 and 2.4.6.4.1.3, the maximum tsunami water level at the site is simulated for a boundary condition with two consecutive sinusoidal tsunami waves of 2.0 meters (6.6 feet) amplitude and 1.5 hours wave period. This boundary condition approximates the 1755 Lisbon tsunami that was generated at the Azores-Gilbaltar region, as simulated by Mader (Reference 209). An initial water surface elevation of 1.36 meters (4.46 feet) MSL is used to evaluate the maximum tsunami water level at the site.

Water level contours at different times are plotted to track the tsunami wave propagation from the open boundary to the site. These time-lapsed snap-shots of water level contours are given in Figures 2.4.6-219a through 2.4.6-219i. As the figures indicate, the tsunami waves propagate from the open boundary to Blake-Bahama Escarpment unimpeded and nearly perpendicular to the escarpment. As the waves reach the Bahama platform, tsunami waves north of the platform (north of Grand Bahama and Abaco Islands) are diffracted southwestward towards the Straits of Florida. The diffracted waves propagate through the Straits of Florida before reaching the site. The tsunami waves reaching the platform are affected by shoaling and travel through the channels and passages between the islands of the Bahamas. These transmitted tsunami waves then interact with the diffracted waves from the north.

From the Straits of Florida the tsunami waves enter the Biscayne Bay first through the openings, cuts, and channels in the barrier islands, and then by overtopping the barrier islands before affecting the site. The maximum tsunami water level at the site is reached as the barrier islands are overtopped. Water level contours in Biscayne Bay corresponding to the time close to the maximum water level at the site is shown in Figure 2.4.6-220.

The site is protected by the Bahamas from direct impact of the tsunami waves. The diffracted tsunami waves have less energy and therefore less flooding potential at the site. In addition, the islands and

the vast extent of the Bahamas dissipate some of the tsunami wave energy before it reaches the deep waters of the Straits of Florida and ultimately the site.

Time history of tsunami water levels at key locations are plotted to show tsunami wave modification as it propagates and reaches shore. Figures 2.4.6-221a through 2.4.6-221d show the locations of the water level monitoring points. Track 1 (Figure 2.4.6-221a) generally follows tsunami wave propagation from the open boundary to east of the Bahamas and then the diffraction towards the Straits of Florida. The tsunami marigrams for the monitoring points are given in Figure 2.4.6-222. The figure shows that as the tsunami waves travel from the open boundary towards the Bahamas, its amplitude increases due to shoaling. The maximum shoaling is seen near the edge of the escarpment north of Little Bahama Bank at monitoring point 4. Waves then dissipate on the shallow waters and diffract towards the Straits of Florida (points 5 and 6). The tsunami amplitudes increase as the diffracted waves interact with the waves passing through the Islands of the Bahamas (points 6 and 7). However, as the tsunami waves travel further south towards the site, its amplitude decreases slightly due to propagation and possibly friction loss.

For Track 2 (Figures 2.4.6-221b and 2.4.6-223), tsunami amplitudes increase as the waves shoal east of the Bahamas similar to that observed for Track 1. Between monitoring points 3 and 4, tsunami amplitude decreases slightly. At monitoring point 5 south of Grand Bahama Island, where the depth is relatively shallow, the wave amplitude increases due to shoaling. In the Straits of Florida, wave modifications are the same as described for Track 1.

Track 3 (Figures 2.4.6-221c and 2.4.6-224 shows modifications of tsunami wave amplitudes along the eastern U.S. Atlantic coast. Between monitoring points 1, 2, and 3, tsunami amplitudes remain nearly the same while the arrival time changes due to their distance from the boundary. However, tsunami amplitudes at monitoring points 4 through 7 are higher owing to the interaction of diffracted and propagated waves from the Bahamas.

Figure 2.4.6-225 shows tsunami marigrams in Biscayne Bay and vicinity. Grid cells (339, 270) and (339, 232) are located within the Straits of Florida adjacent to the site; grid cell (339, 172) is located between Biscayne Bay and the Straits at a shallow water depth (6.1 meters); and grid cells (339, 132), (339, 119), (307, 125), and (272, 146) are located within Biscayne Bay (Figure 2.4.6-221d). As shown in the figure, tsunami amplitudes within the Straits at the selected locations including the location with shallow water depth remain nearly the same. Water level variations within the Biscayne Bay, however, are markedly different compared to that in the Straits of Florida with the minimum water level in the bay considerably higher. This is because the barrier islands do not allow quick draining of the bay during tsunami drawdowns. In addition, the barrier islands dissipate wave energy during overtopping resulting in smaller wave amplitude and delayed arrival.

2.4.6.4.2 Analysis of the Cape Fear Tsunami

2.4.6.4.2.1 Representation of the Cape Fear Slide in the Model

The maximum potential slide at Cape Fear was schematized for modeling purposes as having a Gaussian shape with an elliptical footing that extends from the uppermost head scarp to the salt diapirs in the downslope region. This shape was chosen because a Gaussian shape has been used for several investigations and studies of landslide tsunamis, including benchmark cases (References 237, 242, 243). Grilli and Watts (Reference 237) state that a Gaussian shape is a more realistic representation of a submarine mass failure than other arbitrary fixed shapes. Enet & Grilli (Reference 235) used a Gaussian shape in the experiments that provide the basis for the validation of the model used to simulate the generation of a wave by a submarine slide (Reference 235). The Gaussian shape of the slide was approximated in the numerical model by truncated hyperbolic secant squared functions (Reference 235). The center of the elliptical base of the slide was initially

located near the S1 headwall in Figure 2 of Reference 223, at 33.14° N, 76.29° W, which places the uppermost end of the slide area at a depth of approximately 710 meters (2329.4 feet).

The length (minor axis of the elliptical base) of the slide is 38 kilometers (23.6 miles), based on the distance from the upper scarp (described as S1 in Reference 223 and as the upper headwall scarp in Reference 225) to the salt diapirs downslope shown in Figure 2 of Reference 223. This length represents a conservative upper bound for the length of a potential slide. The width (major axis of the elliptical base) of the slide was assumed to be 50 kilometers (31.1 miles) taken conservatively from the width of the largest scarp S4 (the main scarp). The use of 50 kilometers (31.1 miles) as the width of the slide is conservative as it is five times the width of the upper scarp at the centroid of the postulated slide (reported as 10 kilometers [6.2 miles] in Reference 223).

The maximum thickness of the postulated slide was taken as approximately 120 meters (393.7 feet). This thickness is equal to the maximum height of the main scarp of the Cape Fear slide, S4, located at 2300 meters (7545.9 feet) depth, and is larger than the thicknesses of all the other scarps. For instance, the height of the uppermost scarp at 890 meters (2919.9 feet) depth is much smaller, at about 20 meters (65.6 feet) (Reference 236). Using a thickness of 120 meters (393.7 feet) is therefore a conservative assumption because the centroid of the postulated slide for the tsunami simulations is placed near the uppermost scarp, S1, at much smaller depth than the lower scarp of the Cape Fear slide. The assumed dimensions and shape of the postulated slide give an area of 1492 km^2 (576.1 mi^2) for the base of the slide and a total volume of 68 km^3 (16.3 mi^3).

The bottom slope used was 3.09 degrees, based on a measured depth difference of 1350 meters (4429.1 feet) over a distance of 25 kilometers (15.5 miles) in the area of the downslope movement of the slide. The distance of 25 kilometers (15.5 miles) is based on the presence of a slope break in the Cape Fear profile at about 25 kilometers (15.5 miles) from the initial location of the centroid, after which the slope decreases by approximately one-half. The direction of the downslope movement of the slide forms a 10 degree angle clockwise with the West-East direction. This direction is based on the delineation and orientation of the Cape Fear slide from the GLORIA mapping data.

The initial acceleration of the slide, 0.529 m/s^2 (1.74 ft/s^2) was estimated directly from the bed slope. Using Equation (10) in Reference 235, the terminal velocity of the slide was estimated to be 138 m/s (452.76 ft/s). As stated earlier, this estimate was obtained using a specific gravity for the slide equal to 2 (Reference 223), and a bed slope of 3.09 degrees, and a length of 38 kilometers (23.6 miles). The global drag coefficient was set equal to 1 (Reference 237), which is conservative. Based on its initial acceleration, the slide reaches its terminal velocity within 260 seconds.

2.4.6.4.2.2 Initial Wave Generated by the Cape Fear Slide

Two alternative approaches were used for the generation of the initial wave in the tsunami simulations. The two approaches are referred to as the dynamic source approach and the static source approach. Two source approaches are used as the velocity components from the dynamic source can differ significantly from the static source with respect to the total slide energy.

The dynamic source approach defined the initial condition for the tsunami propagation simulations in terms of both the water surface displacement and the depth-averaged horizontal velocity fields. This source was computed from the slide geometry and its movement using the computer model NHWAVE (Non-Hydrostatic Wave), Version 1.1 (Reference 238). NHWAVE solves the fully non-hydrostatic Navier-Stokes equations in the sigma coordinate system. The model assumes a single-valued water surface and represents turbulent stresses in terms of an eddy viscosity closure scheme. Turbulent stresses are not modeled in this analysis, and thus the model is basically solving the Euler equations for incompressible flow with a moving surface and bottom.

Input to NHWAVE includes the bathymetric grid, the slide dimensions, the initial slide position and orientation, and the terminal velocity. The modeled domain was set up so that the landslide event was centrally located and the generated motion did not reach the lateral boundaries during the simulated time. Bathymetric data for the model domain of NHWAVE and the three nested grids of FUNWAVE-TVD used in the simulations were obtained from the National Geophysical Data Center (NGDC) ETOPO 1 (Reference 244) and the Coastal Relief Model (CRM) (Reference 245) data sets. Results from the NHWAVE model output at 500 seconds were saved and used as initial conditions in the tsunami propagation model FUNWAVE-TVD. The reason for selecting the NHWAVE solution at 500 seconds as input to the tsunami propagation model, was that at that time the maximum wave height is about equal to the maximum thickness of the slide (120 meters [393.7 feet]). After 500 seconds, the NHWAVE model produces wave heights greater than the maximum thickness of the slide, which would be overly conservative.

At 500 seconds, the slide volume moves downslope 64.6 kilometers (40.1 miles), i.e., a distance equal to 1.7 times the length of the minor axis of the elliptical base of the slide, which is aligned with the direction of downslope movement (38 kilometers [23.6 miles]). The present approach neglects the spreading and flattening of the sliding mass during the slide process. This assumption results in a higher and narrower initial elevation hump at the final slide location than what would have occurred if the slide were allowed to deform. The initial and final positions of the slide are displayed in Figure 2.4.6-239. The water depth at the initial location of the centroid of the slide is 1100 meters (3608.9 feet). The water depth at the final position of the centroid of the slide is 3300 meters (10,826.8 feet) (Figure 2.4.6-239).

The resulting water surface displacement from NHWAVE at that time (500 seconds) is shown in Figures 2.4.6-240 and 2.4.6-241, which also shows the water surface profile in the direction of the slide motion simulated with NHWAVE at different times after the initiation of the slide. As shown in Figure 2.4.6-241, the maximum water surface at 500 seconds is 122 meters (400.3 feet), and the minimum –166 meters (-544.6 feet).

The second approach to the generation of the initial condition for the tsunami propagation model used a static source based on the geometry of the initial and final positions of the slide mass. A static source is defined as an initial displacement of the water surface in the form of a depression over the initial slide location, equal in areal extent, shape and volume to the displaced material volume during the submarine slide. It was assumed that the initial slide volume described above translates downslope along its axis in the direction of the slope beyond its original footprint. A positive displacement of the water surface equal to the volume, shape and size of the slide was assumed at that point, i.e., extending over an elliptical area with minor axis equal to 38 kilometers (23.6 miles), a major axis of 50 kilometers (31.1 miles) and maximum thickness 120 meters (393.7 feet), and a corresponding negative displacement representing the missing volume of the slide mass was added at the slide starting point. The centroid of the depression of the water surface was placed at 33.14° N, 76.29° W, same as the initial location of the centroid of the slide for the dynamic source. A water rise equal in shape and size with the depression was assumed downslope of the initial depression and at a distance equal to translation distance of the dynamic case, i.e., over a distance of 64.6 kilometers (40.1 miles). The maximum water surface rise is equal to 120 meters (393.7 feet). Figure 2.4.6-242 shows the assumed initial water surface wave for the Cape Fear tsunami simulation with FUNWAVE-TVD based on a static source. Using an initial static source, it was assumed that the initial horizontal velocities were zero over the entire model domain of FUNWAVE-TVD.

2.4.6.4.2.3 Modeling of Tsunami Propagation and Inundation

The propagation, shoreline runup and inundation caused by the Cape Fear tsunami were simulated using the Boussinesq wave model FUNWAVE-TVD, developed at the University of Delaware. In its present application, FUNWAVE-TVD solved the spherical-polar form of the weakly-nonlinear, weakly-dispersive Boussinesq equations described in Reference 234. Reference 240 describes the

operation of both Cartesian and spherical-polar versions of the code. The model incorporates bottom friction and subgrid lateral turbulent mixing effects.

The Cartesian coordinate version of FUNWAVE-TVD, described in References 240 and 241, has been validated using several PMEL-135 benchmarks (Reference 242), which are the presently accepted benchmarking standards adopted by the National Tsunami Hazard Mitigation Program (NTHMP) for judging model acceptance for use in development of coastal inundation maps and evacuation plans. Benchmark tests for the Cartesian version of FUNWAVE-TVD are described in Reference 240. Benchmark tests for the spherical version of the code are described in Reference 234.

The equations solved by FUNWAVE-TVD consist of a depth-integrated volume conservation equation together with depth-integrated horizontal momentum equations. These equations are summarized in Reference 234. For tsunami applications, FUNWAVE-TVD is run with closed boundaries and an initial hot start condition consisting of either a surface displacement alone (in the case of static initial conditions) or a surface displacement and initial velocity field (in the case of a dynamic initial condition based on the results of calculations with NHWAVE). The model is run from the initial start until past the time when significant wave activity has decayed at the target site.

In most large scale problems, FUNWAVE-TVD is run on more than one nested grid. The grid nesting scheme uses a one-way nesting technique, which passes surface elevation and velocity components calculated from a large domain to a nested small domain through ghost cells at nesting boundaries. A linear interpolation is performed between the large and the small domain at the nesting boundaries. A test of the nesting process is included in the FUNWAVE-TVD verification and validation document (Reference 234).

In the simulations of the Cape Fear tsunami, three nested grids are used, which are referred to as Grid A, Grid B and Grid C. The output from Grid A is used as input to FUNWAVE-TVD on Grid B. The same process is repeated in going from Grid B to Grid C.

The domain covered by each of these three grids is shown in Figure 2.4.6-243. All the grids are based on geographic coordinates. The coordinates of the southwest corner of each grid, the grid spacing, and number of grid cells in each grid are given in Table 2.4.6-205.

It is noted that because of the curvature of the earth, having a uniform grid size in degrees leads to variable-length (in the west-east direction) cells at different latitudes within the model domain.

There is a sponge layer along the open boundaries of the model, which was used for the definition of the boundary conditions. The thickness of the sponge layer was 200 kilometers (124.3 miles) along the eastern boundary, and 100 kilometers (62.1 miles) along the northern and southern boundaries.

The antecedent water surface level was equal to the 10 percent exceedance spring tide level, plus the initial rise and long term sea-level rise, which produce an initial water level equal to 1.68 meters (5.5 feet) mean low water (MLW), or 3.6 feet (1.10 meters) NAVD 88.

2.4.6.4.2.4 Simulation Results

Two sets of simulation results for the tsunami propagation and inundation by the Cape Fear tsunami are presented. The first set of results is for the dynamic initial condition and the second set of results is for a static initial condition.

Dynamic Source Initial Condition

Figures 2.4.6-244 and 2.4.6-245 show the propagation of the tsunami wave over the domain of model Grid A during the first three hours of the FUNWAVE-TVD simulation, presenting snapshots of

the wave height every 20 minutes. Time zero in the FUNWAVE-TVD simulation is 500 seconds after the initiation of the slide. It should be noted that the color scale indicating wave height differs in the different panels of these two figures. As can be seen in these figures, the highest waves travel towards the east. The wave traveling west towards the east coast of the United States is relatively smaller. Relatively high water levels are also predicted towards the southeast. This is illustrated in Figure 2.4.6-246 which shows the maximum water surface elevation within the model domain of Grid A during the simulation period. The highest water levels are within a fan-shaped zone towards the east, and over a relatively narrow zone towards the southeast. The latter seems to coincide with the relatively shallower ocean depths along Blake Ridge (Figure 2.4.6-243).

Figure 2.4.6-247 shows the propagation of the tsunami wave in Grid B, from 100 minutes in the FUNWAVE-TVD simulation, a little after the wave enters the Grid B domain, until 180 minutes after the slide simulation. Snapshots of the wave height every 20 minutes are shown. Figure 2.4.6-248 shows the maximum water surface elevation within the model domain of Grid B during the simulation period. As can be seen in this figure, the highest water levels occur in the northern part of Grid B, while the water levels toward the south and in the vicinity of Units 6 & 7 are much lower.

Figure 2.4.6-249 shows the propagation of the tsunami wave in Grid C, from 140 minutes until 240 minutes in the FUNWAVE-TVD simulation. Snapshots of the wave height every 20 minutes are shown. Figure 2.4.6-250 shows the maximum water level over Grid C. As can be seen in these figures, the area surrounding the site of Units 6 & 7 is inundated. However, the Units 6 & 7 site itself and other parts of the Turkey Point station, which are elevated above the existing grade, are not inundated and remain dry. However, this is not caused by the Cape Fear tsunami. It is a consequence of the assumption regarding the initial sea water level rise which accounts for the 10 percent exceedance spring tide level, 1.097 meters (3.6 feet) MLW, initial rise, 0.274 meter (0.9 foot), and long term sea-level rise, 0.305 meter (1.0 foot), which produce an initial water level, i.e., prior to the arrival of the tsunami, equal to 1.68 meters (5.5 feet) MLW, or 1.10 meters (3.6 feet) NAVD 88. This initial level is enough to inundate a large zone along the Florida coast, including the entire area around Units 6 & 7. This is made clear in Figure 2.4.6-251, which shows the water depth over the area of Grid C relative to two different levels of the water surface. The left panel shows the water depth relative to MLW. The right panel shows the water depth relative to the assumed initial water surface in the Cape Fear tsunami simulations, i.e., relative to 10 percent exceedance spring tide + initial rise + long-term sea-level rise. As can be seen in the right panel of Figure 2.4.6-251, the area surrounding Units 6 & 7 is inundated even prior to the arrival of the tsunami. Again, the Units 6 & 7 site itself and other parts of the Turkey Point station, which are elevated above the existing grade, are not inundated and remain dry. The maximum water surface elevation is 2.32 meters (7.5 feet) MLW or 1.75 meters (5.7 feet) NAVD 88. Figure 2.4.6-252 shows the maximum water surface rise in the vicinity of Units 6 & 7, relative to the initial sea water level.

Figure 2.4.6-253 shows the water level near Units 6 & 7 from the dynamic source simulation as a function of time. The maximum water surface level rise caused by the Cape Fear tsunami is 0.6 meter (1.97 feet) over the initial water level, occurring a little after five hours from the initiation of the Cape Fear slide, and about two hours after the arrival of the first waves caused by the Cape Fear tsunami.

Static Source Initial Condition

Figures 2.4.6-254 and 2.4.6-255 show the propagation of the tsunami wave generated by a static source over the domain of Grid A during the first three hours of the FUNWAVE-TVD simulation, presenting snapshots of the wave height every 20 minutes. The tsunami propagation pattern is similar to that in the dynamic source simulation, but the wave heights away from the source, especially towards the east are much smaller than those for the dynamic source shown in Figures 2.4.6-244 and 2.4.6-245.

Figure 2.4.6-256 shows the maximum water surface elevation within the model domain of Grid A during the simulation period. Comparing Figure 2.4.6-256 with Figure 2.4.6-246 shows that the static source produces much smaller water surface elevations over most of the domain of Grid A, and especially to the east and southeast. An exception is the area right over the slide and its immediate vicinity to the west, where the maximum water surface levels with the static source are substantially higher than those obtained with the dynamic source. This difference could be attributed to the fact that in the case of the dynamic source the initial condition entered in FUNWAVE-TVD includes the velocities obtained with NHWAVE, while in the case of the static source the initial velocities in the vicinity of the source are zero. Assigning a velocity to the initial wave in the dynamic source case results in a higher total energy than in the static source case where the initial velocity is assumed to be zero.

Figure 2.4.6-257 shows the propagation of the tsunami wave in Grid B, from 100 minutes in the FUNWAVE-TVD simulation, a little after the wave enters the Grid B domain, until 180 minutes after the slide simulation. Snapshots of the wave height every 20 minutes are shown. Figure 2.4.6-258 shows the maximum water surface elevation within the model domain of Grid B during the simulation period. The predicted water surface levels in Grid B for the static source are quite similar to those for the dynamic source shown in Figures 2.4.6-247 and 2.4.6-248.

Figure 2.4.6-259 shows the propagation of the tsunami wave in Grid C, from 140 minutes until 240 minutes in the FUNWAVE-TVD simulation. Snapshots of the wave height every 20 minutes are shown. Figure 2.4.6-260 shows the maximum water level over Grid C. Again the predicted water surface elevations over Grid C for the static source are quite similar to those predicted with a dynamic source, shown in Figures 2.4.6-249 and 2.4.6-250.

The maximum water surface elevation is 2.08 meters (6.8 feet) MLW, or 1.51 meters (5.0 feet) NAVD 88. Figure 2.4.6-261 shows the maximum water surface rise in the vicinity of Units 6 & 7, relative to the initial sea water level.

Figure 2.4.6-262 shows the water level (relative to the initial water level) near Units 6 & 7 from the static source simulation as a function of time. The maximum water surface level rise caused by the Cape Fear tsunami is 0.4 meter (1.31 feet), occurring a little after four hours from the initiation of the Cape Fear slide, and about one hour after the arrival of the first waves caused by the Cape Fear tsunami. The maximum water level at Units 6 & 7 predicted with the static source (0.4 meter [1.31 feet]) is slightly lower than that predicted using a dynamic source (0.6 meter [1.97 feet]).

2.4.6.4.2.5 Comparison of the Cape Fear Tsunami with the PMT

The simulations of a tsunami generated by a conservatively large submarine mass failure on the continental margin off Cape Fear suggest that the impact of such an event on water levels near Units 6 & 7 will be smaller than that of the postulated PMT presented in Subsection 2.4.6.4.1. The maximum predicted water level due to the Cape Fear tsunami event is 2.28 meters (7.5 feet) MLW, or 1.75 meters (5.7 feet) NAVD 88, representing a rise of 0.6 meter (1.97 feet) of the initial sea water level. The assumed initial sea water level includes the 10 percent exceedance spring tide, 1.097 meters (3.6 feet) MLW, an initial rise, 0.274 meter (0.9 foot), plus the long-term sea level rise, 0.304 meter (1.0 foot). This water level is much smaller than the maximum tsunami water level of 4.5 meters (14.76 feet) MSL (4.82 meters [15.8 feet] MLW) reported for the PMT case in Subsection 2.4.6.5.

2.4.6.4.3 Analysis of the Florida Escarpment Tsunami

2.4.6.4.3.1 Representation of the Florida Escarpment Slide in the Model Simulations

The maximum potential slide at the Florida Escarpment was schematized for modeling purposes as having a Gaussian shape with an elliptical footing. This shape was chosen because a Gaussian shape has been used for several investigations and studies of landslide tsunamis, including benchmark cases (References 237, 242, 243). Grilli and Watts (Reference 237) state that a Gaussian shape is a more realistic representation of a submarine mass failure than other arbitrary fixed shapes. Enet and Grilli (Reference 235) used a Gaussian shape in the experiments that provide the basis for the validation of the model used to simulate the generation of a wave by a submarine slide (Reference 235). The Gaussian shape of the slide was approximated in the numerical model by truncated hyperbolic secant squared functions (Reference 235). The center of the elliptical base of the slide prior to the initiation of movement is located at 25.92° N, 84.80° W (Figure 2.4.6-264). The length (minor axis of the elliptical base) of the slide shown in Figure 2.4.6-264 is 19.2 kilometers (11.93 miles), and the width (major axis of its elliptical base) of the slide is approximately 42.9 kilometers (26.7 miles). These dimensions were selected so the ellipse approximately covers the area of the outline of maximum credible submarine slide above the Florida Escarpment, and it has an area equal to 647.57 square kilometers (250.03 square miles), given in Reference 239.

The maximum thickness of the postulated slide was taken as approximately 66 meters (216.5 feet). This was estimated so the volume of the schematized slide used in the model is equal to 16.2 cubic kilometers (3.9 cubic miles), which was estimated based on the bathymetric data (Reference 239).

The bottom slope used in the model was 5.8 degrees. This was estimated based on the water depth difference between the centroid of the slide at its initial position and a point downslope at a distance equal to the minor axis of the elliptical base of the slide, i.e., 19.2 kilometers (11.9 miles). The water depth at these two points is 1355 and 3307 meters (4445.5 and 10,849.7 feet), respectively.

The initial acceleration of the slide, 0.992 meter (3.25 feet) per second squared, was estimated directly from the bed slope. The terminal velocity of the slide was estimated as equal to 134.3 meters (440.6 feet) per second, using a specific gravity for the slide equal to 2 and a bed slope of 5.8 degrees and length of 19.2 kilometers (11.9 miles). The global drag coefficient was assumed to be equal to 1 (Reference 237), which is conservative. Based on its initial acceleration, the slide reaches its terminal velocity within 135 seconds.

2.4.6.4.3.2 Initial Wave Generated by the Florida Escarpment Slide

Two alternative approaches were used for the generation of the initial wave in the tsunami simulations. The two approaches are referred to as the dynamic approach and the static source approach. Two source approaches are used as the velocity components from the dynamic source can differ significantly from the static source with respect to the total slide energy.

The dynamic source approach defined the initial condition for the tsunami propagation simulations in terms of both the water surface displacement and the depth-averaged horizontal velocity fields. This source was computed from the slide geometry and its movement using the computer model NHWAVE (Non-Hydrostatic Wave), Version 1.1 (Reference 238).

Input to NHWAVE includes the bathymetric grid, the slide dimensions, the initial slide position and orientation, and the terminal velocity of the slide. The modeled domain was set up so that the landslide event was centrally located and the generated motion did not reach the lateral boundaries during the simulated time. Bathymetric data for the model domain of NHWAVE and the three nested grids of FUNWAVE-TVD used in the simulations were obtained from the National Geophysical Data Center (NGDC) ETOPO 1 (Reference 244) and the Coastal Relief Model (CRM) (Reference 246)

data sets. Results from the NHWAVE model at 250 seconds were saved and used as initial conditions in the tsunami propagation model FUNWAVE-TVD, Version 1.1 (Reference 252).

The assumed runout distance of the slide volume as it moves downslope along its minor axis is 24.5 kilometers (15.2 miles). It is the distance between the centroid of the elliptical base of the slide in its initial position and the intersection of an extension of the bottom slope and the sea floor beyond the base of the escarpment. This is a very conservative assumption because the sea floor beyond 9.6 kilometers (5.97 miles) from the initial position of the centroid of the slide is practically horizontal. Therefore, assuming that the slide will continue moving at the same velocity up to 24.5 kilometers (15.2 miles) from its initial position would produce conservative estimates of the initial wave. The present approach neglects the spreading and flattening of the sliding mass during the slide process in the present simulations. This results in a higher and narrower initial elevation hump at the final slide location than what would have occurred if the slide were allowed to deform. The initial and final positions of the slide are displayed in Figure 2.4.6-266.

The NHWAVE model was run for a period of time, and the surface displacement field and horizontal velocity fields at 250 seconds, the time required to travel the postulated run out distance of 24.5 kilometers (15.2 miles), were saved and used as input into FUNWAVE-TVD. The resulting water surface displacement from NHWAVE at that time (250 seconds) is shown in Figures 2.4.6-267 and 2.4.6-268 which also shows the water surface profile in the direction of the slide motion simulated with NHWAVE at different times after the initiation of the slide. As shown in Figure 2.4.6-268, the maximum water surface at 250 seconds is 47.2 meters (154.9 feet), and the minimum is –77.5 meters (-254.3 feet).

The second approach to the generation of the initial condition for the tsunami propagation model used a static source based on the geometry of the initial and final positions of the slide mass. A static source is defined as an initial displacement of the water surface in the form of a depression over the initial slide location, equal in areal extent, shape and volume to the displaced material volume during the submarine slide. It was assumed that the initial slide volume described above translates downslope along its axis in the direction of the slope beyond its original footprint. A positive displacement of the water surface equal to the volume, shape, and size of the slide was assumed at that point, i.e., extending over an elliptical area with minor axis equal to 19.2 kilometers (11.9 miles), major axis equal to 42.9 kilometers (26.7 miles), maximum thickness equal to 66 meters (216.5 feet), and a corresponding negative displacement representing the missing volume of the slide mass was assumed over the initial position of the slide. The centroid of the depression of the water surface was placed at 25.92° N, 84.80° W, same as the initial location of the centroid of the slide for the dynamic source. A water rise equal in shape and size with the depression was assumed downslope of the initial depression and at a distance equal to translation distance of the dynamic case, i.e., 24.5 kilometers (15.2 miles). The maximum water surface rise is equal to 66 meters (216.5 feet). Figure 2.4.6-281 shows the assumed initial water surface wave for the Florida Escarpment tsunami simulation with FUNWAVE-TVD based on a static source. Using an initial static source, it was assumed that the initial horizontal velocities were zero over the entire model domain of FUNWAVE-TVD.

2.4.6.4.3.3 Modeling of Tsunami Propagation and Inundation

The propagation, shoreline runup, and inundation caused by the Florida Escarpment tsunami were simulated using the Boussinesq wave model FUNWAVE-TVD.

In the simulations of the Florida Escarpment tsunami, three nested grids are used, which are referred to as Grid A, Grid B, and Grid C. The output from Grid A is used as input to FUNWAVE-TVD on Grid B. The same process is repeated in going from Grid B to Grid C. The domain covered by each of these three grids is shown in Figure 2.4.6-265. All the grids are based on geographic coordinates.

The coordinates of the southwest corner of each grid, the grid spacing, and number of grid cells in each grid are given in Table 2.4.6-206.

It is noted that because of the curvature of the earth, having a uniform grid size in degrees leads to variable-length (in the west-east direction) cells at different latitudes within the model domain.

There is a sponge layer along the open boundaries of the model, which was used for the definition of the boundary conditions. The thickness of the sponge layer was 200 kilometers (124.3 miles) along the eastern and northern boundaries, 100 kilometers (62.1 miles) along the southern boundary, and 150 kilometers (93.2 miles) along the western boundary.

The antecedent water surface level used for the model simulation was equal to the 10 percent exceedance high tide level, plus the initial rise and long-term sea level rise, which produce an initial water level equal to 1.68 meters (5.5 feet) MLW or 1.10 meters (3.6 feet) NAVD 88, which is the same as that used for the PMT numerical simulation in Subsection 2.4.6.4 and for the probable maximum storm surge evaluation as explained in Subsection 2.4.5.2.2.1.

2.4.6.4.3.4 Simulation Results

Two sets of simulation results for the tsunami propagation and inundation by the Florida Escarpment tsunami are presented. The first set of results is for the dynamic initial condition and the second set of results is for a static initial condition.

Figures 2.4.6-269 and 2.4.6-270 show the propagation of the tsunami wave over the domain of model Grid A during the first 3 hours after the generation of the initial wave by the slide, presenting snapshots of the wave height every 20 minutes. Time zero in the FUNWAVE-TVD simulation is 250 seconds after the initiation of the slide. It should be noted that the color scale indicating wave height differs in the different panels of these two figures.

Figure 2.4.6-271 shows the maximum water surface elevation within the model domain of Grid A during the simulation period. The highest water levels are in the vicinity and to the west of the slide.

Figures 2.4.6-272 and 2.4.6-273 show the propagation of the tsunami wave in Grid B, from 80 minutes in the FUNWAVE-TVD simulation and after the wave enters the Grid B domain until 240 minutes. Snapshots of the wave height every 20 minutes are shown. Figure 2.4.6-274 shows the maximum water surface elevation within the model domain of Grid B during the simulation period. The maximum water level rise within the domain of Grid B is less than 0.1 meter (0.33 feet). As shown in Figure 2.4.6-274, the highest water levels occur over a relatively shallower area between Florida and Cuba, which can be seen in Figure 2.4.6-265.

Figures 2.4.6-275 and 2.4.6-276 show the propagation of the tsunami wave in Grid C, from 140 minutes to 240 minutes in the simulation. Snapshots of the wave height every 20 minutes are shown. Figure 2.4.6-277 shows the maximum water level over Grid C. As can be seen in these figures, the area surrounding the site of Units 6 & 7 is inundated. However, the Units 6 & 7 site itself and other parts of the Turkey Point station, which are elevated above the existing grade, are not inundated and remain dry. The inundation of the area surrounding the Units 6 & 7 site is not caused by the Florida Escarpment tsunami. It is a consequence of the assumption regarding the initial sea water level that accounts for the 10 percent exceedance tide level, initial rise, and long-term sea level rise, the sum of which produces an initial water level, i.e., prior to the arrival of the tsunami, equal to 1.68 meters (5.5 feet) MLW or 1.10 meters (3.6 feet) NAVD 88. This initial water level rise is enough to inundate a large zone along the Florida coast, including the area around Units 6 & 7. This is made clear in Figure 2.4.6-278, which shows the water depth over the area of Grid C relative to two different levels of the water surface. Figure 2.4.6-278 (a) shows the water depth relative to MLW without the water level rise that is used to define the initial condition for the tsunami propagation simulations.

Figure 2.4.6-278 (b) shows the water depth relative to the assumed initial water surface in the Florida Escarpment tsunami simulations, i.e., relative to 10 percent exceedance tide plus initial rise plus long-term sea-level rise. As can be seen in Figure 2.4.6-278 (b), the area surrounding the Units 6 & 7 site and its vicinity is inundated even prior to the arrival of the tsunami, i.e., under the assumed initial condition for the tsunami propagation simulations. Again, the Units 6 & 7 site itself and other parts of the Turkey Point station, which are elevated above the existing grade, are not inundated and remain dry. Figure 2.4.6-279 shows the maximum water surface rise in the vicinity of Units 6 & 7 relative to the initial seawater level. The maximum water surface level rise over this area, shown in Figure 2.4.6-279, is very small, less than 0.07 meter (0.23 foot).

Figure 2.4.6-280 shows the water level near Units 6 & 7 from the dynamic source simulation as a function of time. The maximum water surface level rise caused by the Florida Escarpment tsunami is less than 0.02 meter (0.065 foot) over the initial water level, occurring after 4 hours from the initiation of the Florida Escarpment slide and about an hour and a half after the arrival of the first waves caused by the Florida Escarpment tsunami. The predicted maximum water surface level is 1.71 meters (5.6 feet) MLW or 1.14 meters (3.5 feet) NAVD 88.

Figures 2.4.6-282 and 2.4.6-283 show the propagation of the tsunami wave generated by a static source over the domain of Grid A during the first 160 minutes, presenting snapshots of the wave height every 20 minutes. As can be seen in these figures, the tsunami propagation pattern is similar to that in the dynamic source simulation, but the wave heights away from the source toward the west are much smaller than those for the dynamic sources shown in Figure 2.4.6-269. The wave propagation to the east toward Florida is quite similar as that simulated with a dynamic source.

This is illustrated in Figure 2.4.6-284, which shows the maximum water surface elevation within the model domain of Grid A during the simulation period. Comparing Figure 2.4.6-284 with Figure 2.4.6-271 shows that the static source produces smaller water surface levels to the west of the source but similar water levels to the east. This could be attributed to the fact that in the case of the dynamic source, the initial condition entered in FUNWAVE-TVD includes the velocities obtained with NHWAVE, while in the case of the static source, the initial velocities in the vicinity of the source are zero. Assigning a velocity to the initial wave in the dynamic source case results in a higher total energy than in the static source case where the initial velocity is assumed to be zero. In the area right over the slide and its immediate vicinity to the west, the maximum water surface levels with the static source are higher than those obtained with the dynamic source.

Figures 2.4.6-285 and 2.4.6-286 show the propagation of the tsunami wave in Grid B, from 80 minutes in the simulation and after the wave enters the Grid B domain until 240 minutes. Snapshots of the wave height every 20 minutes are shown. Figure 2.4.6-287 shows the maximum water surface elevation within the model domain of Grid B during the simulation period. The predicted water surface levels in Grid B for the static source are quite similar to those for the dynamic source shown in Figures 2.4.6-272, 2.4.6-273, and 2.4.6-274.

Figures 2.4.6-288 and 2.4.6-289 show the propagation of the tsunami wave in Grid C, from 140 minutes until 240 minutes in the simulation. Snapshots of the wave height every 20 minutes are shown. Figure 2.4.6-290 shows the maximum water level over Grid C. Again, the predicted water surface elevations over Grid C for the static source are quite similar to those predicted with a dynamic source, shown in Figures 2.4.6-275, 2.4.6-276, and 2.4.6-277.

Figure 2.4.6-291 shows the maximum water surface rise in the vicinity of the Turkey Point Power Station, relative to the initial sea water level. Figure 2.4.6-292 shows the water level at the Turkey Point Power Station from the static source simulation as a function of time. The maximum water surface level rise caused by the Florida Escarpment tsunami is 0.02 meter (0.065 foot), occurring after 4 hours from the initiation of the Florida Escarpment slide and about 1.5 hours after the arrival of the first waves caused by the Florida Escarpment tsunami. The maximum water level near Units 6

and 7 predicted with the static source is the same as that predicted using a dynamic source, i.e., 1.71 meters (5.6 feet) MLW or 1.14 meters (3.7 feet) NAVD 88.

2.4.6.4.3.5 Comparison of the Florida Escarpment Tsunami with the PMT

The simulations of a tsunami generated by a conservatively large submarine mass failure at the Florida Escarpment suggest that the impact of such an event on water levels near Units 6 & 7 will be smaller than that of the postulated PMT presented in Subsection 2.4.6.4.1. The maximum predicted water level near Units 6 & 7 due to this tsunami event will be 1.71 meters (5.6 feet) MLW or 1.14 meters (3.7 feet) NAVD 88, representing a rise of only 0.02 meter (0.065 foot) above the initial sea water level. The assumed initial sea water level in the FUNWAVE model simulation includes the 10 percent exceedance high tide, an initial rise plus the long-term sea level rise, all of which add up to 1.68 meters (5.5 feet) MLW or 1.11 meters (6 feet) NAVD 88. This water level is much smaller than the maximum tsunami water level of 4.5 meters (14.76 feet) MSL (4.82 meters [15.81 feet] MLW) reported for the PMT case in Subsection 2.4.6.5. This conclusion is also consistent with the results of the Florida Escarpment Slide evaluation described in Subsection 2.4.6.1.2.

2.4.6.4.4 Analysis of the Great Bahama Bank Tsunami

2.4.6.4.4.1 Representation of the Great Bahama Bank Slide in the Model

The maximum credible slide was schematized for modeling purposes as having a Gaussian shape with an elliptical footing. This shape was chosen because a Gaussian shape has been used for several investigations and studies of landslide tsunamis, including benchmark cases (References 235, 242, 243). Grilli and Watts (Reference 237) state that a Gaussian shape is a more realistic representation of a submarine mass failure than other arbitrary fixed shapes. Enet & Grilli (Reference 235) used a Gaussian shape in the experiments that provide the basis for the validation of the model used to simulate the generation of a wave by a submarine slide (Reference 235). Although actual slides usually have more pronounced head shapes, the Gaussian surface shape is deemed as providing a reasonable approximation of the shape of actual slides. The Gaussian shape of the slide was approximated in the numerical model by truncated hyperbolic secant squared functions. The center of the elliptical base of the slide before the initiation of movement is located at 25.6134°N, 79.3213°W. The length (minor axis of the elliptical base) of the slide is 3 kilometers, and its width (major axis of its elliptical base) of the slide is approximately 30 kilometers.

The length of the slide is postulated based on the ocean floor profile at the site investigated in detail by Mulder et al. (Reference 260) shown in Figure 2.4.6-296, where the length of the steepest slope in the southern site with a slope up from approximately 1.5 degrees is approximately 3 kilometers. Figure 2.4.6-298 shows that the length of the steepest slope at the Postulated Slide Location of the northern site with slopes greater than 5 degrees is close to 1 kilometer. As a conservative assumption, the larger failure length between the northern and southern sites, i.e., 3 kilometers, is selected to define the source (Case 1) in the numerical simulations.

The width of the slide, i.e., its dimension in the direction normal to the direction of the slope failure, is conservatively selected to be 30 kilometers This width is about twice the combined width of all the scars identified in the southern site through multibeam bathymetric surveys shown in Figure 2.4.6-293.

The height of the three scars in the southern site shown in Figure 2.4.6-293 is between 80 and 110 meters (Reference 260). The upper end of this range is selected as a conservative estimate of the slide thickness at both postulated tsunami source locations along the GBB. It is also noted that the thickness of the material subject to potential mass failure on the seismic profile shown in Figure 2.4.6-298 (Line 5 in Reference 263) near the northern site is of the order of 100 meters.

The slope of the face of the scarp of the southern site shown in Figure 2.4.6-293 ranges from 3.8 to 5.8 degrees as illustrated in Figure 2.4.6-296. The slope of the ocean floor beyond the foot of the scarp is of the order of 1.5 degrees. The slope of the face of the scarp at the Postulated Slide Location in the northern site, based on the profile shown in Figure 2.4.6-300, is approximately 7 degrees. This slope is used in the simulation of a 3-kilometer long slide, presented as Case 1. The center of the elliptical base of the Case 1 slide was placed at 25.59°N, 79.33°W. In addition, the effect of a steeper but shorter potential slide is evaluated in Case 2. Based on the seismic profile shown in Figure 2.4.6-298, reproduced from Reference 263, the source in Case 2 is represented by a bed slope of 20 degrees and a slide length of 1.5 kilometers. The center of the elliptical base of the Case 2 slide was placed at 25.62°N, 79.34°W.

For Case 1, the initial acceleration of the 3-kilometer slide on a 7-degree bed slope is 1.2 meters per second squared, and its terminal velocity 58.3 meters per second. This estimate was obtained using a specific gravity for the slide equal to 2, and global drag coefficient equal to 1. Based on its initial acceleration the slide reaches its terminal velocity within 49 seconds. For Case 2, the initial acceleration of the 1.5-kilometer slide on a 20-degree bed slope is 3.4 meters per second squared, and its terminal velocity 69.1 meters per second, reached in 21 seconds from the initiation of motion.

2.4.6.4.4.2 Initial Wave Generated by the Great Bahama Bank Slide

Two alternative approaches were used for the generation of the initial wave in the tsunami simulations. The two approaches are referred to as the dynamic source approach and the static source approach.

The dynamic source approach defines the initial condition for the tsunami propagation simulations in terms of both the water surface displacement and the depth-averaged horizontal velocity fields. This source was computed from the slide geometry and its movement using the computer model NHWAVE (Non-Hydrostatic Wave), Version 1.1 (Reference 238). NHWAVE solves the fully non-hydrostatic Navier-Stokes equations in the sigma coordinate system.

Input to NHWAVE includes the bathymetric grid, the slide dimensions, the initial slide position and orientation, the terminal velocity, and the down-slope acceleration of the slide. For the dynamic approach, the modeled domain was set up so that the landslide event was centrally located and the generated motion did not reach the lateral boundaries during the simulated time. Results from the NHWAVE model at the time the amplitude of the generated wave becomes equal to the maximum thickness of the slide were saved and used as initial conditions in the tsunami propagation model FUNWAVE-TVD.

The approach conservatively neglects the spreading and flattening of the sliding mass during the slide process in the present simulations. This results in a higher and narrower initial elevation hump at the final slide location than what would have occurred if the slide were allowed to deform. The initial and final positions of the 3-kilometer slide are displayed in Figure 2.4.6-301.

For Case 1 that simulated the 3-kilometer slide on a 7-degree slope, the NHWAVE model was run for a period of time and the surface displacement field and horizontal velocity fields at 110 seconds, the time that the maximum drawdown (negative wave height) became approximately equal to the maximum thickness of the slide were saved and used as input into FUNWAVE-TVD. The resulting water surface displacement from NHWAVE at that time (110 seconds) for the 3-kilometer slide on a 7-degree slope is shown in Figure 2.4.6-302. Figure 2.4.6-303 shows the water surface profile in the direction of the slide motion simulated with NHWAVE at different times after the initiation of the slide. The maximum water surface at 110 seconds is 63 meters, and the minimum –108 meters. Figure 2.4.6-303 shows the evolution of the simulated water surface profile over time.

For Case 2 that simulated the 1.5-kilometer slide on a 20-degree slope, the NHWAVE model was run until the maximum drawdown became about equal to the maximum thickness of the slide, which in this case as 140 seconds. Figure 2.4.6-304 shows the water surface at that time which was used as input in the FUNWAVE-TVD simulation. The maximum water surface is 61 meters and the minimum –120 meters. Figure 2.4.6-305 shows the evolution of the simulated water surface profile over time.

The second approach to the generation of the initial condition for the tsunami propagation model used a static source. A static source is defined as an initial displacement of the water surface in the form of a depression over the initial slide location, equal in areal extent, shape, and volume to the displaced material volume during the submarine slide. A negative displacement of the water surface equal to the volume, shape, and areal extent of the slide was assumed at the initial slide location, i.e., extending over an elliptical area with minor axis equal to 3 kilometers, major axis 30 kilometers and maximum thickness 110 meters. A corresponding positive displacement representing the missing volume of the slide mass was also added. The centroid of the depression of the water surface was placed at 25.63°N, 79.34°W.

2.4.6.4.4.3 Modeling of Tsunami Propagation and Inundation

As in the case of the tsunamis discussed in Subsections 2.4.6.4.2 and 2.4.6.4.3, the propagation, shoreline runup and inundation caused by the GBB slide were simulated using the Boussinesq wave model FUNWAVE-TVD in spherical-polar coordinates (Reference 240).

In the simulations of the tsunami generated by a landslide on the western margin of the GBB, two grids are used, which are referred to as Grid B and Grid C. These are the same grids used in analysis of tsunamis generated by a submarine slide at the Florida Escarpment discussed in Subsection 2.4.6.4.3. The output from Grid B is used as input to FUNWAVE-TVD on Grid C.

The domain covered by each of the grids is shown in Figure 2.4.6-265. All the grids are based on geographic coordinates. The coordinates of the southwest corner of each grid, the grid size and number of grid cells in each grid are given in Table 2.4.6-207.

It is noted that because of the curvature of the earth, having a uniform grid size in degrees leads to variable-length (in the west-east direction) cells at different latitudes within the model domain.

There is a sponge layer along the open boundaries of the model that was used for the definition of the boundary conditions. The thickness of the sponge layer was 40 kilometers along the eastern and the western boundary, 50 kilometers along the southern boundary and 20 kilometers along the northern boundary.

2.4.6.4.4.4 Simulation Results

Simulations were performed for three cases representing different assumptions for the initial tsunami wave that can be generated by a submarine slide at the west margin of the GBB. Case 1 uses a dynamic source, i.e., a wave produced by NHWAVE, for a tsunami generated by a 3-kilometer slide on a 7-degree slope. Case 2 uses also a dynamic source for tsunami generated by a 1.5-kilometer slide on a 20-degree slope. Case 3 uses a static source for a tsunami generated by a 3-kilometer slide on a 7-degree slope.

With respect to Case 1, Figure 2.4.6-306 shows the propagation of the tsunami wave in Grid B, at 2, 4, 6, and 14 minutes in the FUNWAVE-TVD simulation. Figure 2.4.6-307 shows the maximum water surface elevation within the model domain of Grid B during the simulation period.

Figure 2.4.6-308 shows the propagation of the same tsunami wave in Grid C, at 18, 30, 44, and 100 minutes in the FUNWAVE-TVD simulation. Figure 2.4.6-309 shows the maximum water level over

Grid C. As can be seen in these figures, the area surrounding the Turkey Point Units 6 & 7 site is inundated. However, as already discussed in Subsection 2.4.6.4.3.4, the inundation of the area surrounding the site of Units 6 & 7 is not caused by the GBB tsunami. It is a consequence of the assumption regarding the initial seawater level that accounts for the 10 percent exceedance high tide level of 3.6 feet MLW, initial rise of 0.9 feet and long-term sea level rise of 1.0 foot, the sum of which produces an initial water level, i.e., prior to the arrival of the tsunami, equal to 1.68 meters (5.5 feet) MLW, or 3.6 feet (1.10 meters) NAVD 88. This initial water level is enough to inundate a large zone along the Florida coast, including the area around Units 6 & 7 (Figure 2.4.6-278). Figure 2.4.6-310 shows the maximum water surface rise in the vicinity of the site relative to the initial seawater level.

Figure 2.4.6-311 shows the water level at the Turkey Point Units 6 & 7 site as a function of time. The maximum water surface level rise over the initial water level is 2.9 meters, occurring approximately 50 minutes from the initiation of the slide. The predicted maximum water surface level is 4.6 meters (15.0 feet) MLW, or 4.0 meters (13.1 feet) NAVD 88. The predicted maximum water level near the site is derived from Figure 2.4.6-310.

With respect to Case 2, Figure 2.4.6-304 shows the water surface profile simulated with NHWAVE that was used as input in the simulation of the propagation of a tsunami caused by a 1.5-kilometer-long slope failure on a 20-degree slope.

The simulation with FUNWAVE-TVD was again performed in two steps, modeling the propagation of the tsunami wave first within Grid B, then in Grid C using the output from the Grid B as input in Grid C to define the wave surface elevation and velocity conditions along its boundaries. Figure 2.4.6-312 shows the propagation of the tsunami wave in Grid B, at 2, 6, 8, and 14 minutes in the FUNWAVE-TVD simulation. Figure 2.4.6-313 shows the maximum water surface elevation within the model domain of Grid B during the simulation period.

Figure 2.4.6-314 shows the propagation of the same tsunami wave in Grid C, at 18, 30, 44, and 100 minutes in the FUNWAVE-TVD simulation. Figure 2.4.6-315 shows the maximum water level over Grid C. As in Case 1, the area surrounding the Turkey Point Units 6 & 7 site is inundated. The inundation of the area surrounding the site of Units 6 & 7 is not caused by the GBB tsunami. It is a consequence of the assumption regarding the initial seawater level, as explained above. Figure 2.4.6-316 shows the maximum water surface rise in the vicinity of the Turkey Point Units 6 & 7 site relative to the initial seawater level.

Figure 2.4.6-317 shows the time history of the water level at the Turkey Point Units 6 & 7 site. The maximum water surface level caused by this tsunami is 3.0 meters over the initial water level, also occurring after approximately 50 minutes from the initiation of the slide. The predicted maximum water surface level is 4.68 meters (15.4 feet) MLW, or 4.1 meters (13.5 feet) NAVD 88, taking into account the antecedent seawater level. The predicted maximum water level near the site is derived from Figure 2.4.6-316.

With respect to Case 3, the initial displacement of the water surface in this case is in the form of a depression approximately equal to the slide, i.e., extending over an elliptical area with its minor axis equal to 3 kilometers, its major axis equal to 30 kilometers, and maximum thickness 110 meters. The volume of the depression is approximately 3 cubic kilometers. A water rise equal to the depression, both in shape and size, is formed downslope of the initial depression. The displacement volume of the positive wave and negative wave were set equal to the landslide volume. The maximum water surface rise is equal to 110 meters, equal to the height (thickness) of the slide. Figure 2.4.6-318 shows the assumed initial water surface wave for the tsunami simulation with FUNWAVE-TVD based on a static source.

Figure 2.4.6-319 shows the propagation of the tsunami wave in Grid B, at 2, 4, 6, and 14 minutes in the FUNWAVE-TVD simulation. Figure 2.4.6-320 shows the maximum water surface elevation within the model domain of Grid B during the simulation period.

Figure 2.4.6-321 shows the propagation of the tsunami wave in Grid C, at 18, 30, 44, and 100 minutes in the FUNWAVE-TVD simulation. Figure 2.4.6-322 shows the maximum water level over Grid C.

Figure 2.4.6-323 shows the maximum water surface rise in the vicinity of the Turkey Point Units 6 & 7 site relative to the initial seawater level. Figure 2.4.6-324 shows the water level at the site from the static source simulation as a function of time. The maximum water surface rise caused by the tsunami generated by a submarine slide at the Postulated Slide Location is 1.7 meters over the initial water level, occurring after approximately 58 minutes from the initiation of the slide. The predicted maximum water level at the Turkey Point Units 6 & 7 site is 3.38 meters (11.1 feet) MLW, or 2.8 meters (9.2 feet) NAVD 88, taking into account the antecedent seawater level. The predicted maximum water level near the site is derived from Figure 2.4.6-323.

2.4.6.4.4.5 Comparison of the Great Bahama Bank Tsunami with the PMT

Simulations were performed for a tsunami generated by a conservatively large slope failure along the western margin of the GBB. The maximum predicted water level at the Turkey Point Units 6 & 7 site due to this tsunami event is 4.68 meters (15.4 feet) MLW, or 4.1 meters (13.5 feet) NAVD 88. The assumed initial seawater level in the FUNWAVE-TVD model simulation includes the 10 percent exceedance spring tide, an initial rise plus the long-term sea level rise, all of which add up to 1.68 meters (5.50 feet) MLW or 1.10 meters (3.6 feet) NAVD 88.

The maximum predicted water level at the Turkey Point Units 6 & 7 site caused by a tsunami at the GBB is less than the maximum water level predicted for the 1755 Lisbon earthquake PMT scenario, which was estimated to be equal to 4.2 meters (13.9 feet) NAVD 88.

2.4.6.5 Tsunami Water Level

The time history of tsunami water level at the site is given in Figure 2.4.6-226. The maximum tsunami water level at the site from model simulation results is 4.5 meters (14.76 feet) MSL or 4.2 meters (13.9 feet) NAVD 88 including the initial water level of 1.36 meters (4.46 feet) MSL, which is rounded up to 14.0 feet (4.3 meters) NAVD 88. This maximum tsunami water level is 12 feet lower than the entrance floor elevation of all safety-related structures at 26 feet NAVD 88.

2.4.6.6 Hydrography and Harbor or Breakwater Influences on Tsunami

Units 6 & 7 are located adjacent to Biscayne Bay approximately 8 miles west of the Elliott Key barrier island. The PMT water level near Units 6 & 7 is analyzed based on published numerical simulation results and includes a conservatively assumed tsunami run-up. Therefore, the effect of hydrography of the area has been considered in the estimation of the PMT water level. There are no breakwaters located near the Units 6 & 7 that may affect the PMT water level.

2.4.6.7 Effects on Safety-Related Facilities

A conservative estimate of the PMT still water level near Units 6 & 7 is approximately 4.3 meters (14 feet) NAVD 88. This PMT water level along with coincidental wind-wave run-up, as presented in Subsection 2.4.5, would be lower than the design plant grade elevation of 26 feet NAVD 88 for the safety-related facilities. Therefore, the postulated PMT event does not affect the safety functions of Units 6 & 7. Because the PMT water level is lower than the design plant grade, debris, waterborne

projectiles, sediment erosion, and deposits are not a concern to the functioning of the safety-related SSCs of Units 6 & 7.

2.4.6.8 References

201. Prasad, R., *Tsunami Hazard Assessment at Nuclear Power Plant Sites in the United States of America (Draft Report for Comments)*, Pacific Northwest National Laboratory, PNNL-1-7397, Office of New Reactors, U.S. NRC, NUREG/CR-6966, August 2008.

202. Atlantic and Gulf of Mexico Tsunami Hazard Assessment Group, *Evaluation of Tsunami Sources with the Potential to Impact the U.S. Atlantic and Gulf Coasts — An Updated Report to the Nuclear Regulatory Commission*, U.S. Geological Survey, Administrative Report, August 2008.

203. Twichell, D., W. Dillon, C. Paull, and N. Kenyon, *Morphology of Carbonate Escarpments as an Indicator of Erosional Processes, Geology of the Unites States Seafloor — A View from GLORIA*, Cambridge University Press, 1996.

204. Ward, S., and S. Day, *Cumbre Vieja Volcano — Potential Collapse and Tsunami at La Palma, Canary Islands,* Geophysical Research Letters, Vol. 28, No. 17, pp. 3397–3400, 2001.

205. Mader, C., *Modeling the La Palma Landslide Tsunami,* Science of Tsunami Hazards, Vol. 19, No. 50–70, 2001.

206. Pararas-Carayannis, G., *Evaluation of the Threat of Mega Tsunami Generation from Postulated Massive Slope Failures of Island Stratovolcanos on La Palma, Canary Islands, and on the Island of Hawaii,* Science of Tsunami Hazards, Vol. 20, No. 5, pp. 251–277, 2002.

207. Gisler, G., R. Weaver, and M. Gittings, *Sage Calculations of the Tsunami Threat from La Palma,* Science of Tsunami Hazards, Vol. 24, No. 4, pp. 288–301, 2006.

208. Lockridge, P., S. Lowell, and J. Lander, *Tsunamis and Tsunami-Like Waves of the Eastern United States,* Science of Tsunami Hazards, Vol. 20, No. 3, pp. 120–157, 2002.

209. Mader, C., *Modeling the 1755 Lisbon Tsunami,* Science of Tsunami Hazards, Vol. 19, No. 2, pp. 93–98, 2001.

210. Lander, J., L. Whiteside, and P. Lockridge, *A Brief History of Tsunamis in the Caribbean Sea,* Science of Tsunami Hazards, Vol. 20, No. 2, pp. 57–94, 2002.

211. Knight, B., *Model Prediction of Gulf and Southern Atlantic Coast Tsunami Impacts from a Distribution of Sources,* Science of Tsunami Hazards, Vol. 24, No. 5, pp. 304–312, 2006.

212. National Geophysical Data Center, *Significant Earthquake Database*, revised August 27, 2008. Available at http://www.ngdc.noaa.gov/hazard/earthqk.shtml, accessed August 27, 2008.

213. National Earthquake Information Center, *M 5.8 Gulf of Mexico Earthquake of 10 September 2006*, U.S. Geological Survey, September 2006.

214. National Geophysical Data Center, *Historical Tsunami Database*, revised August 27, 2008. Available at http://www.ngdc.noaa.gov/seg/hazard/tsu_db.shtml, accessed August 1, 2008.

215. Hornbach, M., S. Mondziel, N. Grindlay, C. Frohlich, and P. Mann, *Did a Submarine Slide Trigger the 1918 Puerto Rico Tsunami?,* Science of Tsunami Hazards, Vol. 27, No. 2, pp. 22–31, 2008.

216. Geist, E., *Local Tsunamis and Earthquake Source Parameters*, R. Dmowska and B. Saltsman (eds.), Tsunamigenic Earthquakes and their Consequences, Advances in Geophysics, Vol. 39, pp. 117–209, 1998.

217. Ocean Drilling Program, Shipboard Scientific Party, *Chapter 5. Site 626: Straits of Florida,* J. Austin, Jr. and W. Schlager (eds.), Proceedings of the Ocean Drilling Program, Initial Report, Vol. 101, pp. 49-109, 1986.

218. Iturralde-Vinent, M. (ed.), *Geologia de Cuba para Todos*, Edicion Cientifica, Museo Nacional de Historia Natural-CITMA, preprint, 2009.

219. Deltares, *Delft3D-FLOW*, Simulation of Multi-Dimensional Hydrodynamic Flows and Transport Phenomena, Including Sediments, Rotterdamseweg 185, 2009.

220. Stelling, G. and S. Duinmeijer, *A Staggered Conservative Scheme for Every Froude Number in Rapidly Varied Shallow Water Flows,* International Journal for Numerical Methods in Fluids, Vol. 43, pp. 1329–1354, 2003.

221. Apotsos, A., M. Buckley, and G. Gelfenbaum, *Tsunami Benchmark Simulations Using Delft3D,* ISEC Community Workshop: Simulation & Large-Scale Testing of Nearshore Wave Dynamics, Corvallis, July 8–10, 2009.

222. Imamura, F., A. Yalciner, and G. Ozyurt, *Tsunami Modeling Manual*, International Oceanographic Commission, 2006.

223. Hornbach, M., L. Lavier, and C. Ruppel, *Triggering Mechanism and Tsunamogenic Potential of the Cape Fear Slide Complex, U.S. Atlantic Coastal Margin,* Geochemistry, Geophysics, and Geosystems, Vol. 8, No. 10, 2007.

224. Apotsos, A., B. Jaffe, and G. Gelfenbaum, *Wave Characteristics and Morphologic Effects on the Onshore Hydrodynamic Response of Tsunamis,* Coastal Engineering, Vol. 58, pp. 1034–1048, November 2011.

225. Popenoe, P., E. Schmuck, and W. Dillon, *The Cape Fear Landslide: Slope Failure Associated with Salt Diapirism and Gas Hydrate Decomposition,* in *Submarine Landslides: Selected Studies in the U.S. Exclusive Economic Zone*, W. Schwab, H. Lee, and D. Twichell (eds.), U.S. Geological Survey, Bulletin 2002, pp. 40–53, 1993.

226. Popenoe, P., and W. Dillon, *Characteristics of the Continental Slope and Rise Off North Carolina from GLORIA and Seismic-Reflection Data: The Interaction of Downslope and Contour Current Processes,* J. Gardner, M. Field, and D. Twichell (eds.), Geology of the United States' Seafloor, The View from GLORIA, Cambridge University Press, Cambridge, United Kingdom, pp. 59–80, 1996.

227. Paull, C., R. Matsumoto, P. Wallace, et al., *Chapter 1: Introduction,* Proceedings of the Ocean Drilling Program, Initial Reports, Vol. 164, pp. 5–12, 1996.

228. Paull, C., W. Buelow, W. Ussler III, and W. Borowski, *Increased Continental-Margin Slumping Frequency During Sea-Level Lowstands Above Gas Hydrate-BearingSediments,* Geology, Vol. 24, No. 2, pp. 143–146, 1996.

229. Lee, H., *Timing of Occurrence of Large Submarine Landslides on the Atlantic Ocean Margin,* Marine Geology, Vol. 264, No. 1-2, pp. 53–64, 2009.

230. Rodriguez, N., and C. Paull, *Chapter 32. Data Report: 14C Dating of Sediment of the Uppermost Cape Fear Slide Plain: Constraints on the Timing of this Massive Submarine Landslide,* C. Paull, R. Matsumoto, P. Wallace, and W. Dillon (eds.), Proceedings of the Ocean Drilling Program, Scientific Results, Vol. 164, pp. 325–327, 2000.

231. Owen, M., S. Day, and M. Maslin, *Late Pleistocene Submarine Mass Movements: Occurrence and Causes,* Quaternary Science Reviews, Vol. 26, No. 7-8, pp. 958–978, 2007.

232. Tappin, D., *Submarine Mass Failures as Tsunami Sources: Their Climate Control,* Philosophical Transactions of the Royal Society, Vol. 368, pp. 2417–2434, 2010.

233. Twichell, D., J. Chaytor, U. ten Brink, and B. Buczkowski, *Morphology of Late Quaternary Submarine Landslides Along the U.S. Atlantic Continental Margin*, Marine Geology, Vol. 264, pp. 4–15, 2009.

234. Shi, F., J. Kirby, and B. Tehranirad, *Tsunami Benchmark Results for Spherical Coordinate Version of FUNWAVE-TVD* (Ver. 1.1), Research Report No. CACR-12-02, Center for Applied Coastal Research, University of Delaware, Newark, 2012.

235. Enet, F., and S. Grilli, *Experimental Study of Tsunami Generation By Three-Dimensional Rigid Underwater Landslides*, Journal of Waterway, Port, Coastal and Ocean Engineering, Vol. 133, No. 6, pp. 442–454, 2007.

236. Carpenter, G., *Coincident Sediment Slump/Clathrate Complexes on the US Atlantic Continental Slope*, Geo-Marine Letters, Vol. 1, No. 1, pp. 29–32, 1981.

237. Grilli, S., and P. Watts, *Tsunami Generation by Submarine Mass Failure, Part I: Modeling, Experimental Validation, and Sensitivity Analyses*, Journal of Waterway, Port, Coastal, and Ocean Engineering, Vol. 131, No. 6, pp. 283–297, 2005.

238. Ma, G., F. Shi, and J. Kirby, *Shock-Capturing Non-Hydrostatic Model for Fully Dispersive Surface Wave Processes*, Ocean Modeling, Vol. 43-44, pp. 22–35, 2011.

239. ten Brink, U., D. Twichell, P. Lynett, E. Geist, J. Chaytor, H. Lee, B. Buczkowski, and C. Flores, *Regional Assessment Of Tsunami Potential in the Gulf of Mexico: U.S. Geological Survey Administrative Report*, Report to the National Tsunami Hazard Mitigation Program, Revision, September 2, 2009.

240. Tehranirad, B., F. Shi, J. Kirby, J. Harris, and S. Grilli, *Tsunami Benchmark Results for Fully Nonlinear Boussinesq Wave Model FUNWAVE-TVD,* Ver. 1.0, Research Report No. CACR-11-02, Center for Applied Coastal Research, University of Delaware, Newark, 2011.

241. Shi, F., J. Kirby, B. Tehranirad, J. Harris, and S. Grilli, *FUNWAVE-TVD Version 1.0, Fully Nonlinear Boussinesq Wave Model with TVD Solver, Documentation and User's Manual*, Research Report No. CACR-11-04, Center for Applied Coastal Research, University of Delaware, Newark, 2011.

242. Synolakis, C., E. Bernard, V. Titov, U. Kanoglu, and F. Gonzalez, *Standards, Criteria, and Procedures for NOAA Evaluation of Tsunami Numerical Models*, NOAA Technical Memorandum OAR PMEL-135, Pacific Marine Environmental Laboratory, Seattle, Washington, 2007.

243. Liu, P., P. Lynett, and C. Synolakis, *Analytical Solutions for Forced Long Waves on a Sloping Beach*, J. Fluid Mech. 478: pp. 101–109, 2003.

244. Amante, C., and B. Eakins, *ETOPO1 1 Arc-Minute Global Relief Model: Procedures, Data Sources and Analysis*, NOAA Technical Memorandum NESDIS NGDC-24, 2009.

245. National Oceanic and Atmospheric Administration, *NGDC 3 Arc-Second Coastal Relief Model Development*. Available at http://www.ngdc.noaa.gov/mgg/coastal/model.html, accessed April 20, 2012.

246. National Oceanic and Atmospheric Administration, *National Geophysical Data Center*, U.S. Coastal Relief Model, Vol. 2 (U.S. South East Atlantic Coast Grids) and Vol. 3 (Florida and Eastern Gulf of Mexico Grids). Available at http://www.ngdc.noaa.gov/mgg/coastal/crm.html, accessed June 13 and June 17, 2011.

247. U.S. Geological Survey, *2012: Gulf of Mexico GLORIA Geology Interpretation Map,* U.S. Geological Survey, GLORIA Mapping Program, U.S. EEZ Gulf of Mexico Region, GLORIA Geology Interpretation. Available at http://coastalmap.marine.usgs.gov/gloria/gomex/geology.html, accessed February 14, 2012.

248. Mullins, H., A. Gardulski, and A. Hine, *Catastrophic Collapse of the West Florida Carbonate Platform Margin*, Geology, Vol. 14, No. 2, pp. 167–170, 1986.

249. Doyle, L., and C. Holmes, *Shallow Structure, Stratigraphy, and Carbonate Sedimentary Processes of West Florida Upper Continental Slope*, American Association of Petroleum Geologists Bulletin, Vol. 69, pp. 1133–1144, 1985.

250. Twichell, D., P. Valentine, and L. Parson, *Slope Failure of Carbonate Sediment on the West Florida Slope,* in W. Schwab, H. Lee, and D. Twichell, (eds.), Submarine Landslides: Selected Studies in the U.S. Exclusive Economic Zone: U.S. Geological Survey, Bulletin 2002, pp. 69–78, 1993.

251. Holmes, C., *Accretion of the South Florida Platform, Late Quaternary Development*, American Association of Petroleum Geologists Bulletin, Vol. 69, pp. 149–160, 1985.

252. Shi, F., J. Kirby, B. Tehranirad, J. Harris, and S. Grilli, *FUNWAVE-TVD Version 1.1, Fully Nonlinear Boussinesq Wave Model with TVD Solver*, Documentation and User's Manual, Research Report No. CACR-11-04, Center for Applied Coastal Research, University of Delaware, Newark, 2012.

253. Fulthorpe, C. and A. Melillo *Chapter 12, Middle Miocene Carbonate Gravity Flows in the Straits of Florida* at Site 626, J. Austin, Jr. and W. Schlager (eds.), Proceedings of the Ocean Drilling Program, Scientific Results, Vol. 101, pp. 179–191, 1988.

254. Anselmetti, F., G. Eberli, and Z. Dong Ding, *From the Great Bahama Bank into the Straits of Florida: A Margin Architecture Controlled by Sea Level Fluctuations and Ocean Currents*, Geological Society of America, Bulletin, Vol. 112, pp. 829–844, 2000.

255. Mullins, H., and A. Neumann, *Deep Carbonate Bank Margin Structure and Sedimentation in the Northern Bahamas*, The Society of Economic Paleontologists and Mineralogists, SEPM Special Publication, No. 27, pp. 165–192, 1979.

256. Kuhn, G. and D. Meischner Chapter *14, Quaternary and Pliocene Turbidites in the Bahamas*, Leg 101, Sites 628, 632, and 635, J. Austin, Jr. and W. Schlager (eds.), Proceedings of the Ocean Drilling Program, Scientific Results, Vol. 101, pp. 203–212, 1988.

257. Eberli, G., C. Kendall, P. Moore, G. Whittle, and R. Cannon, *Testing a Seismic Interpretation of Great Bahama Bank with a Computer Simulation*, AAPG Bulletin, Vol. 78, No. 6, pp. 981–1004, 1994.

258. Betzler, C., J. Reijmer, K. Bernet, G. Eberli, and F. Anselmetti, *Sedimentary Patterns and Geometries of the Bahamian Outer Carbonate Ramp (Miocene-Lower Pliocene, Great Bahama Bank)*, Sedimentology, Vol. 46, pp. 1127–1143, 1999.

259. Betzler, C., M. Pfeiffer, and S. Saxena, *Carbonate Shedding and Sedimentry Cyclicities of a Distally Steepened Carbonate Ramp (Miocene, Great Bahama Bank)*, International Journal of Earth Science, Vol. 89, pp. 140–153, 2000.

260. Mulder, T., E. Ducassou, G. Eberli, V. Hanquiez, E. Gonthier, P. Kindler, M. Principaud, F. Fournier, P. Léonide, I. Billeaud, B. Marsset, J. Reijmer, C. Bondu, R. Joussiaume, and M. Pakiades, *New Insights into the Morphology and Sedimentary Processes Along the Western Slope of Great Bahama Bank*, Geology, Vol. 40, No. 7, pp. 603–606, July 2012.

261. Eberli, G., and T. Mulder, *Geometry and Initiation of Large Slope Failure Along Little and Great Bahama Bank*, in the Research Program Prospectus of the Comparative Sedimentology Laboratory, Rosenstiel School of Marine and Atmospheric Science, University of Miami, 2011.

262. Correa, T., M. Grasmueck, G. Eberli, J. Reed, K. Verwer, and S. Purkis, *Variability of Cold-Water Coral Mounds in a High Sediment Input and Tidal Current Regime*, *Straits of Florida*, Sedimentology 59, pp. 1278–1304, 2012.

263. Wilber, R., J. Milliman, and R. Halley, *Accumulation of Bank-Top Sediment on the Western Slope of Great Bahama Bank: Rapid Progradation of a Carbonate Megabank*, Geology, Vol. 18, pp. 970–974, 1990.

264. Eberli, G., P. Swart, M. Malone, et al., *Proceedings of the Ocean Drilling Program*, Initial Reports, 166. 1997. Available at http://www-odp.tamu.edu/publications/166IR/166TOC.HTM, accessed January 8, 2013.

265. Austin, J., J. Ewing, J. Ladd, H. Mullins, and R. Sheridan, *Seismic Stratigraphic Implications of ODP Leg 101 Site Surveys*, J. Austin, Jr., W. Schlager et al. (eds.), Proceedings of the Ocean Drilling Program, Scientific Results, Vol. 101, pp. 391–424, 1988.

266. Swart, P., G. Eberli, M. Malone, et al., *Proceedings of the Ocean Drilling Program*, Scientific Results, Bahamas Transect, Ocean Drilling Program, Vol. 166, 2000.

267. Grasmueck, M., G. Eberli, T. Correa, D. Viggiano, J. Luo, G. Wyatt, J. Reed, A. Wright, and S. Pomponi, *AUV-Based Environmental Characterization of Deep-Water Coral Mounds in the Straits of Florida*, Presented at the 2007 Offshore Technology Conference, Houston, Texas, April 30–May 3, 2007.

268. Freile, D, and J. Milliman, *Sedimentary Facies of Western Great Bahama Bank: Bank-Edge Margin to Slope Transition*, Proceedings of the 9th Symposium on the Geology of the Bahamas and Other Carbonate Regions, H. Curran and J. Mylroie, (eds.), Bahamian Field Station, Ltd. San Salvador, Bahamas, pp. 36–57, 1999.

Table 2.4.6-201
Characteristics of Landslides on the U.S. Atlantic Margin

Dimension	Minimum	Maximum	Mean	Median
Area (square kilometer)	9	15,241	1,880	424
Length (kilometer)	2.7	>291	85	51
Width (kilometer)	2.1	151	21	12
Source Depth (meter)	92	3,263	1,630	1,785
Toe Depth (meter)	2,126	4,735	3,101	2,991
Scarp Height (meter)	3	410	90	63

Source: Reference 202

Table 2.4.6-202 (Sheet 1 of 2)
Summary of Historical Tsunami Run-Up Events in the East Coast of U.S.

Date[a]	Time (Hours)	Validity Code[b]	Cause Code[c]	Source Location (latitude, longitude)	Run-Up Location Along U.S. East Coast (lat, long)	Run-Up Type[d]	Run-Up Height (meters)
11/01/1755	08:50	4	1	Lisbon, Portugal (36.0°N 11.0°W)	—[e]	—	—
09/24/1848		3	8	Fishing Ships Harbor, Newfoundland, Canada (52.616°N 55.766°W)	—	—	—
06/27/1864	22:30	3	1	SW Avalon Peninsula, Newfoundland, Canada (46.5°N 53.7°W)	—	—	—
09/01/1886	02:51	4	1	Charleston, SC (32.9°N 80.0°W)	Jacksonville, FL (30.317°N 81.65°W) Mayport, FL (30.39°N 81.43°W) Copper River, SC (32.87°N 79.93°W)	1 1 1	—
09/01/1895	11:09	3	1	High Bridge, NJ (40.667°N 74.883°W)	Long Island, NY (40.591°N 73.796°W)	1	—
10/11/1918	14:14	4	1	Puerto Rico, Mona Passage (18.5°N 67.5°W)	Atlantic City, NJ (39.364°N 74.423°W)	2	0.06
11/18/1929	20:32	4	3	Grand Banks[f], Newfoundland, Canada (44.69°N 56.0°W)	Ocean City, MD (38.333°N 75.083°W) Atlantic City, NJ (39.35°N 74.417°W) Charleston, SC (32.75°N 79.916°W)	2 2 2	0.30 0.68 0.12
08/04/1946	17:51	4	1	Northeastern Cost, Dominican Republic (19.3°N 68.9°W)	Daytona Beach, FL (29.20°N 81.017°W) Atlantic City, NJ (39.364°N 74.423°W)	2 2	—
08/08/1946	13:28	4	1	Northeastern Cost, Dominican Republic (19.71°N 69.51°W)	Daytona Beach, FL (29.21°N 81.02°W) Atlantic City, NJ (39.364°N 74.423°W)	2 2	—
05/19/1964	00:00	3	8	Long Island, NY[f] (40.8°N 73.10°W)	Montauk, NY (41.033°N 71.950°W) Plum Island, NY (41.181°N 72.194°W) Willetts Point, NY (40.683°N 73.283°W) Newport, RI (41.493°N 71.327°W)	2 2 2 2	0.10 0.28 0.10 0.10
12/26/2004	00:58	4	1	Off Sumatra, Indonesia (3.295°N 95.982°E)	Trident Pier, FL (28.415°N 80.593°W) Atlantic City, NJ (39.35°N 74.417°W) Cape May, NJ (38.97°N 74.96°W)	2 2 2	0.17 0.11 0.06

Table 2.4.6-202 (Sheet 2 of 2)
Summary of Historical Tsunami Run-Up Events in the East Coast of U.S.

(a) Date and time given in Universal Coordinated Time (also known as Greenwich Mean Time).
(b) Tsunami event validity:
Valid values: 0 to 4
Validity of the actual tsunami occurrence is indicated by a numerical rating of the reports of that event:
0 = Erroneous entry
1 = Very doubtful tsunami
2 = Questionable tsunami
3 = Probable tsunami
4 = Definite tsunami
(c) Tsunami cause code:
Valid values: 0 to 11
The source of the tsunami:
0 = Unknown cause
1 = Earthquake
2 = Questionable earthquake
3 = Earthquake and landslide
4 = Volcano and earthquake
5 = Volcano, earthquake, and landslide
6 = Volcano
7 = Volcano and landslide
8 = Landslide
9 = Meteorological
10 = Explosion
11 = Astronomical tide
(d) Type of run-up measurement:
Valid values: 1 to 7
1 = Water height measurement
2 = Tide-gage measurement
3 = Deep ocean gage
4 = Paleodeposit
5 = Computer modeled
6 = Atmospheric pressure wave
7 = Seiche
(e) Data not available
(f) Only locations with measured run-up values are presented

Source: Reference 214

Table 2.4.6-203
Grid Resolution and Sizes of the Subdomains

	Grid Resolution (m)	Grid Spacing along M[(a)] Axis (m)	Grid Spacing along N[(a)] Axis (m)
SITE	450 – 540	260 – 410	620 – 800
ISLANDS	1,240 – 3,710	970 – 3,010	950 – 7,050
DEEP	3,120 – 22,320	1,850 – 24,080	2,630 – 27,340

(a) M and N are the principal axes of the model curvilinear grid system

Table 2.4.6-204
Horizontal and Vertical Resolutions of Depth Data

	Biscayne Bay Sounding	LiDAR	Coastal Relief	ETOPO1
Horizontal Resolution	30 m	0.1 m[(a)]	3 arc-seconds (90 m)	1 arc-minute (1,800 m)
Vertical Resolution	0.01 m	0.01 m	1 m for land 0.1 m for sea	1 m

(a) ~ 1 meter resolution for about 10 percent of the data

Table 2.4.6-205
Nested Grids in FUNWAVE-TVD for Cape Fear Tsunami

Grid	Coordinates of SW Corner		Grid Spacing (Δx = Δy)	Number of Grid Cells
	x	y		
	degrees	degrees	seconds	cells
A	-82.0	23.0	60	780 x 900
B	-80.75	23.0	15	480 x 1260
C	-80.517	25.322	3	592 x 768

Table 2.4.6-206
Nested Grids in FUNWAVE-TVD for Florida Escarpment Tsunami

Grid	Coordinates of SW Corner		Grid Spacing (Δx = Δy)	Number of Grid Cells
	x	y		
	degrees	degrees	seconds	cells
A	-89.0	22.0	60	780 x 420
B	-80.75	23.0	15	480 x 1260
C	-80.517	25.156	3	592 x 768

Table 2.4.6-207
Nested Grids in FUNWAVE-TVD for Great Bahama Bank Tsunami

Grid	Coordinates of SW Corner		Grid Spacing (Δx = Δy)	Number of Grid Cells
	x	y		
	degrees	degrees	seconds	cells
B	-80.75	23.0	15	480 x 1260
C	-80.517	25.156	3	592 x 768

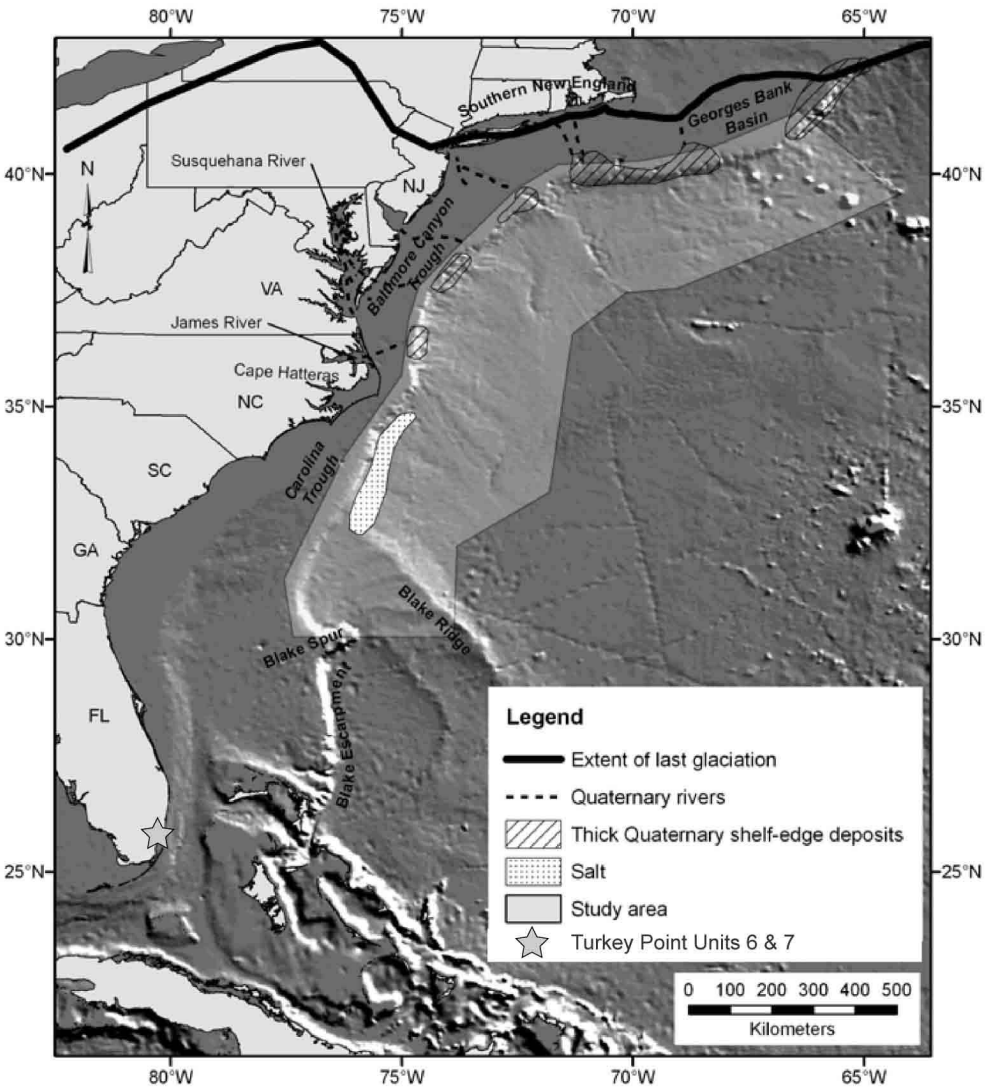

Modified from Reference 202

Figure 2.4.6-201 Location Map Showing the Extent of the AGMTHAG Study Area and Geologic Features That May Influence Landslide Distribution Along the U.S. Atlantic Margin

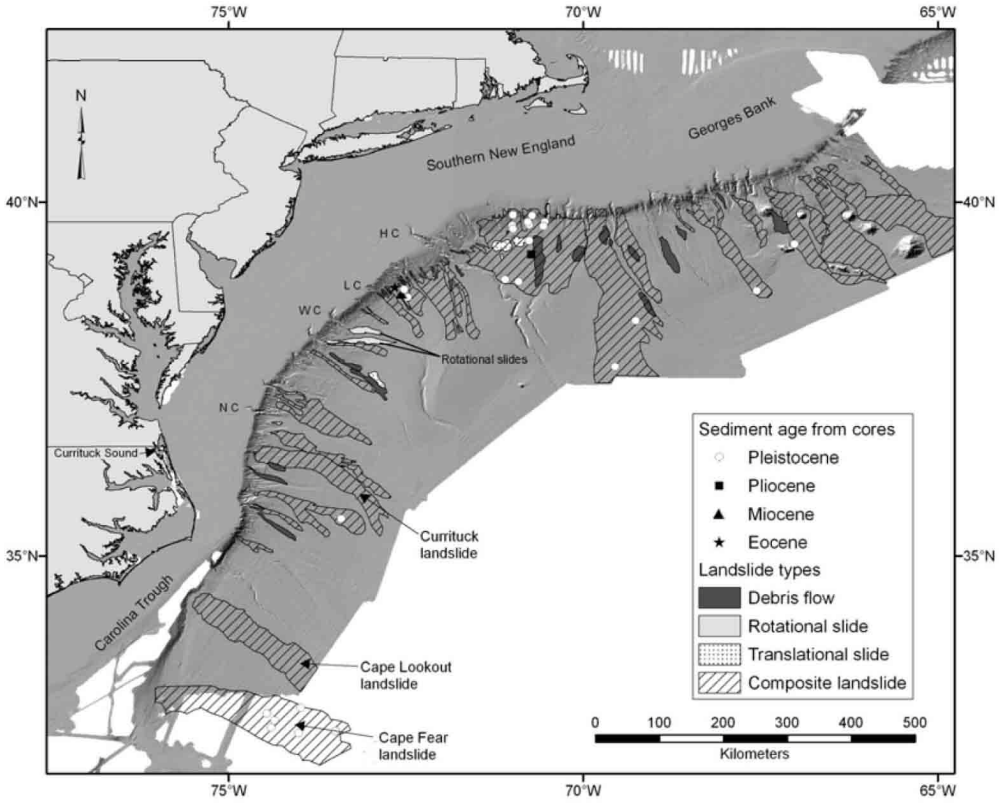

Notes: HC = Hudson Canyon; LC = Lindenkohl Canyon; WC = Wilmington Canyon; NC = Norfolk Canyon
Source: Reference 202

Figure 2.4.6-202 Distribution of Different Landslide Types Along the U.S. Atlantic Margin

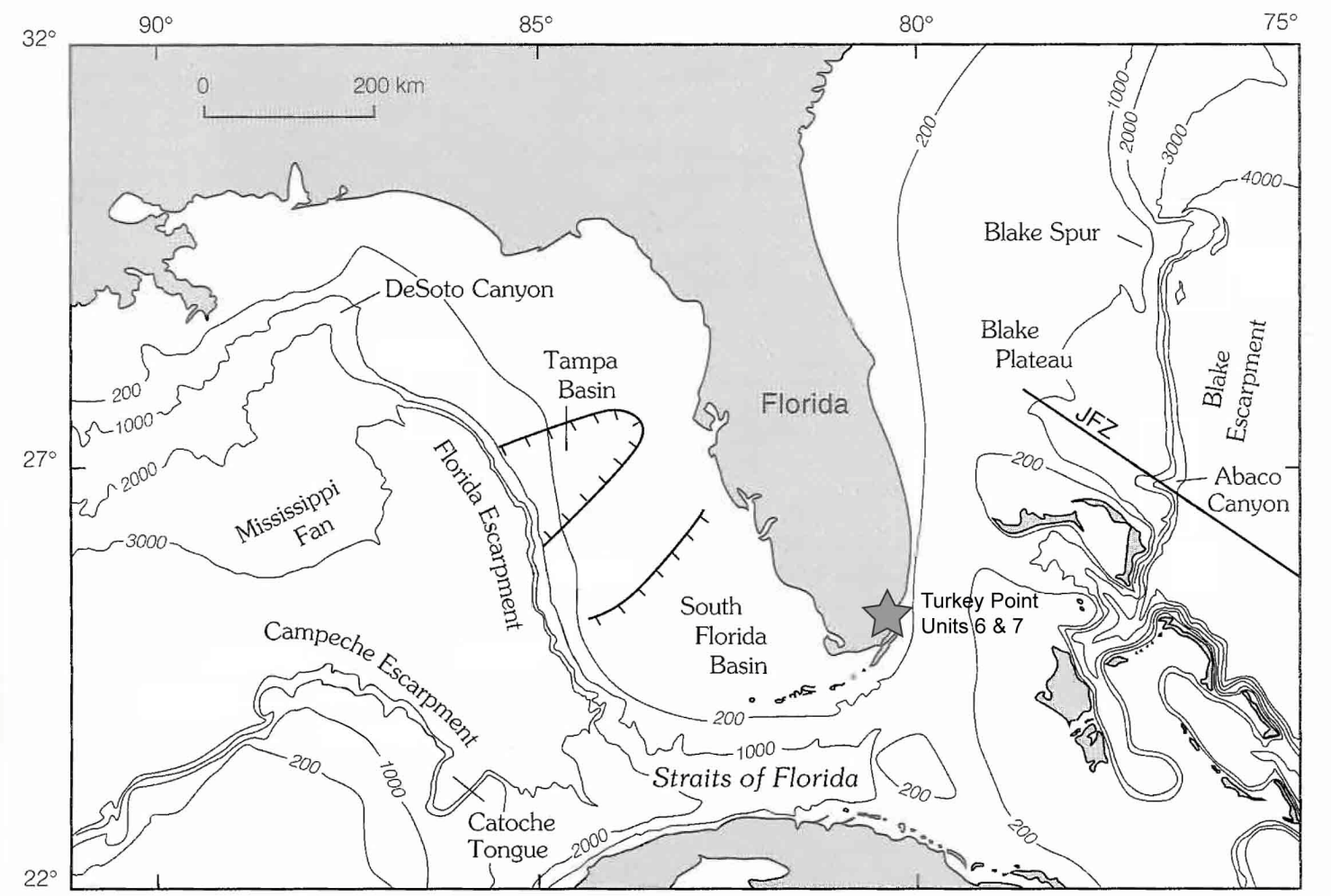

JFZ = Jacksonville fracture zone from Klitgord and Schouten (1986)

Note: Depth contours are in meters.
Modified from Reference 203

Figure 2.4.6-203 Location of Blake Escarpment Offshore of the Florida Coast

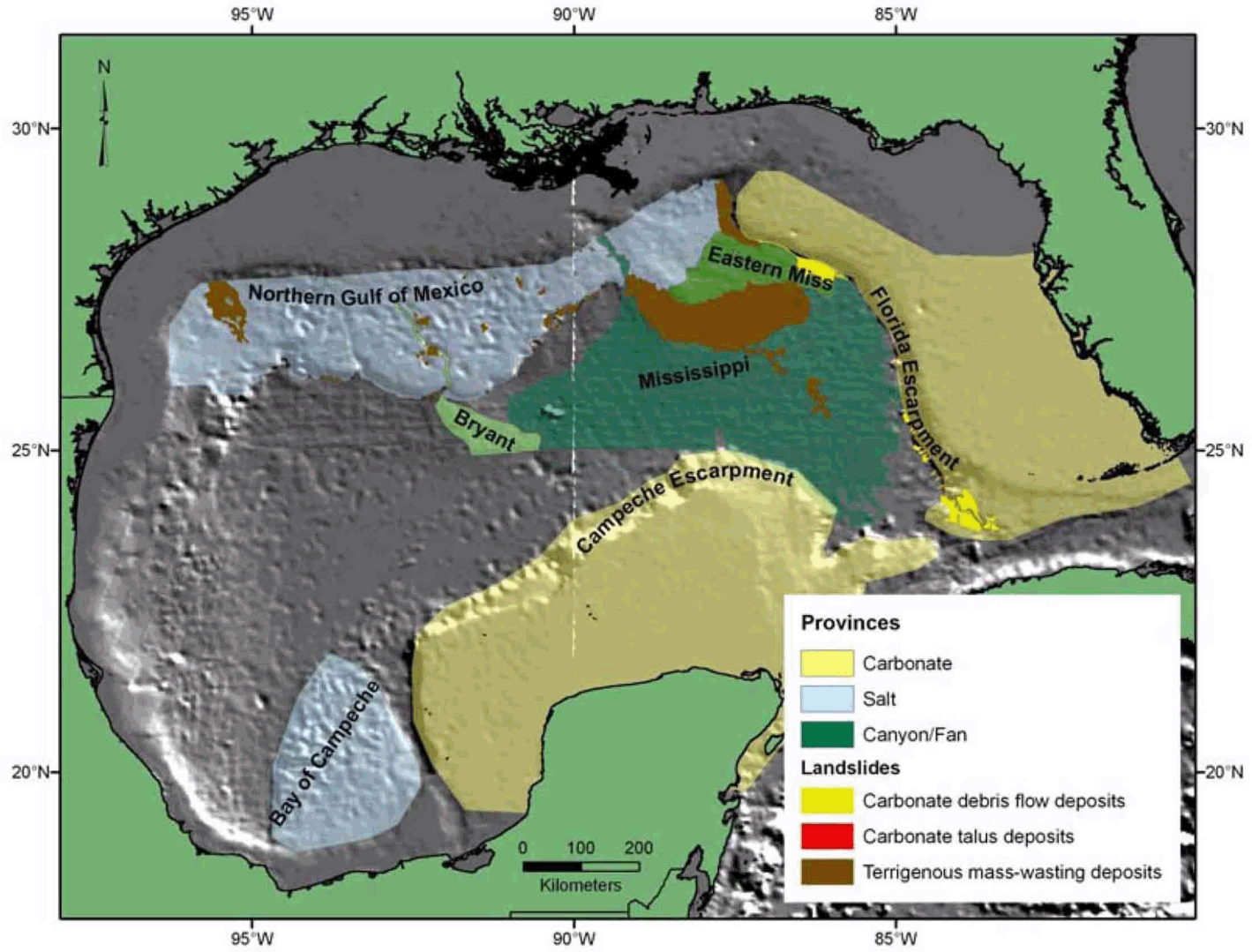

Source: Reference 202

Figure 2.4.6-204 Location Map Showing the Extent of the Physiographic Features in the Gulf of Mexico Basin

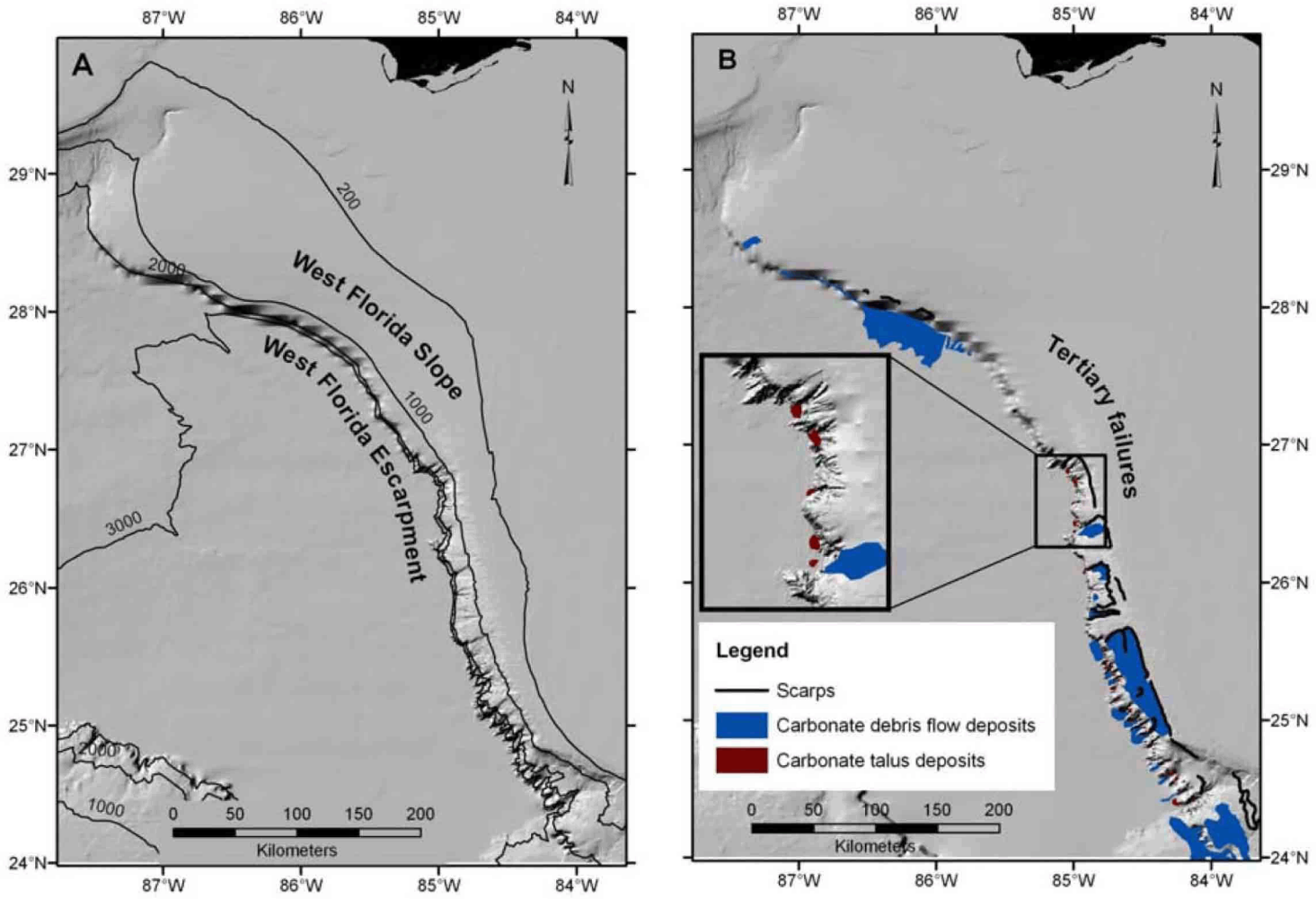

Note: Depth contours are in meters.
Modified from Reference 202

Figure 2.4.6-205 (A) Morphology of the Florida Escarpment and the West Florida Slope, and (B) the Extent and Distribution of Carbonate Debris Flow Deposits and Talus Deposits

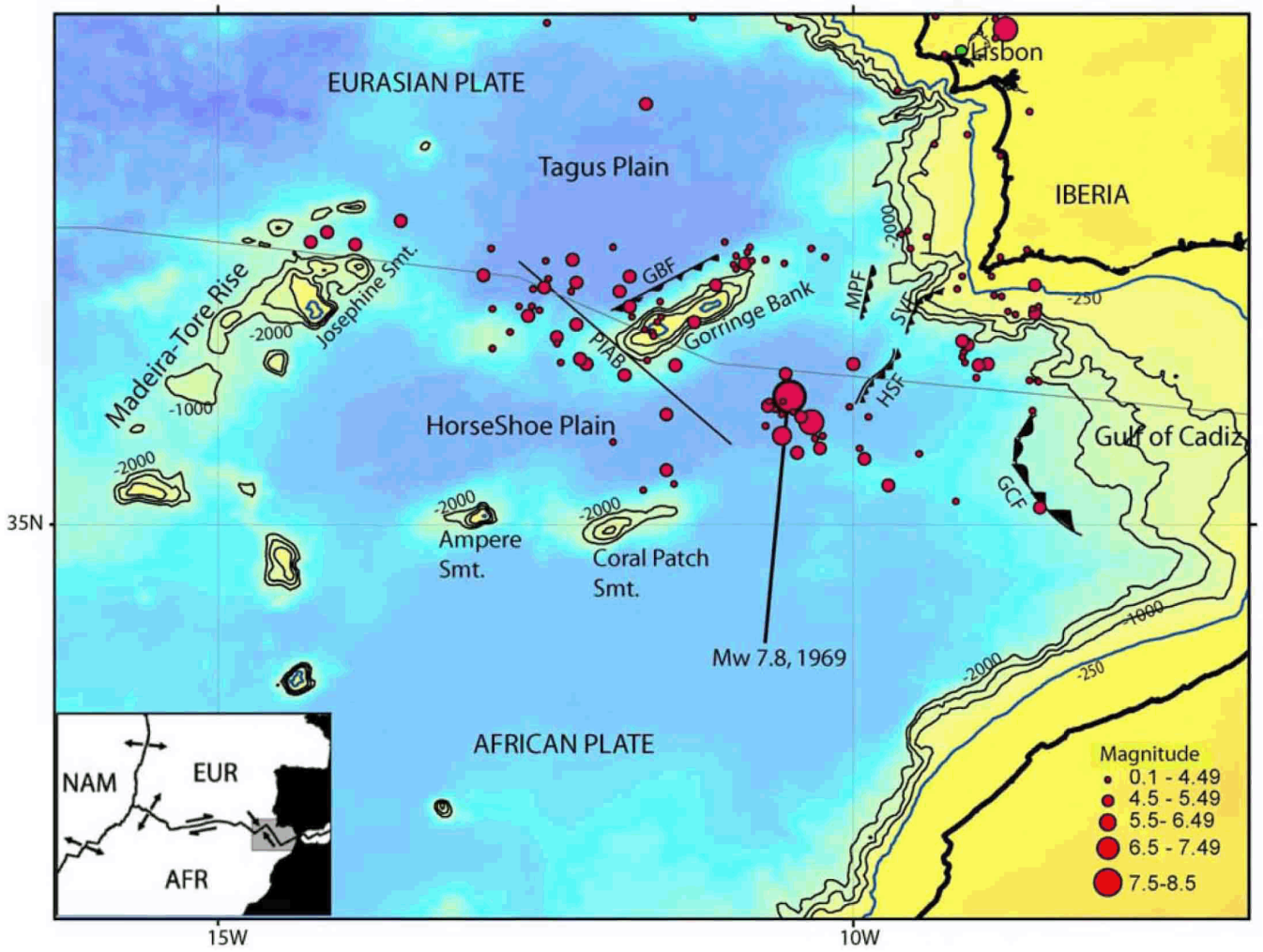

Note: Barbed lines show faults proposed in various past studies, GBF — Gorringe Bank Fault; MPF — Marqués de Pombal Fault; SVF — St. Vicente Fault; HSF — Horseshoe Fault; GCF — Gulf of Cádiz Fault; PIAB - Paleo Iberia-Africa Plate Boundary. Inset plates: NAM - North American Plate; EUR — Eurasian Plate; AFR — African Plate. Depth contours are in meters (only contours from –250 to –2000 meters are shown).
Source: Reference 202

Figure 2.4.6-206 Plate Tectonic Setting and Bathymetry of the Eastern Azores-Gibraltar Region

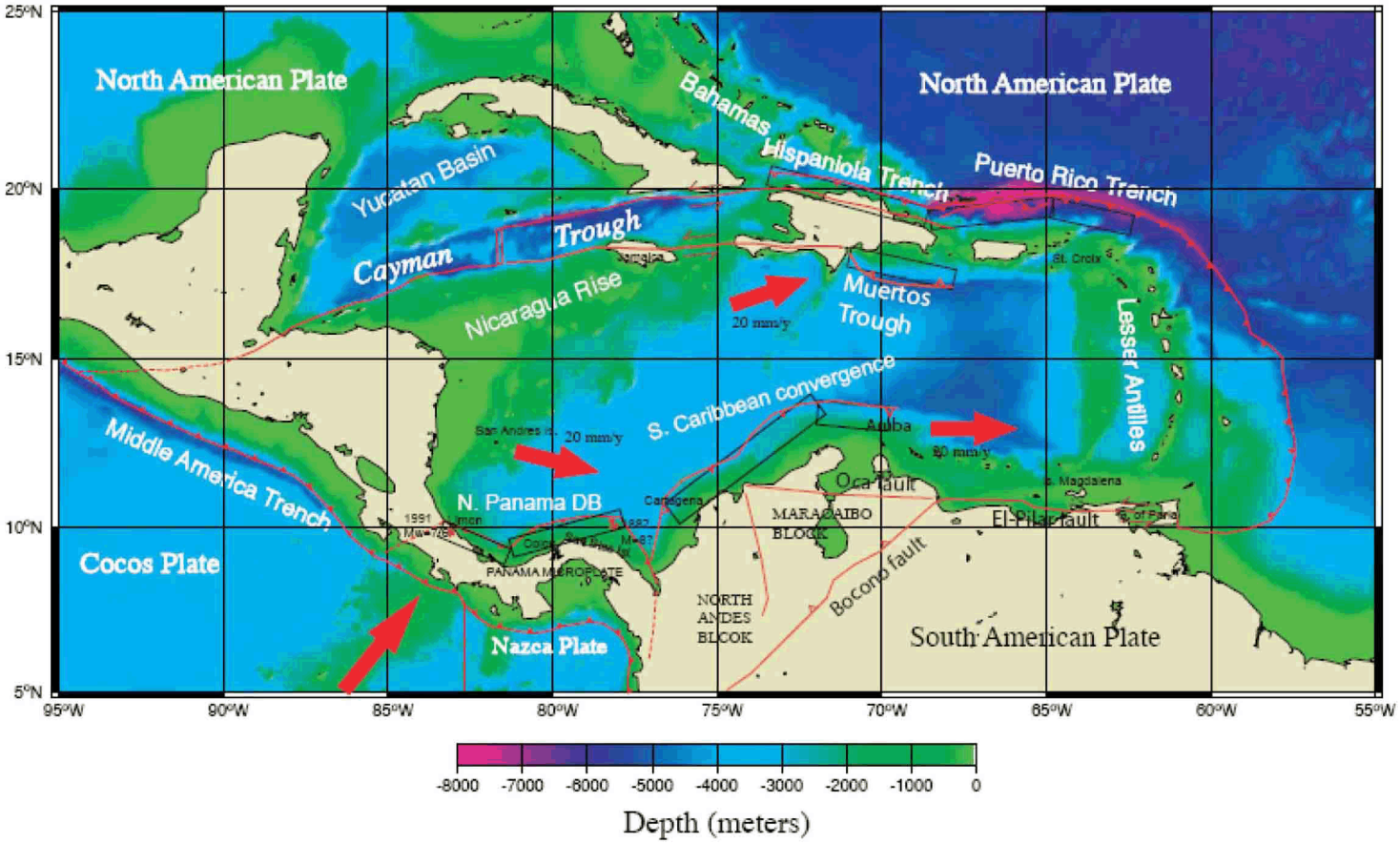

Note: Red lines are plate boundaries and red arrows indicate relative plate movement
Source: Reference 202

Figure 2.4.6-207 The Caribbean Plate Boundary and its Tectonic Elements

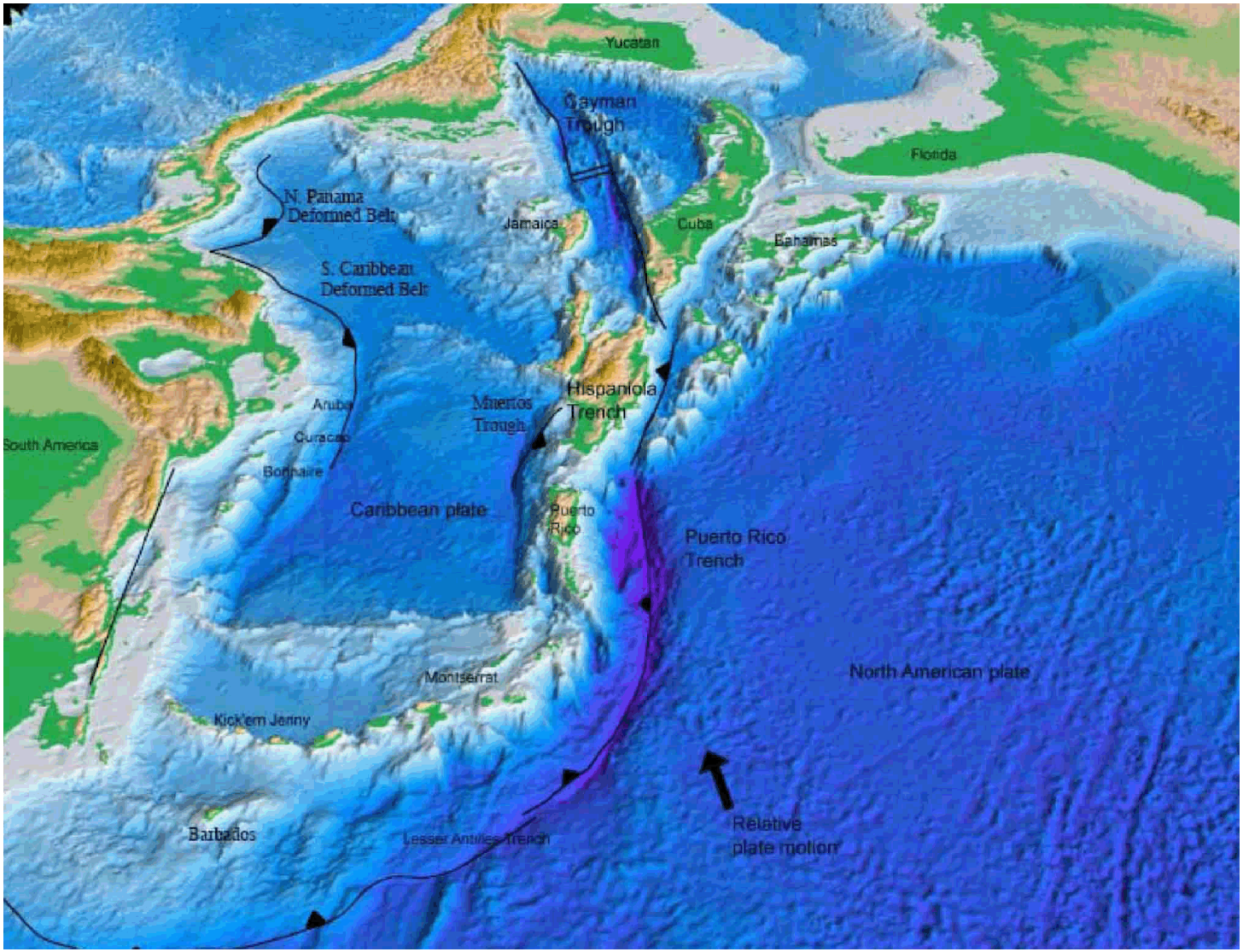

Source: Reference 202

Figure 2.4.6-208 Perspective (Schematic) View of the Tectonic Elements in the Caribbean Plate and Seafloor Topography

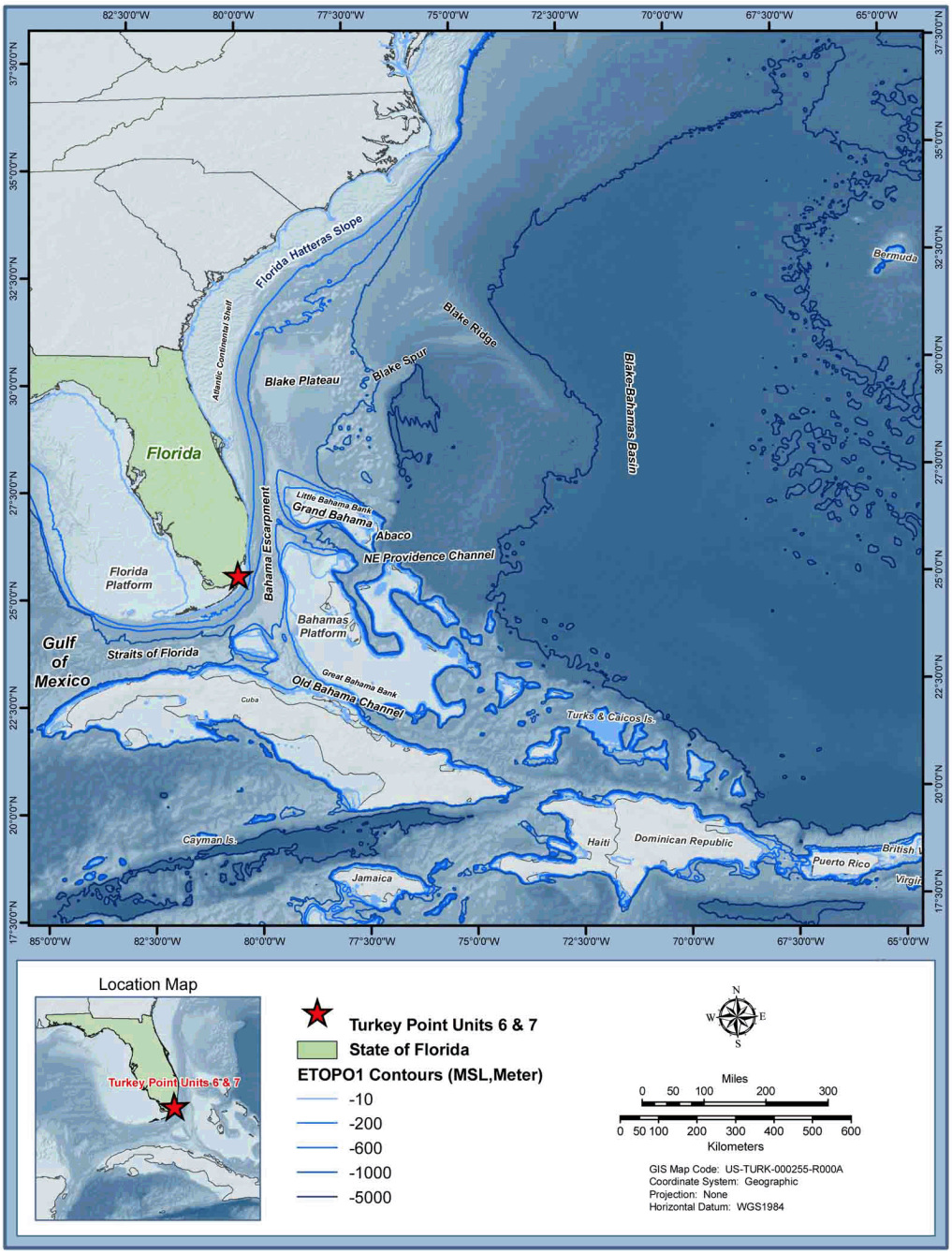

Figure 2.4.6-209 Geophysical Setting and Seafloor Topography East of Southeast U.S. Coast and North of the Caribbean

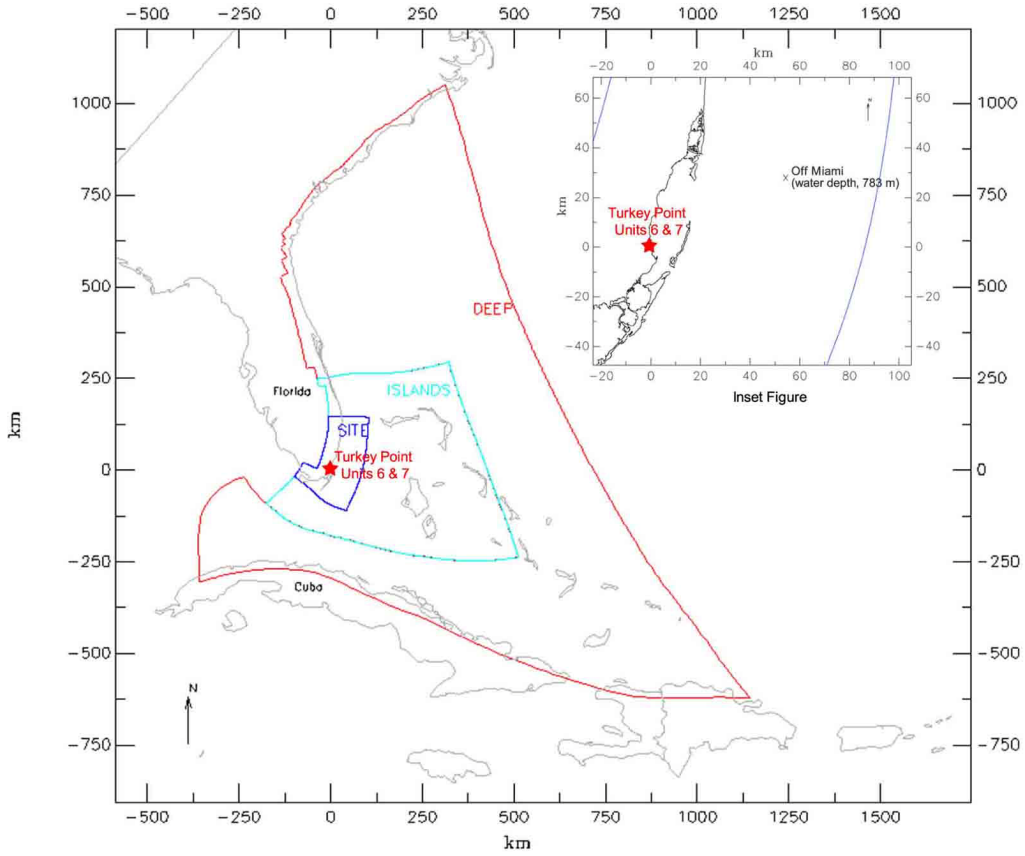

Figure 2.4.6-210 Extent of Selected Tsunami Model Domain and Subdomains SITE, ISLANDS, and DEEP

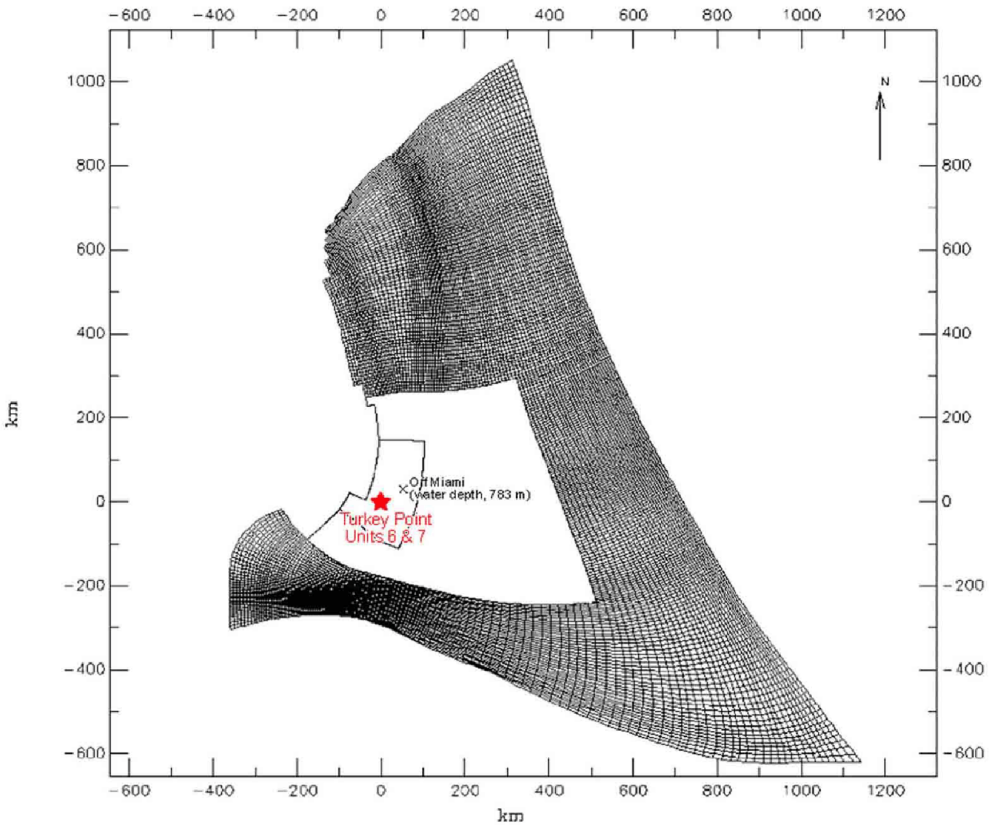

Figure 2.4.6-211 Model Grids of the DEEP Subdomain

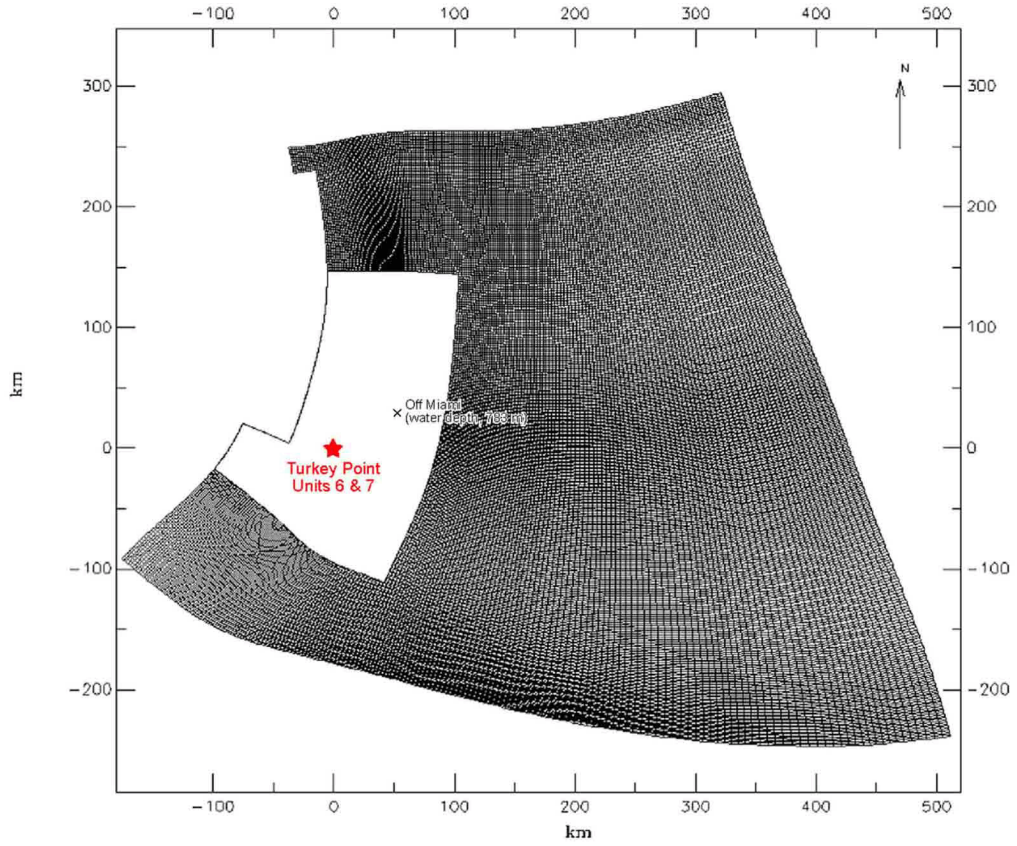

Figure 2.4.6-212 Model Grids of the ISLANDS Subdomain

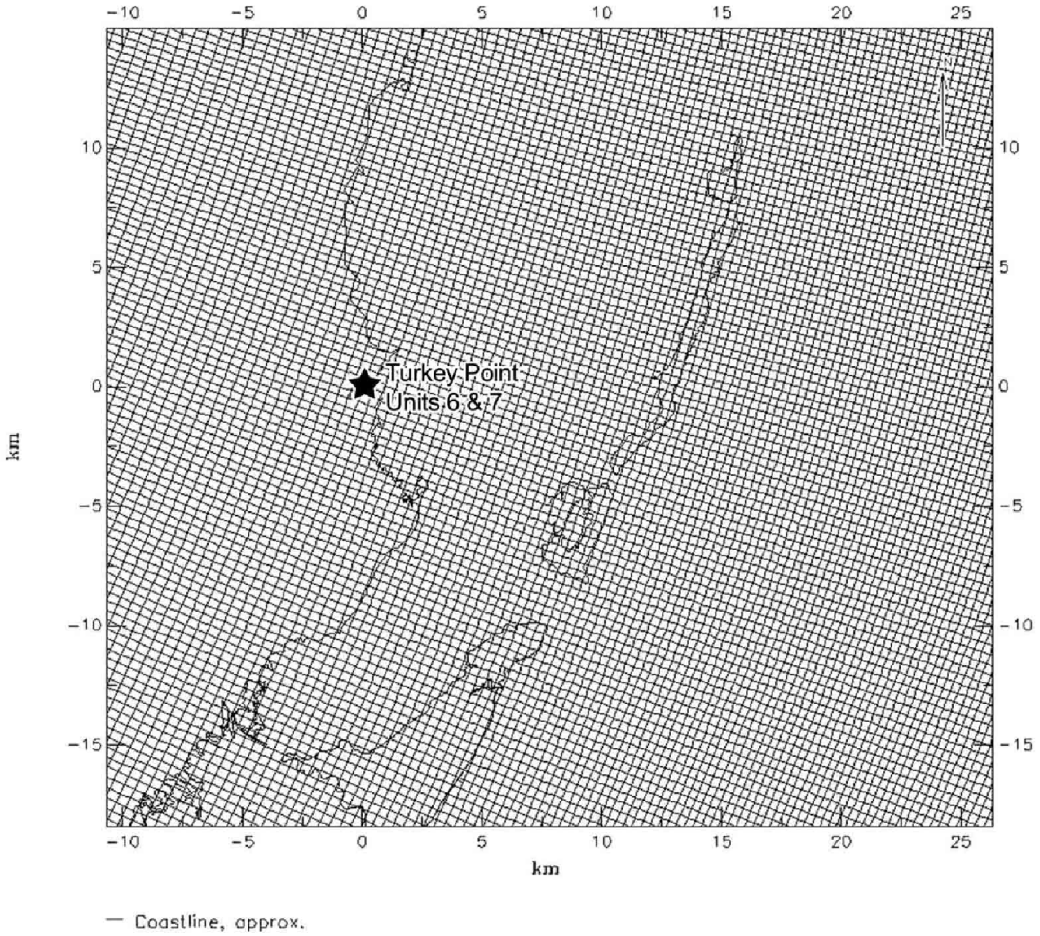

Figure 2.4.6-213 Model Grids of the SITE Subdomain near Units 6 & 7

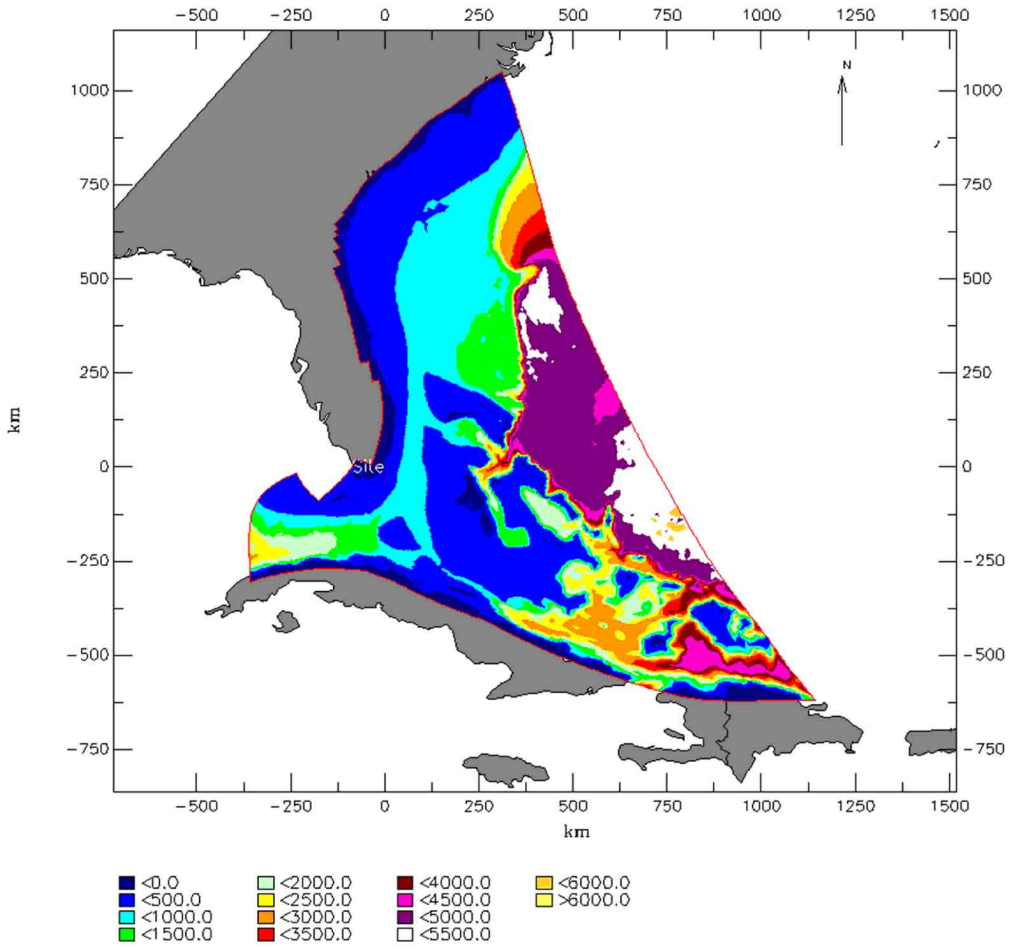

Note: Depths to the seabed are in meters relative to MSL

Figure 2.4.6-214 Contours of Model Bathymetry

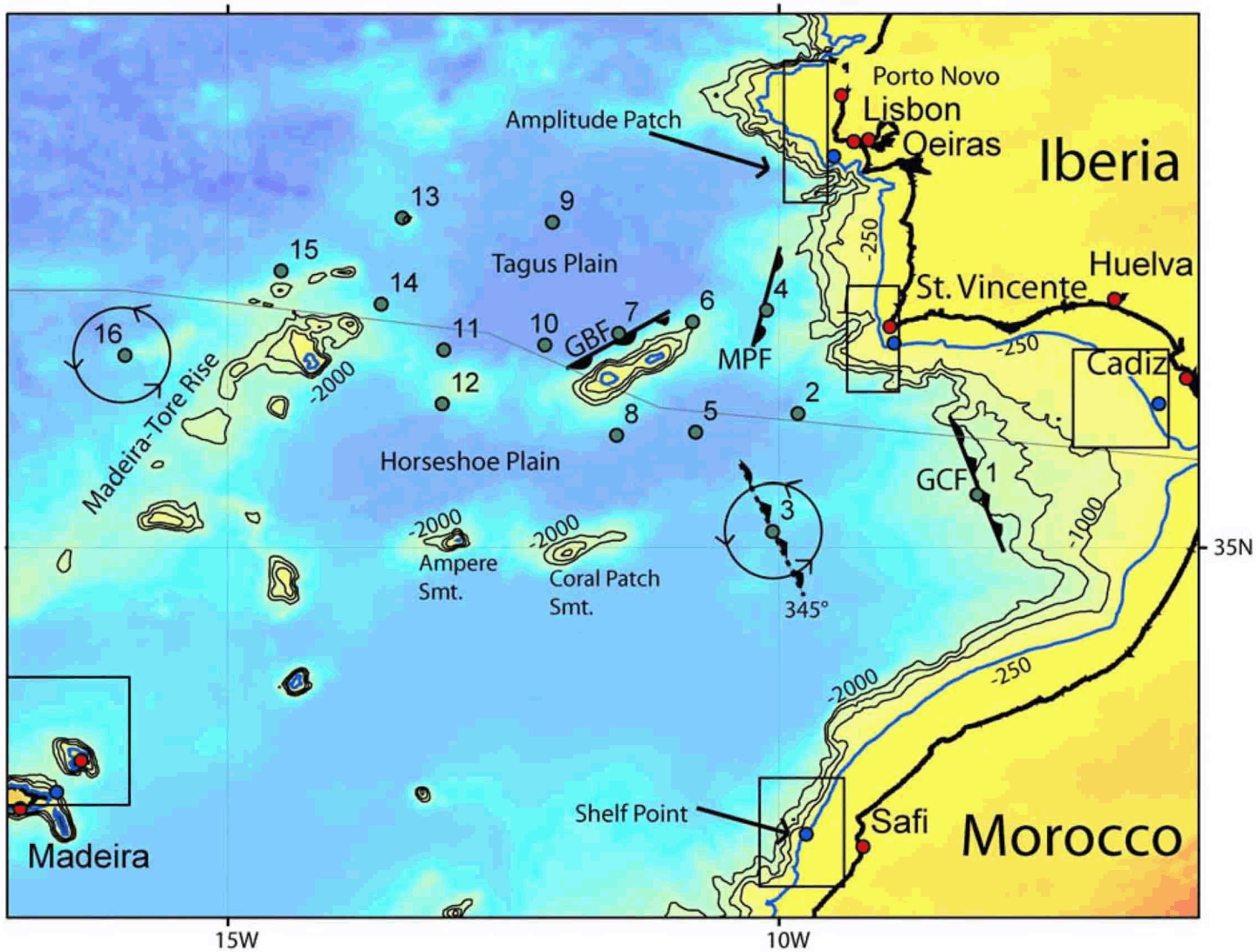

Note: Fault orientation for source locations 3 and 16 were rotated 360° at 15° to test the optimal strike angle generating maximum tsunami amplitude in the Caribbean. Depth contours are in meters.
Source: Reference 202

Figure 2.4.6-215 Postulated Epicenter Locations for the 1755 Lisbon Earthquake by AGMTHAG

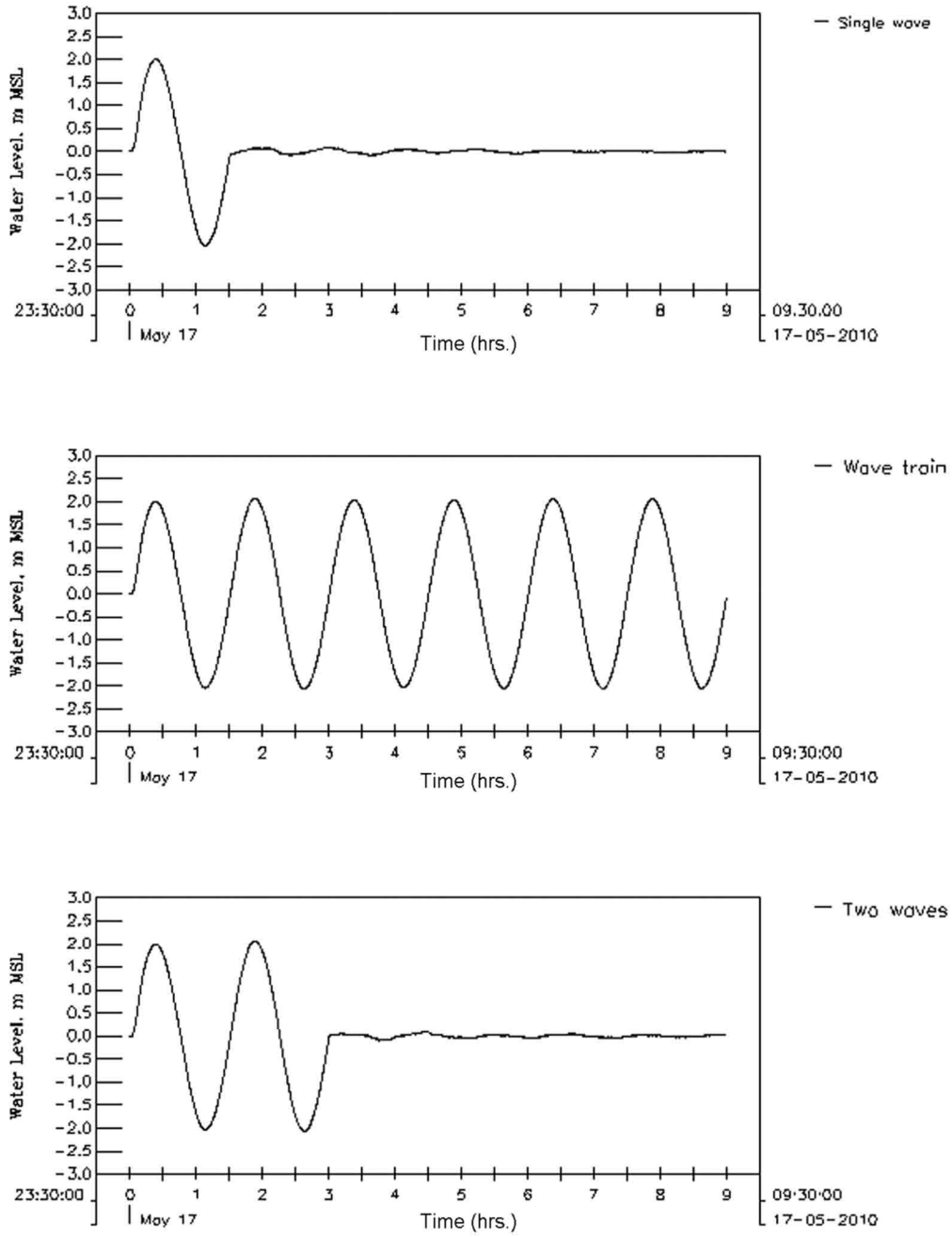

Figure 2.4.6-216 Input Tsunami Marigrams at the Model Open Boundary for Conditions with Single Wave, Continuous Wave Train, and Two Consecutive Waves

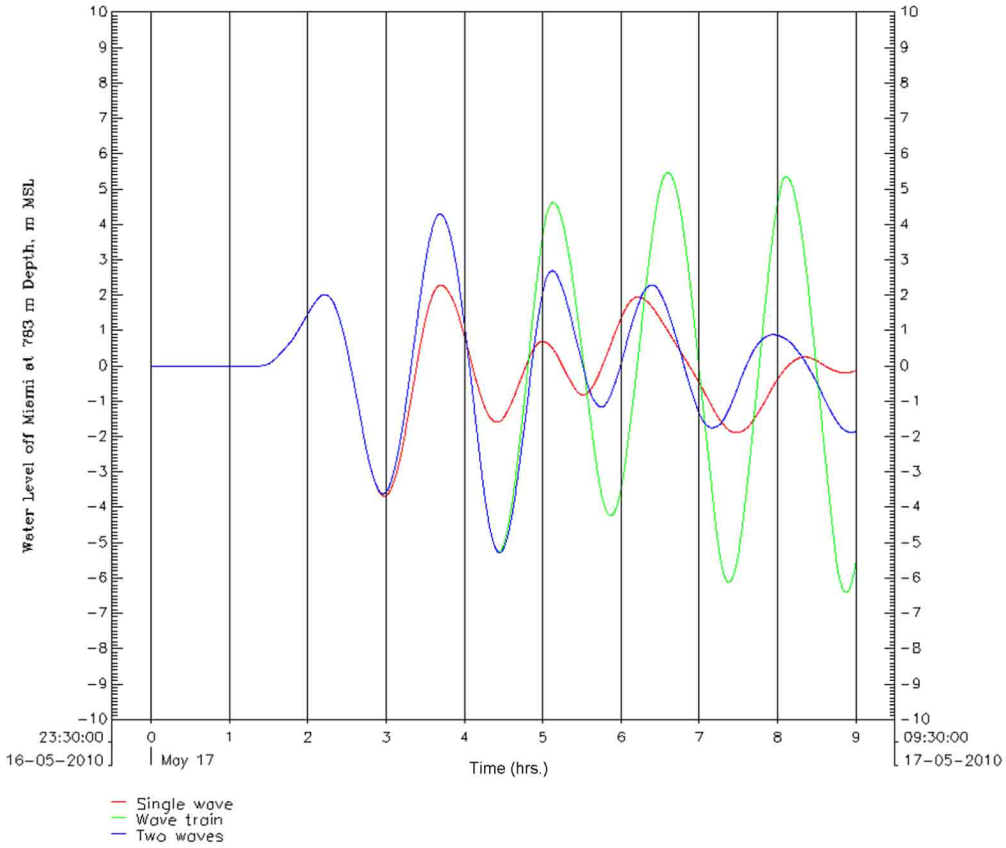

Note: Initial water level at MSL.

Figure 2.4.6-217 Simulated Tsunami Marigrams at 783 meters (2569 feet) Water Depth off Miami, Florida

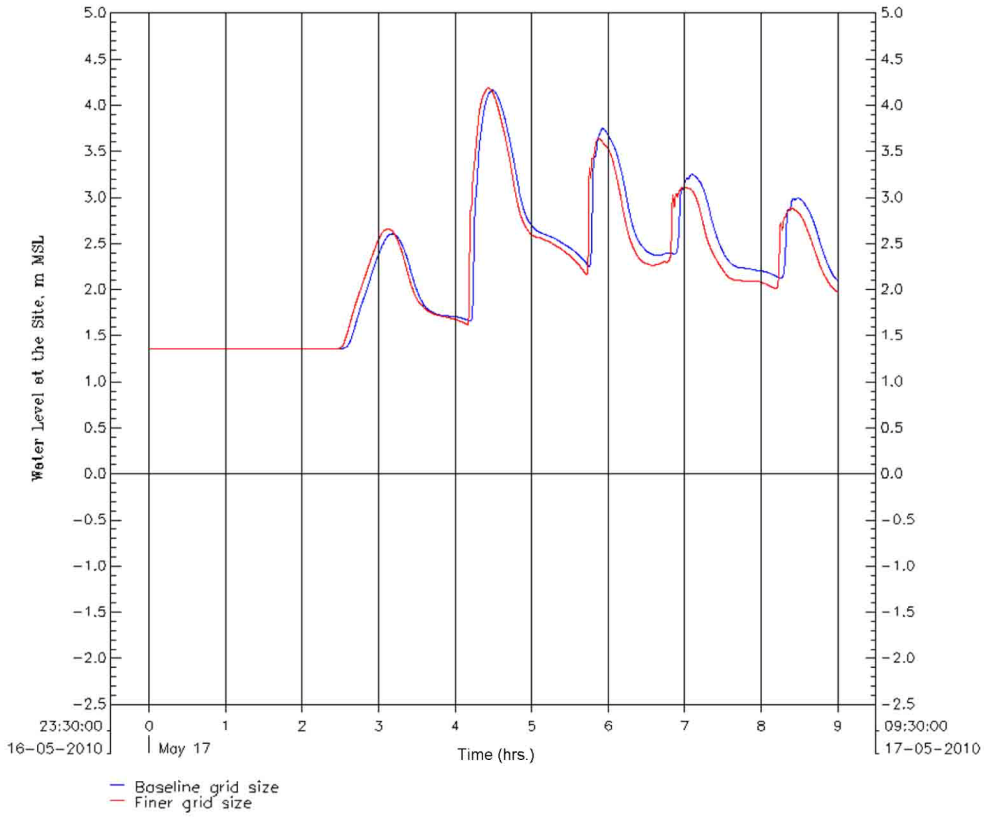

Note: Initial water level at 1.36 meters (4.46 feet) MSL.

Figure 2.4.6-218 Simulated Tsunami Water Levels at the Units 6 & 7 Site for the Selected (Baseline) and Finer Grid Sizes

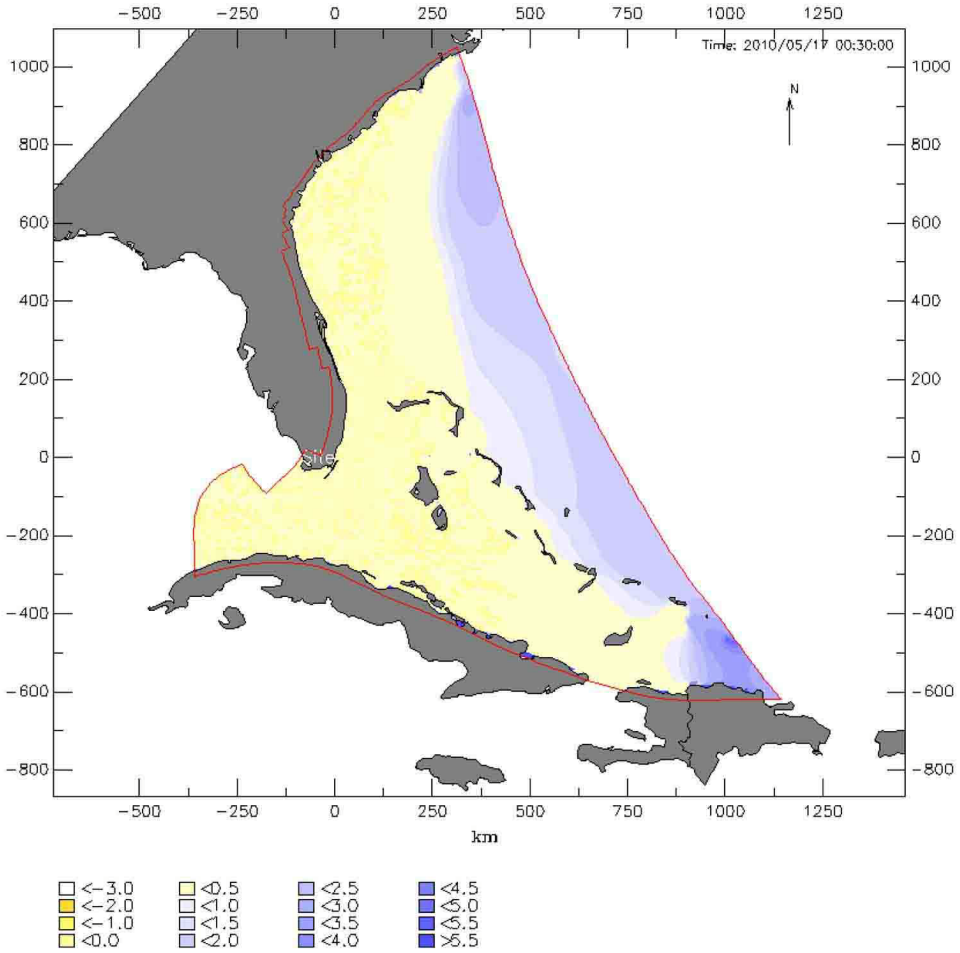

Note: Water levels are in meters **relative to 1.36 m** MSL.

Figure 2.4.6-219a Tsunami Water Level Contours 30 Minutes into the Model Simulation (with Manning's n of 0.02 and non-reflective boundaries)

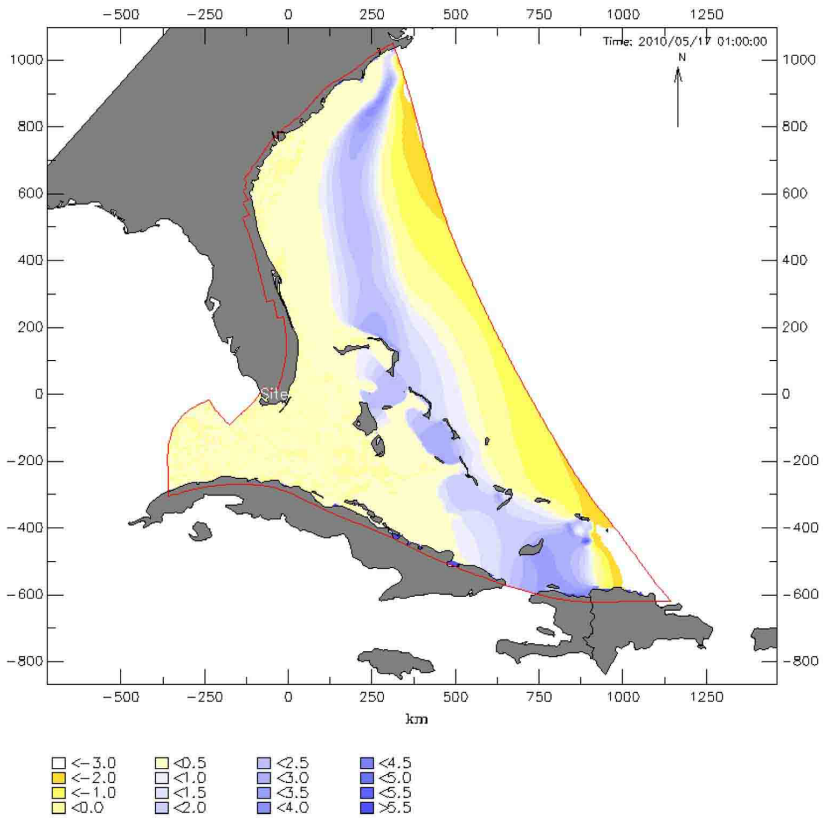

Note: Water levels are in meters **relative to 1.36 m** MSL.

Figure 2.4.6-219b Tsunami Water Level Contours 1.0 Hour into the Model Simulation (with Manning's n of 0.02 and non-reflective boundaries)

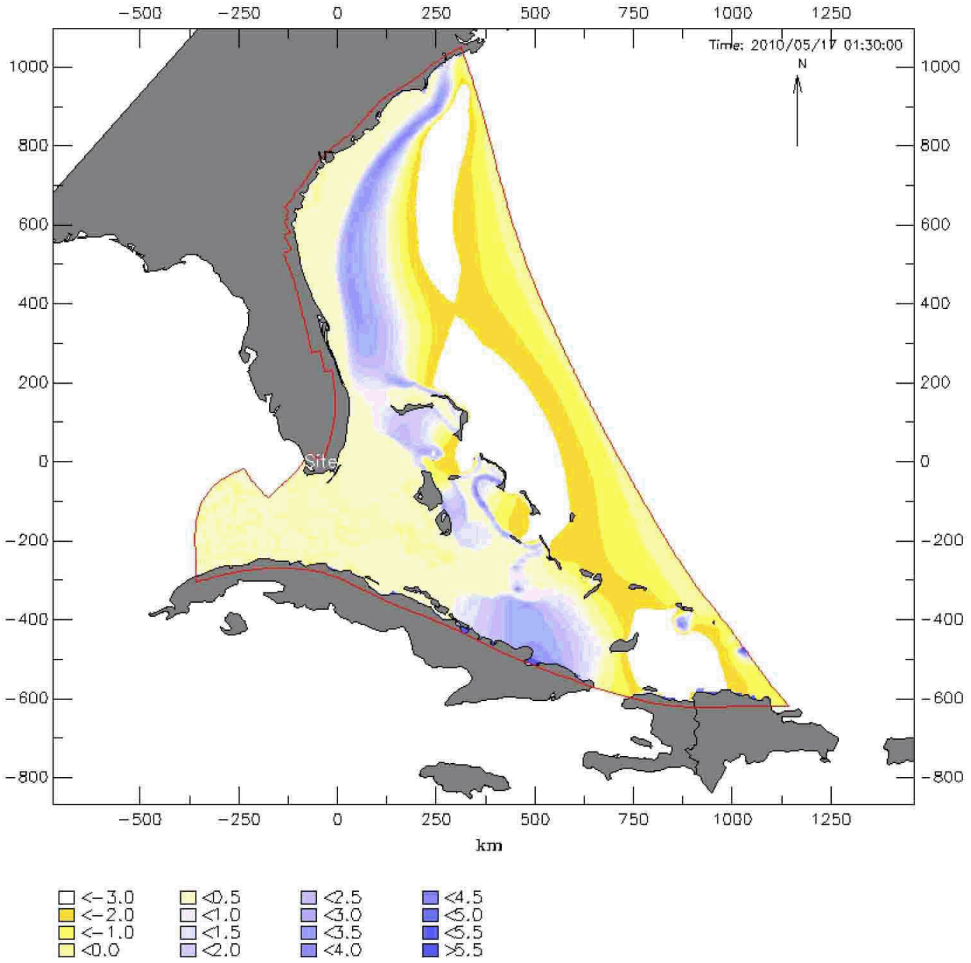

Note: Water levels are in meters **relative to 1.36 m** MSL.

Figure 2.4.6-219c Tsunami Water Level Contours 1.5 Hours into the Model Simulation (with Manning's n of 0.02 and non-reflective boundaries)

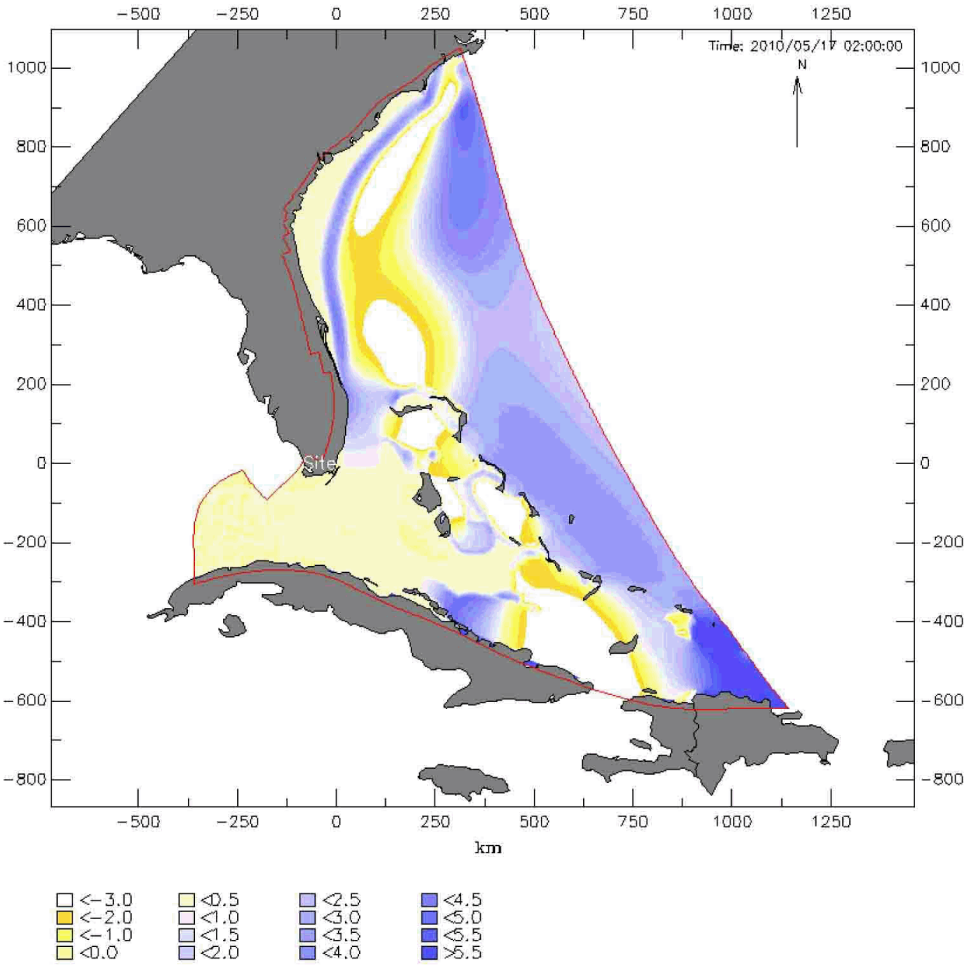

Note: Water levels are in meters **relative to 1.36 m** MSL.

Figure 2.4.6-219d Tsunami Water Level Contours 2.0 Hours into the Model Simulation (with Manning's n of 0.02 and non-reflective boundaries)

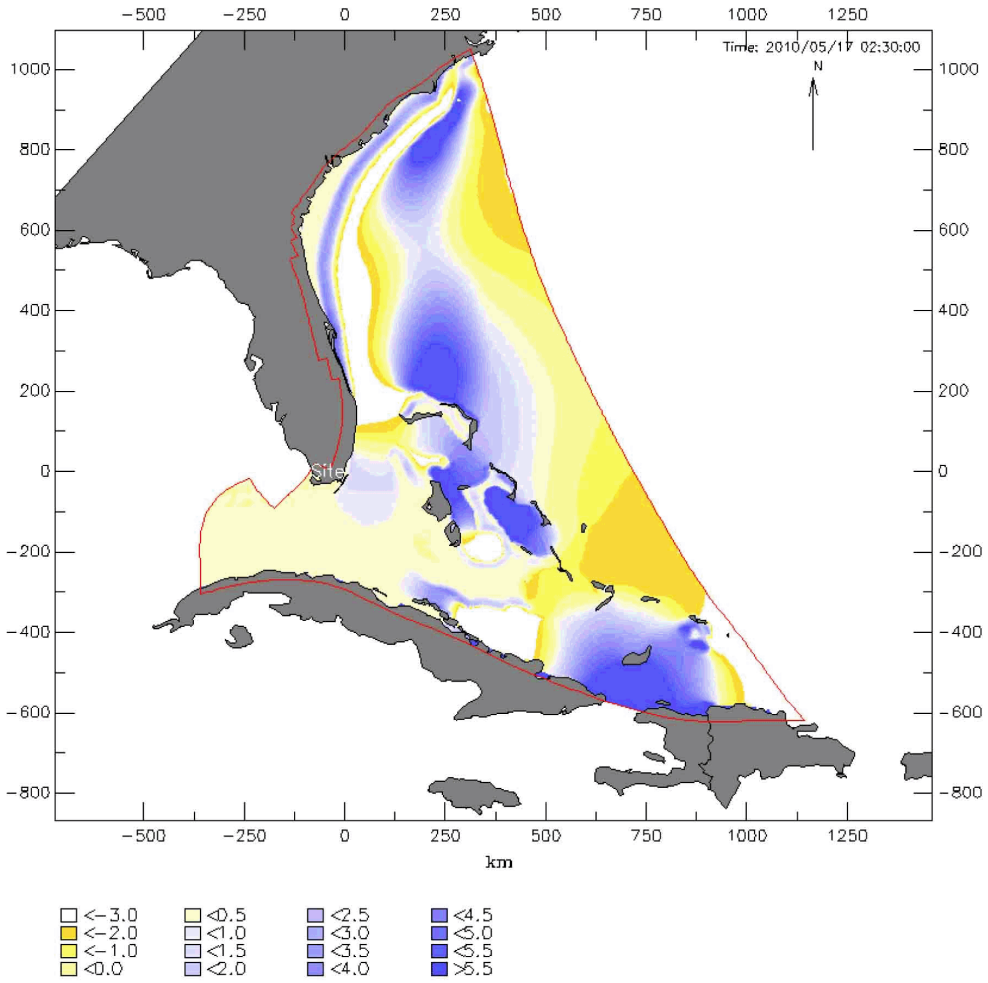

Note: Water levels are in meters **relative to 1.36 m** MSL.

Figure 2.4.6-219e Tsunami Water Level Contours 2.5 Hours into the Model Simulation (with Manning's n of 0.02 and non-reflective boundaries)

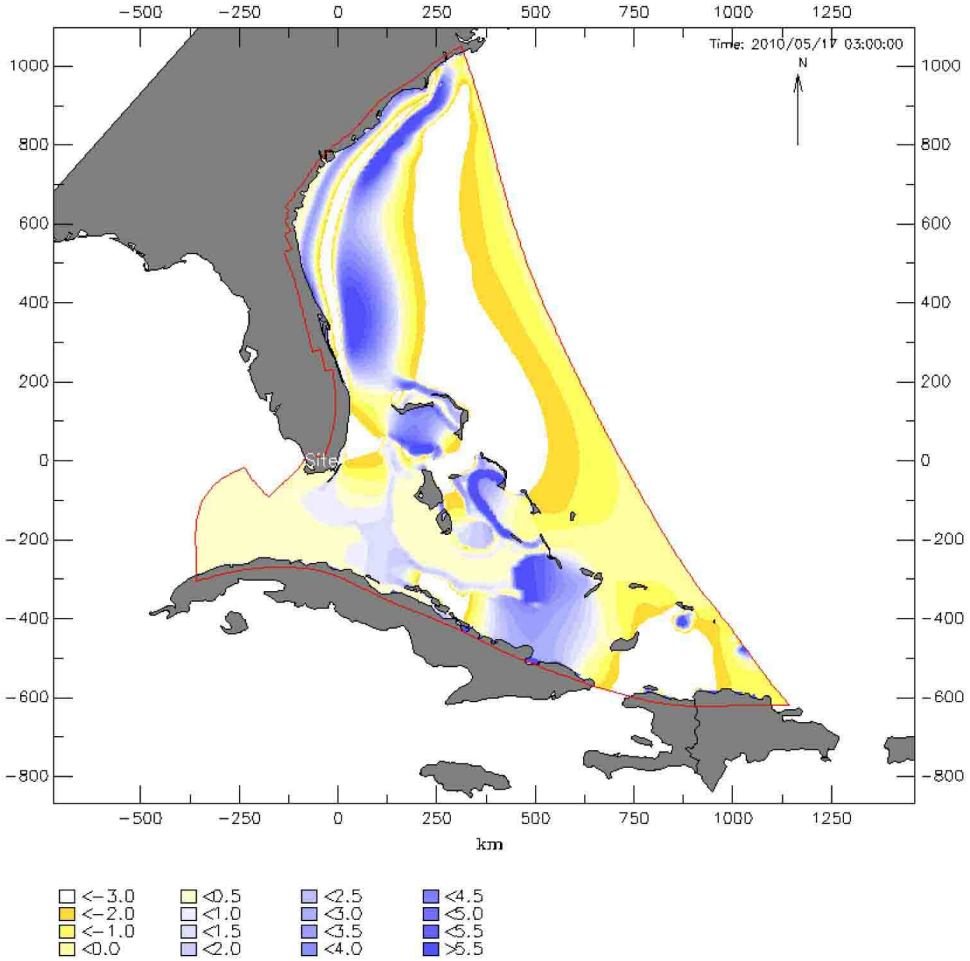

Note: Water levels are in meters **relative to 1.36 m** MSL.

Figure 2.4.6-219f Tsunami Water Level Contours 3.0 Hours into the Model Simulation (with Manning's n of 0.02 and non-reflective boundaries)

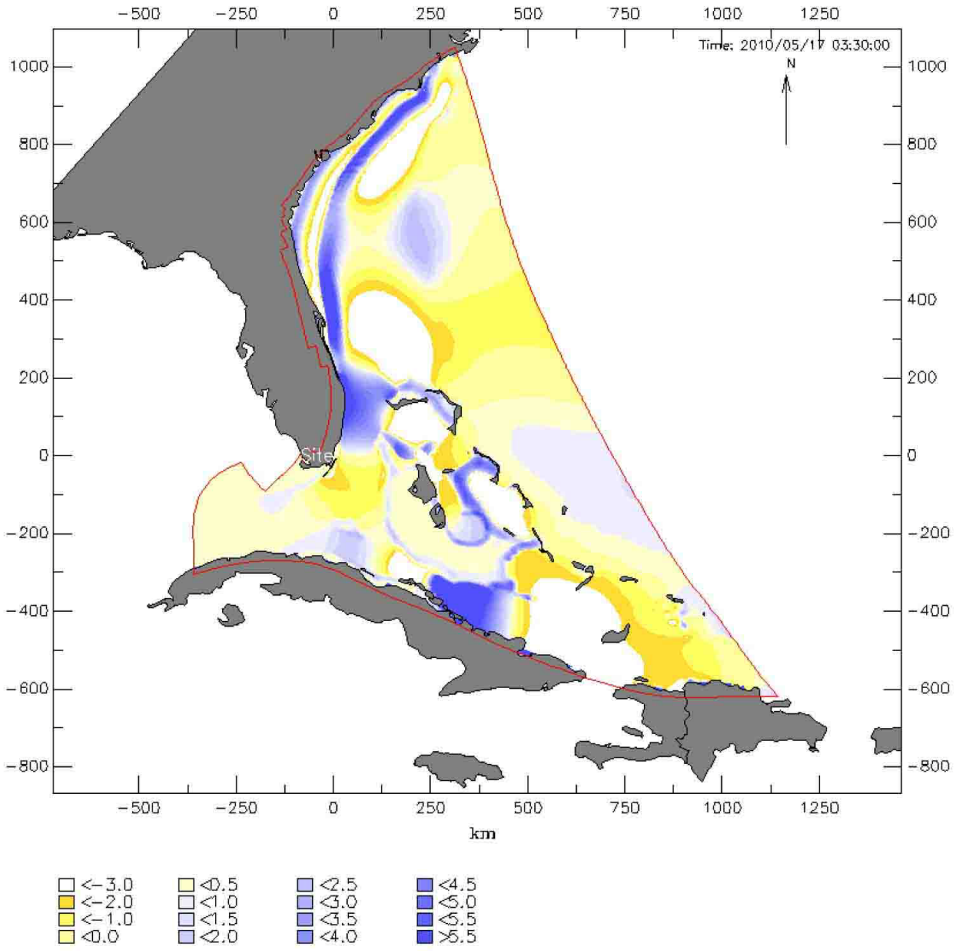

Note: Water levels are in meters **relative to 1.36 m** MSL.

Figure 2.4.6-219g Tsunami Water Level Contours 3.5 Hours into the Model Simulation (with Manning's n of 0.02 and non-reflective boundaries)

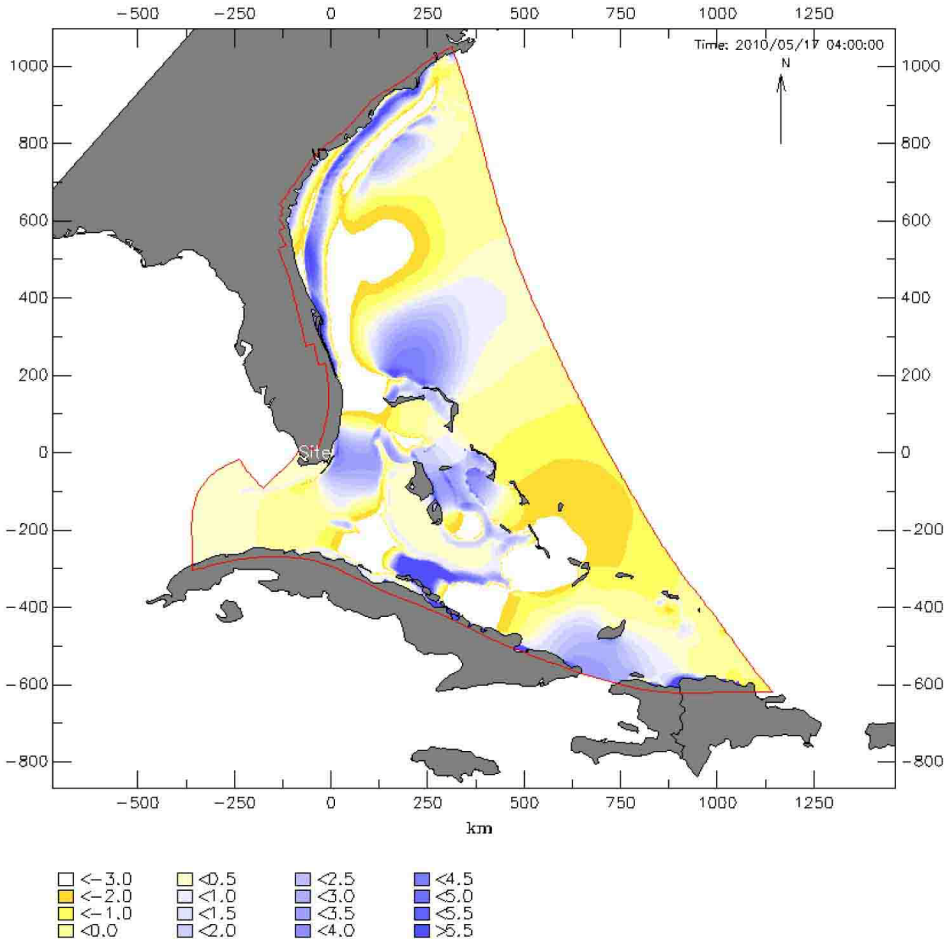

Note: Water levels are in meters **relative to 1.36 m** MSL.

Figure 2.4.6-219h Tsunami Water Level Contours 4.0 Hours into the Model Simulation (with Manning's n of 0.02 and non-reflective boundaries)

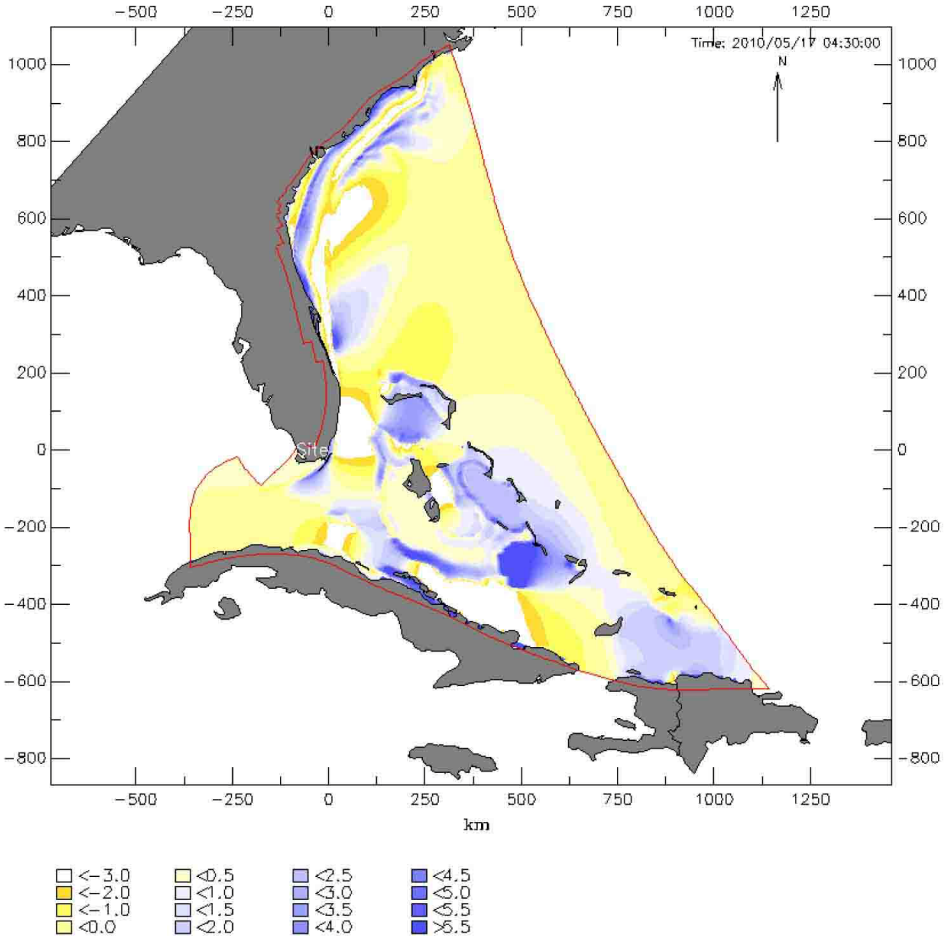

Note: Water levels are in meters **relative to 1.36 m** MSL.

Figure 2.4.6-219i Tsunami Water Level Contours 4.5 Hours into the Model Simulation (with Manning's n of 0.02 and non-reflective boundaries)

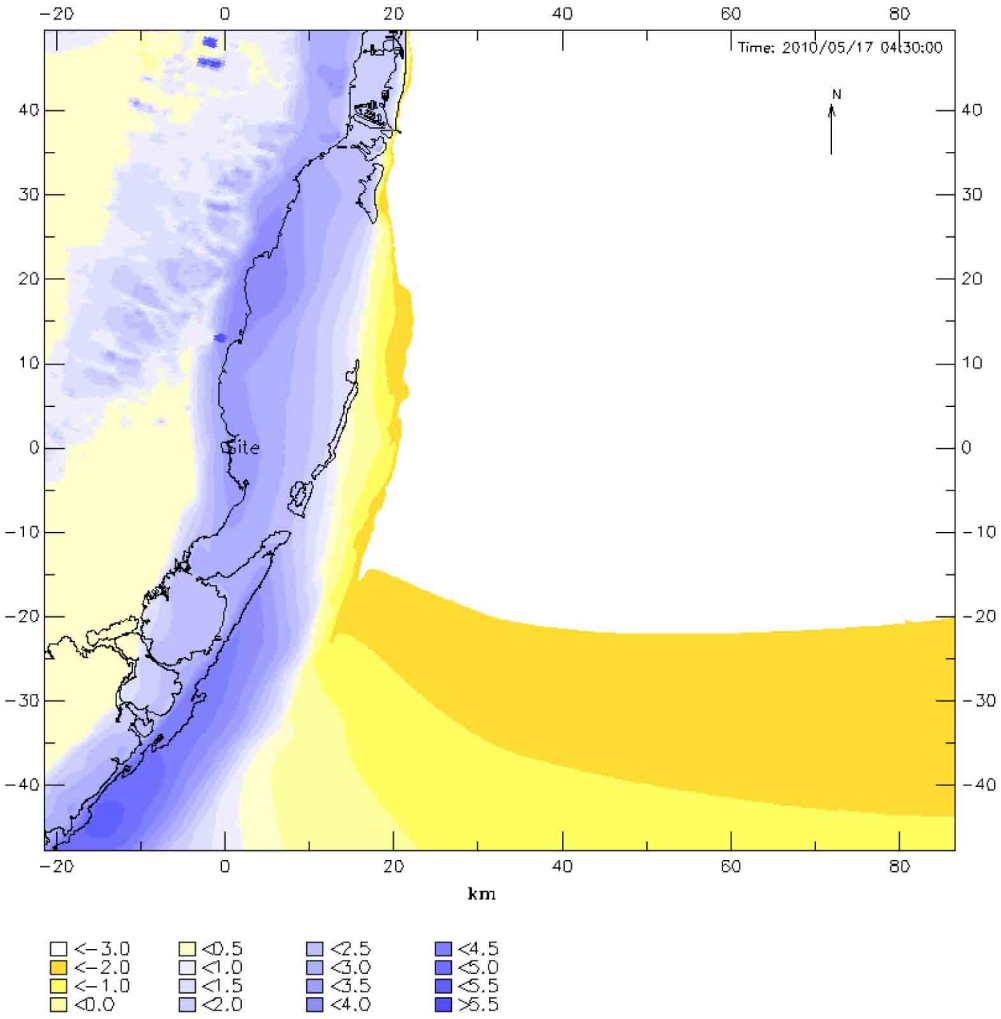

Note: Water levels are in meters **relative to 1.36 m** MSL; some (dry) land elevations are shown as flood water levels according to designation in Delft3D-FLOW.

Figure 2.4.6-220 Tsunami Water Level Contours near the Units 6 & 7 Site 4.5 Hours into the Model Simulation Corresponding to the Time Close to the Maximum Water Level at Site (with Manning's n of 0.02 and non-reflective boundaries)

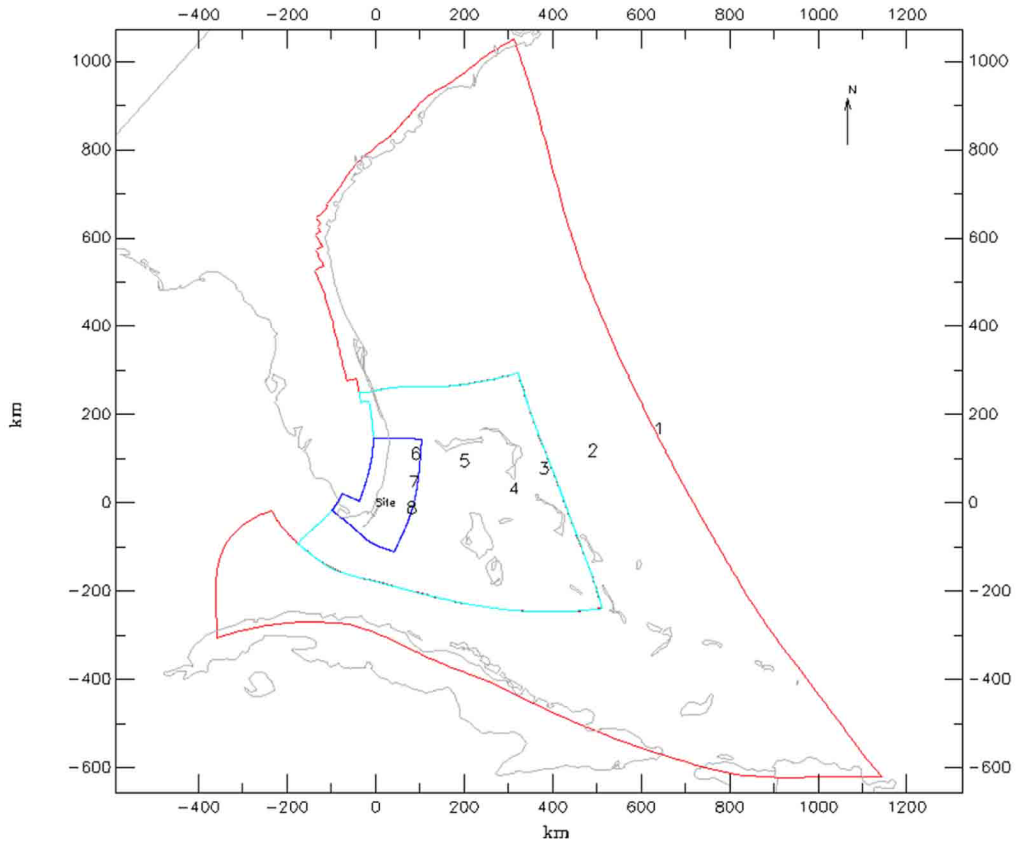

Figure 2.4.6-221a Location of Simulated Water Level Monitoring Points along Track 1

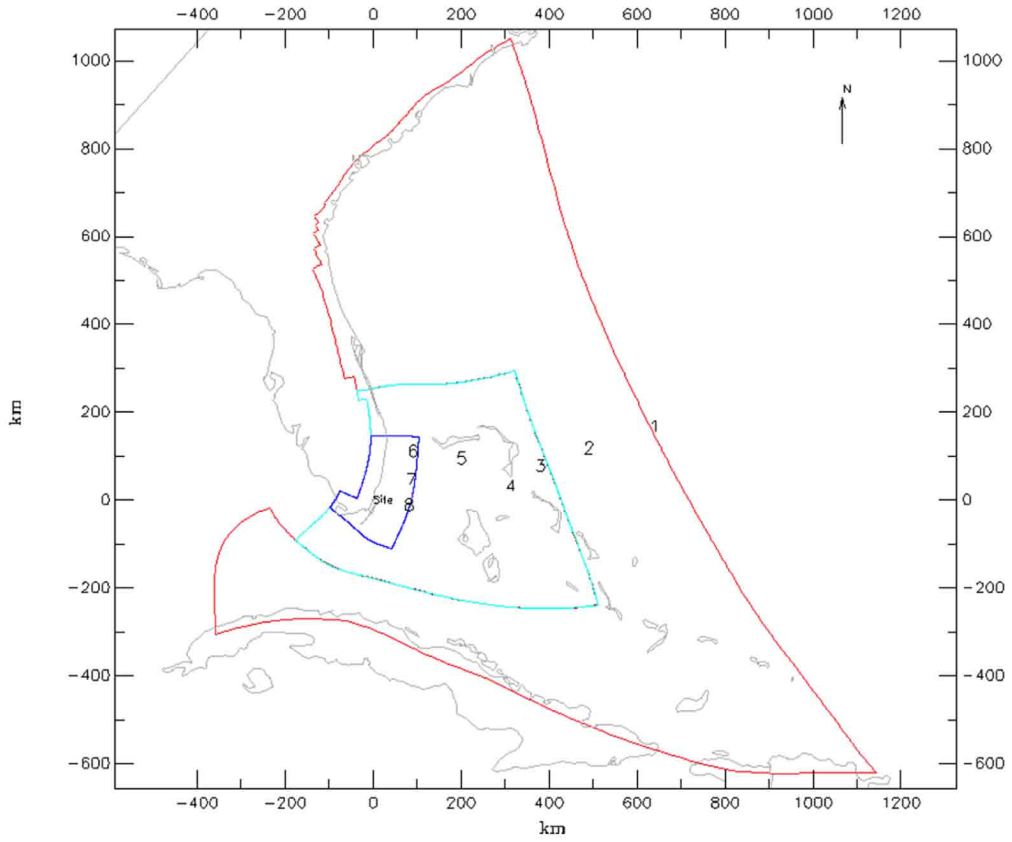

Figure 2.4.6-221b Location of Simulated Water Level Monitoring Points along Track 2

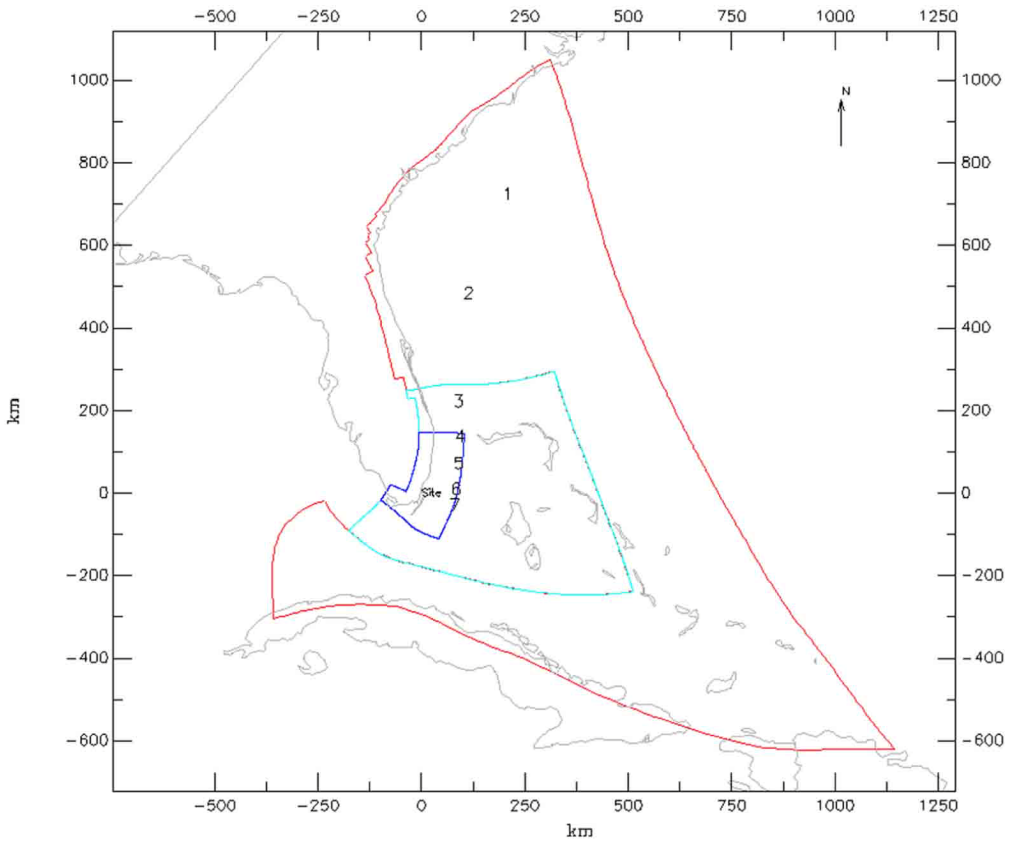

Figure 2.4.6-221c Location of Simulated Water Level Monitoring Points along Track 3

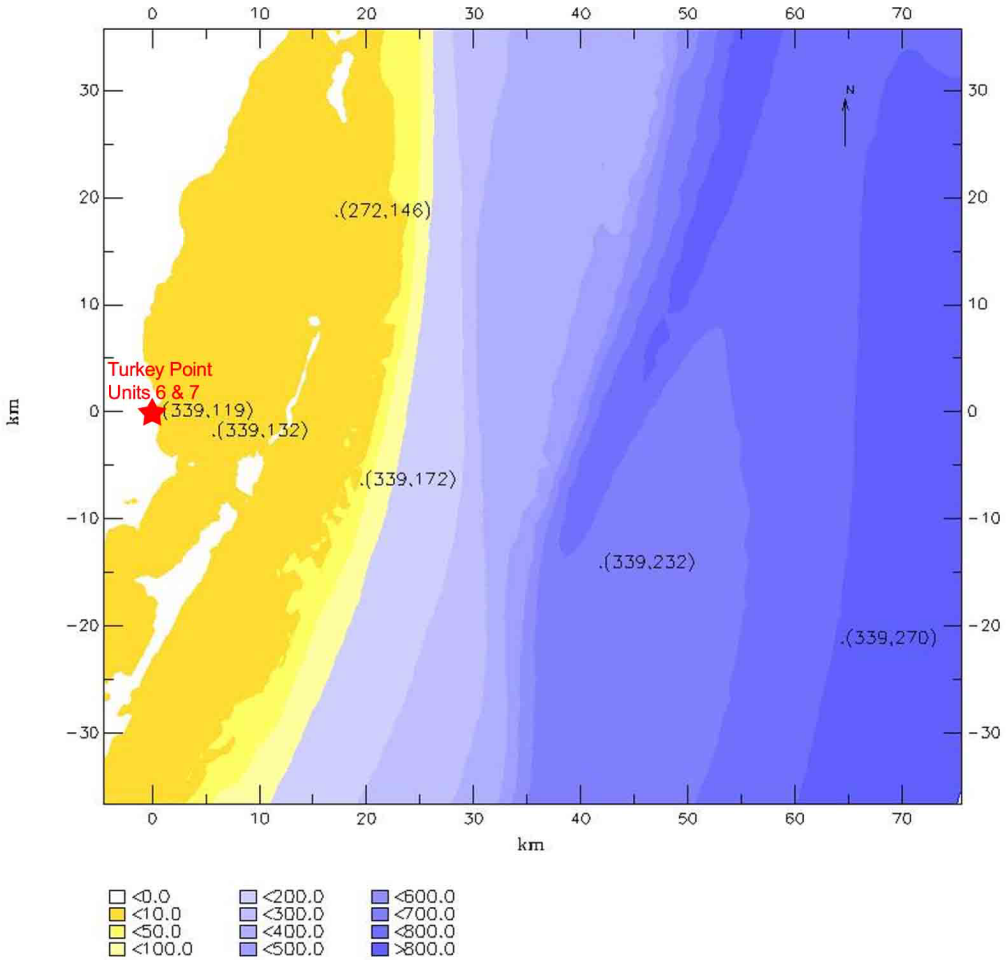

Note: Depths to the seabed are in meters relative to MSL.

Figure 2.4.6-221d Location of Simulated Water Level Monitoring Points in Biscayne Bay and Vicinity (along with water depth contours)

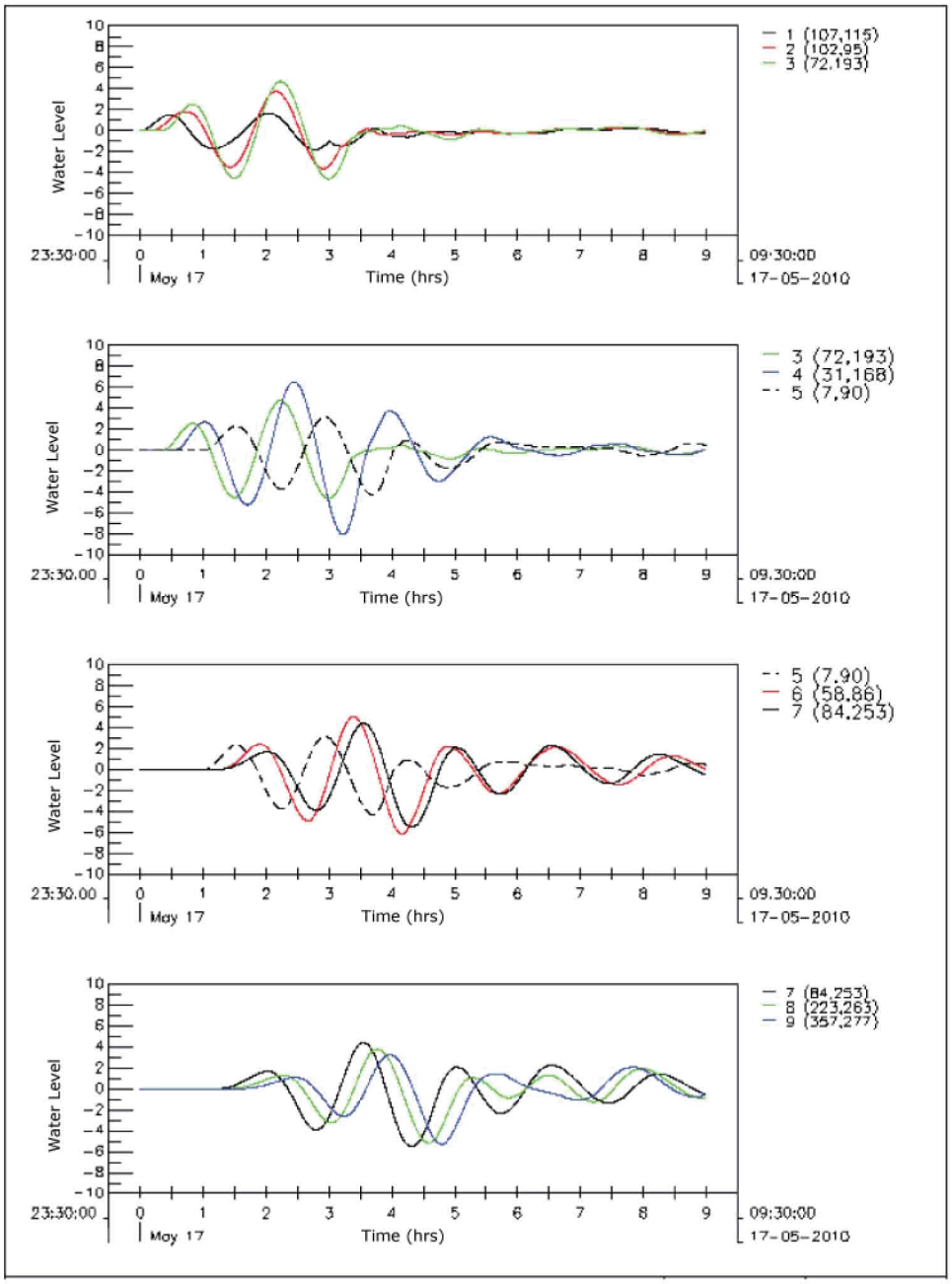

Figure 2.4.6-222 Tsunami Marigrams at Monitoring Points along Track 1, relative to 1.36 m MSL (with Manning's n of 0.02 and non-reflective boundaries)

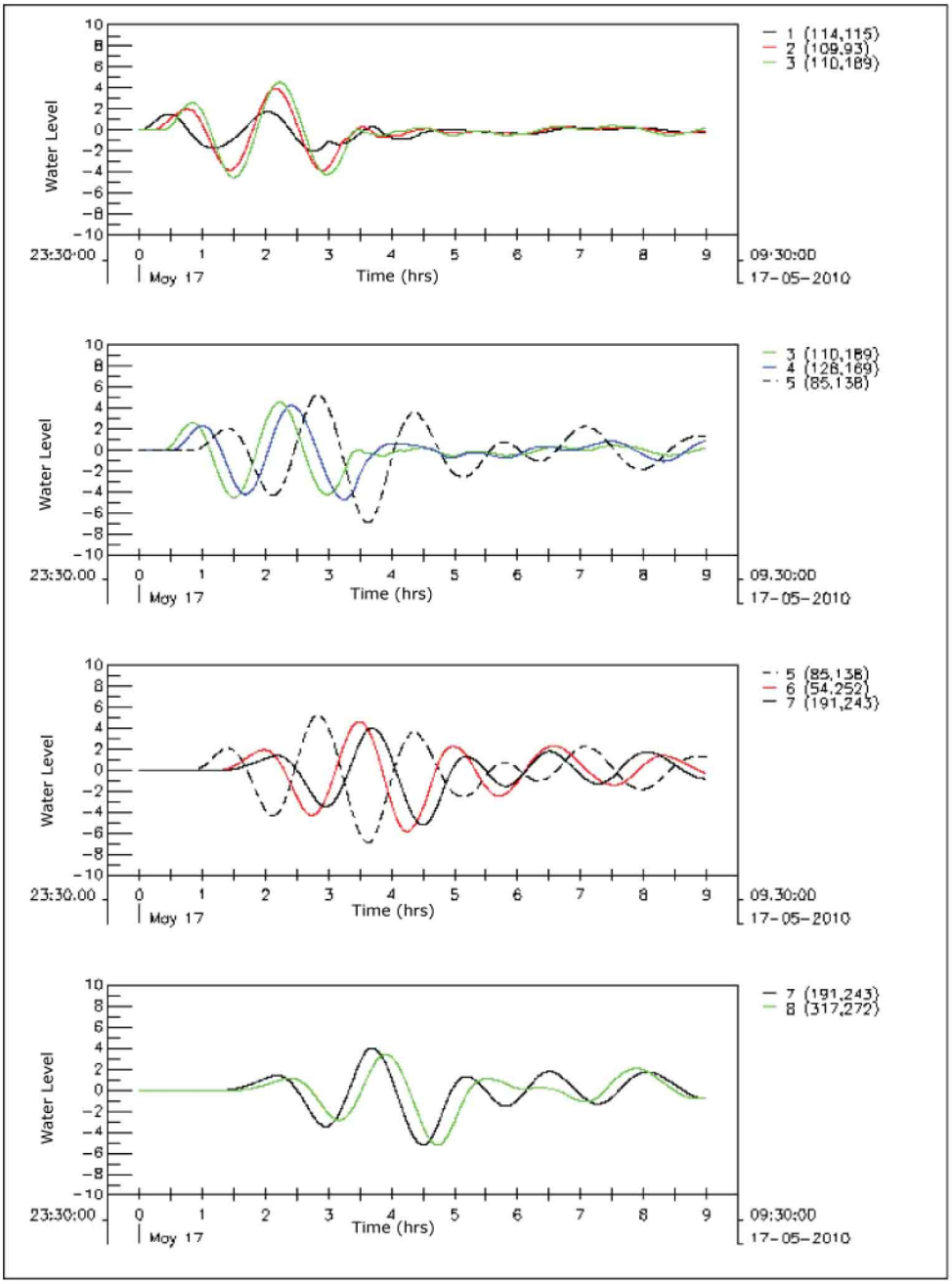

Figure 2.4.6-223 Tsunami Marigrams at Monitoring Points along Track 2, relative to 1.36 m MSL (with Manning's n of 0.02 and non-reflective boundaries)

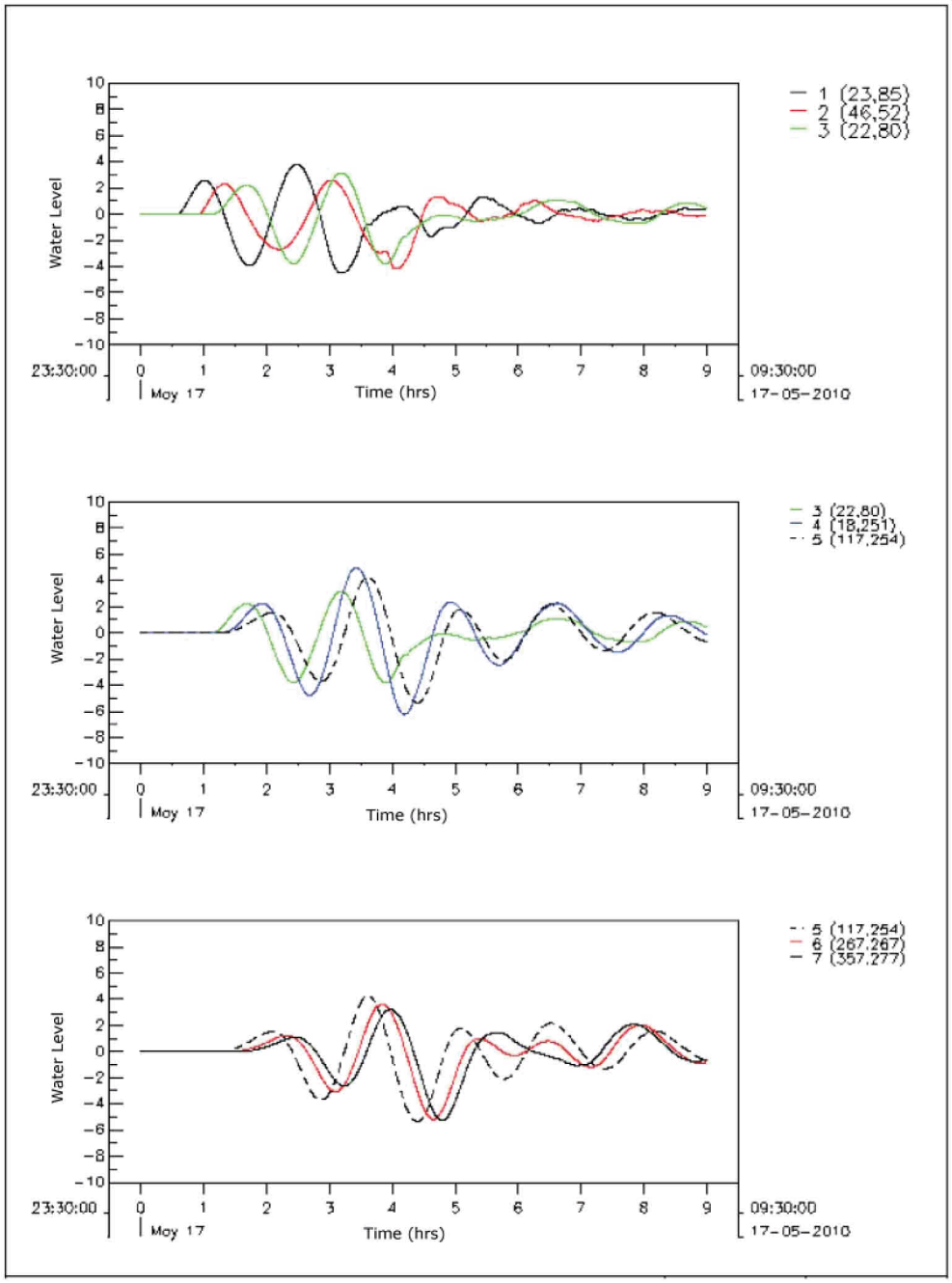

Figure 2.4.6-224 Tsunami Marigrams at Monitoring Points along Track 3, relative to 1.36 m MSL (with Manning's n of 0.02 and non-reflective boundaries)

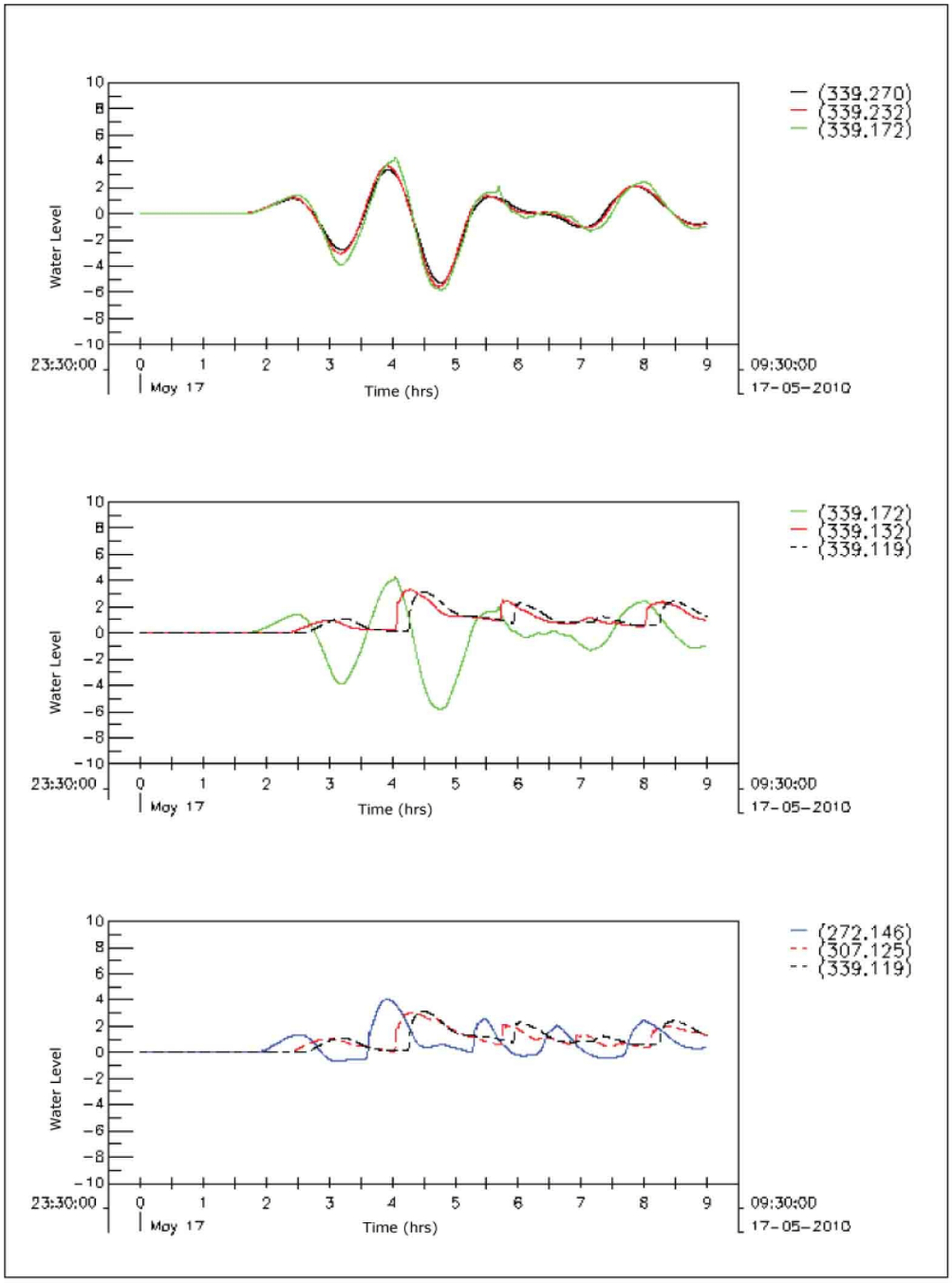

Figure 2.4.6-225 Tsunami Marigrams at Monitoring Points in Biscayne Bay and Vicinity, relative to 1.36 m MSL (with Manning's n of 0.02 and non- reflective boundaries)

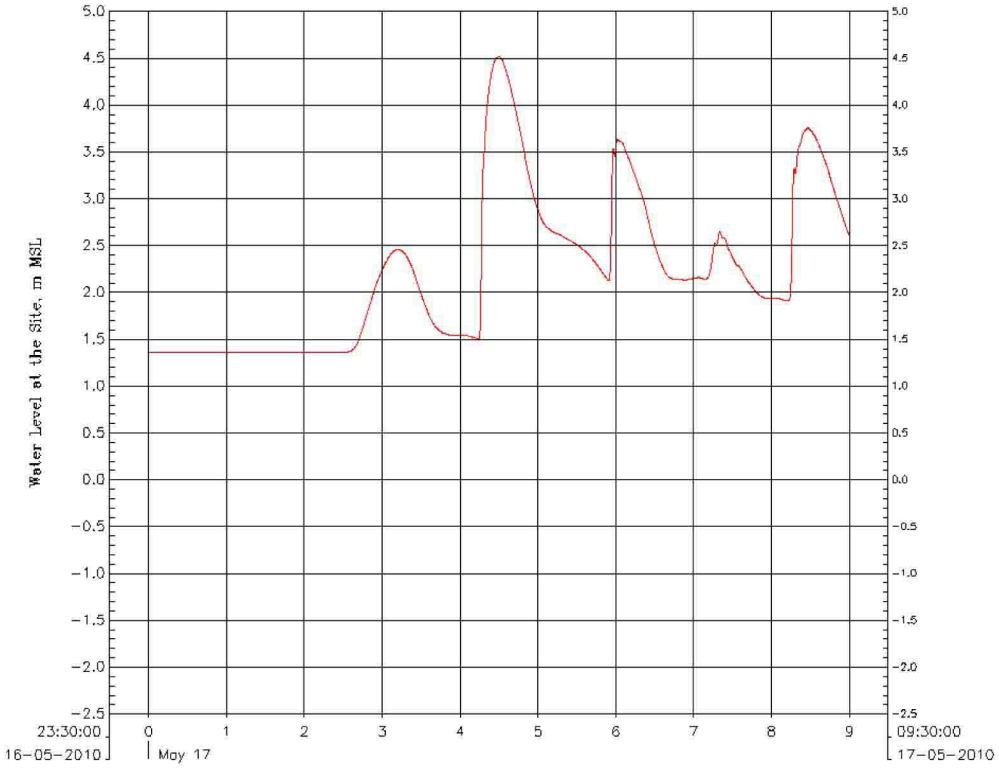

Figure 2.4.6-226 Simulated Tsunami Marigram at the Units 6 & 7 Site (with Manning's n of 0.02 and non-reflective boundaries)

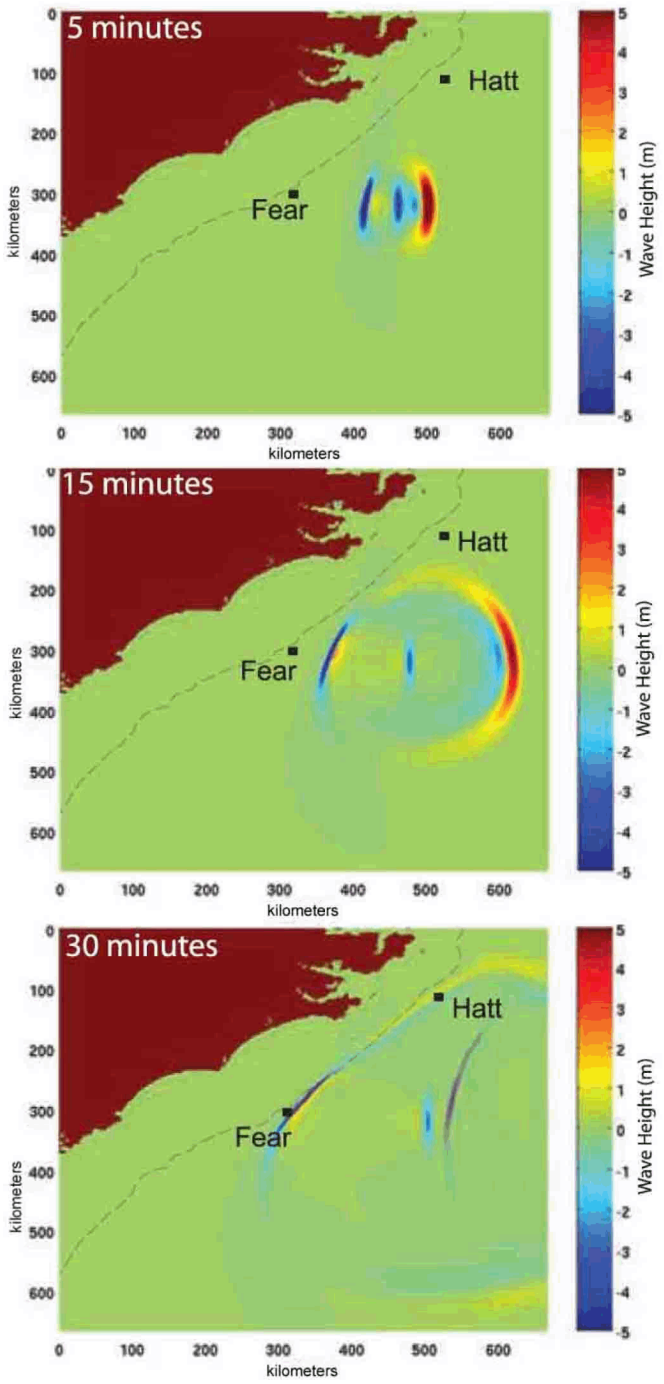

Source: Reference 223

Figure 2.4.6-227 Tsunami Wave Amplitude Results for 5, 15, and 30 Minutes after Slide Initiation of the Largest Landslide Within Cape Fear Slide Complex

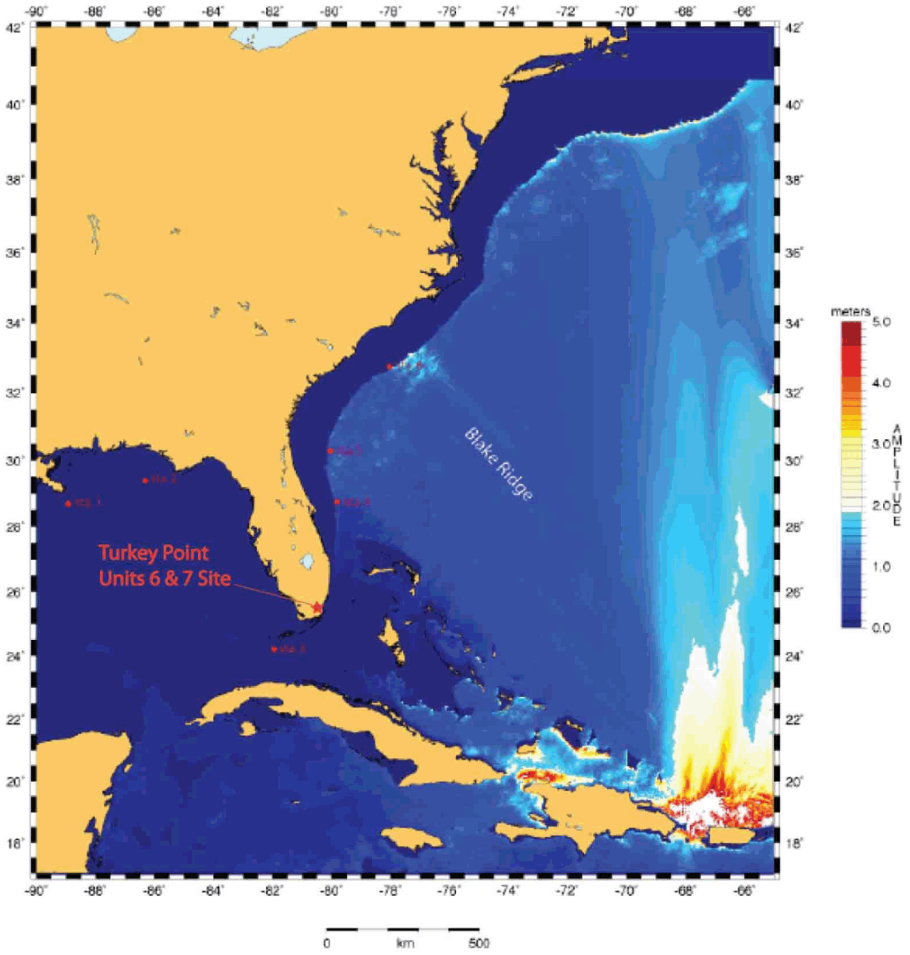

Source: Reference 202

Figure 2.4.6-228 A Simulation Result of Maximum Open-Ocean Tsunami Amplitude Over 4.4 Hours of Propagation Time for North Puerto Rico/Lesser Antilles Subduction Zone

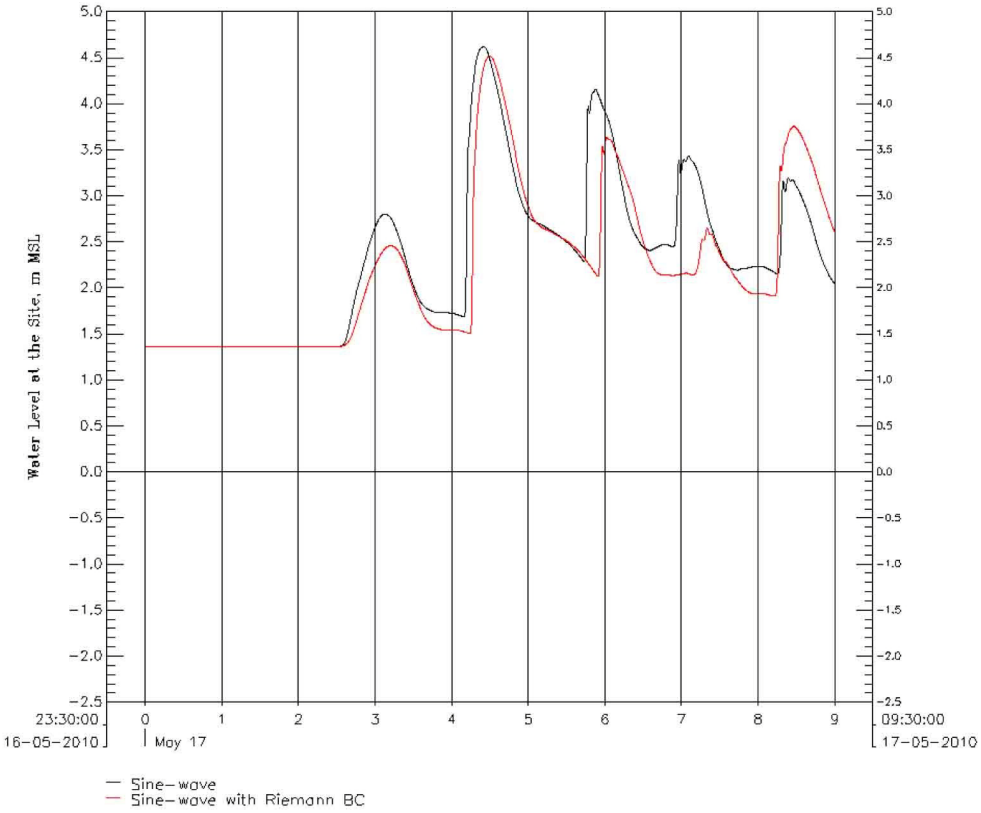

Figure 2.4.6-229 Water Levels at the Site for Incoming Tsunami Sine-Wave With and Without Riemann BC

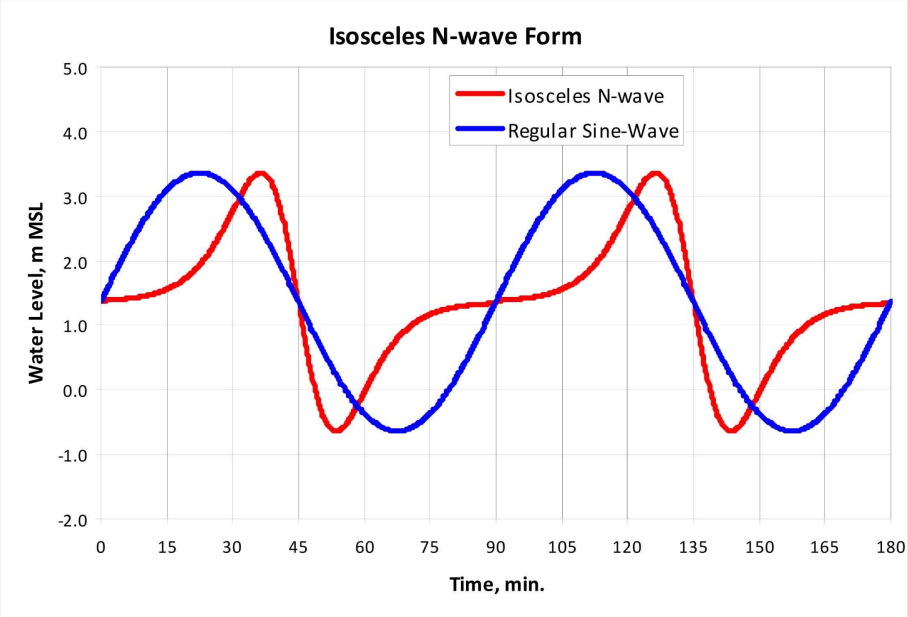

Figure 2.4.6-230 Isosceles N-Wave Form in Comparison with a Sine-Wave Form

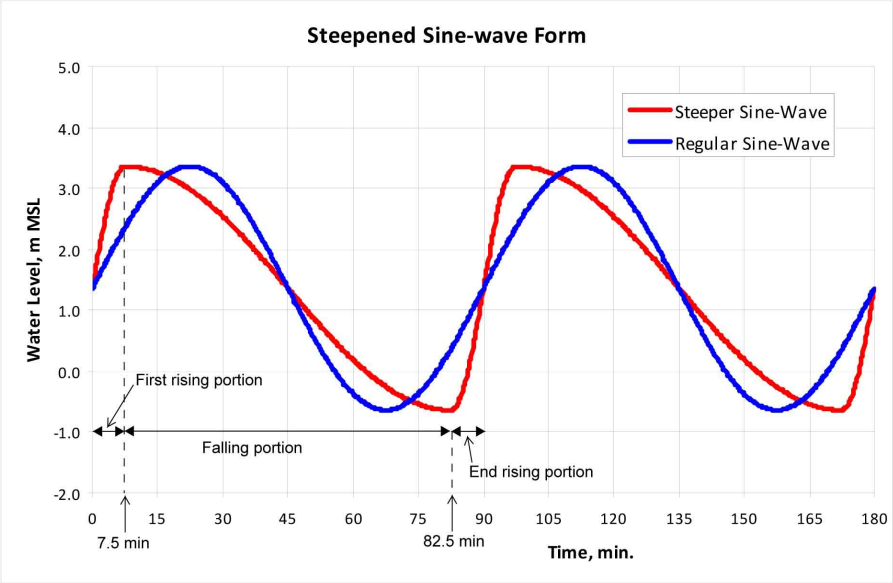

Figure 2.4.6-231 Steepened Sine-Wave Form in Comparison with a Regular Sine-Wave Form

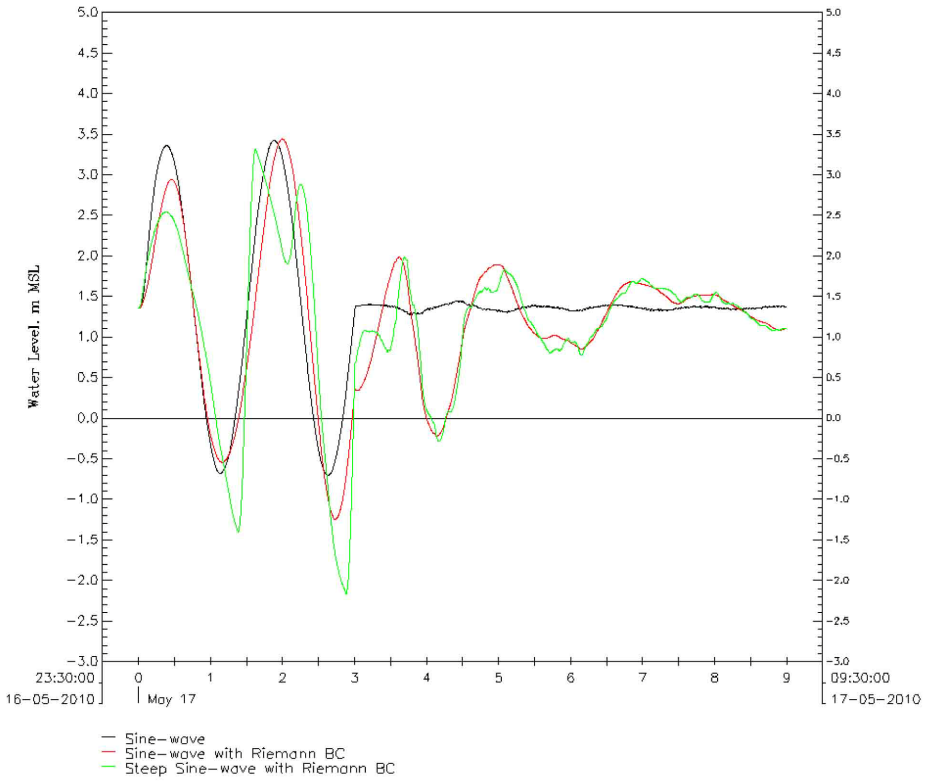

Figure 2.4.6-232 Time History of Water Level at the Forcing Boundary for Steepened Sine-Wave Form

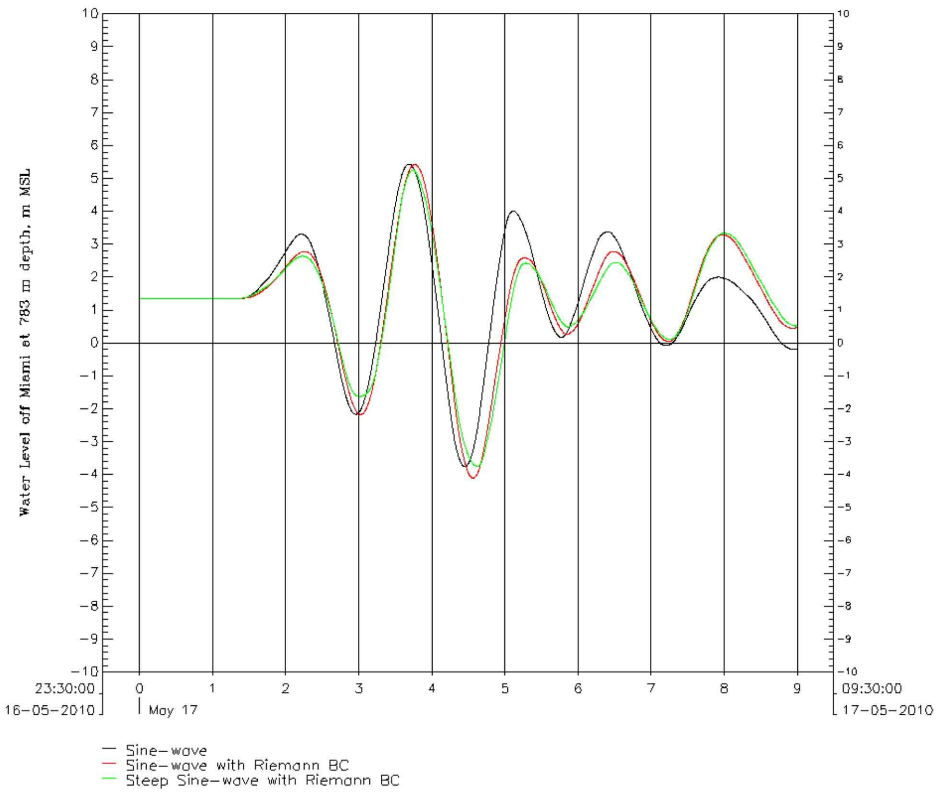

Figure 2.4.6-233 Time History of Water Level Off Miami at Water Depth of 783 Meters (2569 Feet) for Steepened Sine-Wave Form

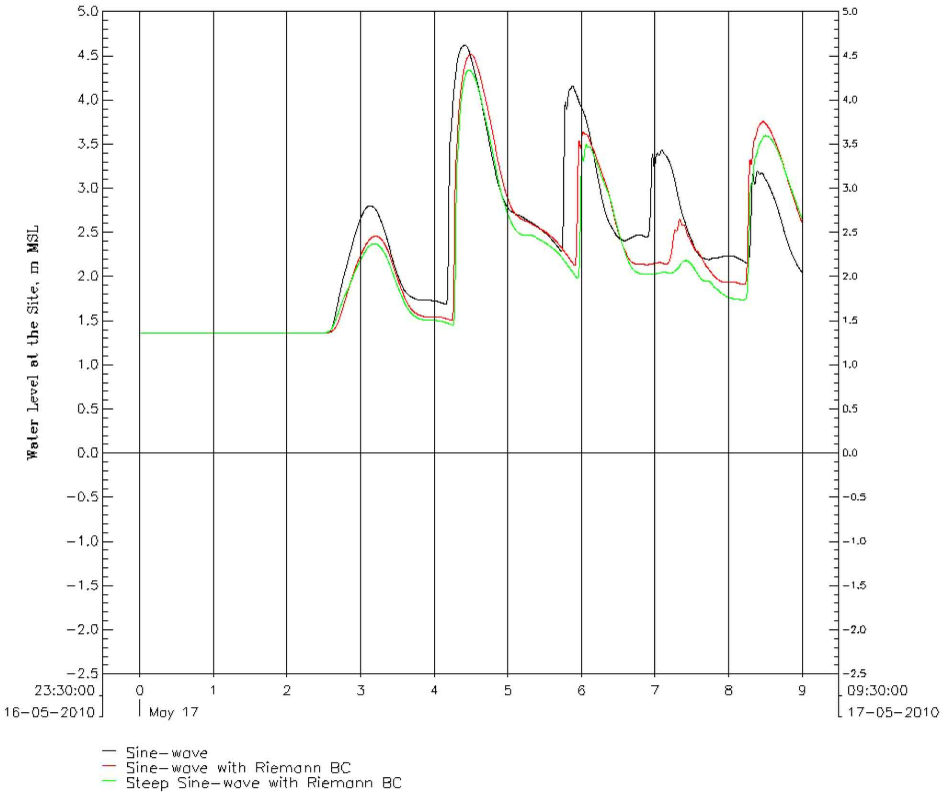

Figure 2.4.6-234 Time History of Water Level at the Site for Steepened Sine-Wave Form

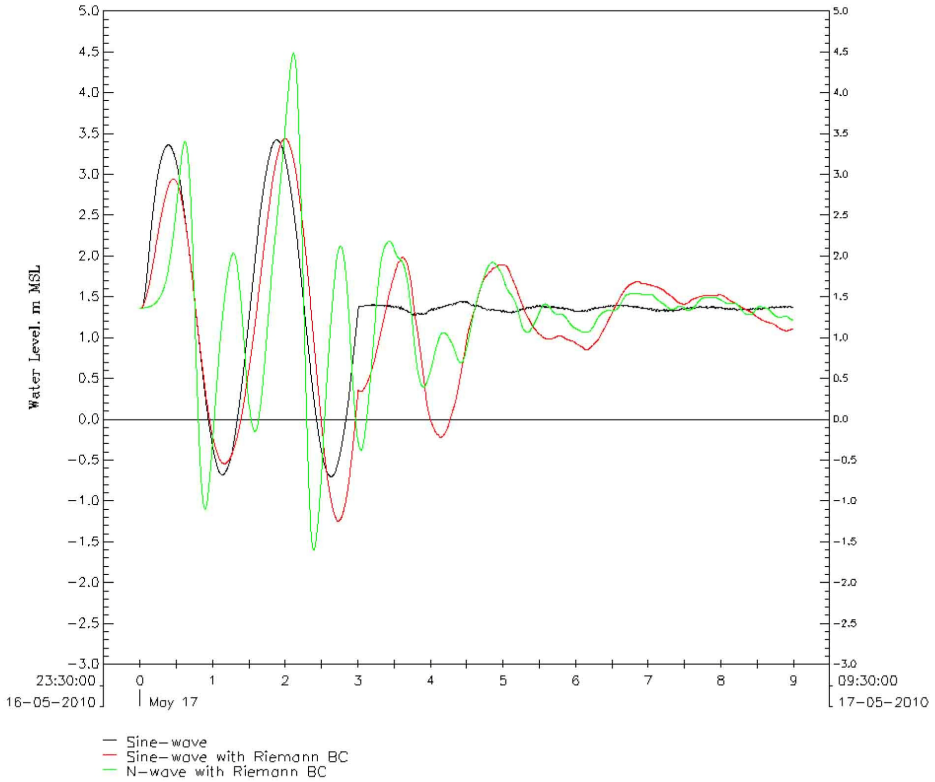

Figure 2.4.6-235 Time History of Water Level at the Forcing Boundary for Isosceles N-Wave Form

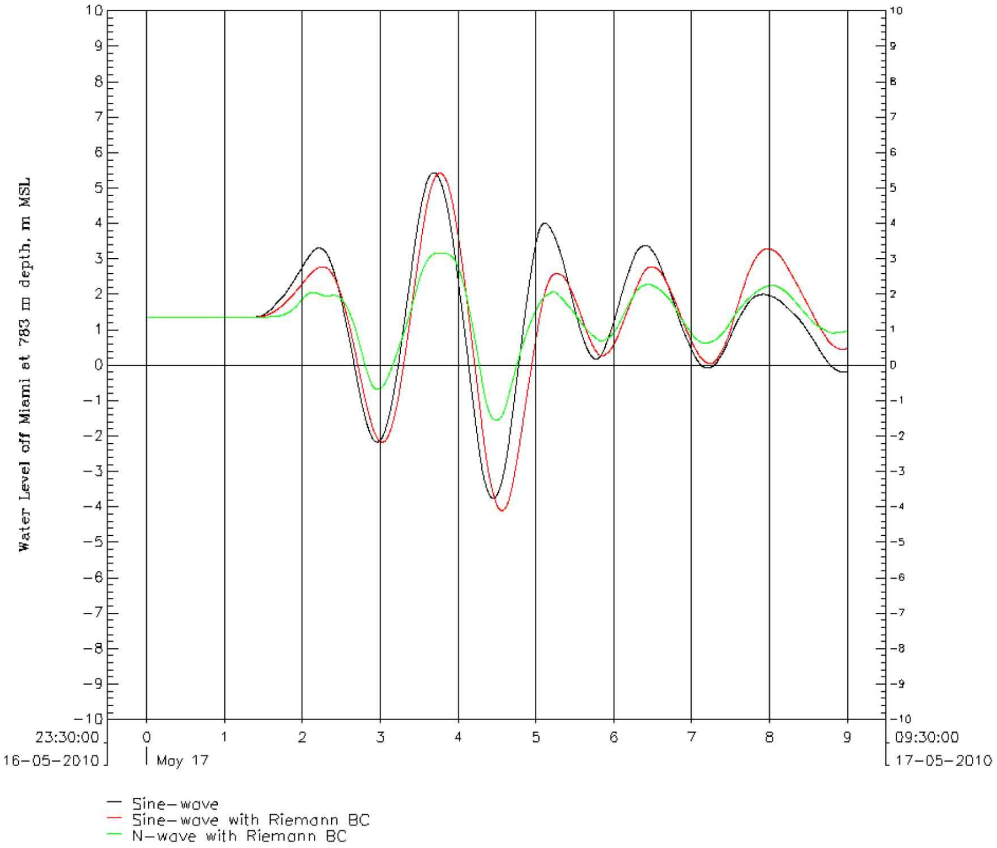

Figure 2.4.6-236 Time History of Water Level Off Miami at Water Depth of 783 Meters (2569 Feet) for Isosceles N-Wave Form

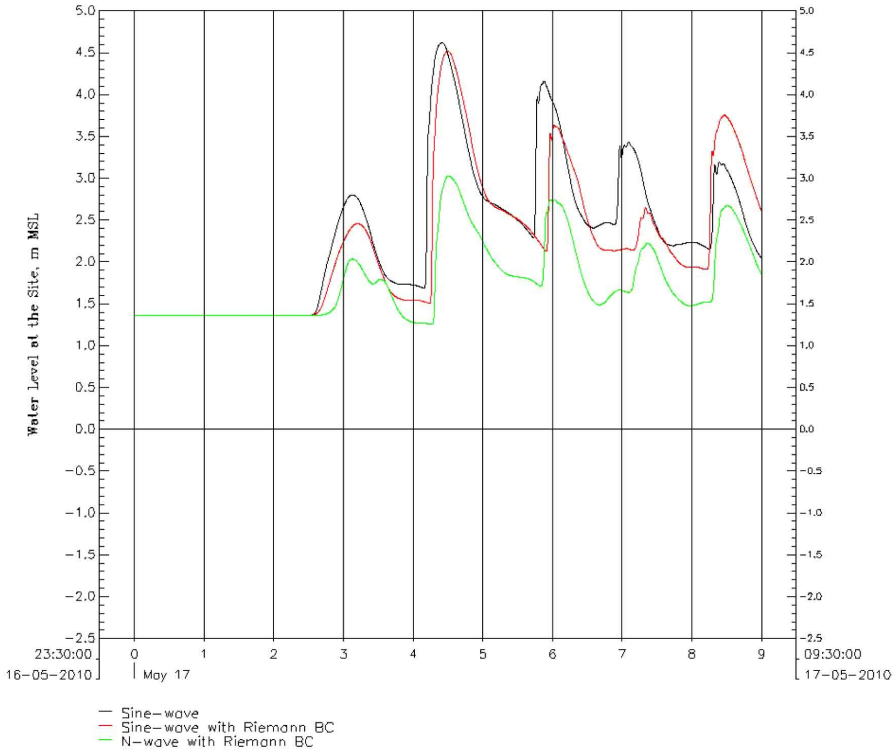

Figure 2.4.6-237 Time History of Water Level at the Site for Isosceles N-Wave Form

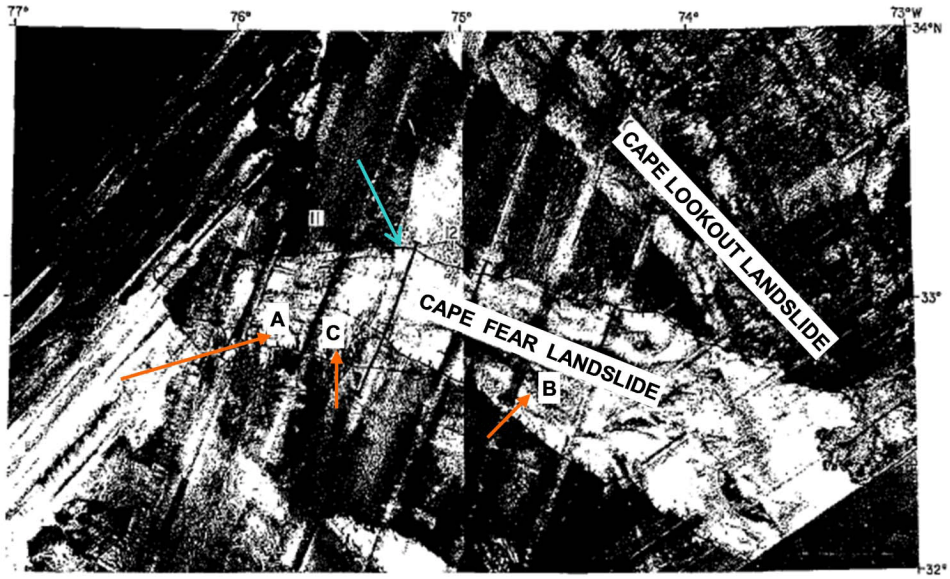

Source: Reference 225.

Note: Hachures pointing downslope represents scarps. The lighter acoustic return seen in the image represent mass movement deposits and the dark return are the undisturbed sedimentary deposits. The location (A) is the longitudinal lines representing both debris chutes between the salt diapirs at the head of the landslide area, and flow paths of debris further down slope, which is shown with location (B). Location (C) is an area of irregular, hummocky sea floor that has been crumpled and buckled by mass movement near the head of the slide. The blue arrow indicates the northern limit of the Cape Fear landslide.

Figure 2.4.6-238 GLORIA Sidescan-sonar Image of the Cape Fear Slide

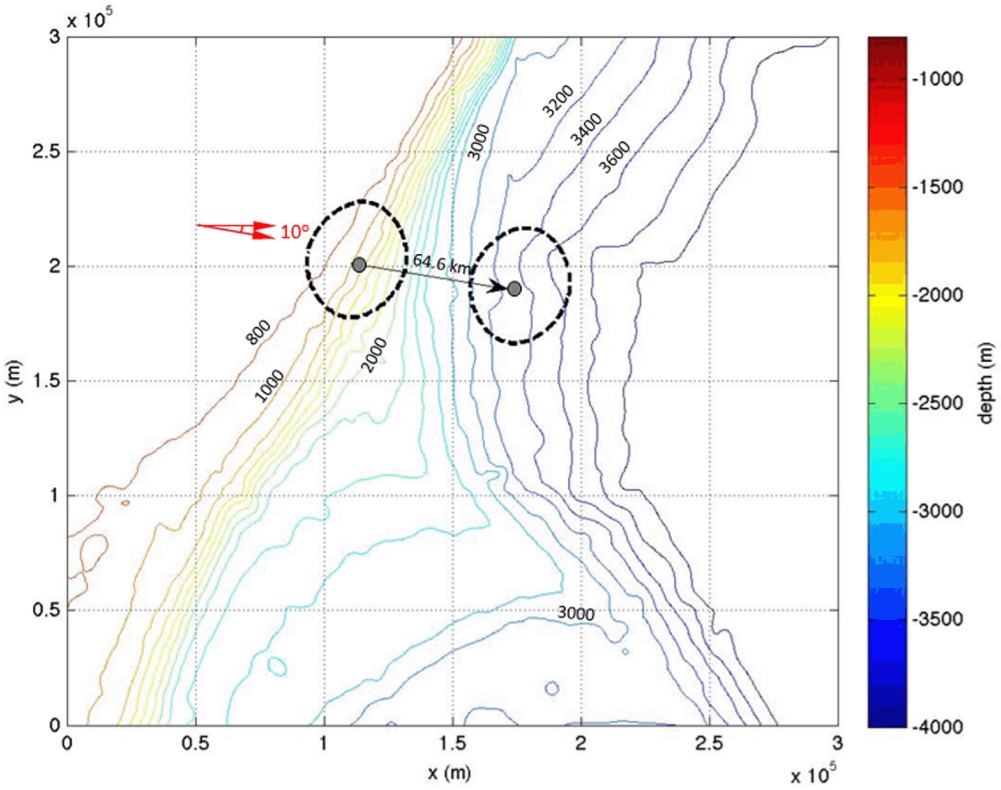

Note: Bathymetry contours indicate water depths (MSL).

Figure 2.4.6-239 Location and Lateral Extent of the Postulated Submarine Mass Failure for the Cape Fear Simulations and Local Bathymetry

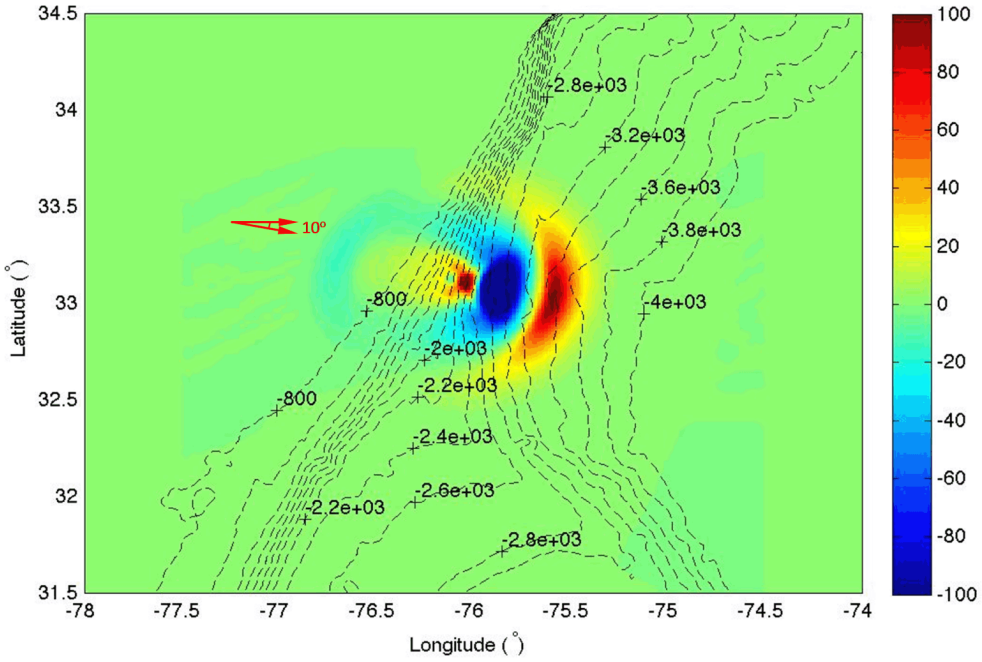

Note: Colors in elevation legend indicate water surface elevation (MSL) in meters. Bathymetry contours indicate water depths (m MSL).

Figure 2.4.6-240 Initial Wave Generated by NHWAVE (Dynamic Source) for the Cape Fear Submarine Failure Shown in Figure 2.4.6-239

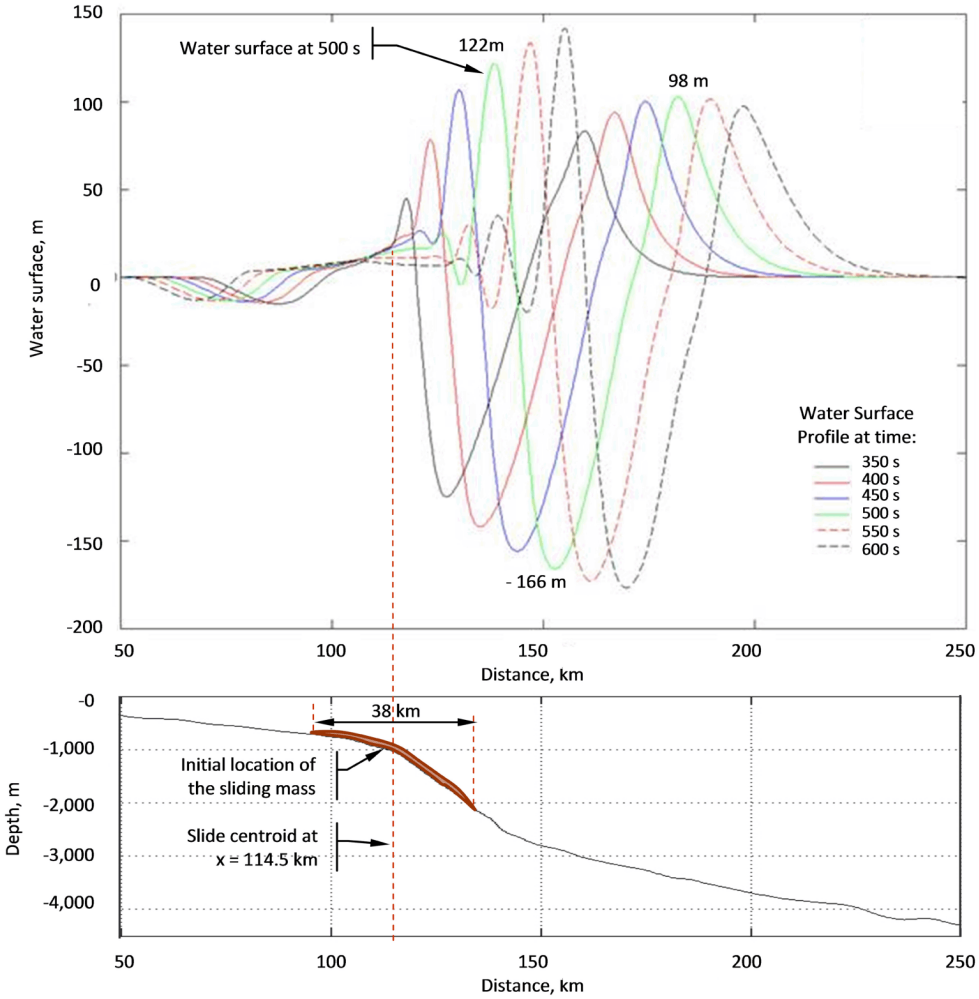

Note: Water surface elevations (upper panel) and water depths (lower panel) are relative to MSL.

Figure 2.4.6-241 Water Surface Profile in the Direction of the Slide Motion at Different Times after the Initiation of the Slide (Upper Panel) and Ocean Floor Profile (Lower Panel)

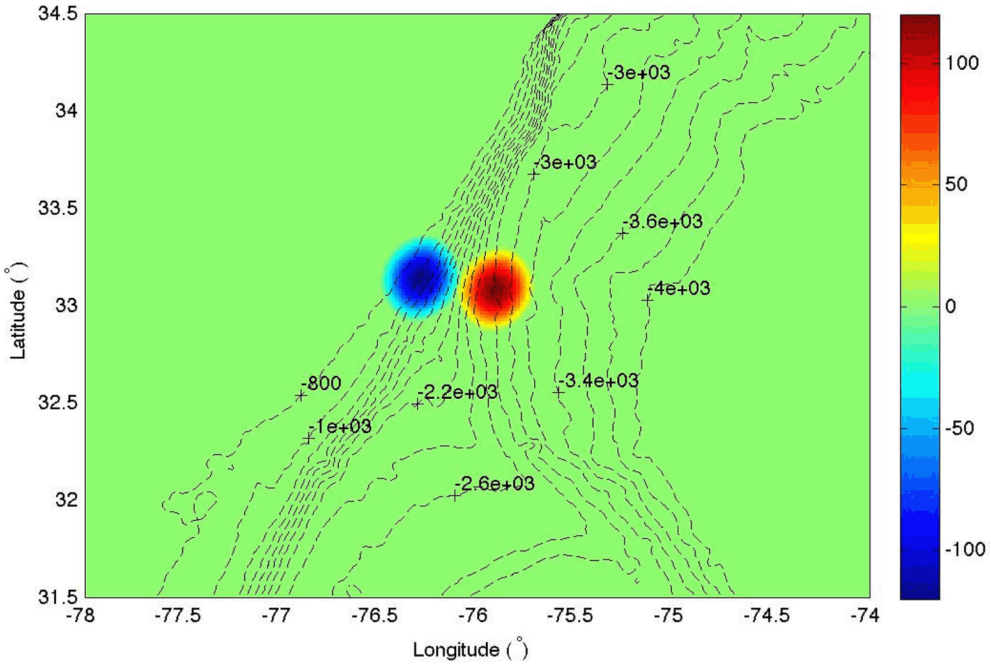

Note: Colors in elevation legend indicate water surface elevation (MSL) in meters. Bathymetry contours indicate water depths (MSL).

Figure 2.4.6-242 Initial Wave for a Static Source Representation of the Cape Fear Submarine Failure Shown in Figure 2.4.6-239

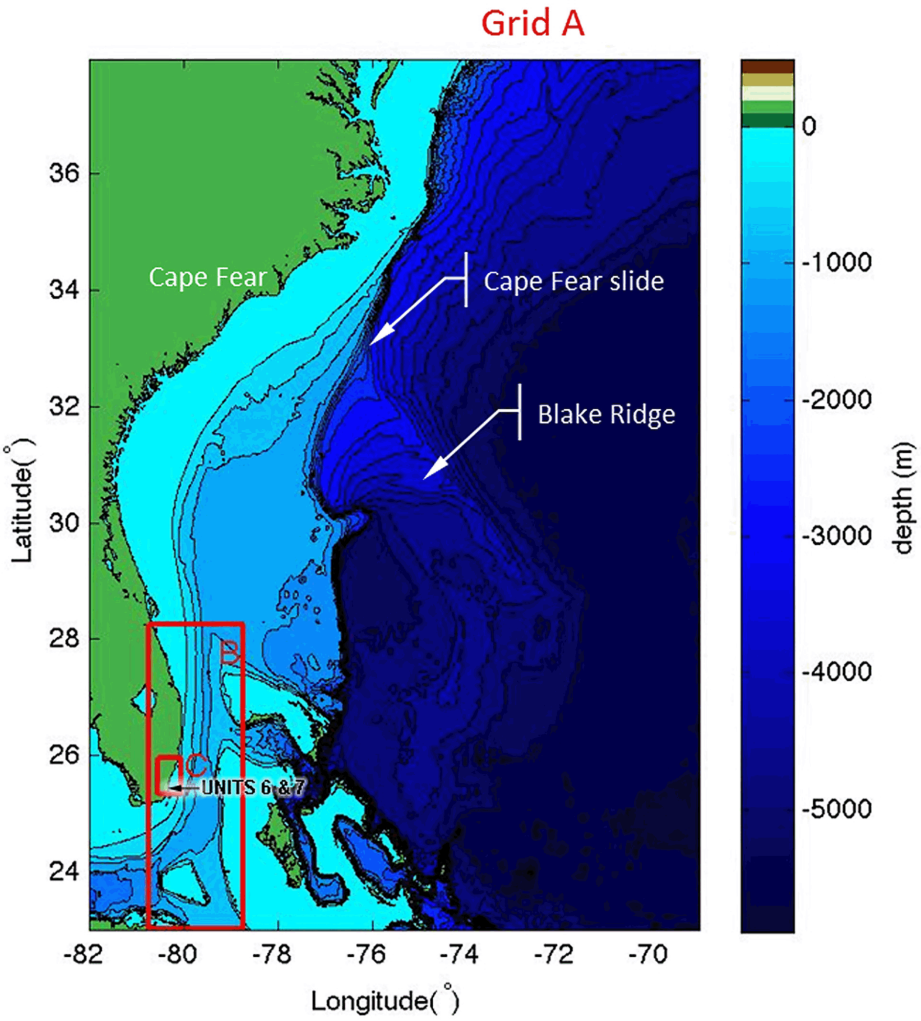

Note: Colors in elevation legend represent water surface elevations relative to MSL for ETOPO1 data and MLW for Coastal Relief Model data.

Figure 2.4.6-243 Model Domain And Bathymetry in the Three Nested Grids Used in the FUNWAVE-TVD Simulations

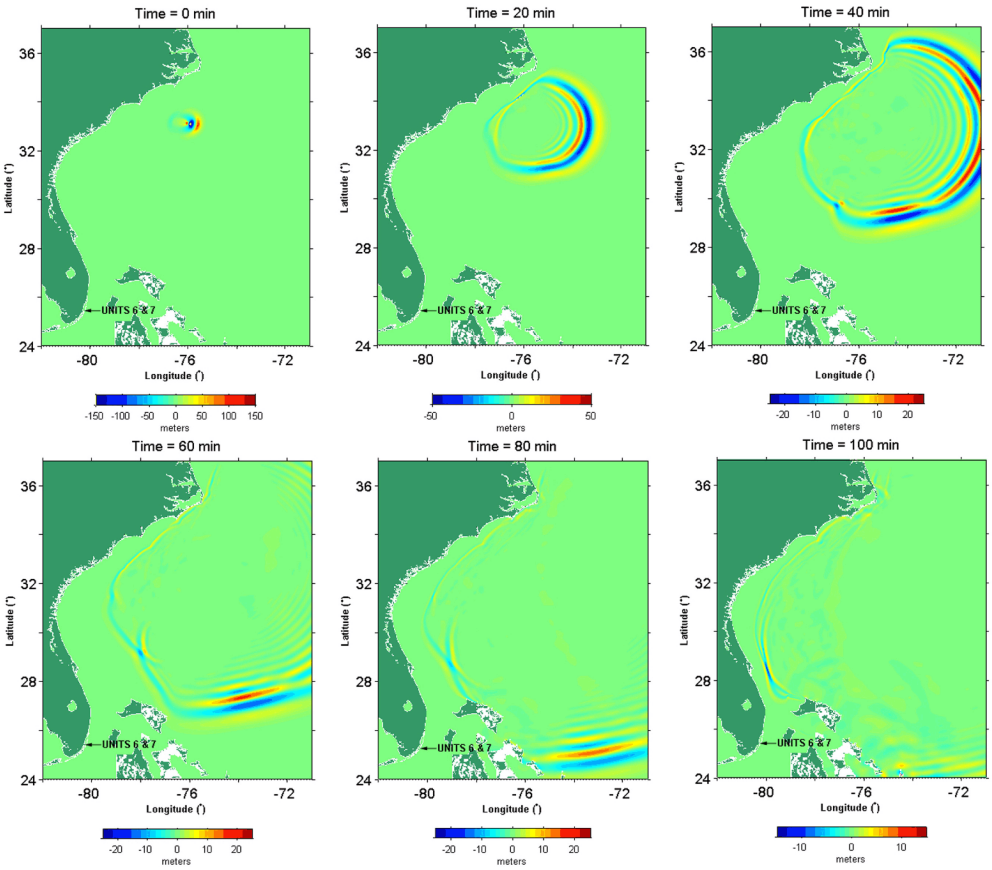

Note: Colors in elevation legend represent water surface elevations relative to MSL for ETOPO1 data and MLW for Coastal Relief Model data.

Figure 2.4.6-244 Simulated Propagation of the Cape Fear Tsunami (Dynamic Source) in Grid A at 0, 20, 40, 60, 80, and 100 Minutes after the Submarine Failure

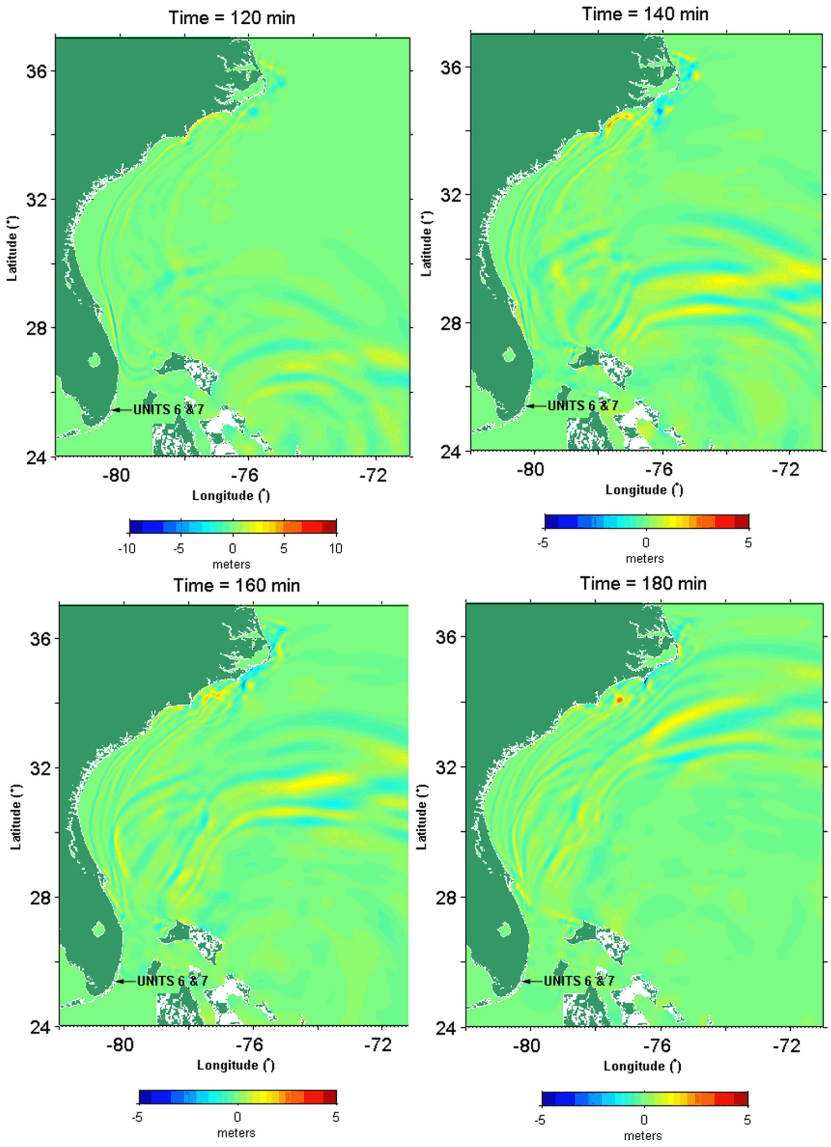

Note: Colors in elevation legend represent water surface elevations relative to MSL for ETOPO1 data and MLW for Coastal Relief Model data.

Figure 2.4.6-245 Simulated Propagation of the Cape Fear Tsunami (Dynamic Source) in Grid A at 120, 140, 160, and 180 Minutes after the Submarine Failure

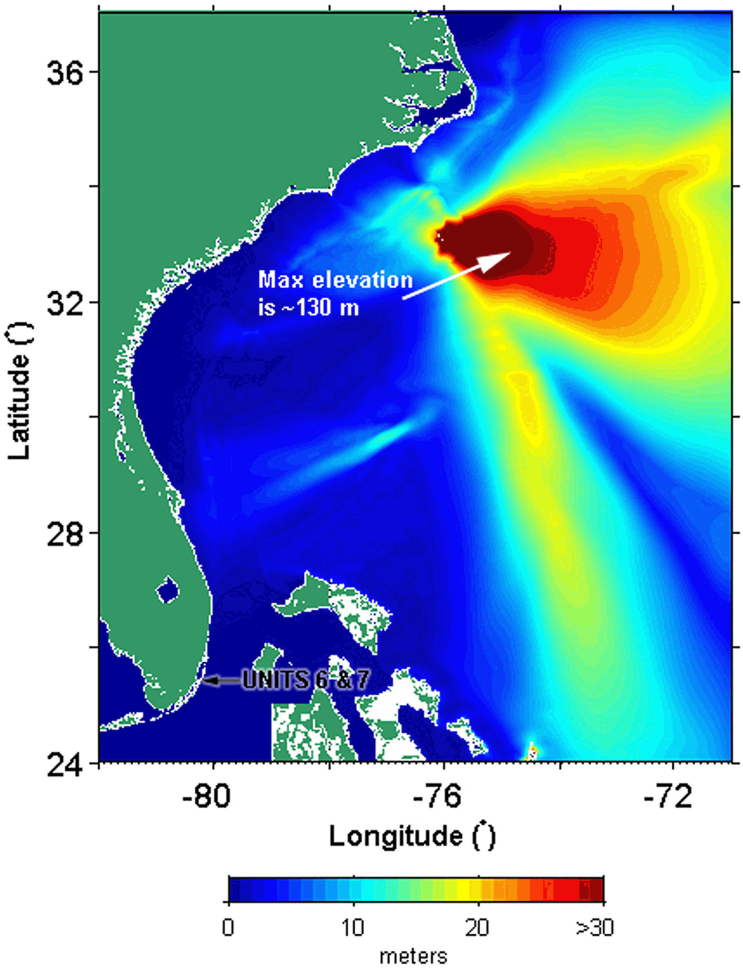

Note: Colors in elevation legend represent water surface elevations relative to MSL for ETOPO1 data and MLW for Coastal Relief Model data.

Figure 2.4.6-246 Simulated Maximum Water Surface Elevation during the Propagation of the Cape Fear Tsunami (Dynamic Source) in Grid A

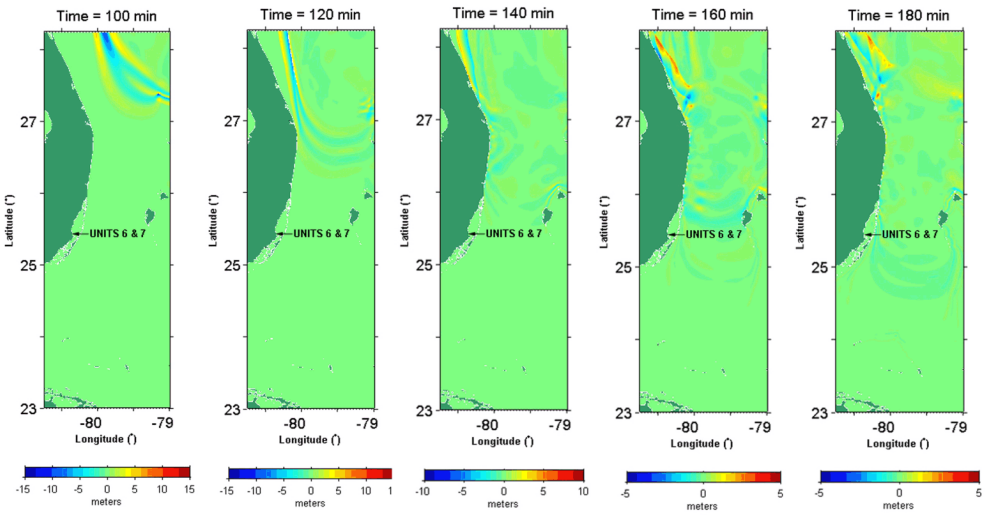

Note: Colors in elevation legend represent water surface elevations relative to MSL for ETOPO1 data and MLW for Coastal Relief Model data.

Figure 2.4.6-247 Simulated Propagation of the Cape Fear Tsunami (Dynamic Source) in Grid B at 100, 120, 140, 160, and 180 Minutes after the Submarine Failure

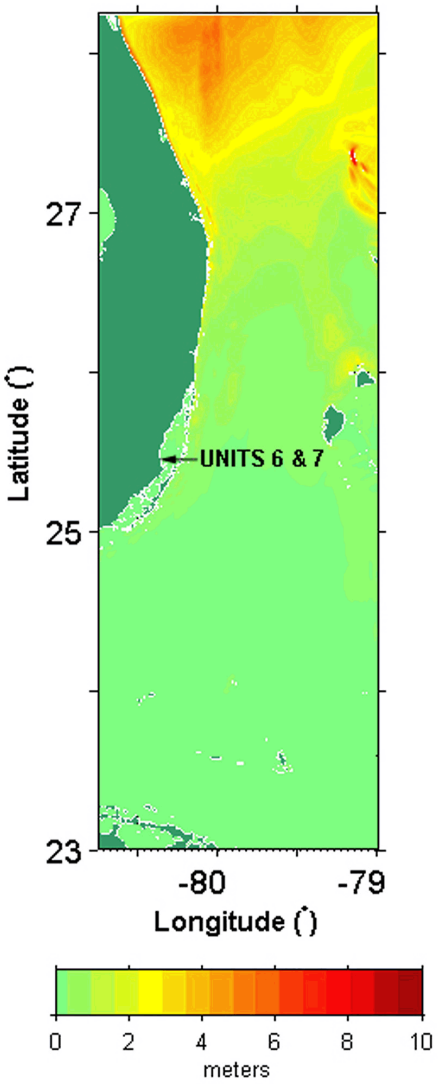

Note: Colors in elevation legend represent water surface elevations relative to MSL for ETOPO1 data and MLW for Coastal Relief Model data.

Figure 2.4.6-248 Simulated Maximum Water Surface Elevation during the Propagation of the Cape Fear Tsunami (Dynamic Source) In Grid B

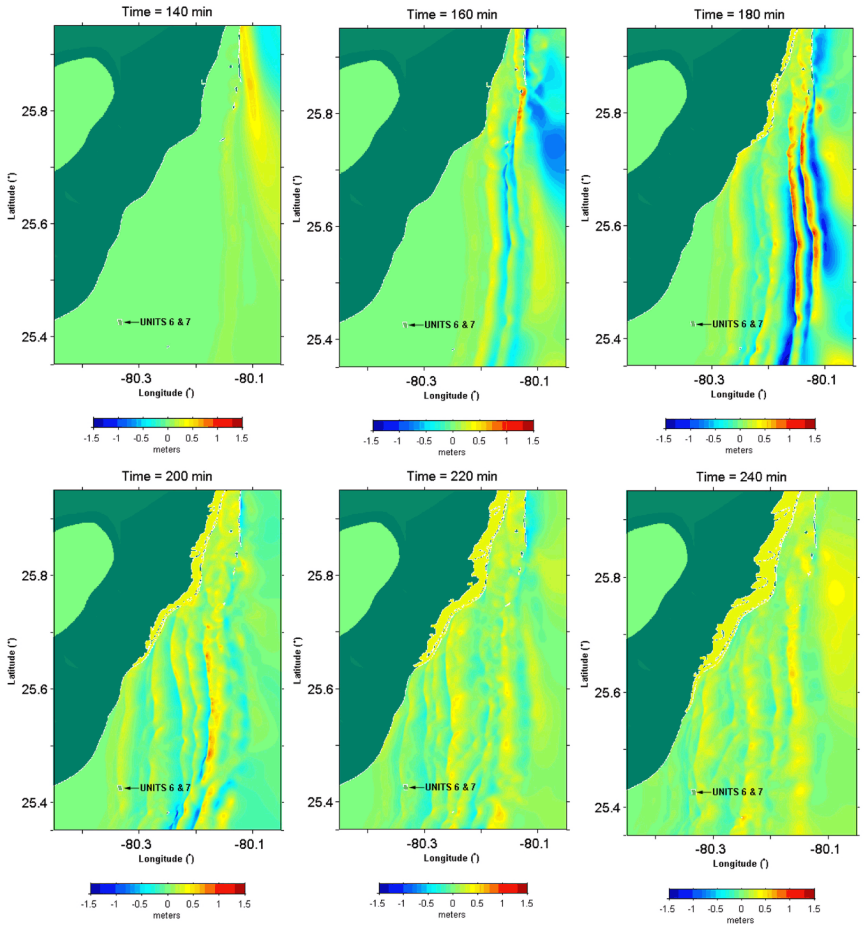

Note: Colors in elevation legend represent water surface elevations relative to MLW.

Figure 2.4.6-249 Simulated Propagation of the Cape Fear Tsunami (Dynamic Source) in Grid C at 140, 160, 180, 200, 220, and 240 Minutes after the Submarine Failure

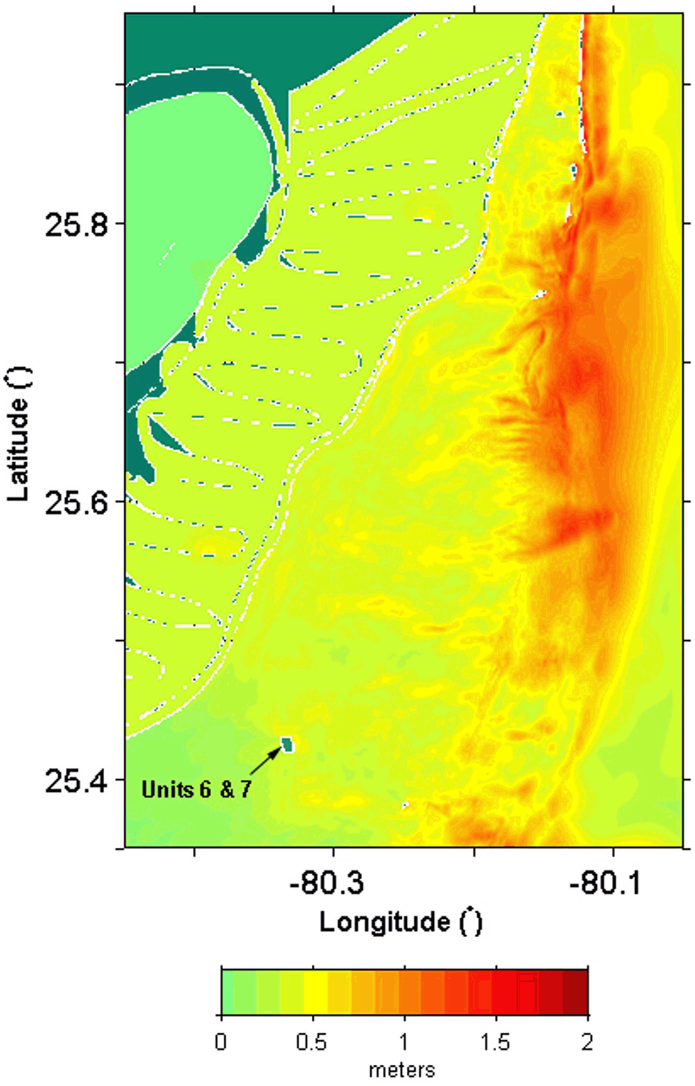

Note: Colors in elevation legend represent water surface elevations relative to MLW.

Figure 2.4.6-250 Simulated Maximum Water Surface Elevation during the Propagation of the Cape Fear Tsunami (Dynamic Source) In Grid C

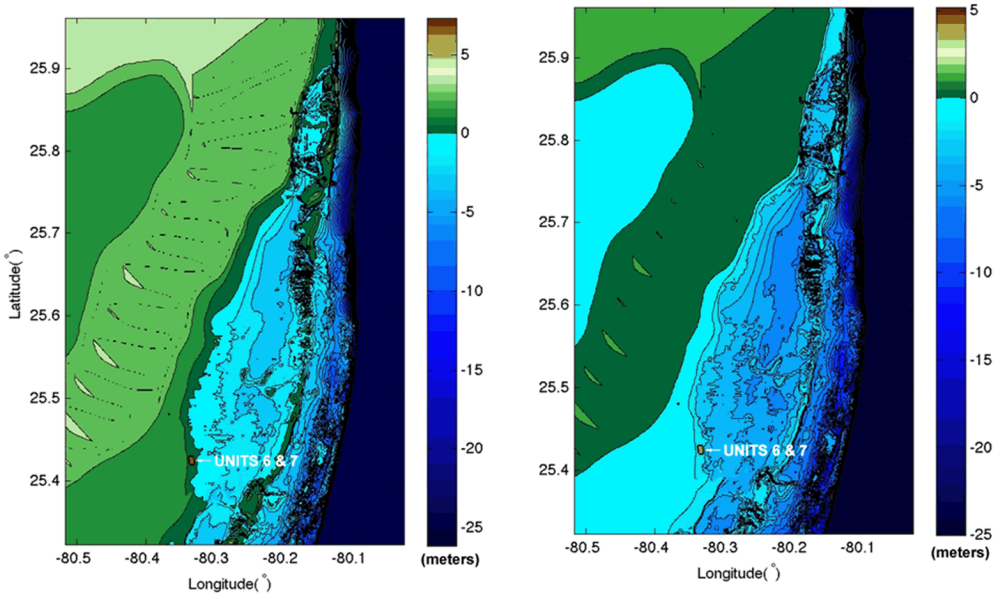

Note: Colors in elevation legend represent water surface elevations relative to MLW.

Figure 2.4.6-251 (a) Water Depth Relative to MLW over the Area of Grid C; and (b) Water Depth Relative to the Assumed Initial Water Surface in the Cape Fear Tsunami Simulations

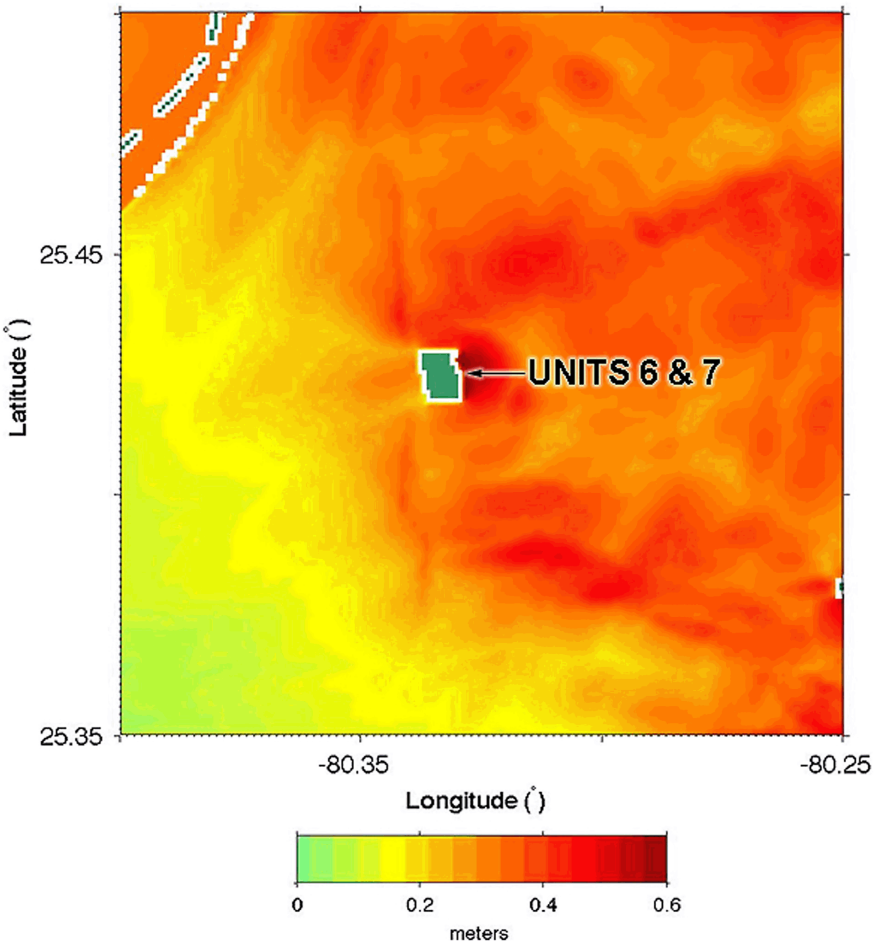

Note: Colors in elevation legend represent water surface elevations relative to MLW.

Figure 2.4.6-252 Simulated Maximum Water Surface Rise, relative to the Initial Sea Water Level, during the Propagation of the Cape Fear Tsunami (Dynamic Source) in the Vicinity of Units 6 & 7

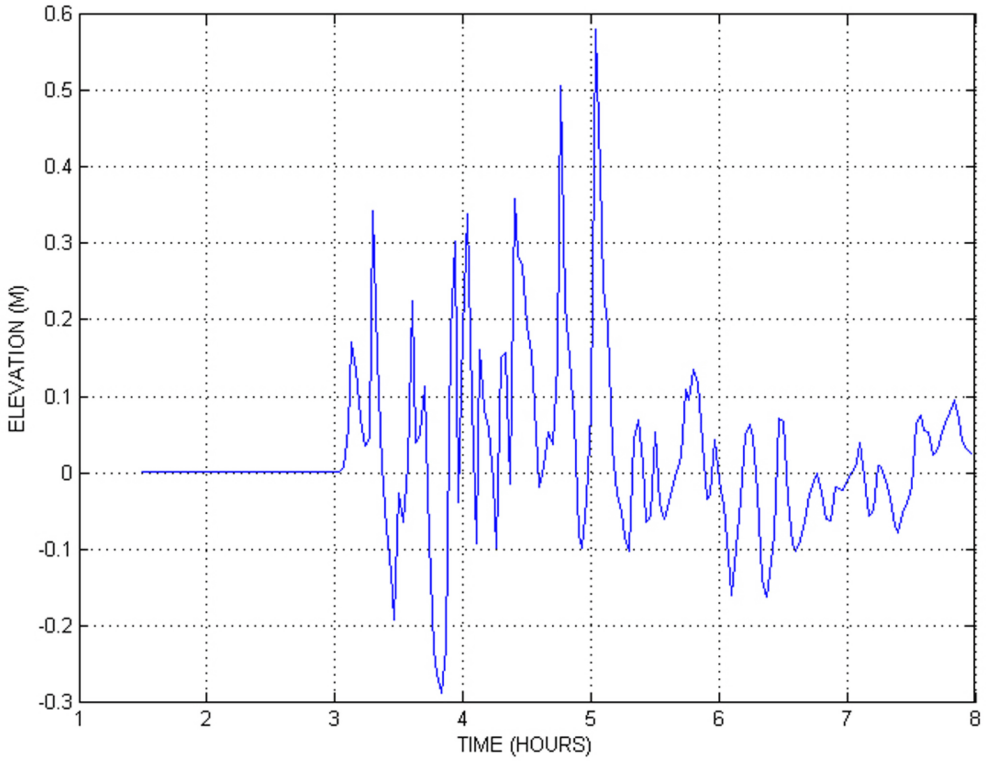

Note: Water surface elevations are relative to the initial water level.

Figure 2.4.6-253 Water Surface Elevation Near Units 6 & 7 as a Function of Time Following the Cape Fear Tsunami (Dynamic Source)

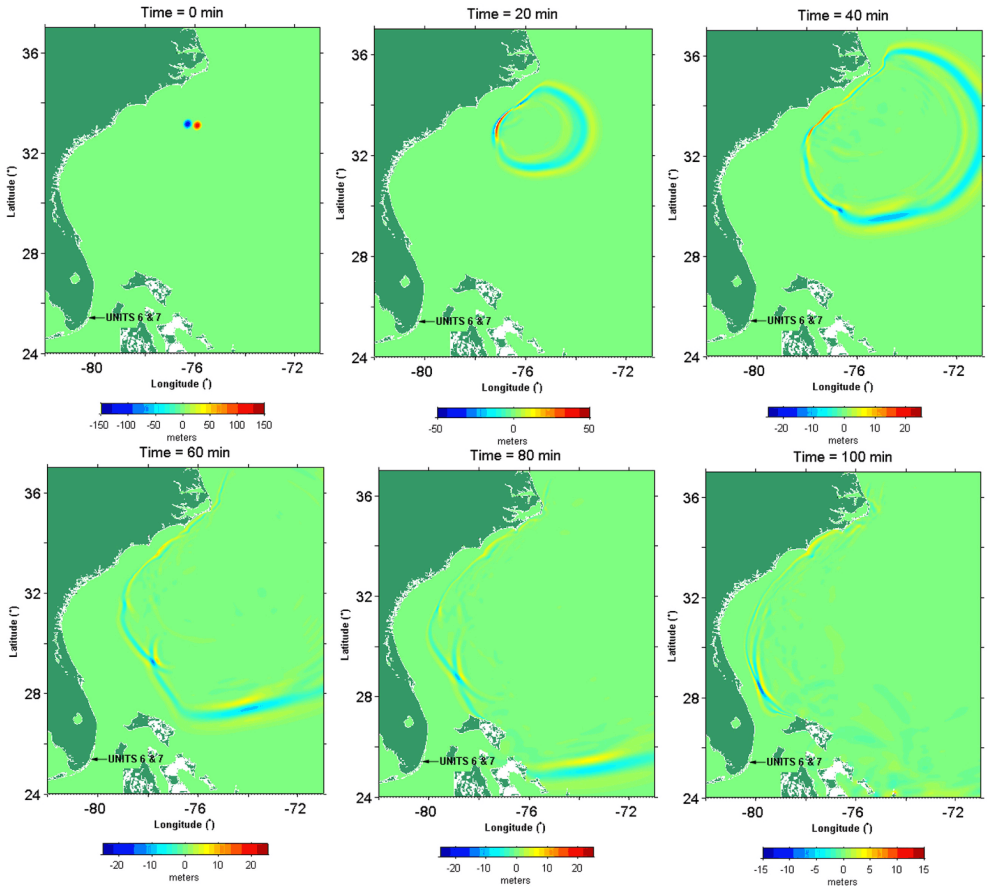

Note: Colors in elevation legend represent water surface elevations relative to MSL for ETOPO1 data and MLW for Coastal Relief Model data.

Figure 2.4.6-254 Simulated Propagation of the Cape Fear Tsunami (Static Source) in Grid A at 0, 20, 40, 60, 80, and 100 Minutes after the Submarine Failure

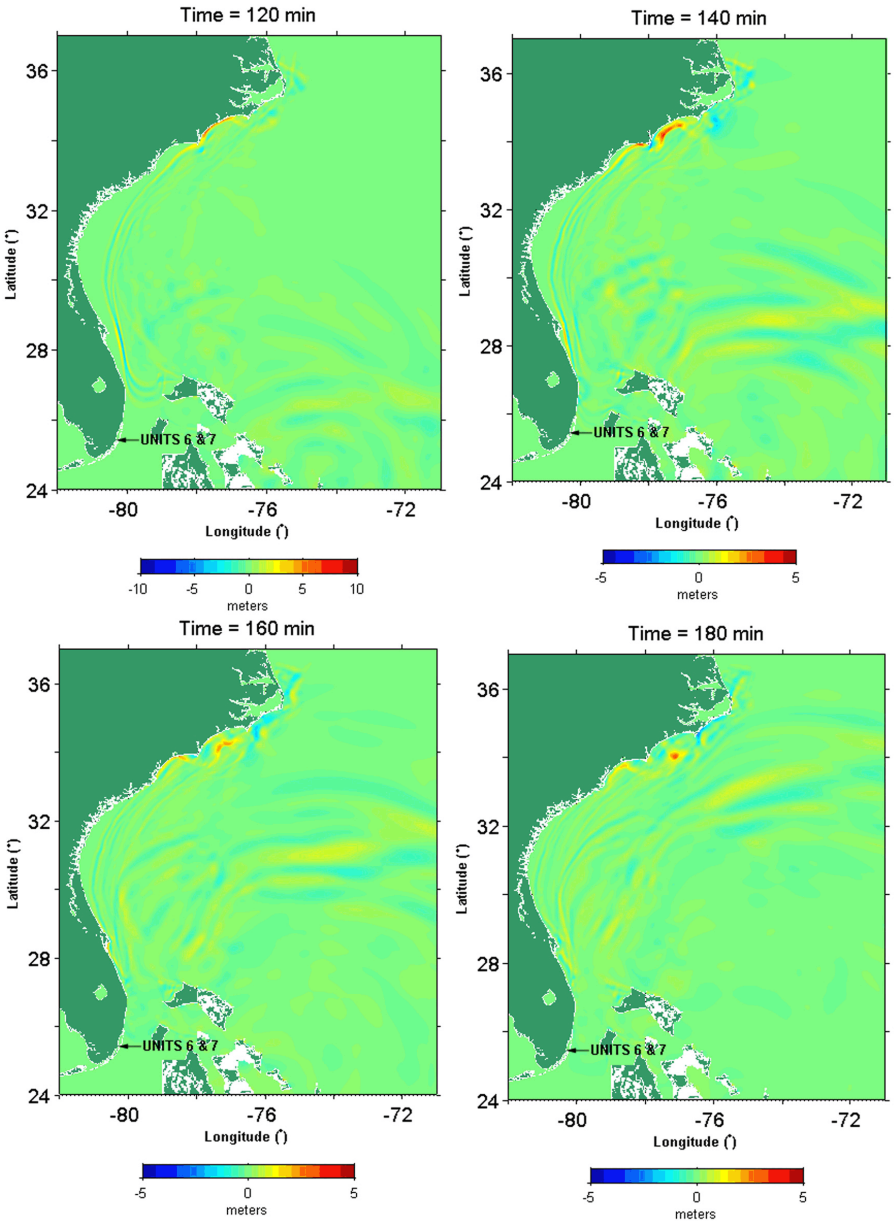

Note: Colors in elevation legend represent water surface elevations relative to MSL for ETOPO1 data and MLW for Coastal Relief Model data.

Figure 2.4.6-255 Simulated Propagation of the Cape Fear Tsunami (Static Source) in Grid A at 120, 140, 160, and 180 Minutes after the Submarine Failure

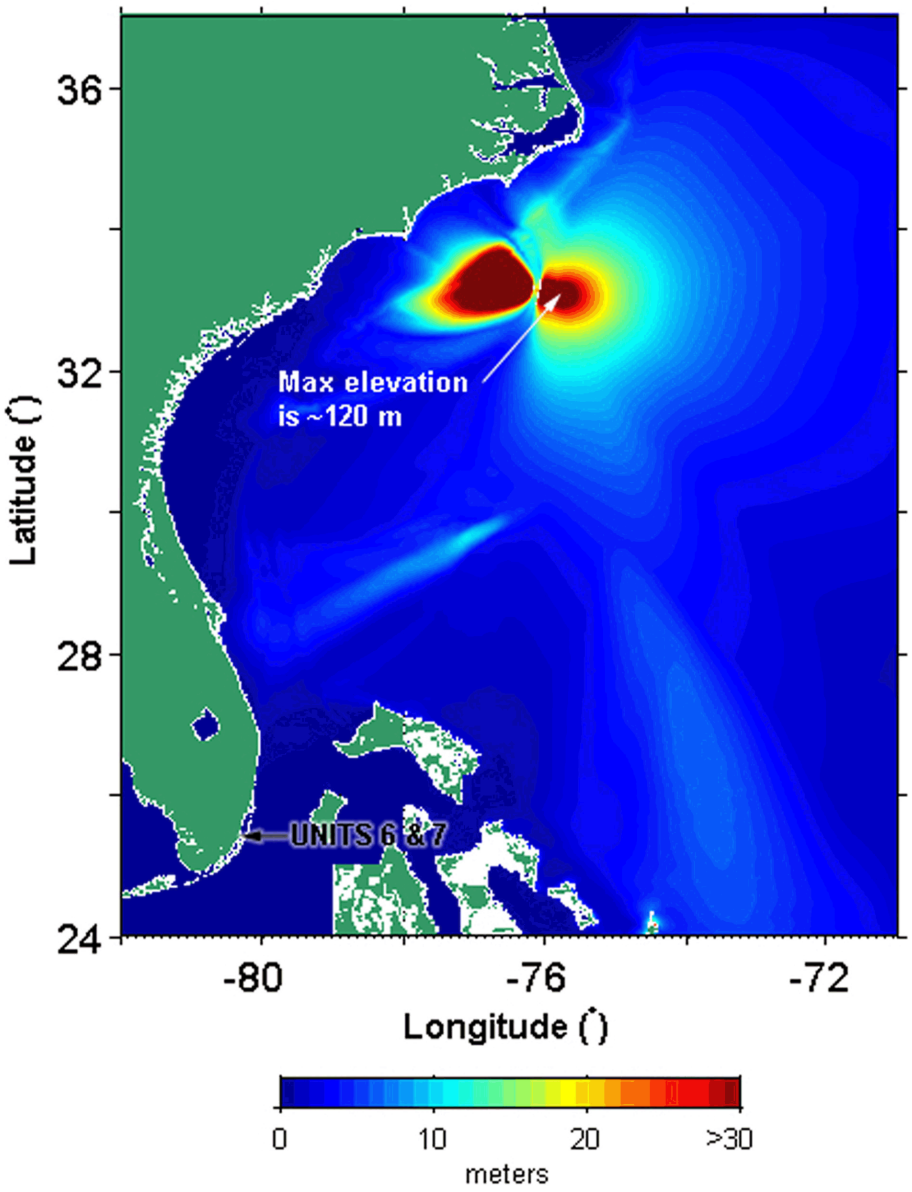

Note: Colors in elevation legend represent water surface elevations relative to MSL for ETOPO1 data and MLW for Coastal Relief Model data.

Figure 2.4.6-256 Simulated maximum water surface elevation during the Propagation of the Cape Fear Tsunami (static source) in Grid A

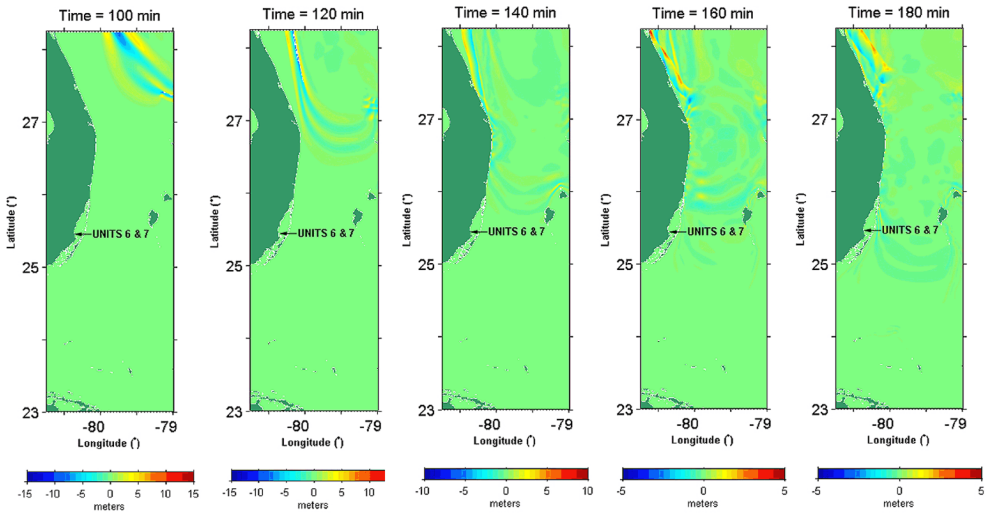

Note: Colors in elevation legend represent water surface elevations relative to MSL for ETOPO1 data and MLW for Coastal Relief Model data.

Figure 2.4.6-257 Simulated Propagation of the Cape Fear Tsunami (Static Source) in Grid B at 100, 120, 140, 160, and 180 Minutes after the Submarine Failure

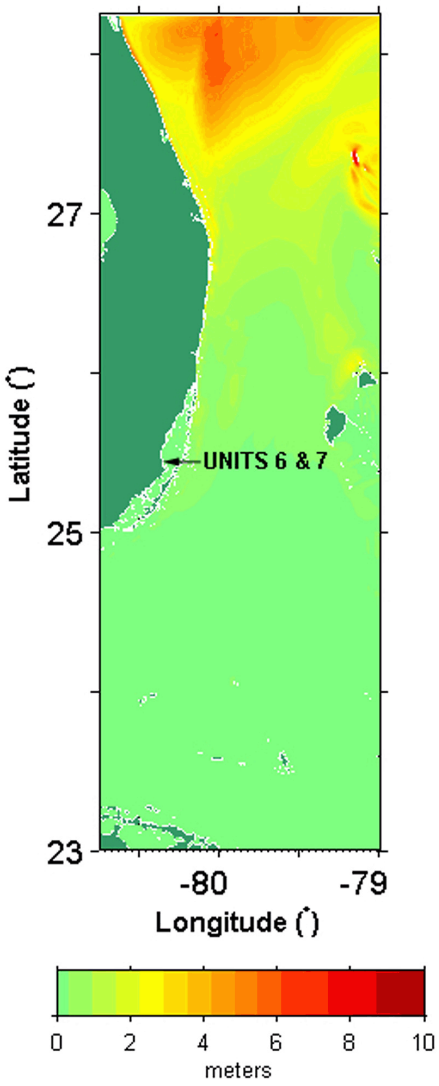

Note: Colors in elevation legend represent water surface elevations relative to MSL for ETOPO1 data and MLW for Coastal Relief Model data.

Figure 2.4.6-258 Simulated Maximum Water Surface Elevation during the Propagation of the Cape Fear Tsunami (Static Source) in Grid B

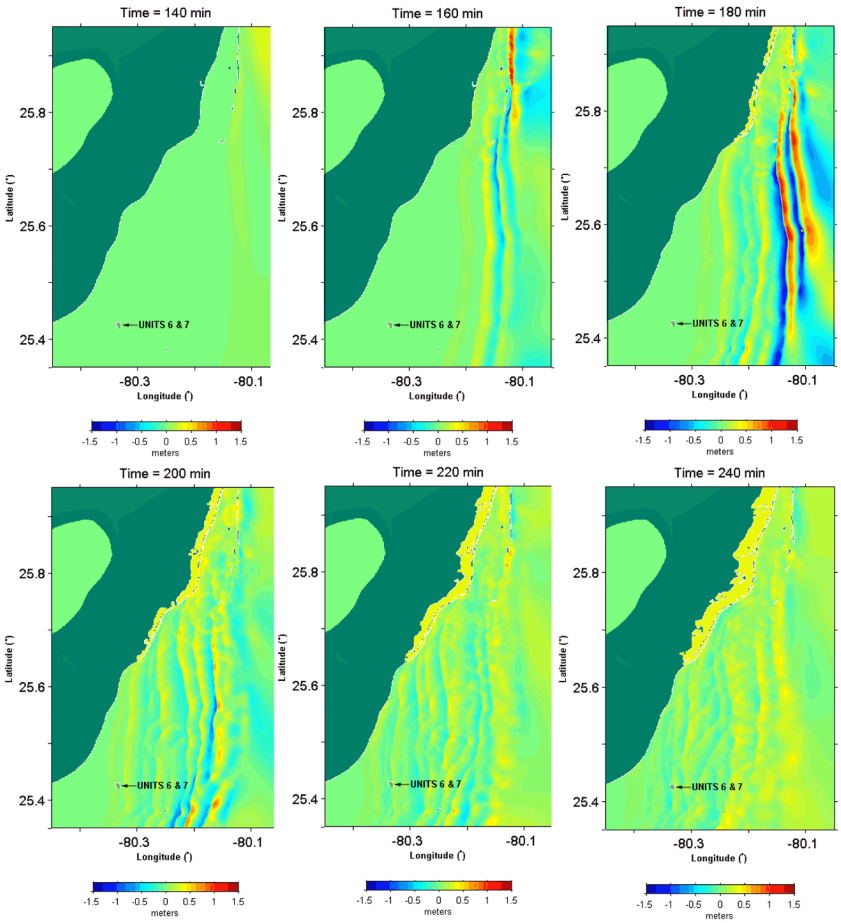

Note: Colors in elevation legend represent water surface elevations relative to MLW.

Figure 2.4.6-259 Simulated Propagation of the Cape Fear Tsunami (Static Source) in Grid C at 140, 160, 180, 200, 220, and 240 Minutes after the Submarine Failure

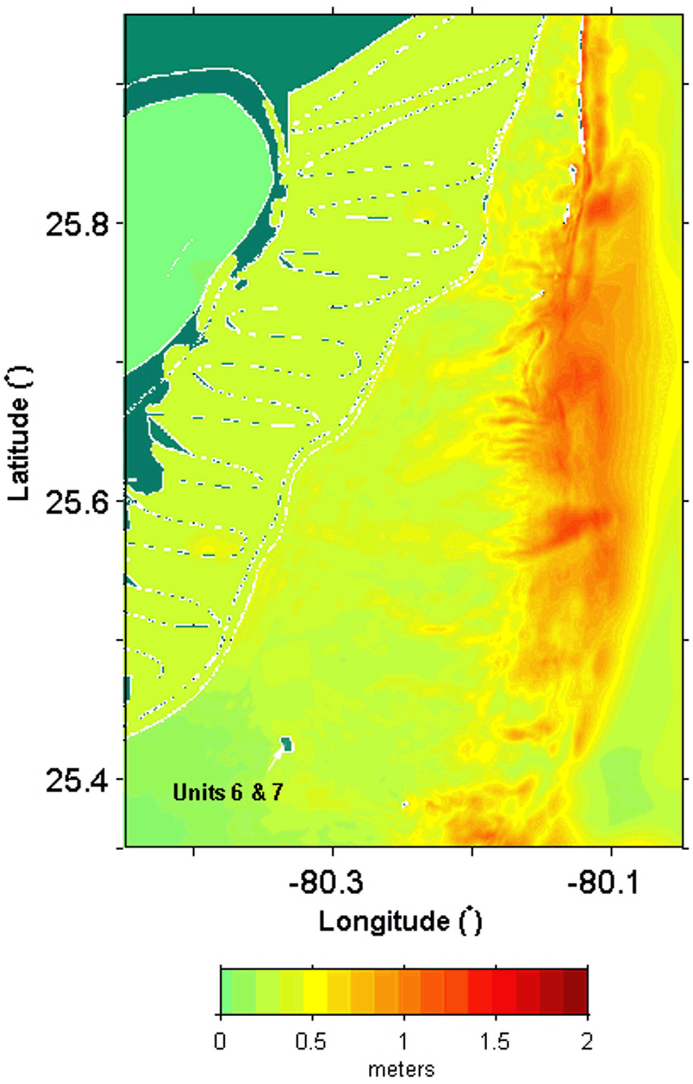

Note: Colors in elevation legend represent water surface elevations relative to MLW.

Figure 2.4.6-260 Simulated Maximum Water Surface Elevation during the Propagation of the Cape Fear Tsunami (Static Source) in Grid C

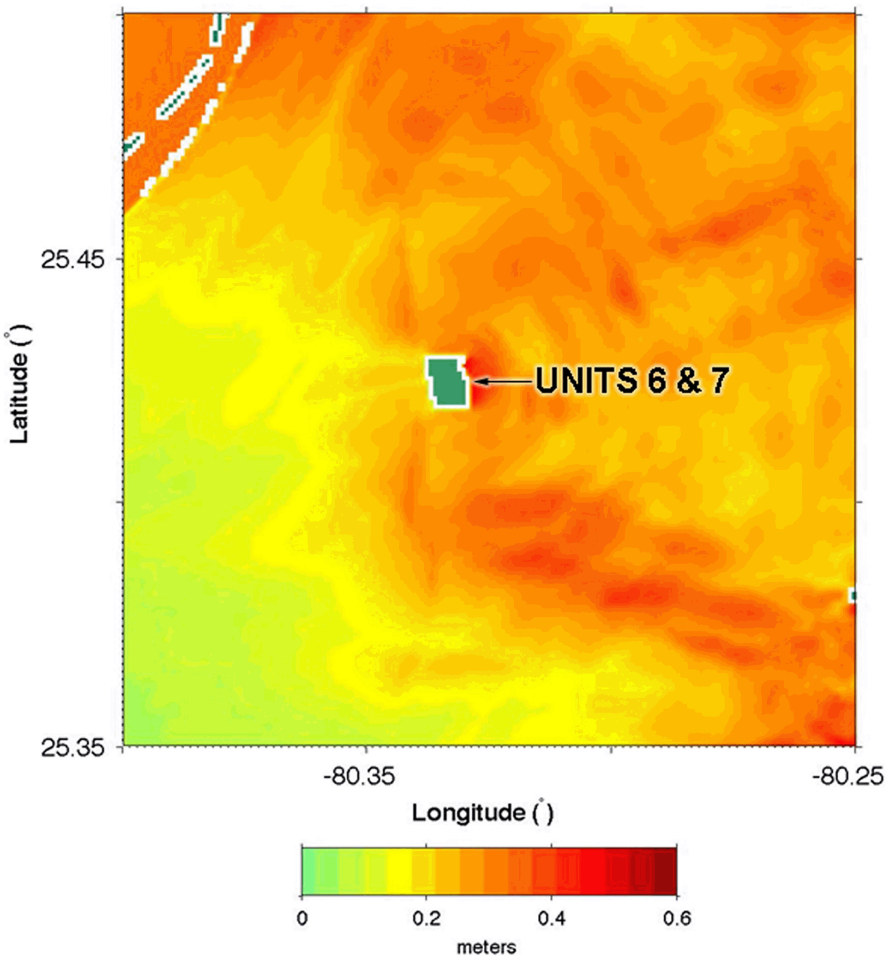

Note: Colors in elevation legend represent water surface elevations relative to MLW.

Figure 2.4.6-261 Simulated Maximum Water Surface Rise, relative to the Initial Sea Water Level, during the Propagation of the Cape Fear Tsunami (Static Source) in the Vicinity Of Units 6 & 7

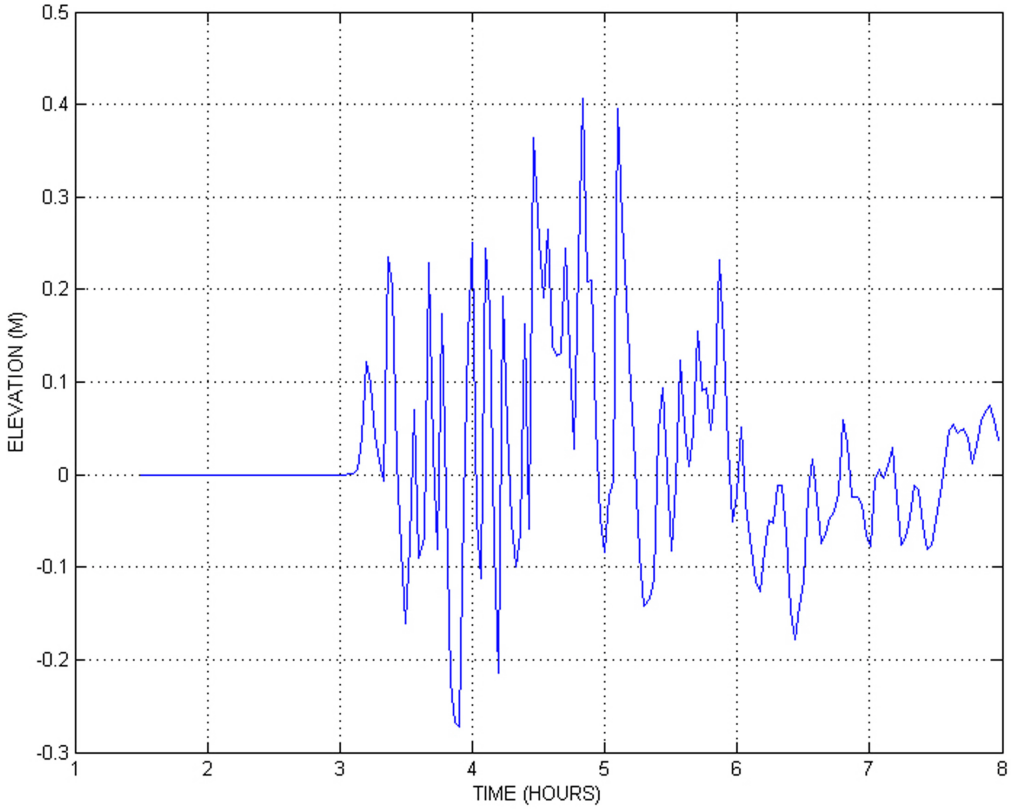

Note: Water surface elevations are relative to the initial water level.

Figure 2.4.6-262 Water Surface Elevation near Units 6 & 7 as a Function of Time Following the Cape Fear Tsunami (Static Source)

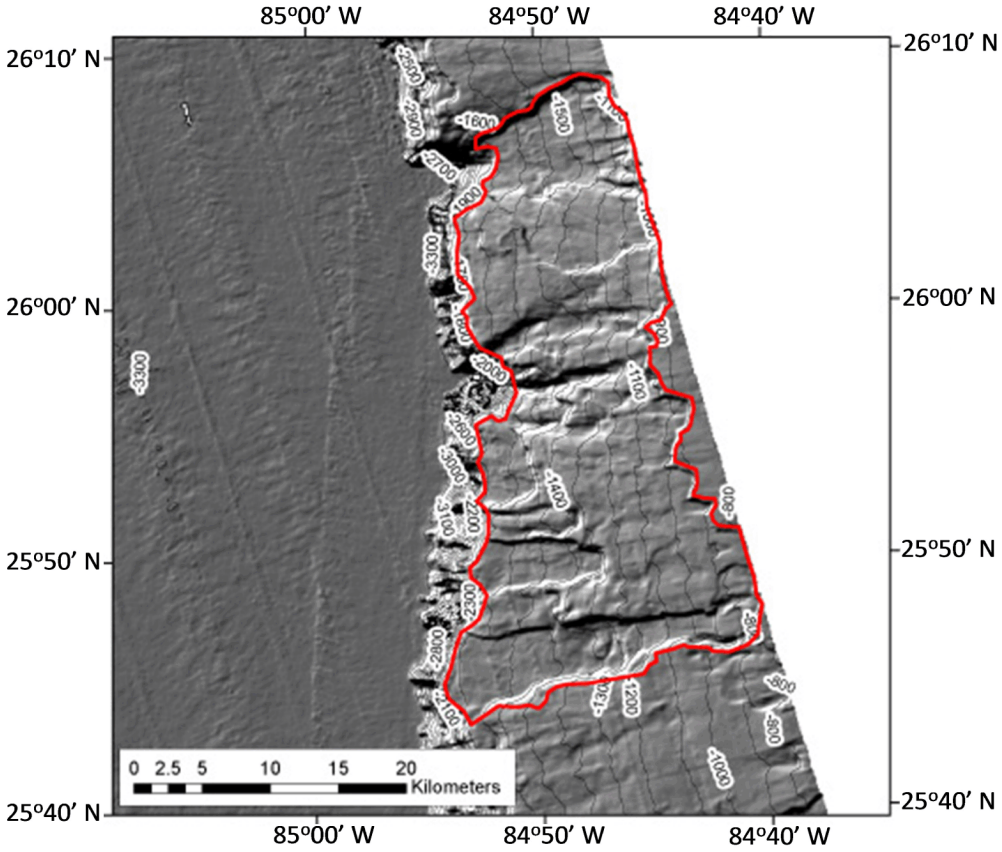

Source: Reference 239

Figure 2.4.6-263 Outline of Maximum Credible Submarine Slide above the Florida Escarpment, Developed from Multibeam Bathymetric Data

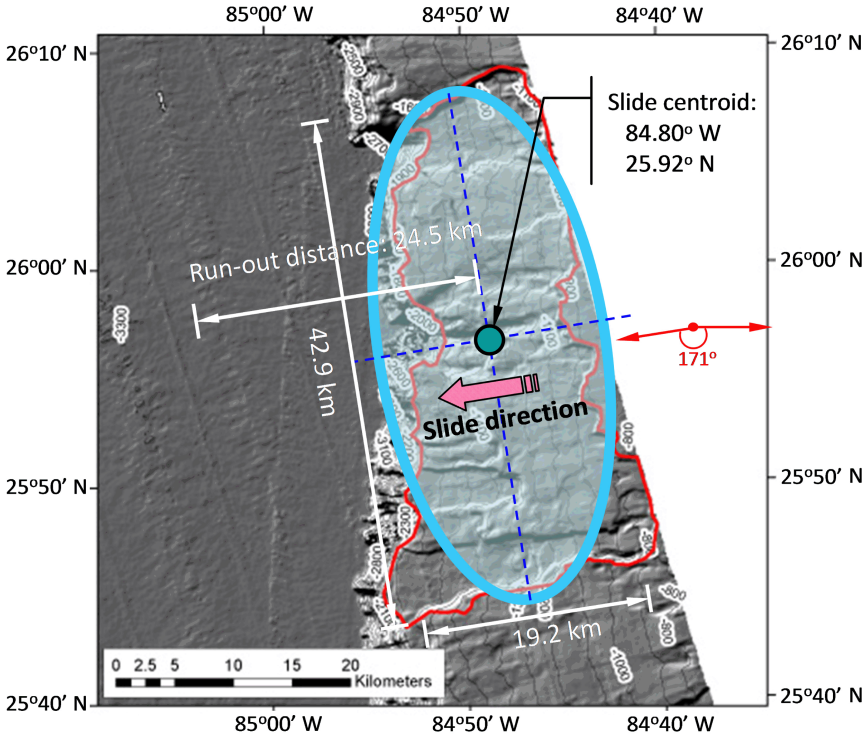

Source: Reference 239

Figure 2.4.6-264 Approximation of the Maximum Credible Submarine Slide above the Florida Escarpment with an Ellipse

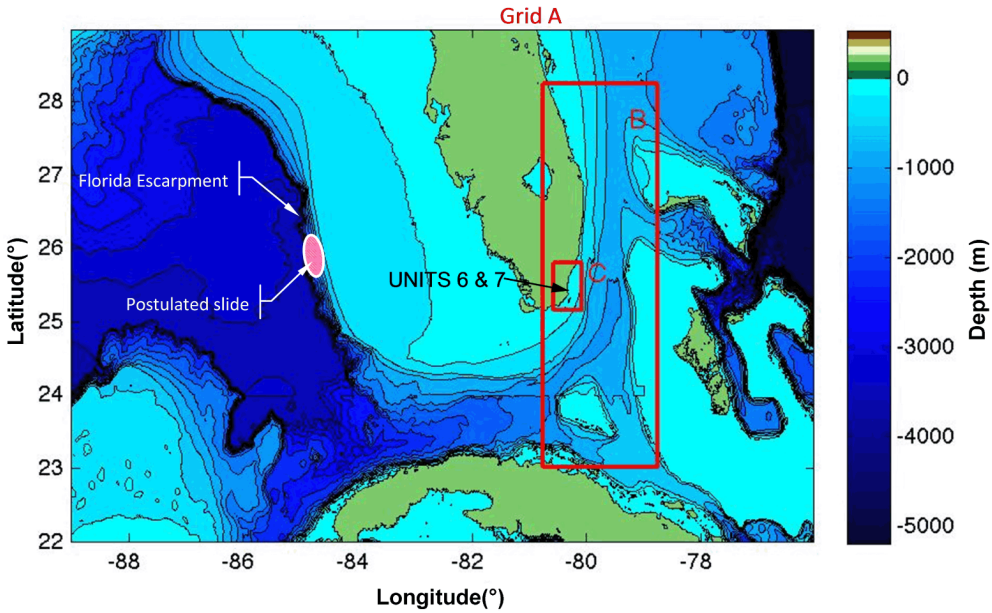

Note: Colors in elevation legend represent water depths relative to MSL for ETOP01 data and MLW for Coastal Relief Model data.
Source: References 244 and 246

Figure 2.4.6-265 Model Domain and Bathymetry in the Three Nested Grids Used in the FUNWAVE Simulations

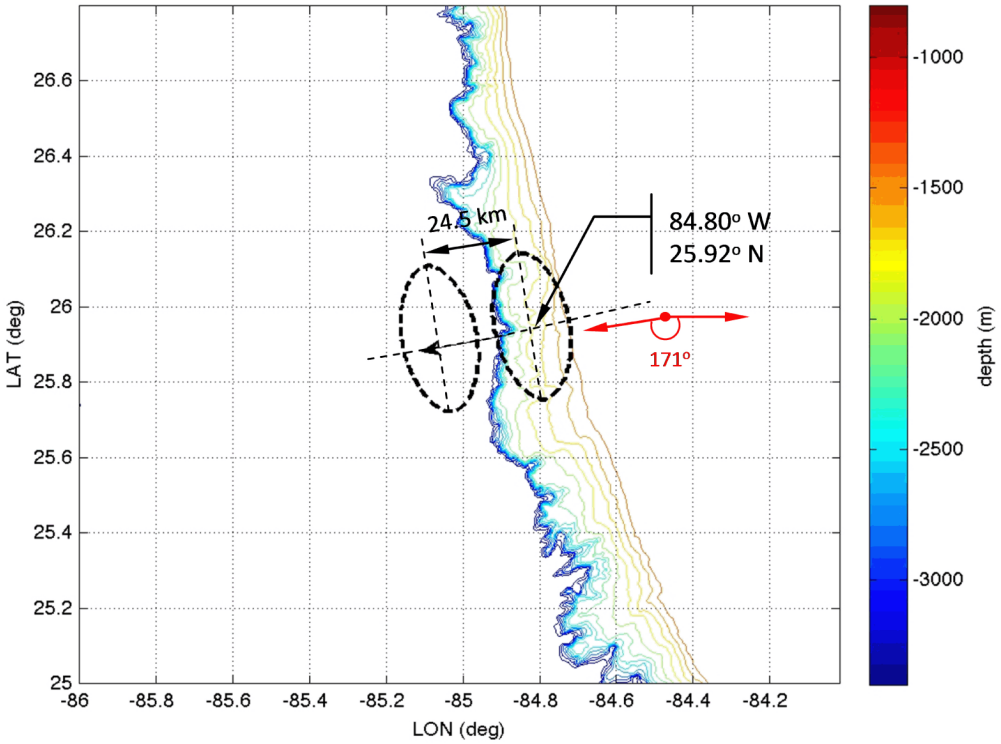

Note: Colors in elevation legend represent water depths relative to MLW.
Source: Reference 246

Figure 2.4.6-266 Location and Lateral Extent of the Postulated Submarine Mass Failure for the Florida Escarpment Slide Simulations and Local Bathymetry

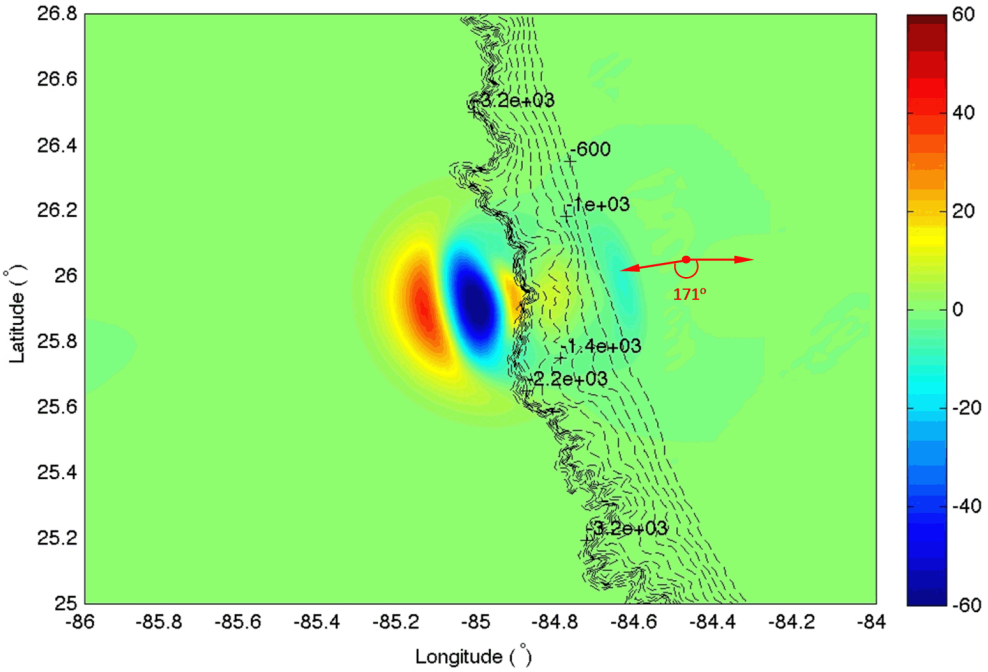

Note: Colors in elevation legend indicate water surface elevation (MLW). Bathymetry contours indicate water depths (MLW) in meters.

Figure 2.4.6-267 Initial Wave Generated by NHWAVE (Dynamic Source) for the Florida Escarpment Submarine Failure

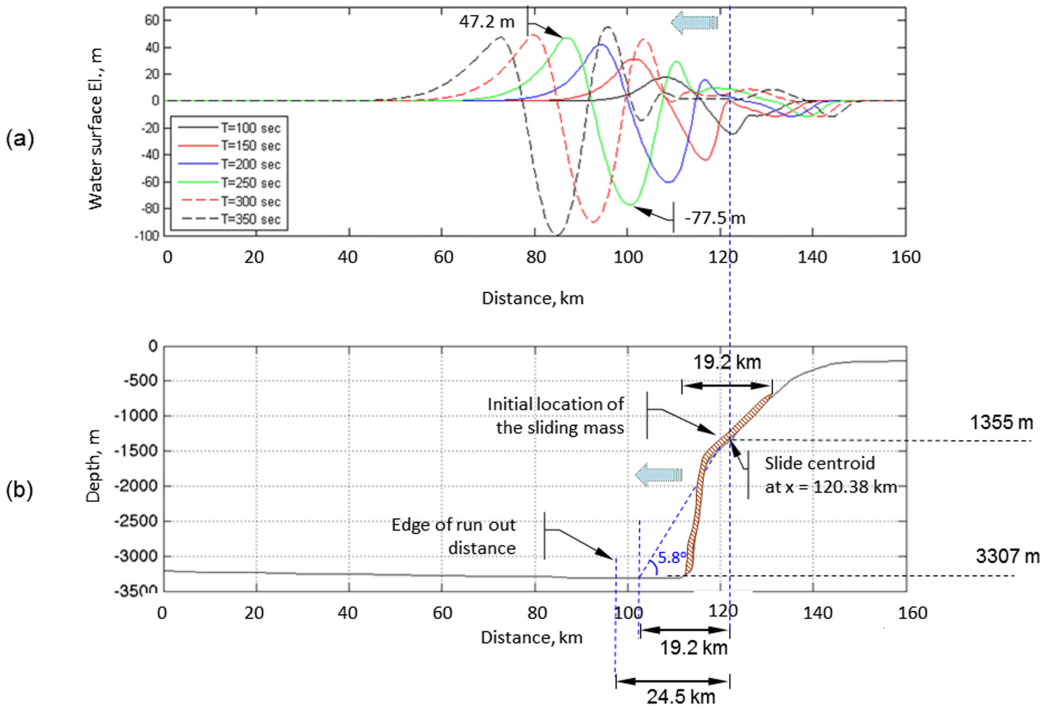

Note 1: The water surface profiles and cross section shown in this figure are along the minor axis of the ellipse shown in Figure 2.4.6-264.
Note 2: Water surface elevations in the upper panel and depths in the lower panel are relative to MLW, respectively.

Figure 2.4.6-268 (a) Water Surface Profiles in the Direction of the Slide Motion at Different Times after the Initiation of the Slide Obtained from NHWAVE and (b) Ocean Floor Profile (Lower Panel)

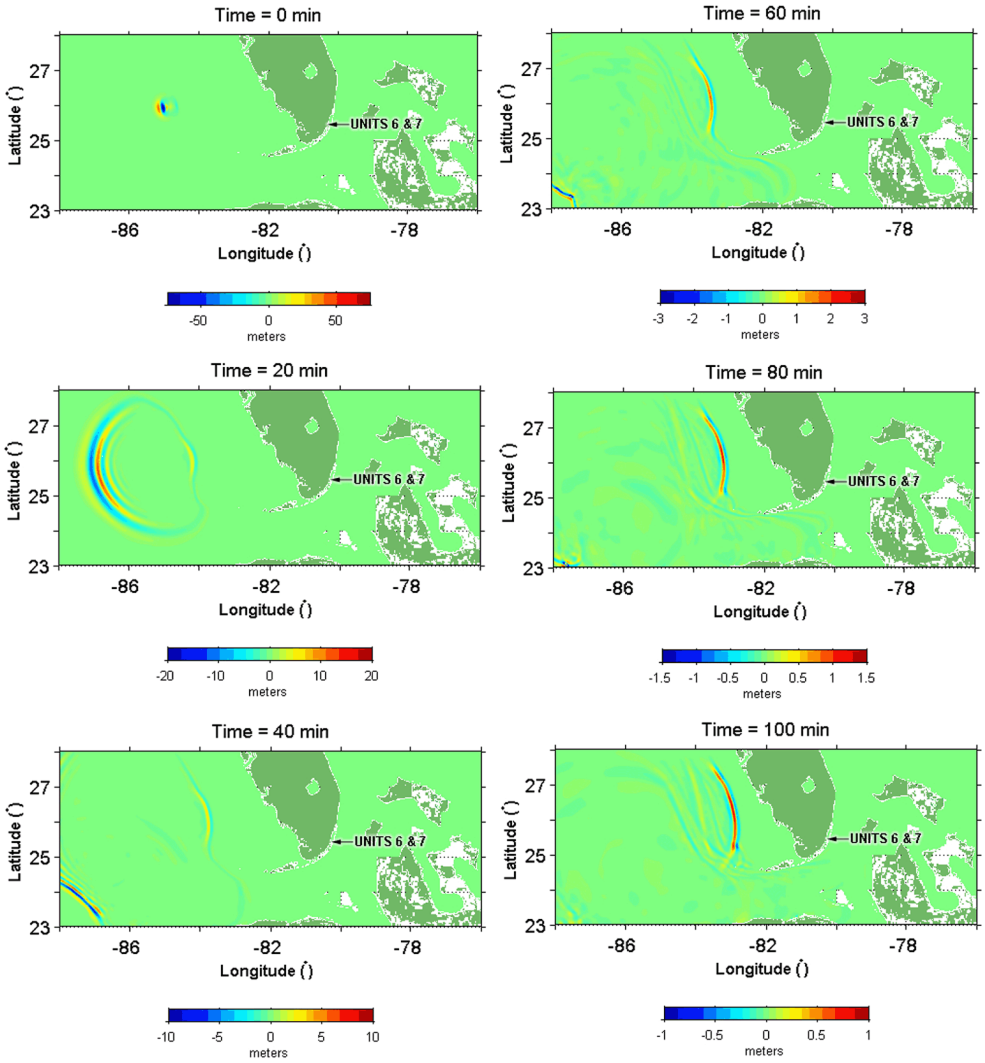

Note: Colors in elevation legend represent water surface elevations in meters relative to MSL for ETOPO1 data and MLW for Coastal Relief Model data.

Source: References 244 and 246

Figure 2.4.6-269 Simulated Propagation of the Florida Escarpment Tsunami (Dynamic Source) in Grid A at 0, 20, 40, 60, 80, and 100 Minutes after the Submarine Mass Failure

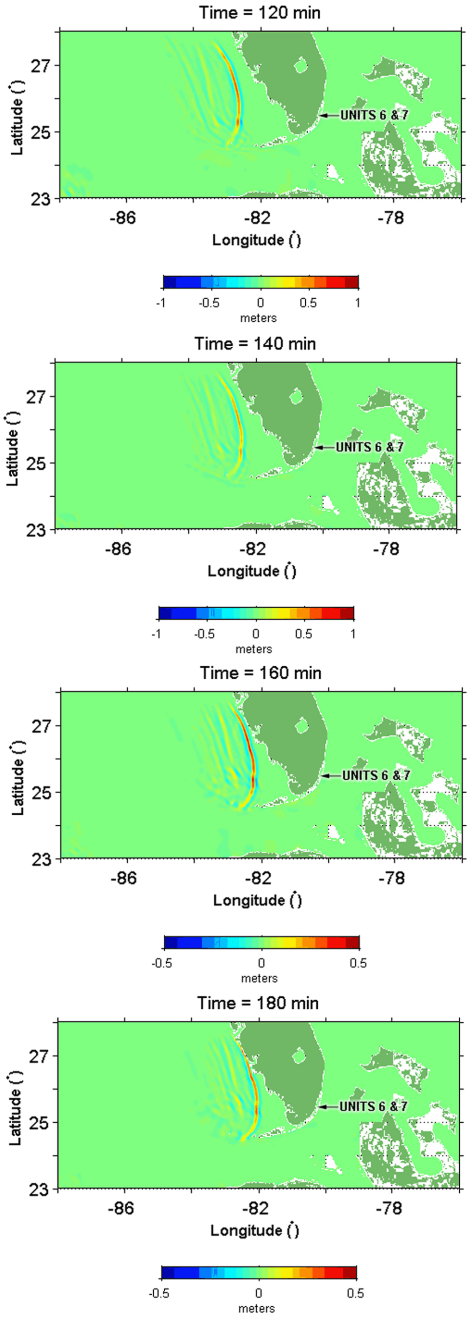

Note: Colors in elevation legend represent water surface elevations in meters relative to MSL for ETOPO1 data and MLW for Coastal Relief Model data.

Source: References 244 and 246

Figure 2.4.6-270 Simulated Propagation of the Florida Escarpment Tsunami (Dynamic Source) in Grid A at 120, 140, 160, and 180 Minutes after the Submarine Mass Failure

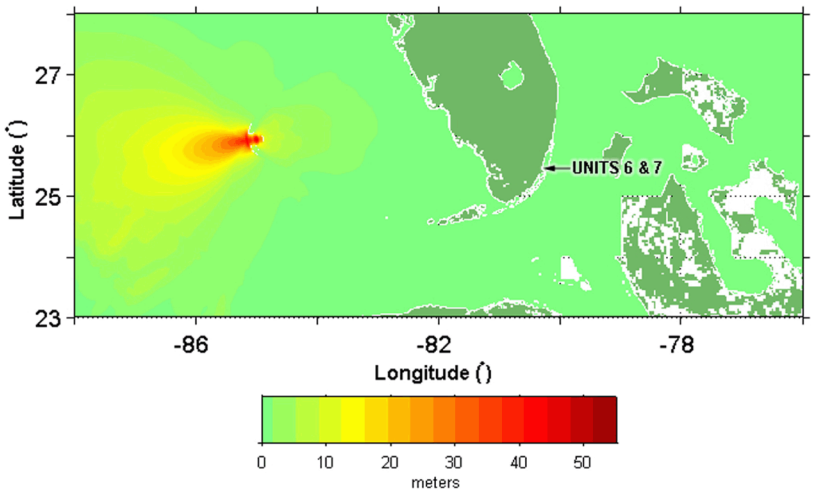

Note: Colors in elevation legend represent water surface elevations relative in meters to MSL for ETOPO1 data and MLW for Coastal Relief Model data.

Source: References 244 and 246

Figure 2.4.6-271 Simulated Maximum Wave Height during the Propagation of the Florida Escarpment Tsunami (Dynamic Source) in Grid A

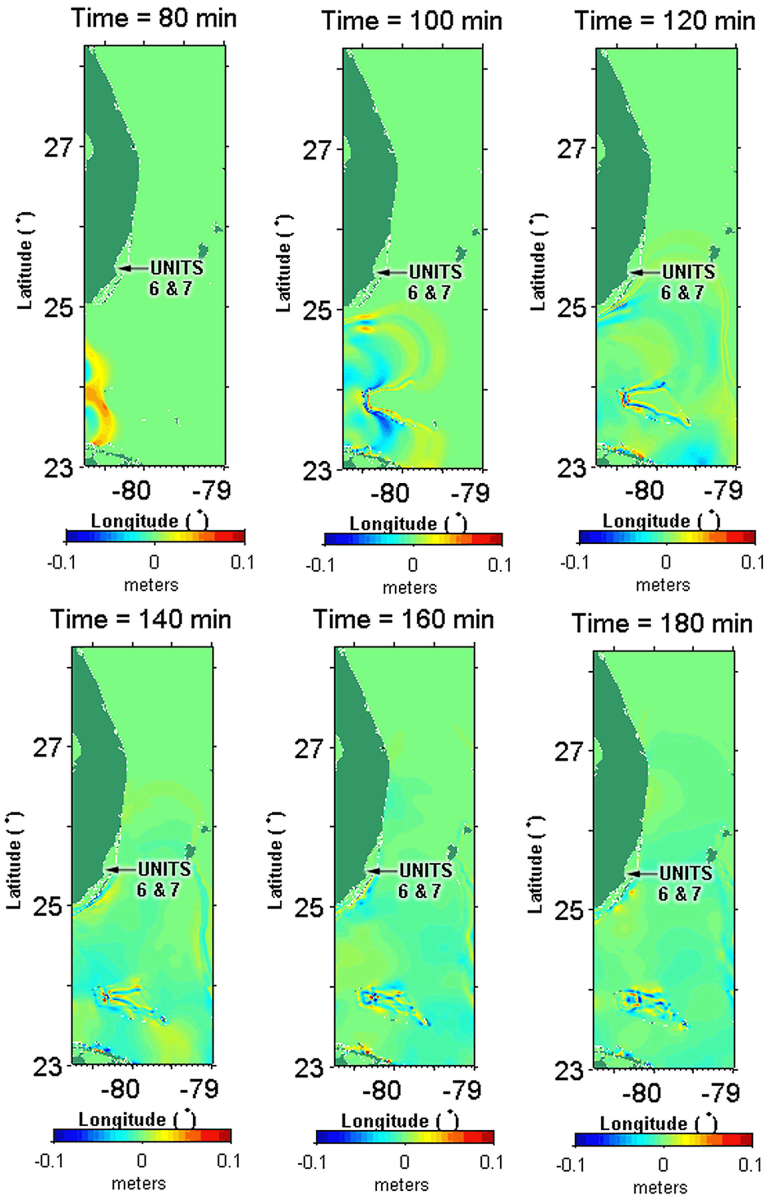

Note: Colors in elevation legend represent water surface elevations in meters relative to MSL for ETOPO1 data and MLW for Coastal Relief Model data.

Source: References 244 and 246

Figure 2.4.6-272 Simulated Propagation of the Florida Escarpment Tsunami (Dynamic Source) in Grid B at 80, 100, 120, 140, 160, and 180 Minutes after the Submarine Mass Failure

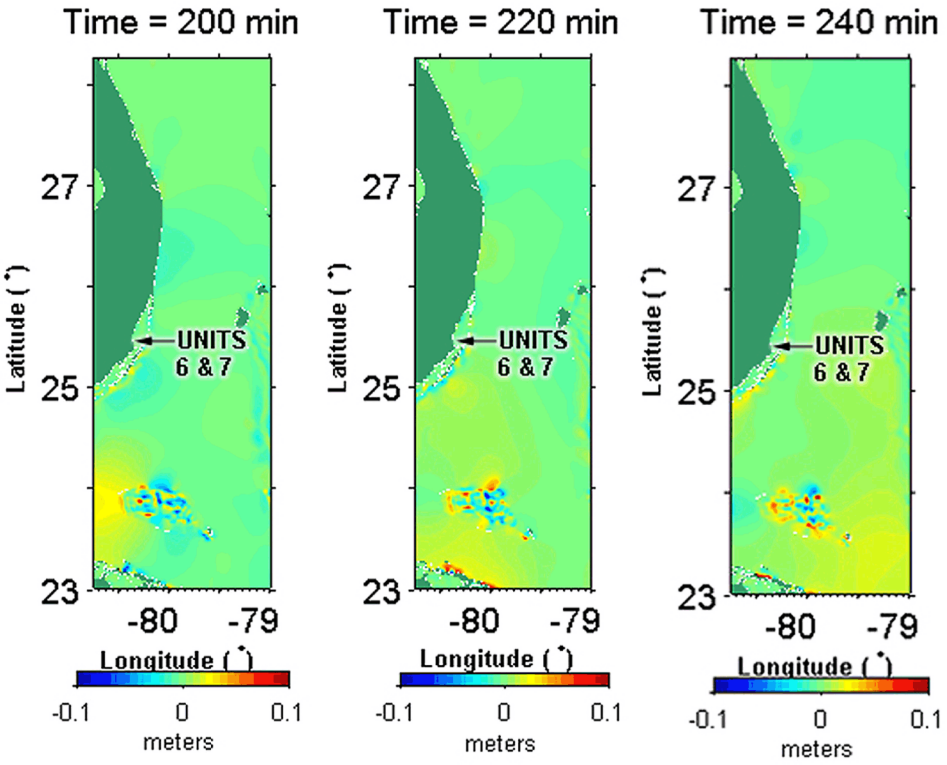

Note: Colors in elevation legend represent water surface elevations in meters relative to MSL for ETOPO1 data and MLW for Coastal Relief Model data.

Source: References 244 and 246

Figure 2.4.6-273 Simulated Propagation of the Florida Escarpment Tsunami (Dynamic Source) in Grid B at 200, 220, and 240 Minutes after the Submarine Mass Failure

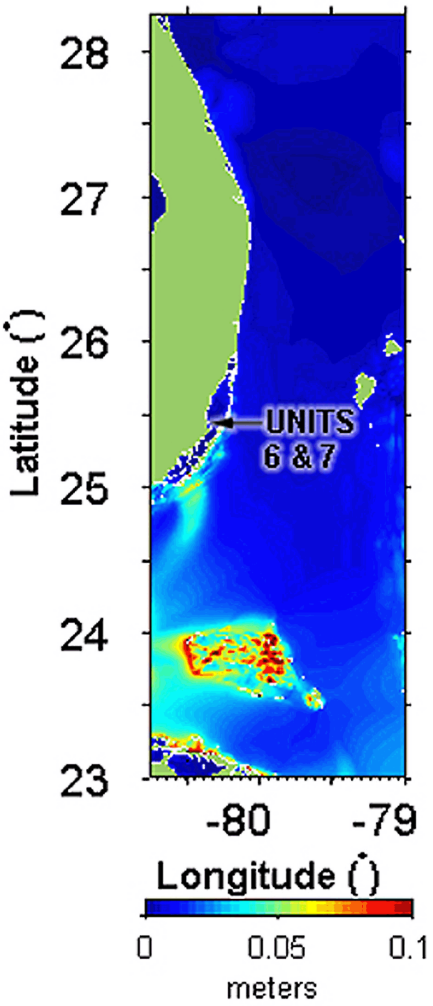

Note: Colors in elevation legend represent water surface elevations in meters relative to MSL for ETOPO1 data and MLW for Coastal Relief Model data.

Source: References 244 and 246

Figure 2.4.6-274 Simulated Maximum Wave Height during the Propagation of the Florida Escarpment Tsunami (Dynamic Source) In Grid B

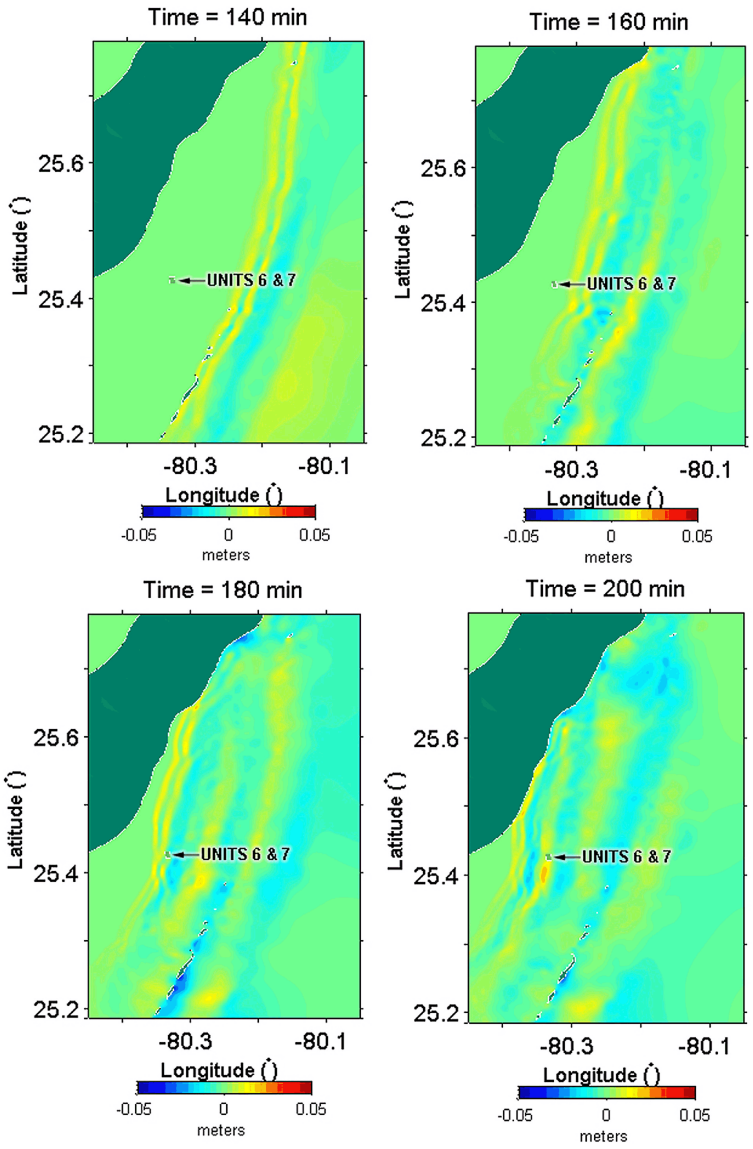

Note: Colors in elevation legend represent water surface elevations in meters relative to MLW.

Figure 2.4.6-275 Simulated Propagation of the Florida Escarpment Tsunami (Dynamic Source) in Grid C at 140, 160, 180, and 200 Minutes after the Submarine Failure

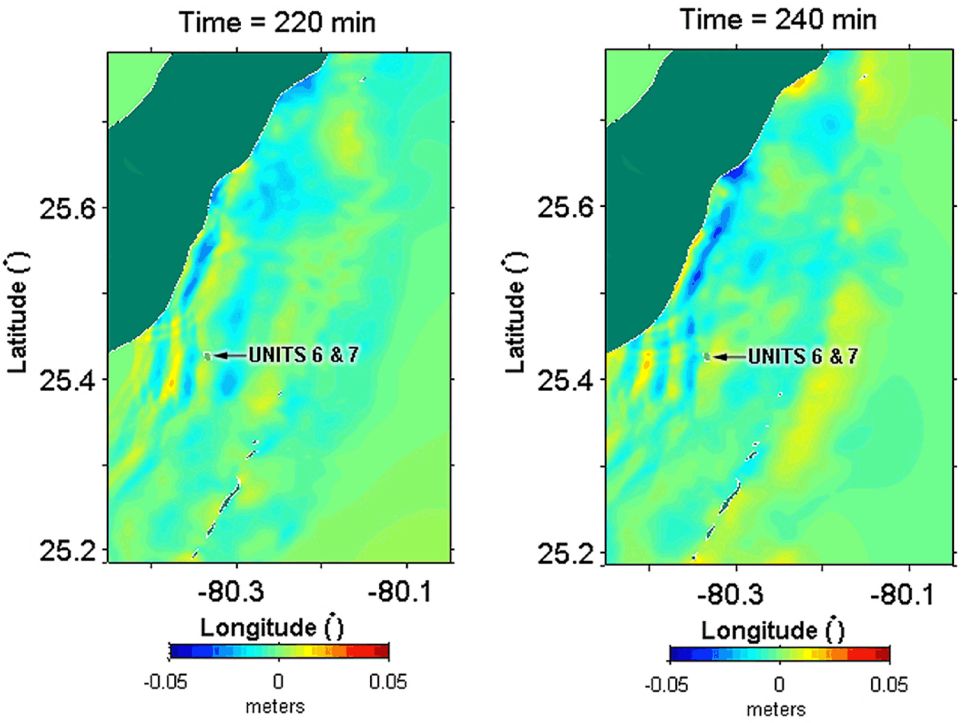

Note: Colors in elevation legend represent water surface elevations in meters relative to MLW.

Figure 2.4.6-276 Simulated Propagation of the Florida Escarpment Tsunami (Dynamic Source) in Grid C at 220 and 240 Minutes after the Submarine Failure

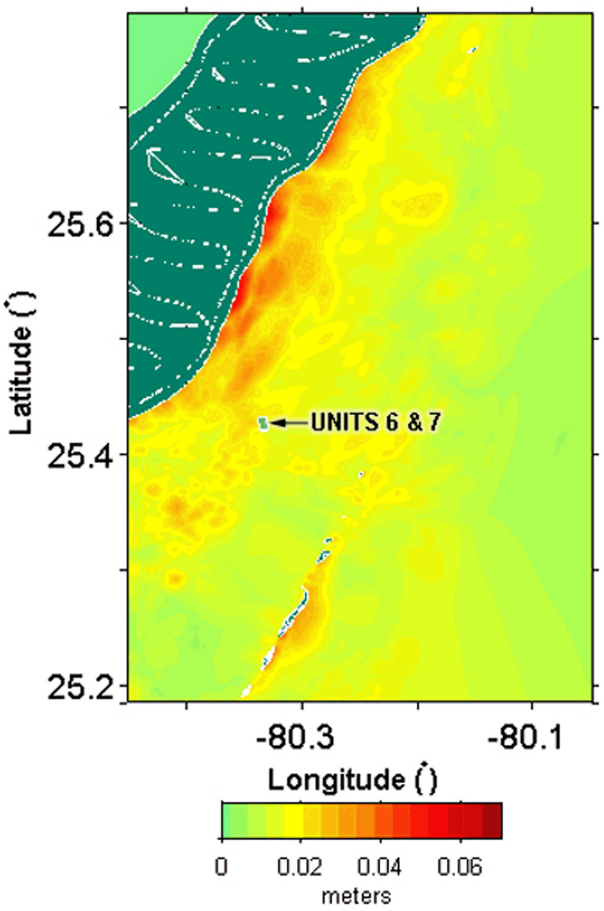

Note: Colors in elevation legend represent water surface elevations in meters relative to MLW.

Figure 2.4.6-277 Simulated Maximum Water Surface Elevation during the Propagation of the Florida Escarpment Tsunami (Dynamic Source) in Grid C

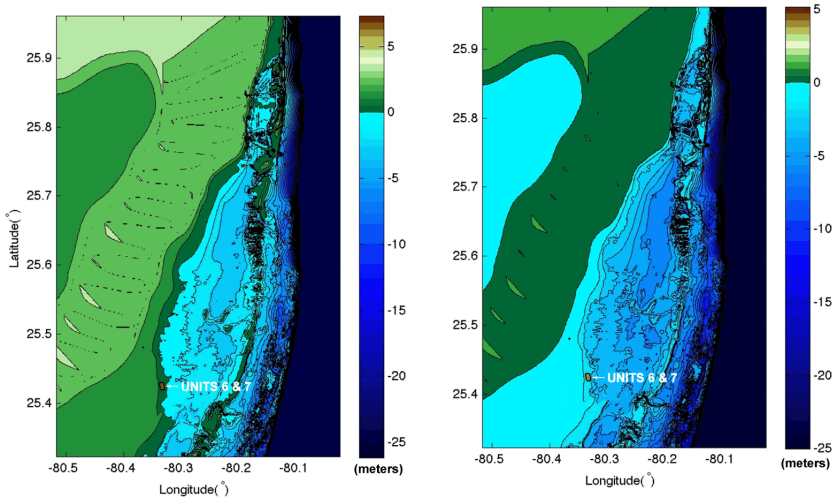

Note: Colors in elevation legend represent water depths relative to MLW.

Figure 2.4.6-278 (a) Water Depth Relative to MLW over the Area of Grid C without the Water Level Rise that is Used to Define the Initial Condition for the Tsunami Propagation Simulations; and (b) Water Depth Relative to the Assumed Initial Water Surface in the Florida Escarpment Tsunami Simulations

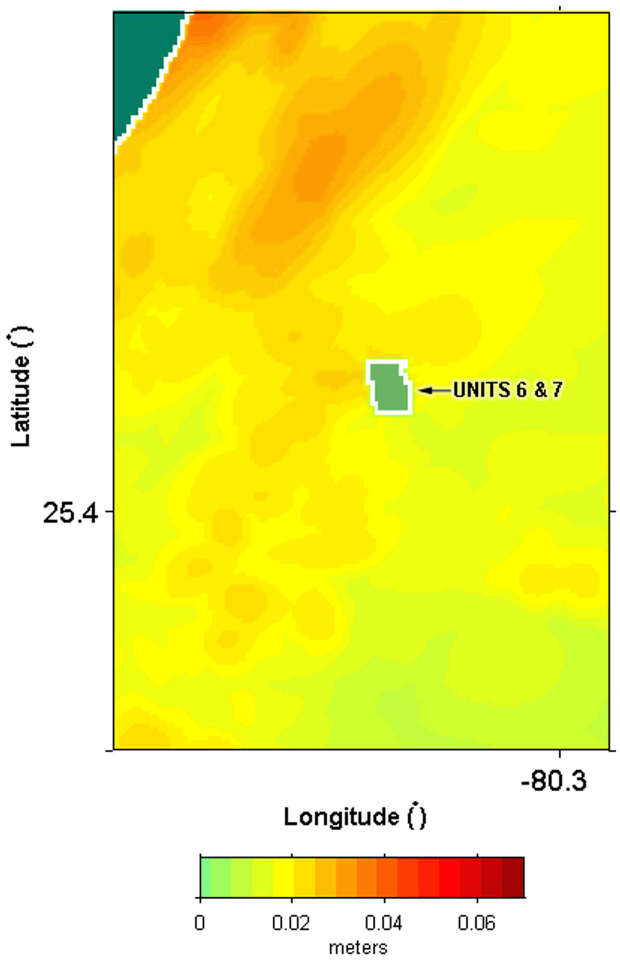

Note: Colors in elevation legend represent water surface elevations in meters relative to MLW.

Figure 2.4.6-279 Simulated Maximum Water Surface Rise, relative to the Initial Sea Water Level, during the Propagation of the Florida Escarpment Tsunami (Dynamic Source) in the Vicinity of Units 6 & 7

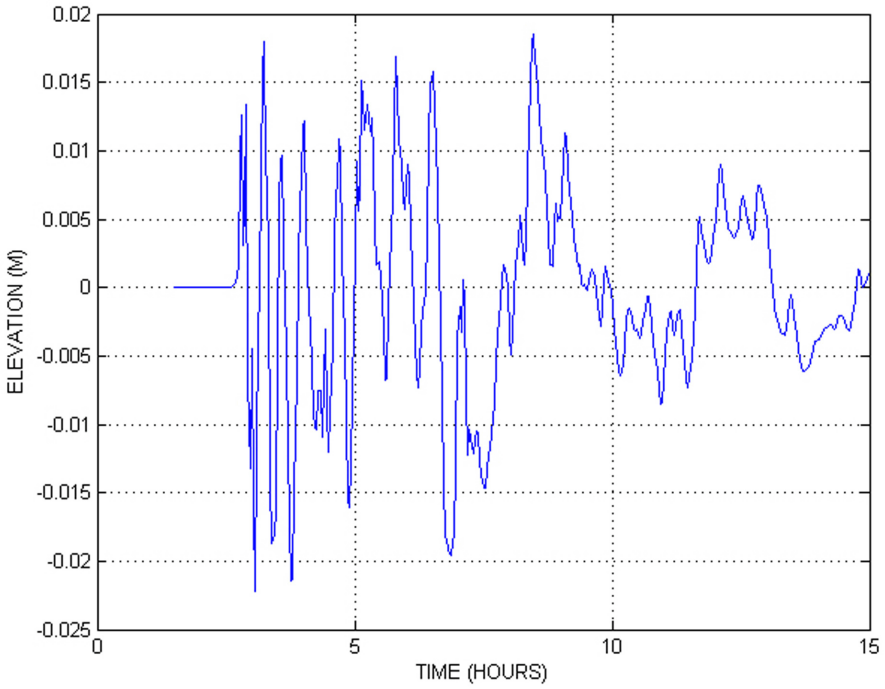

Note: Water surface elevations are relative to MLW and the initial water level.

Figure 2.4.6-280 Water Surface Elevation near Units 6 & 7 as a Function of Time Following the Florida Escarpment Tsunami (Dynamic Source)

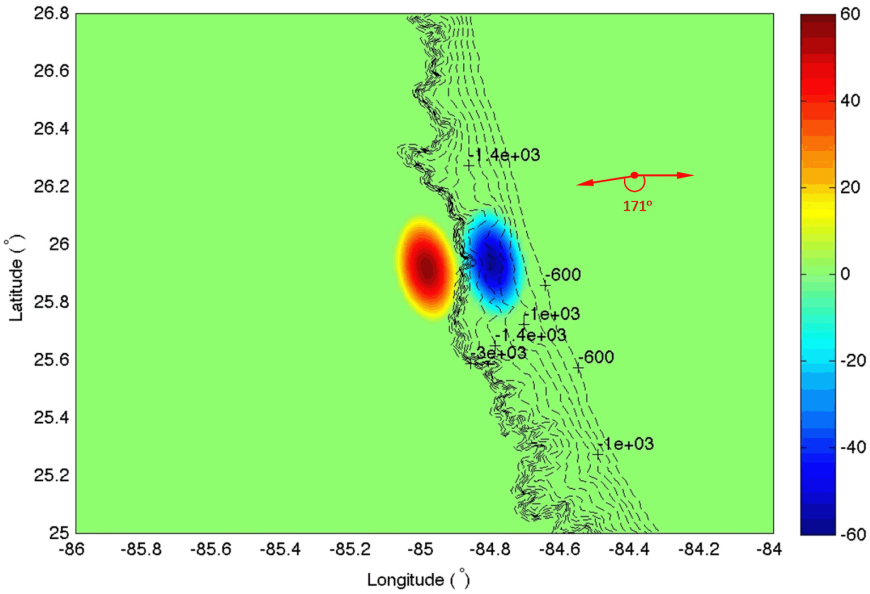

Note: Colors in elevation legend indicate water surface elevation (MLW). Bathymetry contours indicate water depths (MLW) in meters.

Figure 2.4.6-281 Initial Wave for a Static Source Representation of the Florida Escarpment Submarine Failure Shown in Figure 2.4.6-254

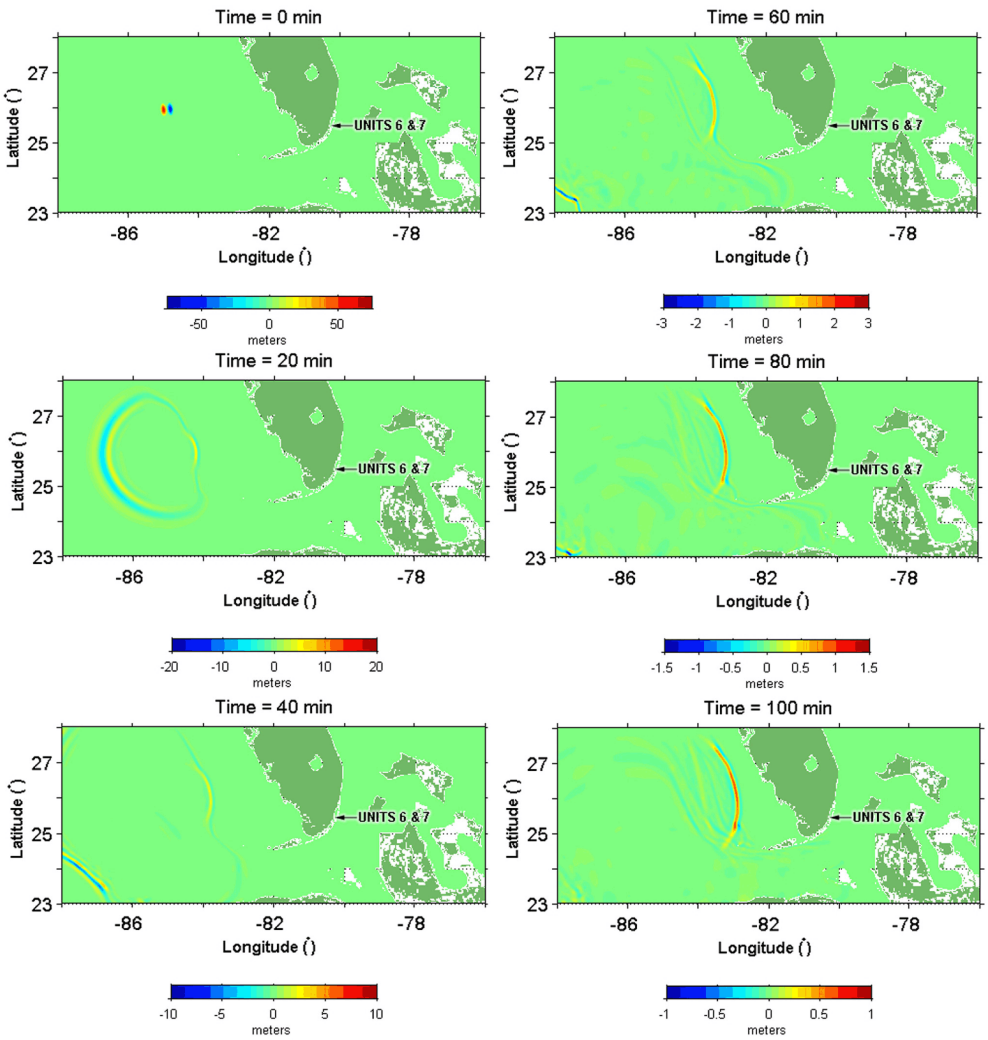

Note: Colors in elevation legend represent water surface elevations in meters relative to MSL for ETOPO1 data and MLW for Coastal Relief Model data.

Source: References 244 and 246

Figure 2.4.6-282 Simulated Propagation of the Florida Escarpment Tsunami (Static Source) in Grid A at 0, 20, 40, 60, 80, and 100 Minutes after the Submarine Failure

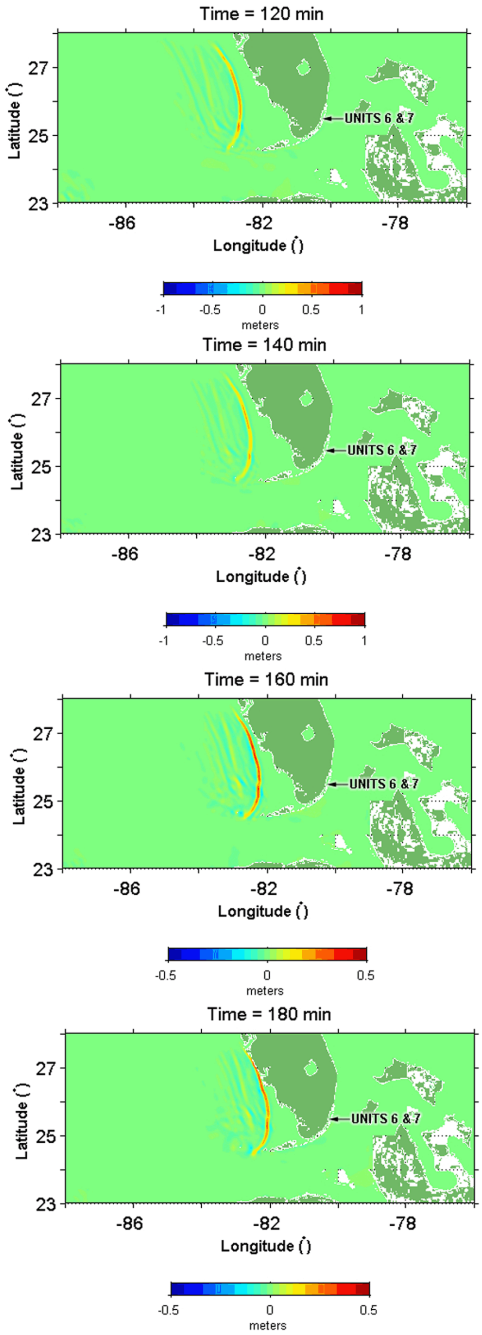

Note: Colors in elevation legend represent water surface elevations in meters relative to MSL for ETOPO1 data and MLW for Coastal Relief Model data.

Source: References 244 and 246

Figure 2.4.6-283 Simulated Propagation of the Florida Escarpment Tsunami (Static Source) in Grid A at 120, 140, 160, and 180 Minutes after the Submarine Failure

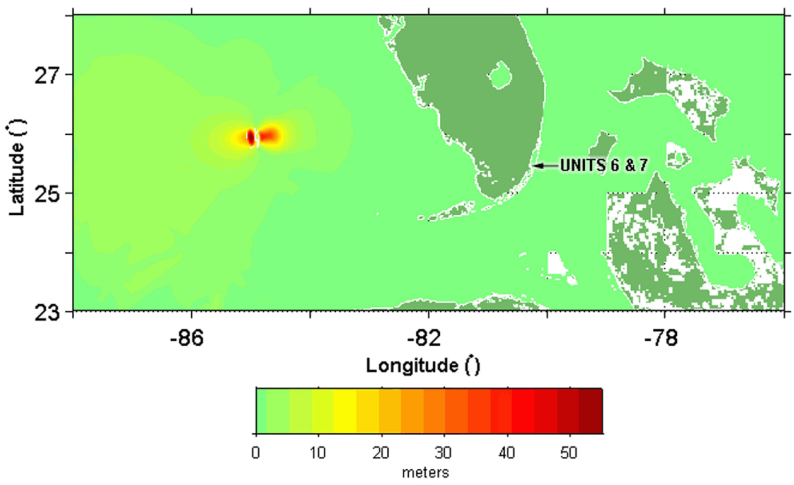

Note: Colors in elevation legend represent water surface elevations relative in meters to MSL for ETOPO1 data and MLW for Coastal Relief Model data.

Source: References 244 and 246

Figure 2.4.6-284 Simulated Maximum Water Surface Elevation during the Propagation of the Florida Escarpment Tsunami (Static Source) in Grid A

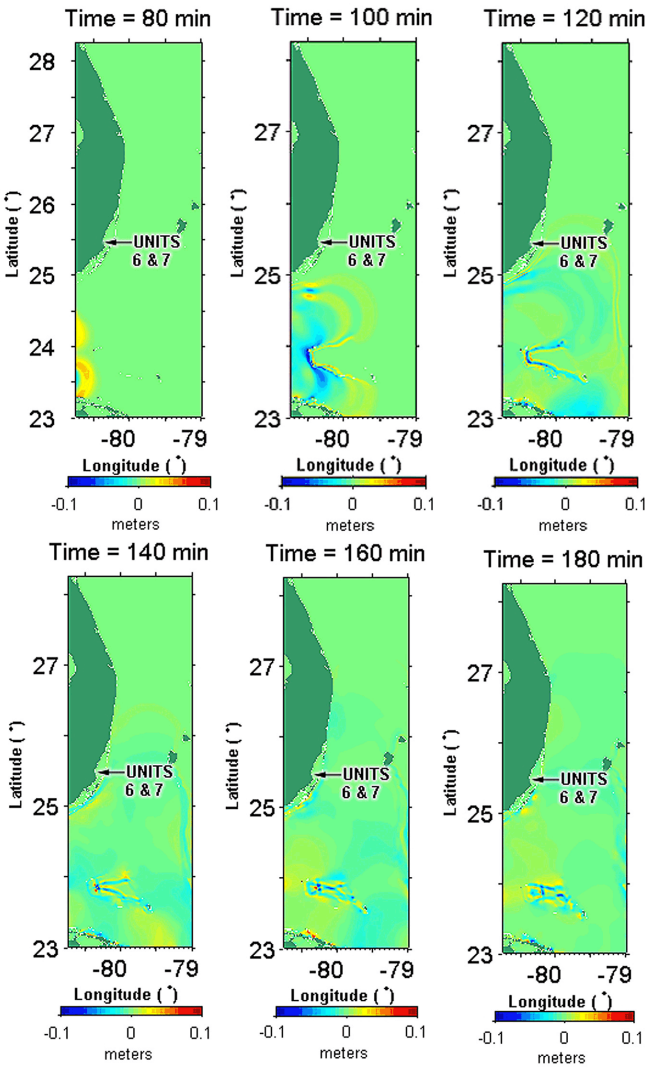

Note: Colors in elevation legend represent water surface elevations in meters relative to MSL for ETOPO1 data and MLW for Coastal Relief Model data.

Source: References 244 and 246

Figure 2.4.6-285 Simulated Propagation of the Florida Escarpment Tsunami (Static Source) in Grid B at 80, 100, 120, 140, 160, and 180 Minutes after the Submarine Failure

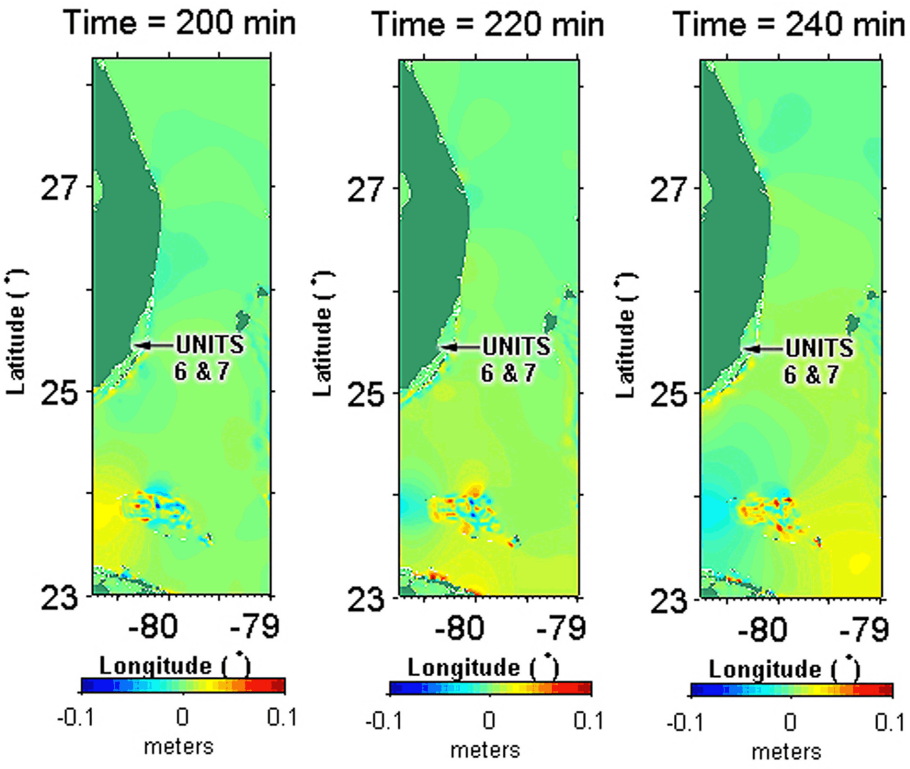

Note: Colors in elevation legend represent water surface elevations in meters relative to MSL for ETOPO1 data and MLW for Coastal Relief Model data.

Source: References 244 and 246

Figure 2.4.6-286 Simulated Propagation of the Florida Escarpment Tsunami (Static Source) in Grid B at 200, 220, and 240 Minutes after the Submarine Failure

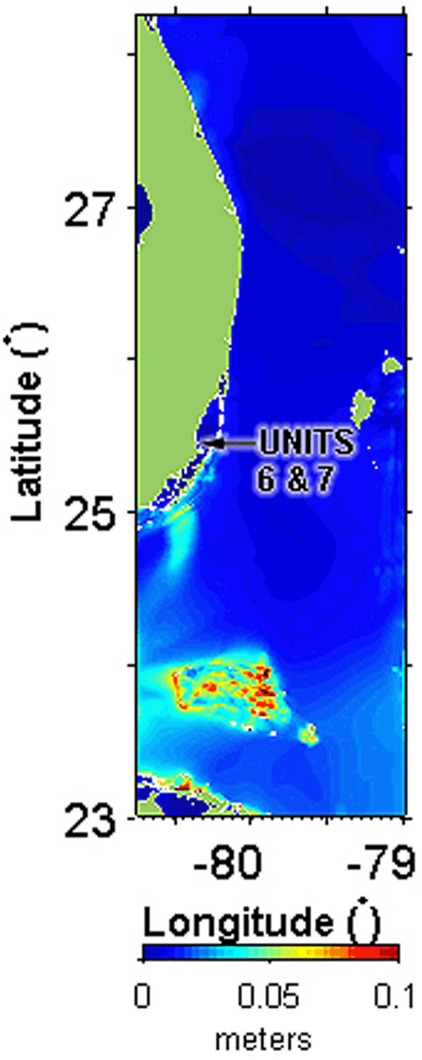

Note: Colors in elevation legend represent water surface elevations relative in meters to MSL for ETOPO1 data and MLW for Coastal Relief Model data.

Source: References 244 and 246

Figure 2.4.6-287 Simulated Maximum Water Surface Elevation during the Propagation of the Florida Escarpment Tsunami (Static Source) in Grid B

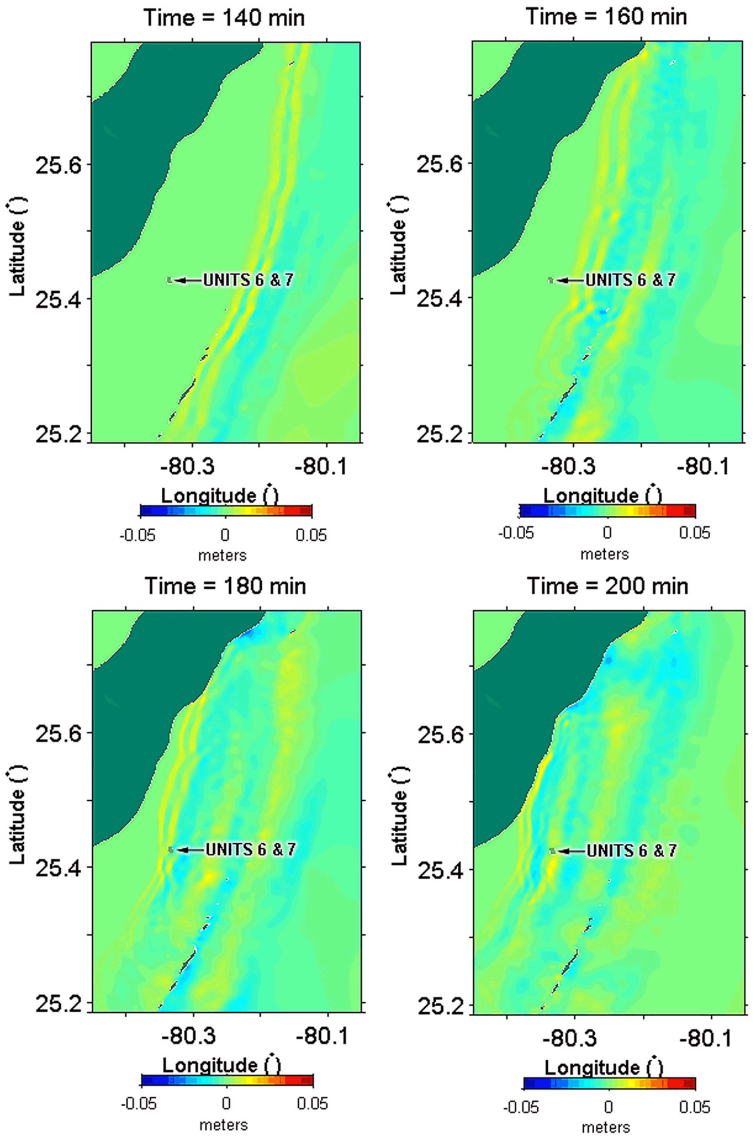

Note: Colors in elevation legend represent water surface elevations in meters relative to MLW.

Figure 2.4.6-288 Simulated Propagation of the Florida Escarpment Tsunami (Static Source) in Grid C at 140, 160, 180, and 200 Minutes after the Submarine Failure

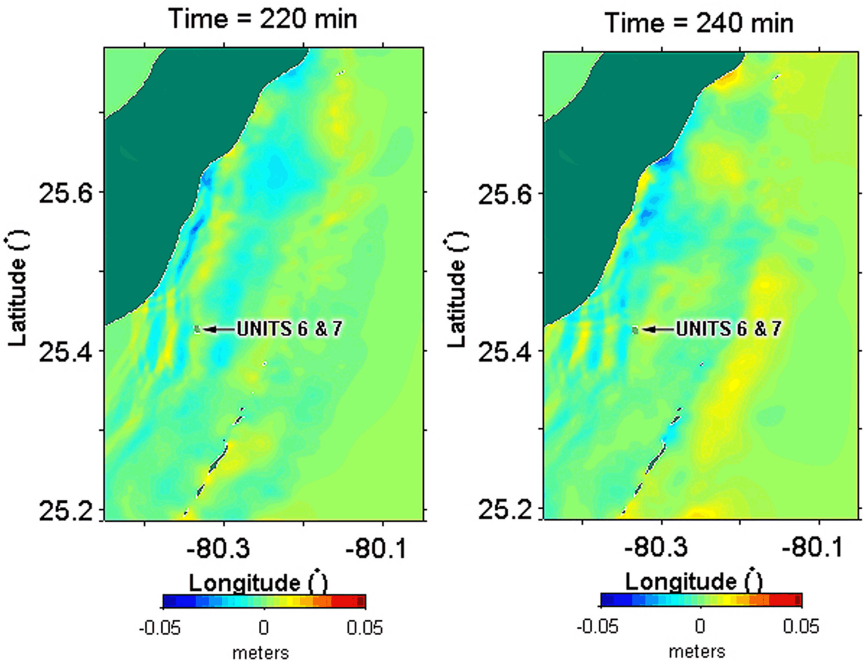

Note: Colors in elevation legend represent water surface elevations in meters relative to MLW.

Figure 2.4.6-289 Simulated Propagation of the Florida Escarpment Tsunami (Static Source) in Grid C at 220 and 240 Minutes after the Submarine Failure

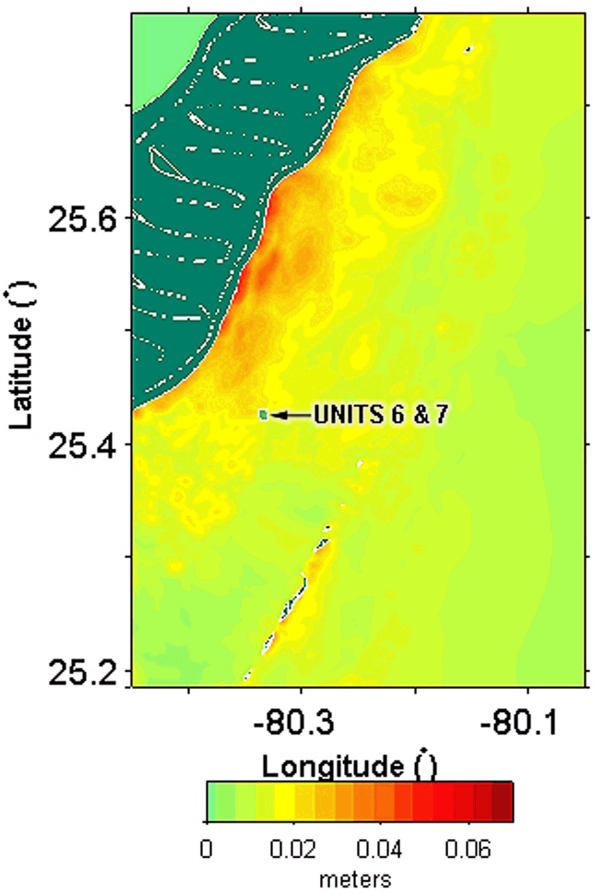

Note: Colors in elevation legend represent water surface elevations in meters relative to MLW.

Figure 2.4.6-290 Simulated Maximum Water Surface Elevation during the Propagation of the Florida Escarpment Tsunami (Static Source) in Grid C

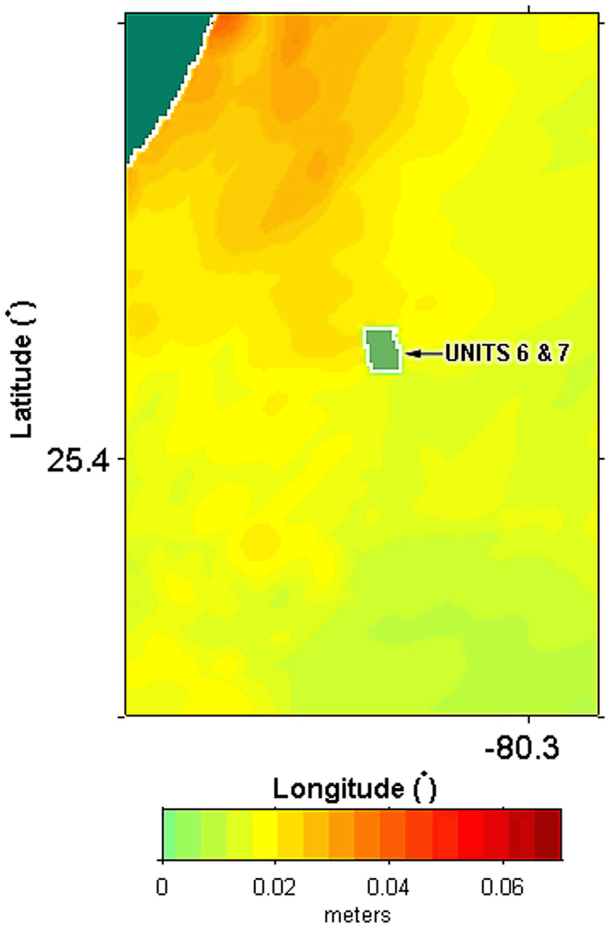

Note: Colors in elevation legend represent water surface elevations in meters relative to MLW.

Figure 2.4.6-291 Simulated Maximum Water Surface Rise, Relative to the Initial Sea Water Level, during the Propagation of the Florida Escarpment Tsunami (Static Source) in the Vicinity of Units 6 & 7

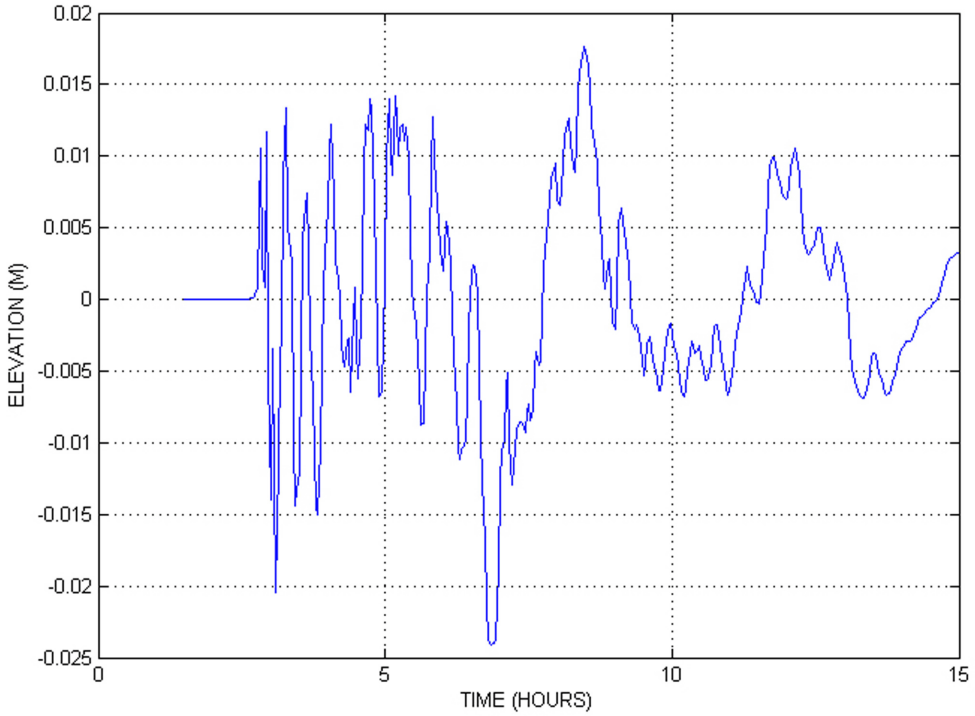

Note: Water surface elevations in meters are relative to the initial water level.

Figure 2.4.6-292 Water Surface Elevation near the Units 6 & 7 as a Function of Time Following the Florida Escarpment Tsunami (Static Source)

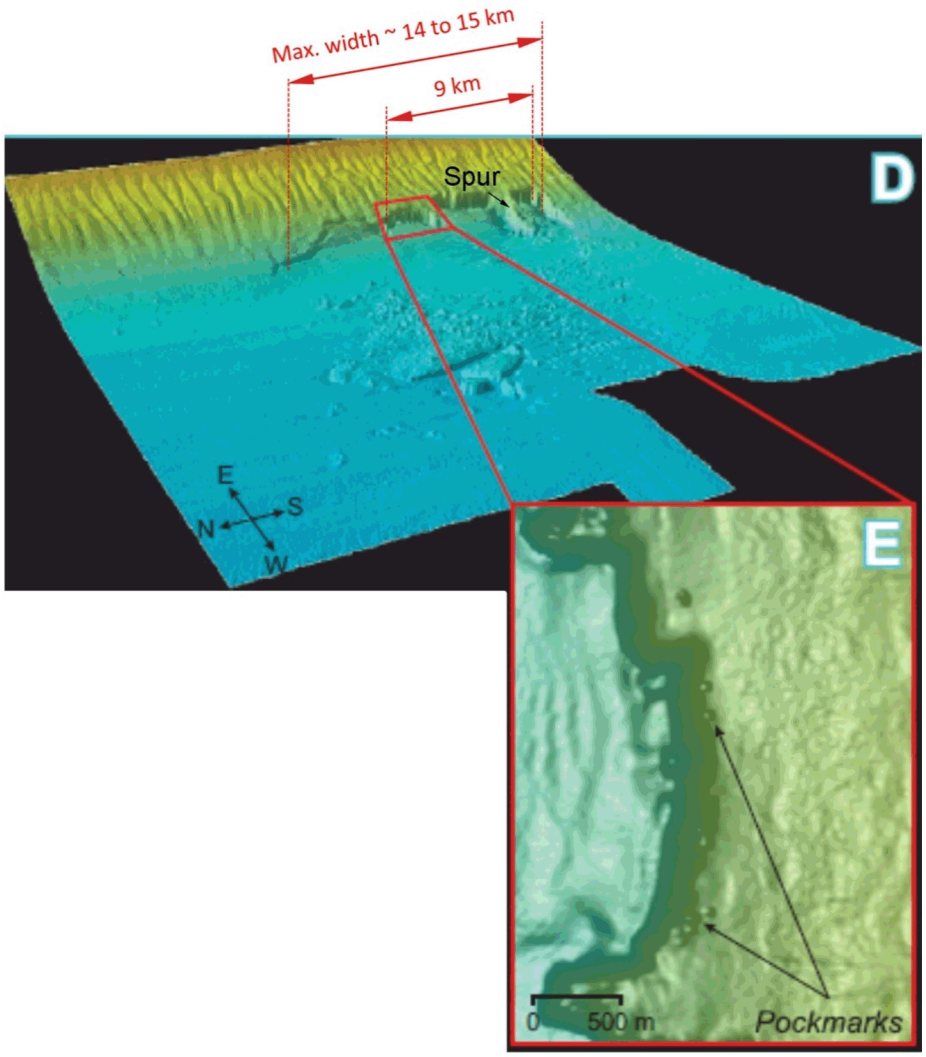

Source: Modified from Figure 1D of Reference 260.

Figure 2.4.6-293 Three-Dimensional View of Mass Transport Complex at the Great Bahama Bank

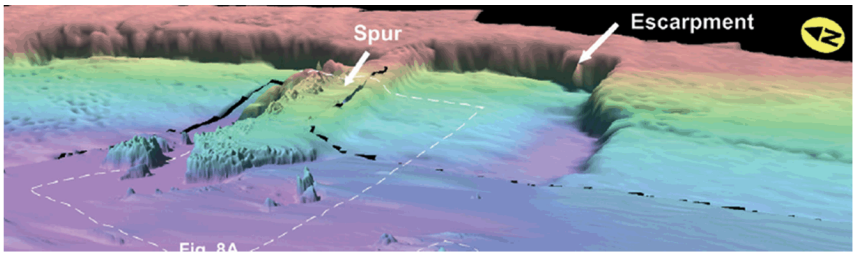

(a)

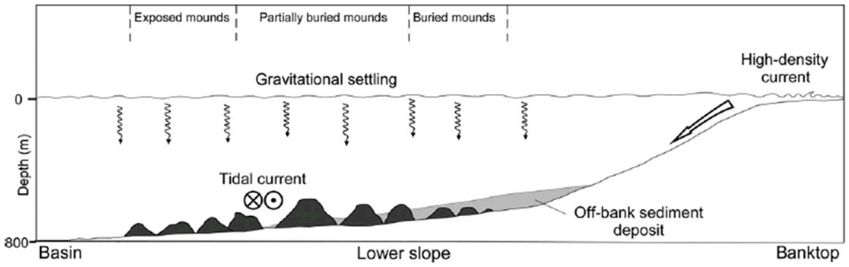

(b)

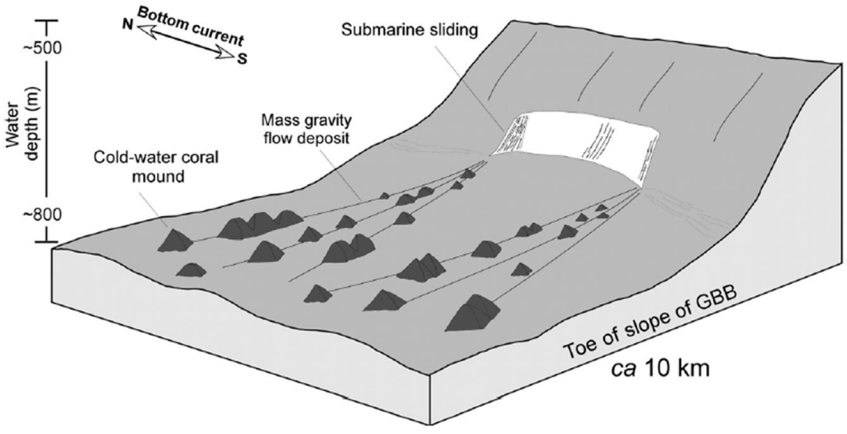

(c)

Source: Modified from Reference 262.

Figure 2.4.6-294 (a) Three-Dimensional View of the Two Southern Scars (b) Generalized Profile Showing the Variability of Mound Size with Respect to the Off-Bank Sediment Deposits Across the GBB Slope, and (c) Schematic Three-Dimensional Representation of the Slide

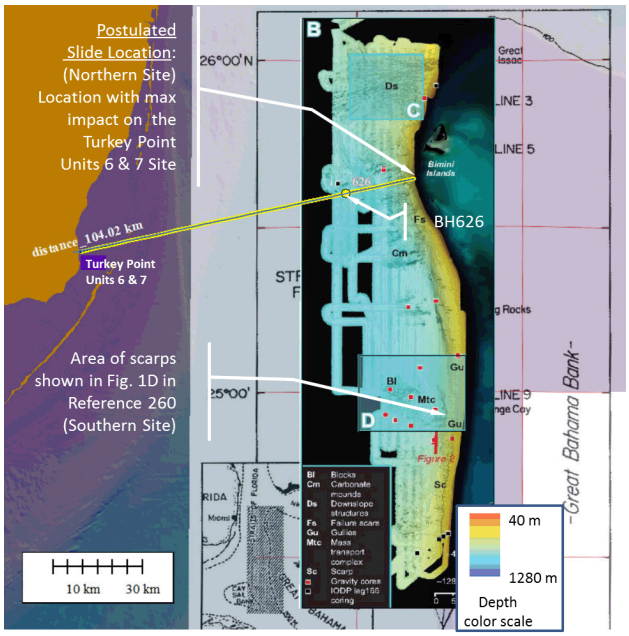

Source: Modified from Reference 260.

Figure 2.4.6-295 Location of Potential Submarine Slide Locations Along the Great Bahama Bank

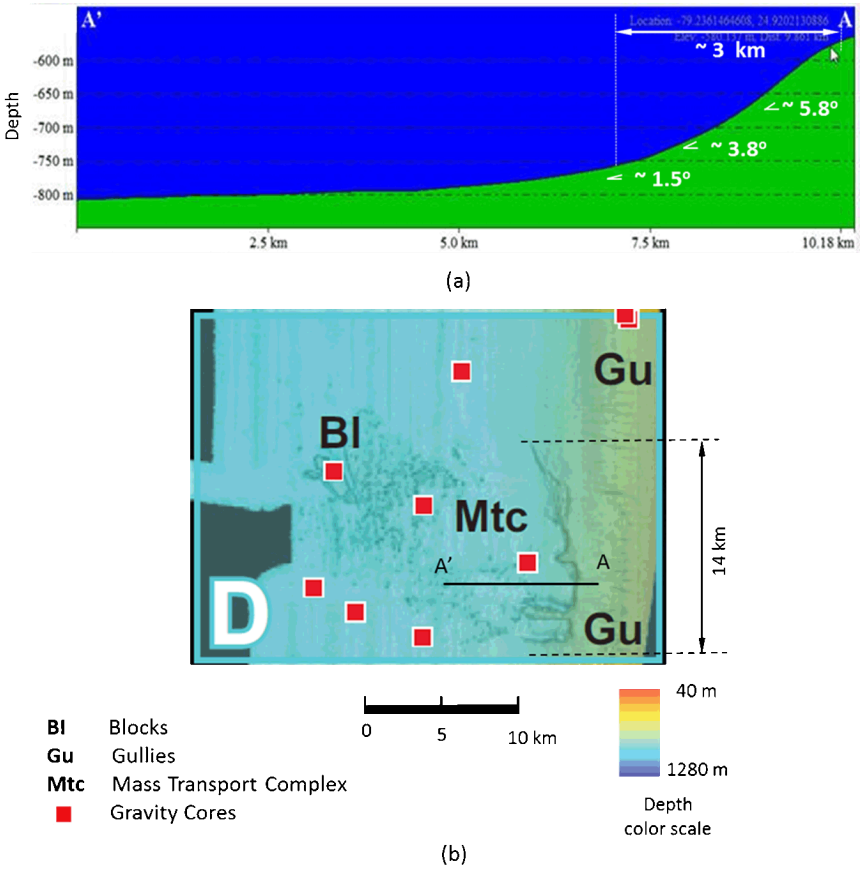

Note: The location of rectangle D is shown in Figure 2.4.6-295.
Source: Modified from Reference 260.

Figure 2.4.6-296 (a) Ocean Bottom Profile Along Line A-A', (b) Map Showing the Location of Line A-A'

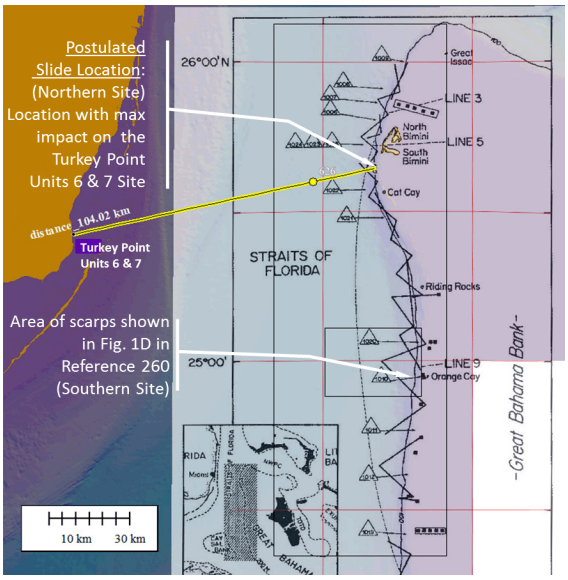

Source: Modified from Reference 263.

Figure 2.4.6-297 Location of Postulated Slide Location Along the Great Bahama Bank and Location of Seismic Profiles

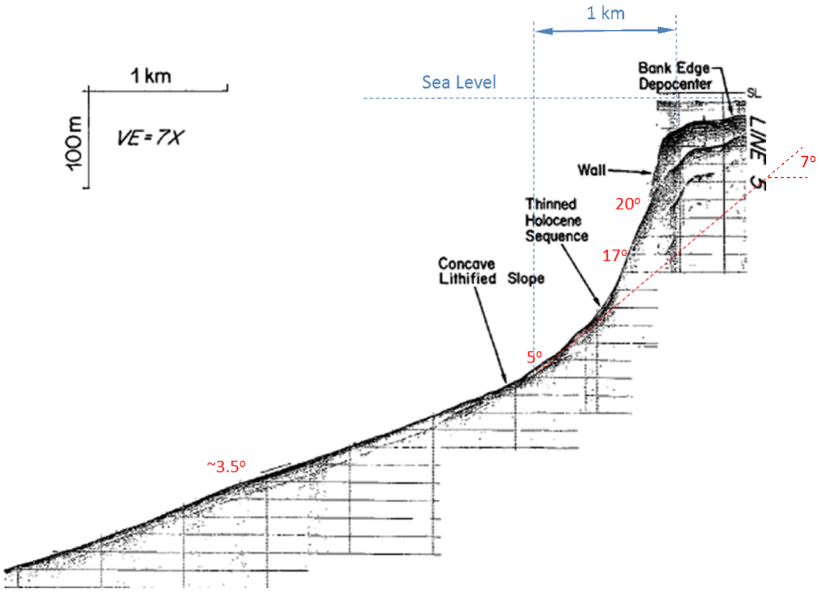

Note:
1. The location of this profile is shown in Figure 2.4.6-297.
2. VE represents Vertical Exaggeration.

Source: Modified from Reference 263.

Figure 2.4.6-298 Seismic Profile Line 5

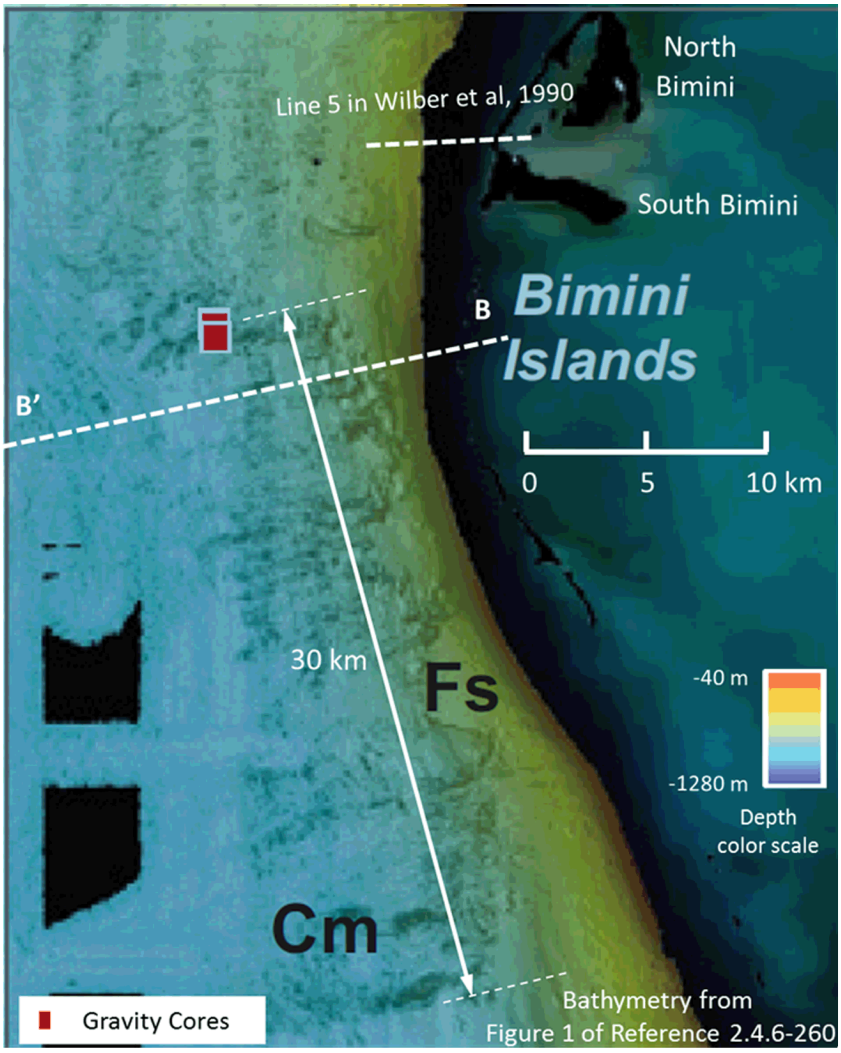

Source: Modified from Reference 260.

Figure 2.4.6-299 Bathymetry in the Vicinity of the Postulated Slide Location

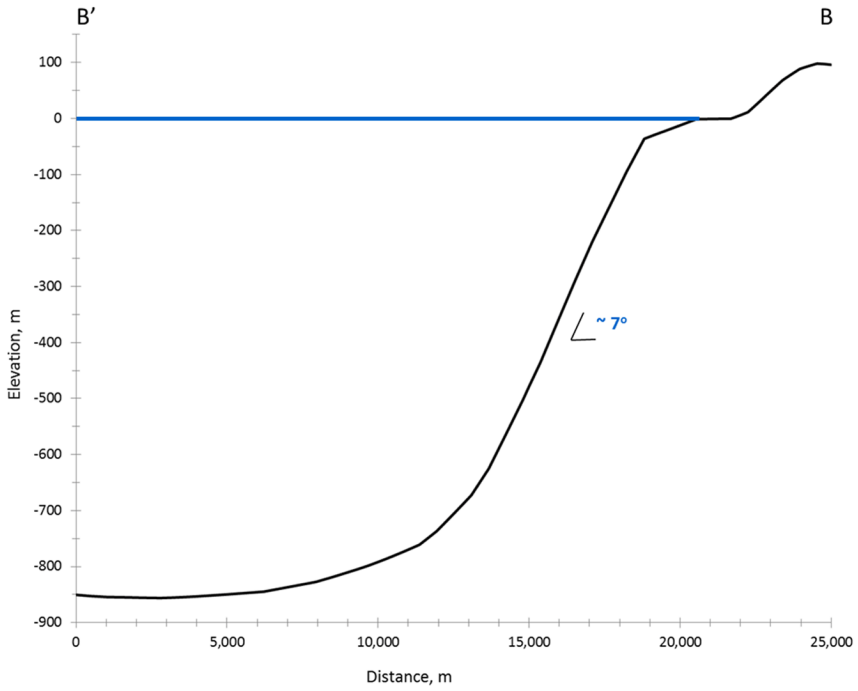

Note: The location of this profile is shown in Figure 2.4.6-299.

Figure 2.4.6-300 Ocean Bottom Profile Along the Line B-B'

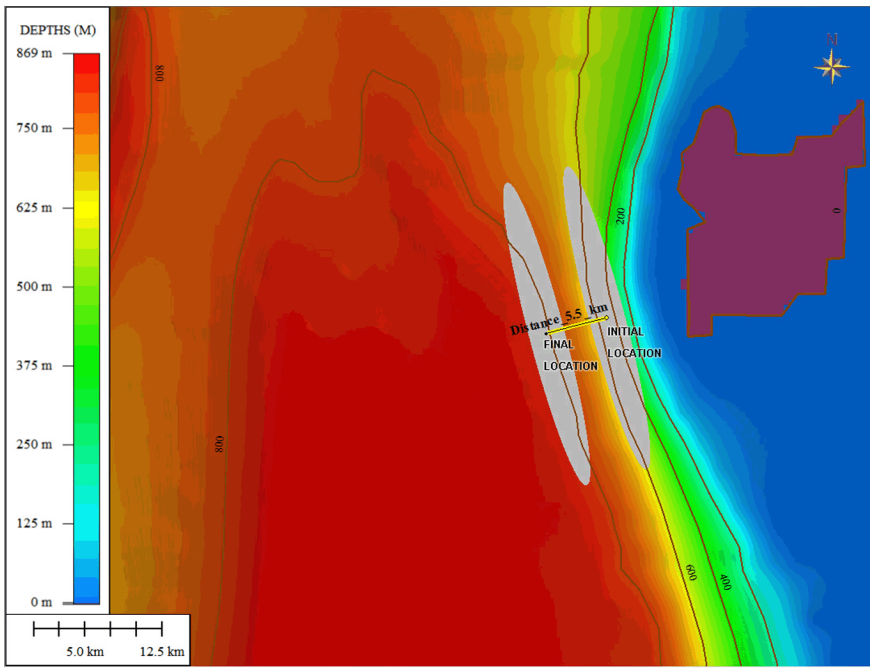

Notes:
1. Bathymetry contour elevations relative to MLW.
2. Also shown is the final position of the slide at the end of the run-out distance.

Figure 2.4.6-301 Location and Lateral Extent of the Postulated Slope Failure Along the GBB for Case 1

Figure 2.4.6-302 Initial Wave Generated by NHWAVE for Case 1 (Dynamic Source, 7-Degree Slope), at 110 Seconds after Initialization of the Slide

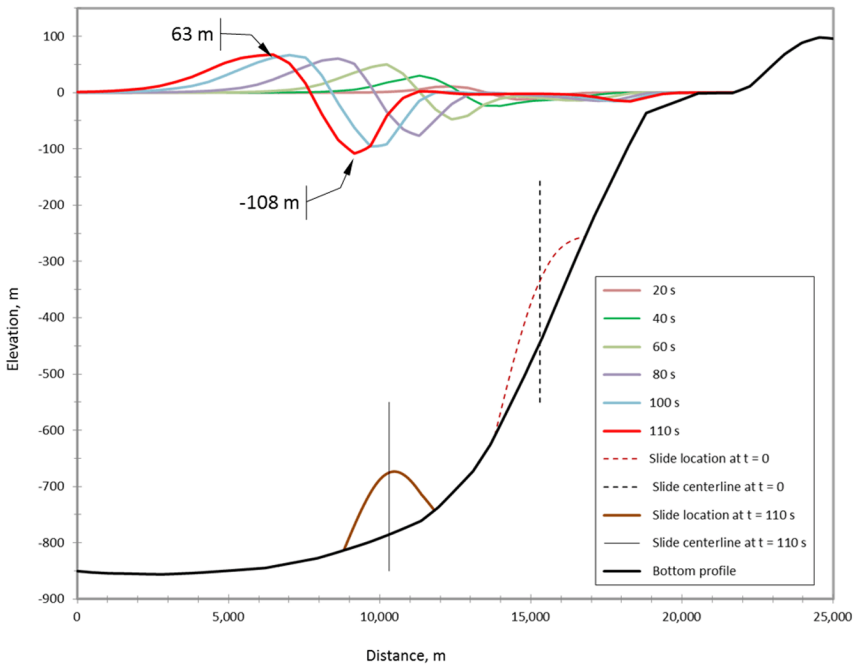

Note: The water surface profiles and cross section shown in this figure are along the minor axis of the ellipse shown in Figure 2.4.6-302.

Figure 2.4.6-303 Case 1 (Dynamic Source, 7-Degree Slope): Water Surface Profiles in the Direction of the Slide Motion at Different Times after the Initiation of the Slide Obtained from NHWAVE

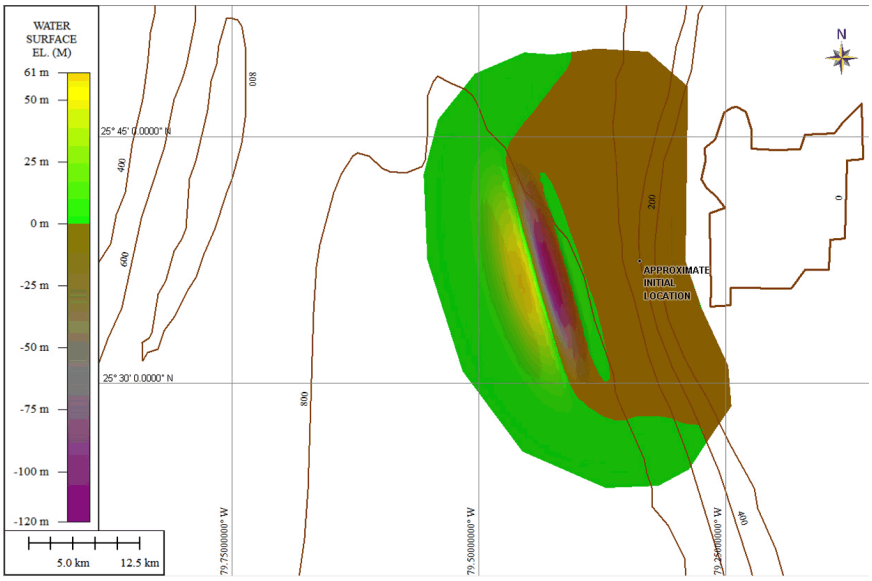

Figure 2.4.6-304 Case 2 (Dynamic Source, 20-Degree Slope): Initial Wave Generated by NHWAVE at 140 Seconds after Initialization of the Slide

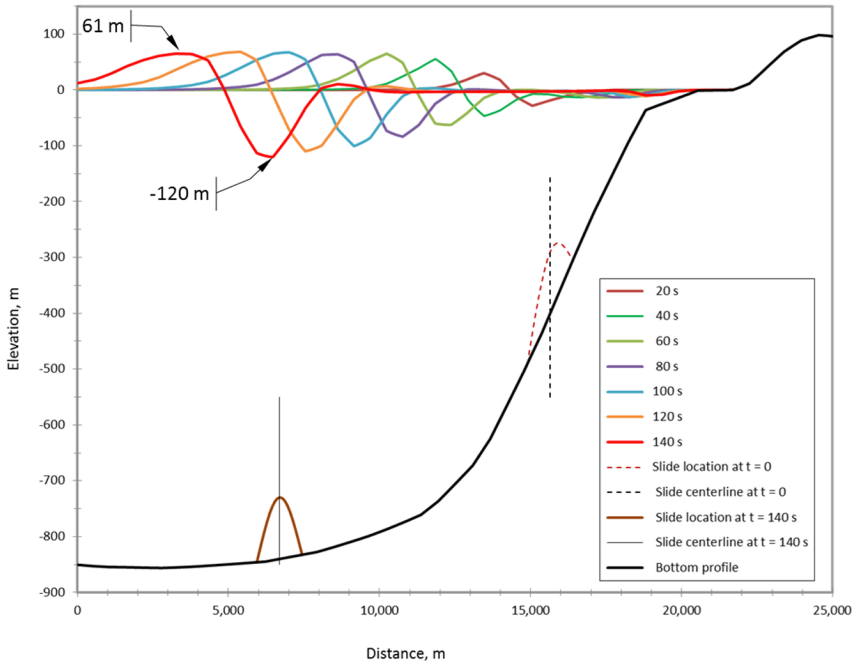

Figure 2.4.6-305 Case 2 (Dynamic Source, 20-Degree Slope): Water Surface Profile in the Direction of the Slide Motion at Different Times after the Initiation of the Slide

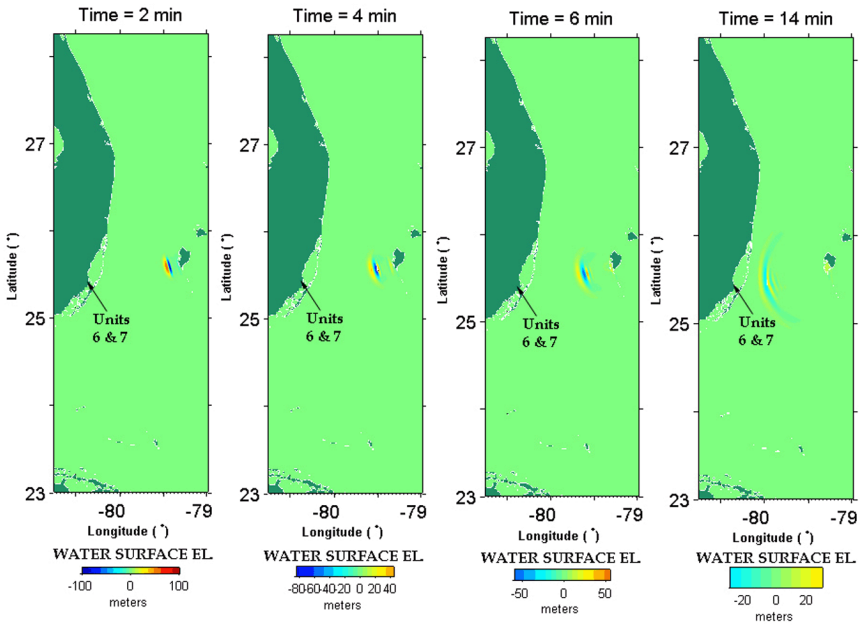

Notes:
1. The above time steps assume a hot-start initial condition.
2. The total time since initiation of the slide includes an additional 110 seconds (1.8 minutes).
3. Water surface elevations presented in the above figure are relative to the initial water surface level in FUNWAVE-TVD.
4. The initial water surface level in FUNWAVE-TVD is 1.68 meters MLW.

Figure 2.4.6-306 Case 1 (Dynamic Source, 7-Degree Slope): Simulated Propagation of the Tsunami Wave in Grid B at 2, 4, 6, and 14 Minutes after the Slope Failure

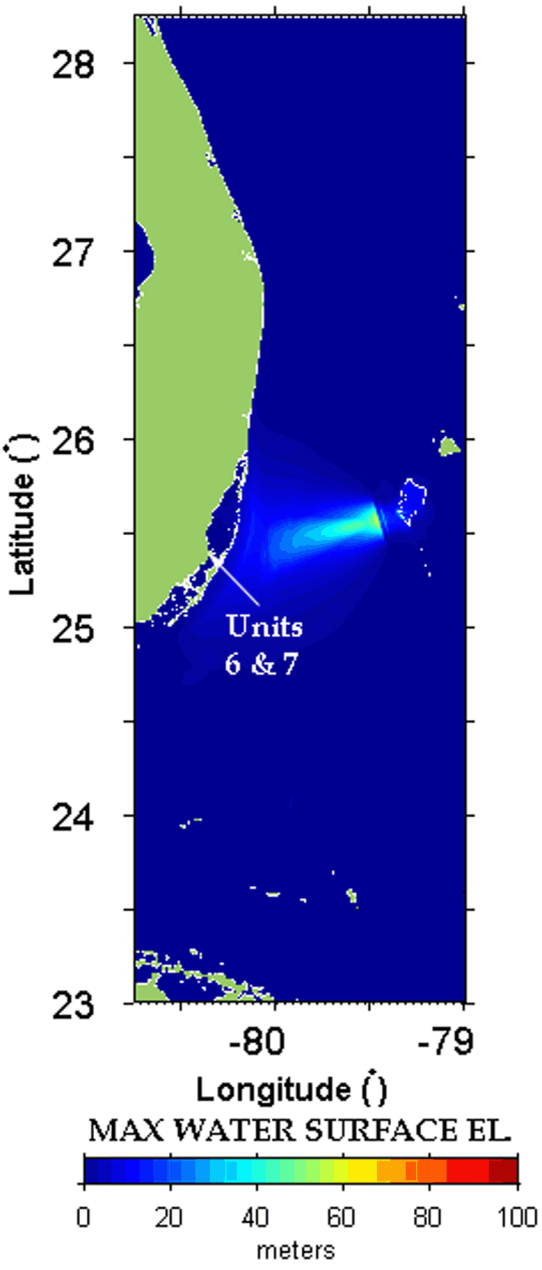

Notes:
1. Water surface elevations presented in the above figure are relative to the initial water surface level in FUNWAVE-TVD.
2. The initial water surface level in FUNWAVE-TVD is 1.68 meters MLW.

Figure 2.4.6-307 Case 1 (Dynamic Source, 7-Degree Slope): Simulated Maximum Wave Height in Grid B during the Propagation of the Tsunami Generated by the Slope Failure

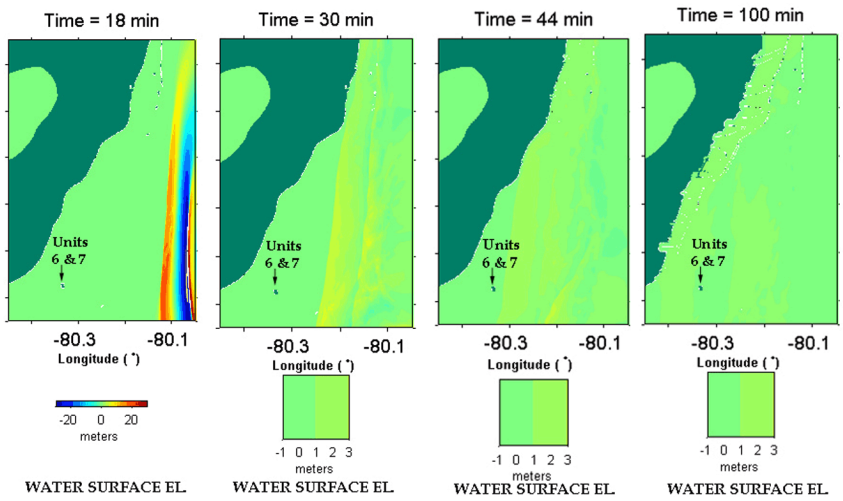

Notes:
1. The above time steps assume a hot-start initial condition.
2. The total time since initiation of the slide includes an additional 110 seconds (1.8 minutes).
3. Water surface elevations presented in the above figure are relative to the initial water surface level in FUNWAVE-TVD.
4. The initial water surface level in FUNWAVE-TVD is 1.68 meters MLW.

Figure 2.4.6-308 Case 1 (Dynamic Source, 7-Degree Slope): Simulated Propagation of the Tsunami Wave in Grid C at 18, 30, 44, and 100 Minutes after the Slope Failure

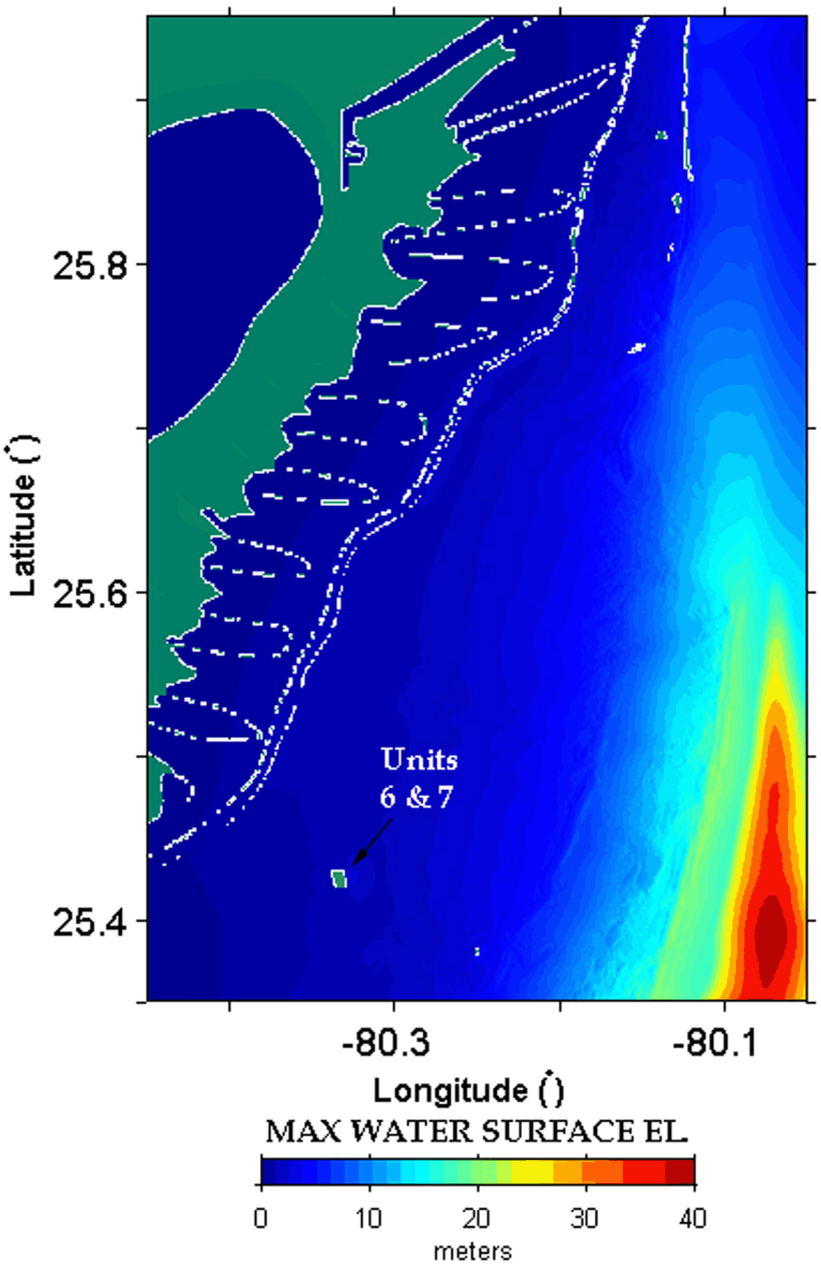

Notes:
1. Water surface elevations presented in the above figure are relative to the initial water surface level in FUNWAVE-TVD.
2. The initial water surface level in FUNWAVE-TVD is 1.68 meters MLW.

Figure 2.4.6-309 Case 1 (Dynamic Source, 7-Degree Slope): Simulated Maximum Wave Height in Grid C during the Propagation of the Tsunami Wave Generated by the Slope Failure

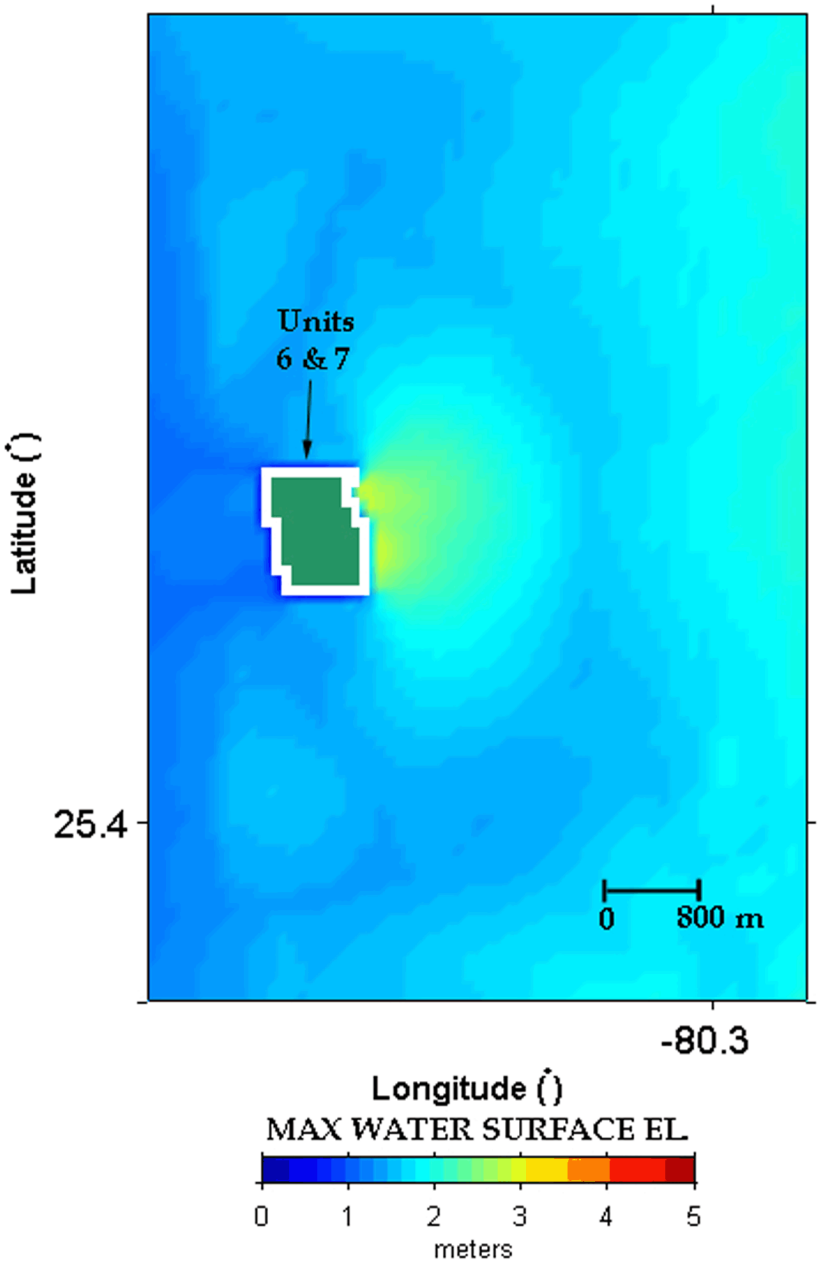

Notes:
1. Water surface elevations presented in the above figure are relative to the initial water surface level in FUNWAVE-TVD.
2. The initial water surface level in FUNWAVE-TVD is 1.68 meters MLW.

Figure 2.4.6-310 Case 1 (Dynamic Source, 7-Degree Slope): Simulated Maximum Water Surface Rise, Relative to the Initial Seawater Level, in the Vicinity of the Turkey Point Units 6 & 7 Site during the Propagation of the Tsunami Wave Generated by the Slope Failure

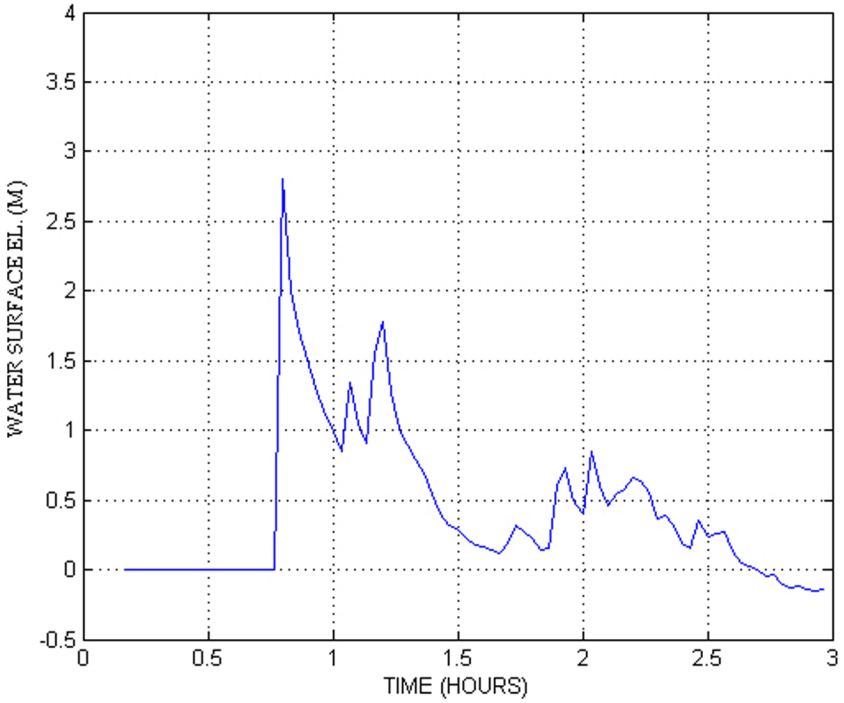

Notes:
1. Water surface elevations presented in the above figure are relative to the initial water surface level in FUNWAVE-TVD.
2. The initial water surface level in FUNWAVE-TVD is 1.68 meters MLW.
3. Time zero is at the start of FUNWAVE-TVD simulation. The total time since initiation of the slide includes an additional 110 seconds (1.8 minutes).

Figure 2.4.6-311 Case 1 (Dynamic Source, 7-Degree Slope): Water Surface Elevation at the Turkey Point Units 6 & 7 Site as a Function of Time Following the Tsunami Wave Generated by the Slope Failure

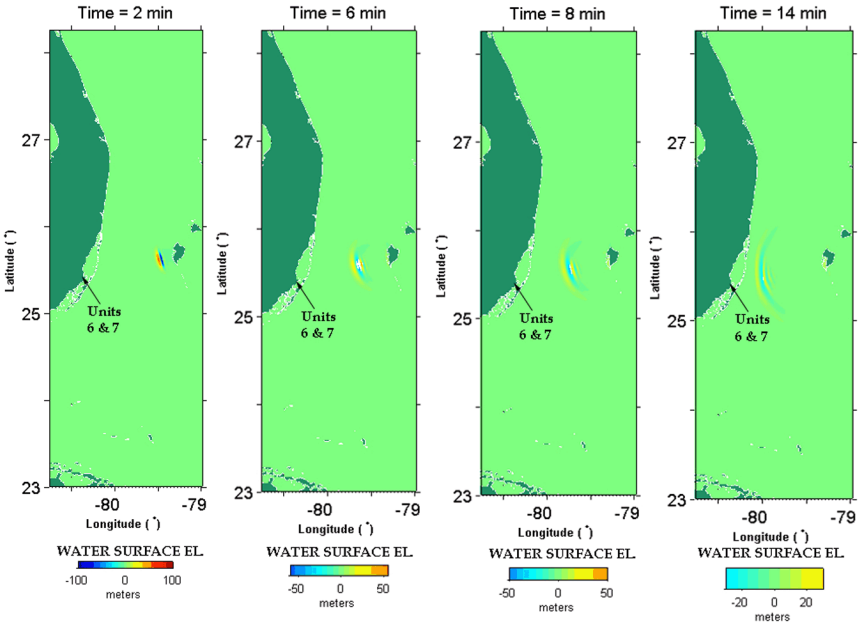

Notes:
1. The above time steps assume a hot-start initial condition.
2. The total time since initiation of the slide includes an additional 140 seconds (2.3 minutes).
3. Water surface elevations presented in the above figure are relative to the initial water surface level in FUNWAVE-TVD.
4. The initial water surface level in FUNWAVE-TVD is 1.68 meters MLW.

Figure 2.4.6-312 Case 2 (Dynamic Source, 20-Degree Slope): Simulated Propagation of the Tsunami Wave in Grid B at 2, 6, 8, and 14 Minutes after the Slope Failure

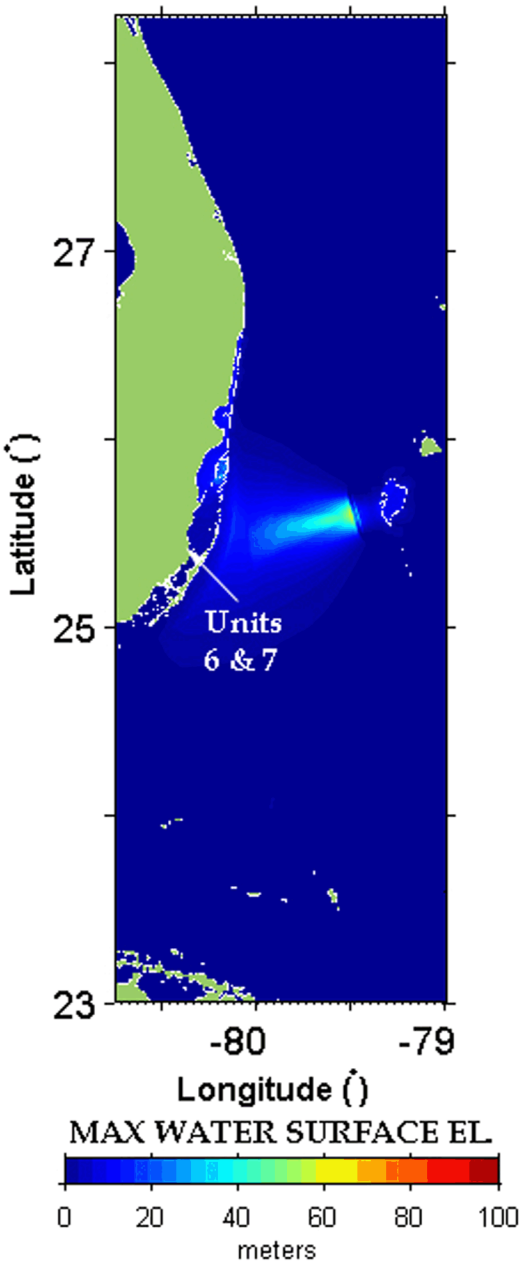

Notes:
1. Water surface elevations presented in the above figure are relative to the initial water surface level in FUNWAVE-TVD.
2. The initial water surface level in FUNWAVE-TVD is 1.68 meters MLW.

Figure 2.4.6-313 Case 2 (Dynamic Source, 20-Degree Slope): Simulated Maximum Wave Height in Grid B during the Propagation of the Tsunami Generated by the Slope Failure

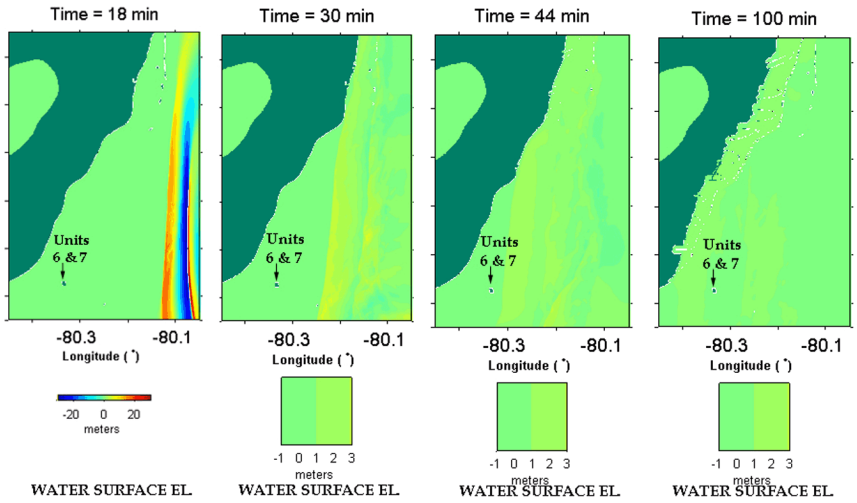

Notes:
1. The above time steps assume a hot-start initial condition.
2. The total time since initiation of the slide includes an additional 140 seconds (2.3 minutes).
3. Water surface elevations presented in the above figure are relative to the initial water surface level in FUNWAVE-TVD.
4. The initial water surface level in FUNWAVE-TVD is 1.68 meters MLW.

Figure 2.4.6-314 Case 2 (Dynamic Source, 20-Degree Slope): Simulated Propagation of the Tsunami Wave in Grid C at 18, 30, 44, and 100 Minutes after the Slope Failure

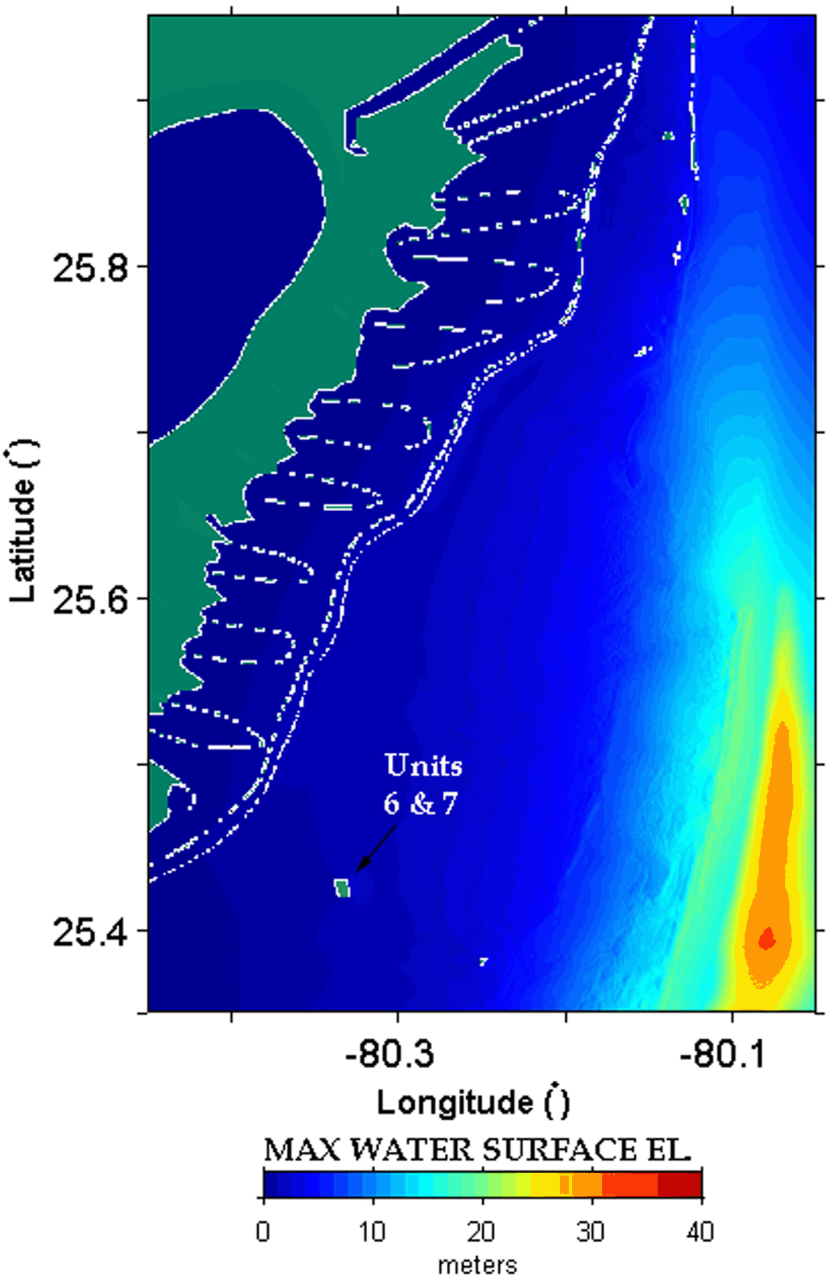

Notes:
1. Water surface elevations presented in the above figure are relative to the initial water surface level in FUNWAVE-TVD.
2. The initial water surface level in FUNWAVE-TVD is 1.68 meters MLW.

Figure 2.4.6-315 Case 2 (Dynamic Source, 20-Degree Slope): Simulated Maximum Wave Height in Grid C during the Propagation of the Tsunami Wave Generated by the Slope Failure

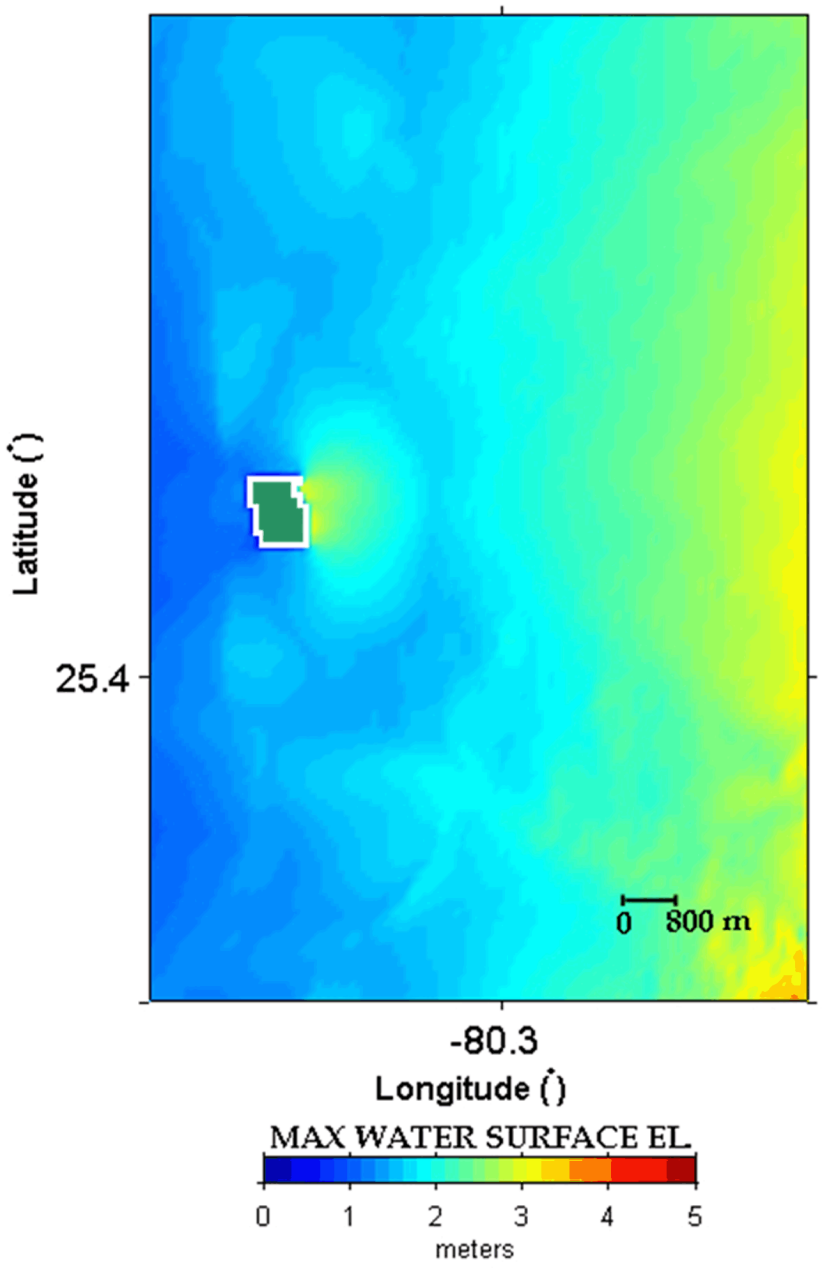

Notes:
1. Water surface elevations presented in the above figure are relative to the initial water surface level in FUNWAVE-TVD.
2. The initial water surface level in FUNWAVE-TVD is 1.68 meters MLW.

Figure 2.4.6-316 Case 2 (Dynamic Source, 20-Degree Slope): Simulated Maximum Water Surface Rise, Relative to the Initial Seawater Level, in the Vicinity of the Turkey Point Units 6 & 7 Site during the Propagation of the Tsunami Wave Generated by the Slope Failure

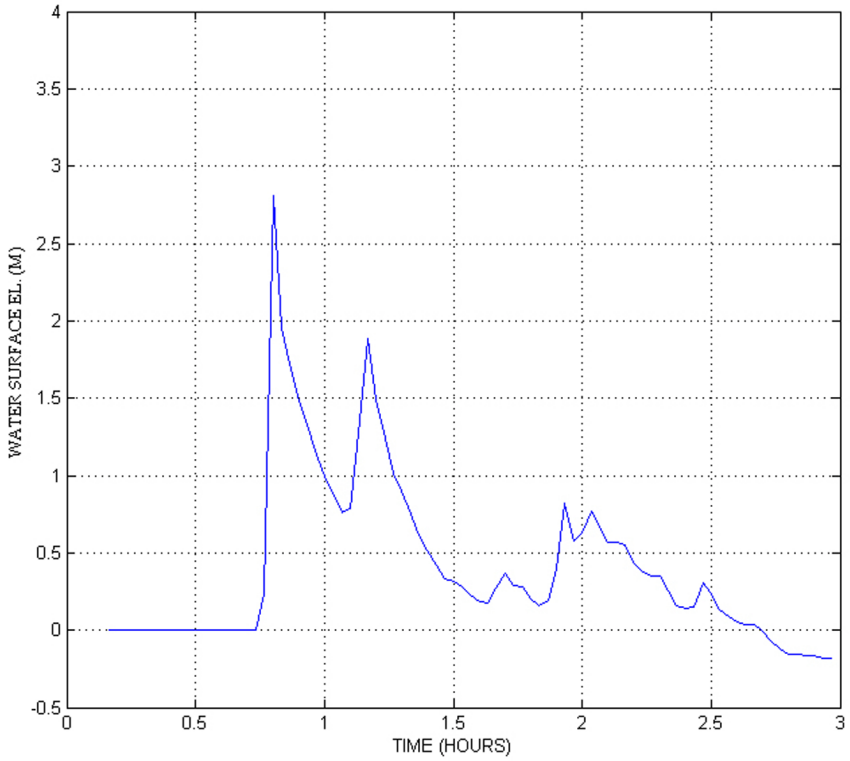

Notes:
1. Water surface elevations presented in the above figure are relative to the initial water surface level in FUNWAVE-TVD.
2. The initial water surface level in FUNWAVE-TVD is 1.68 meters MLW.
3. Time zero is at the start of FUNWAVE-TVD simulation. The total time since initiation of the slide includes an additional 140 seconds (2.3 minutes).

Figure 2.4.6-317 Case 2 (Dynamic Source, 20-Degree Slope): Water Surface Elevation at the Turkey Point Units 6 & 7 Site as a Function of Time Following the Tsunami Wave Generated by the Slope Failure

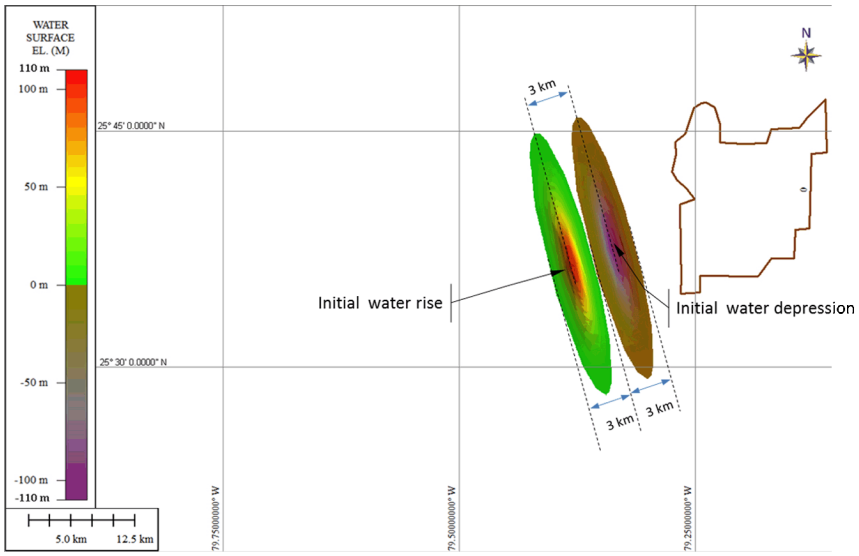

Notes:
1. In the definition of the static source, the initial water depression shown above is directly above the initial position of the slide, i.e., before the initiation of movement.
2. The final position of the slide does not enter in the definition of the static source.

Figure 2.4.6-318 Case 3 (Static Source): Initial Wave for a Static Source Equal to the Postulated Slide at the Great Bahama Bank

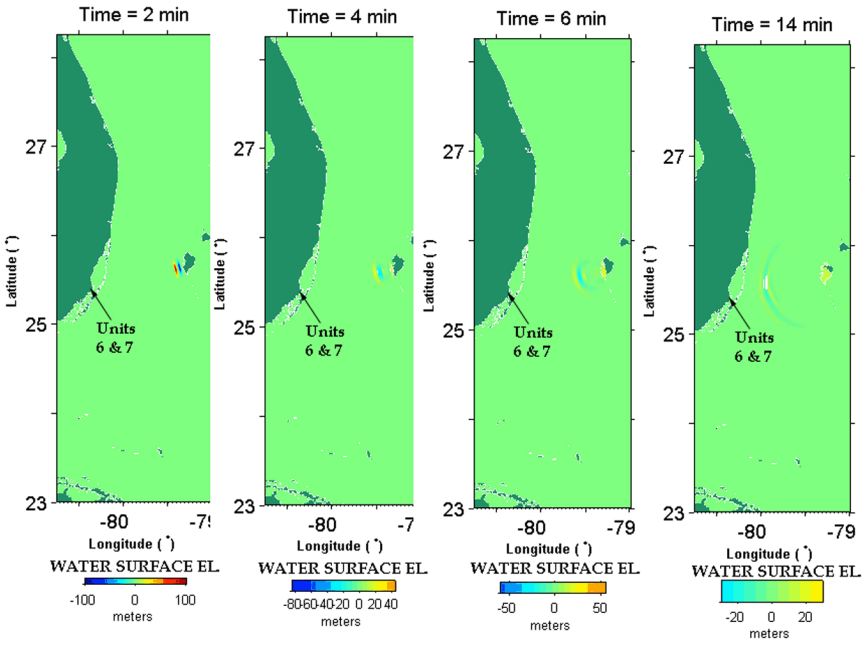

Notes:
1. Water surface elevations presented in the above figure are relative to the initial water surface level in FUNWAVE-TVD.
2. The initial water surface level in FUNWAVE-TVD is 1.68 meters MLW.

Figure 2.4.6-319 Case 3 (Static Source): Simulated Propagation of the Tsunami Wave in Grid B at 2, 4, 6, and 14 Minutes after the Slope Failure

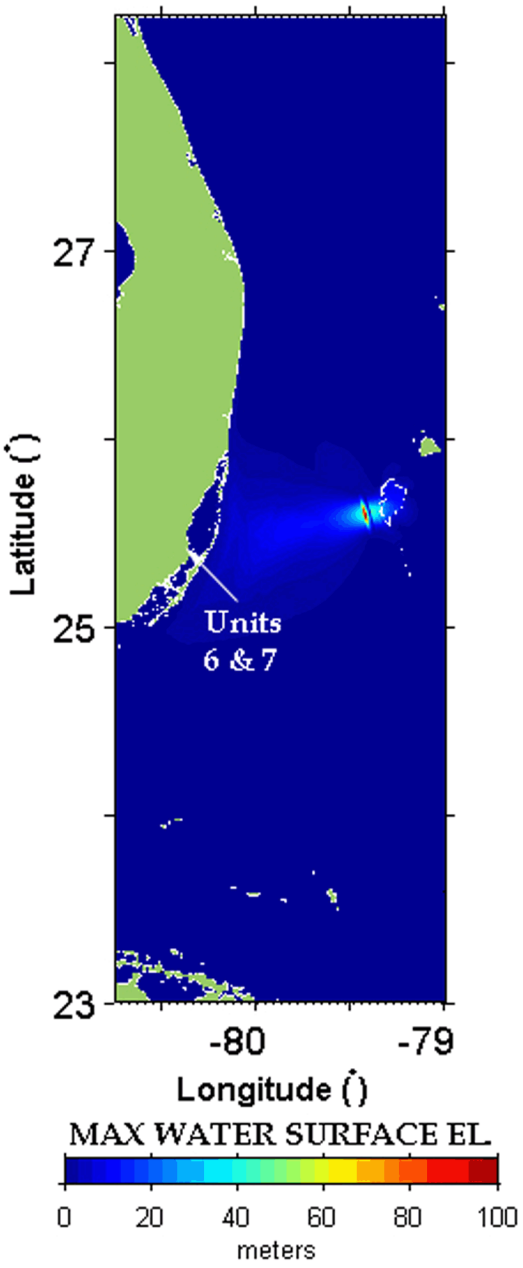

Notes:
1. Water surface elevations presented in the above figure are relative to the initial water surface level in FUNWAVE-TVD.
2. The initial water surface level in FUNWAVE-TVD is 1.68 meters MLW.

Figure 2.4.6-320 Case 3 (Static Source): Simulated Maximum Wave Height in Grid B during the Propagation of the Tsunami Generated by the Slope Failure

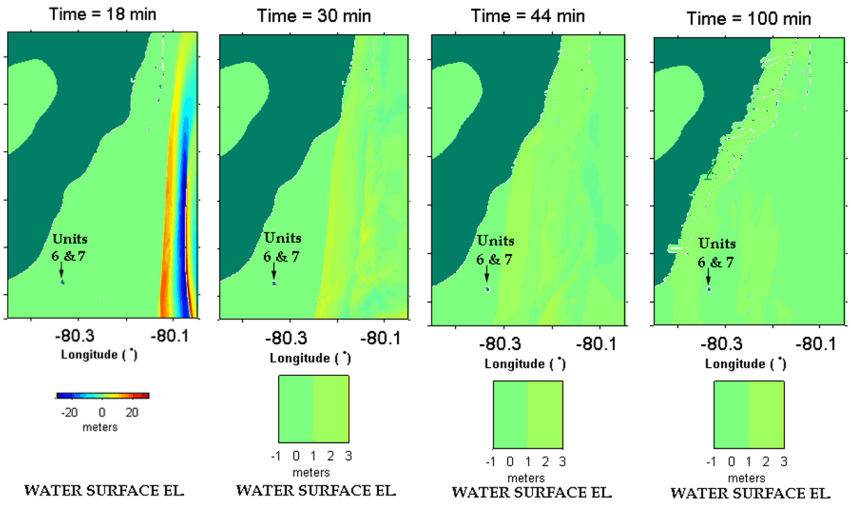

Notes:
1. Water surface elevations presented in the above figure are relative to the initial water surface level in FUNWAVE-TVD.
2. The initial water surface level in FUNWAVE-TVD is 1.68 meters MLW.

Figure 2.4.6-321 Case 3 (Static Source): Simulated Propagation of the Tsunami Wave in Grid C at 18, 30, 44, and 100 Minutes after the Slope Failure

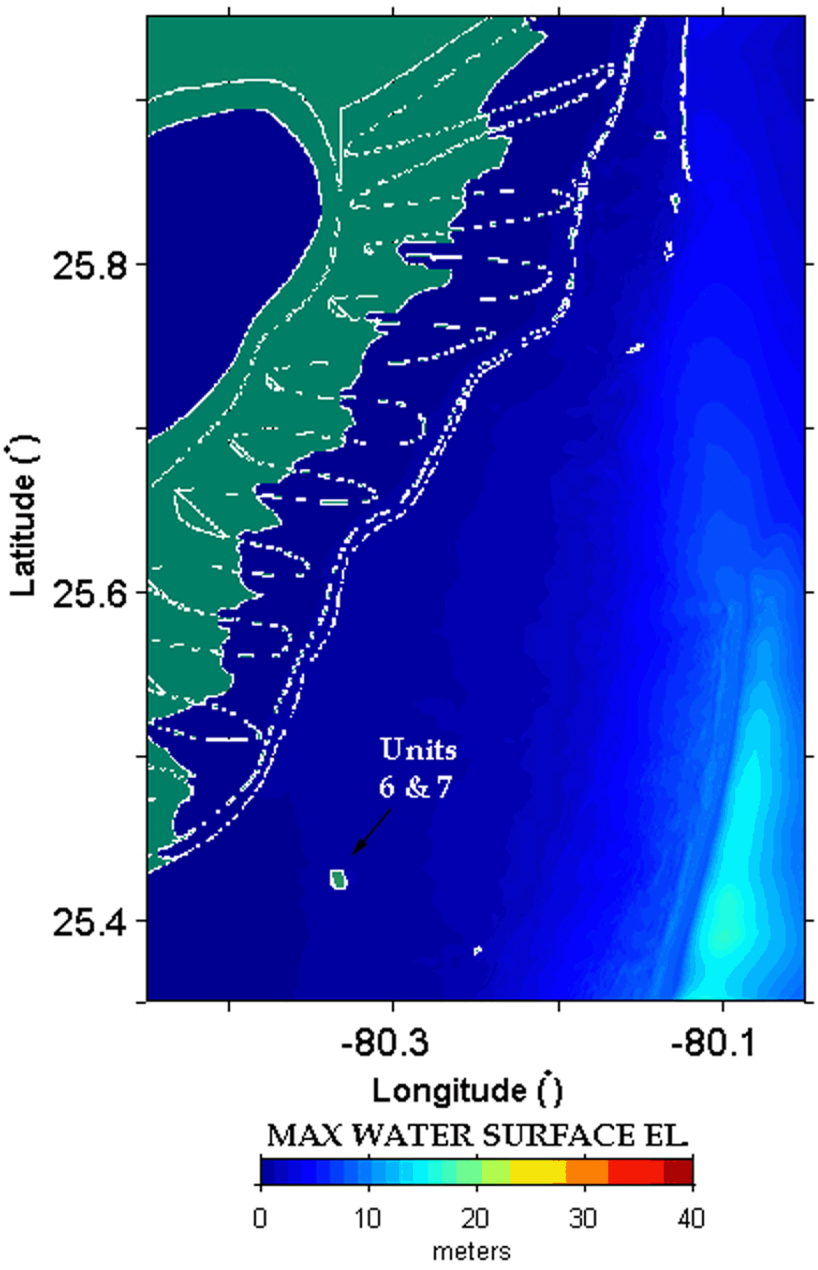

Notes:
1. Water surface elevations presented in the above figure are relative to the initial water surface level in FUNWAVE-TVD.
2. The initial water surface level in FUNWAVE-TVD is 1.68 meters MLW.

Figure 2.4.6-322 Case 3 (Static Source): Simulated Maximum Wave Height in Grid C during the Propagation of the Tsunami Wave Generated by the Slope Failure

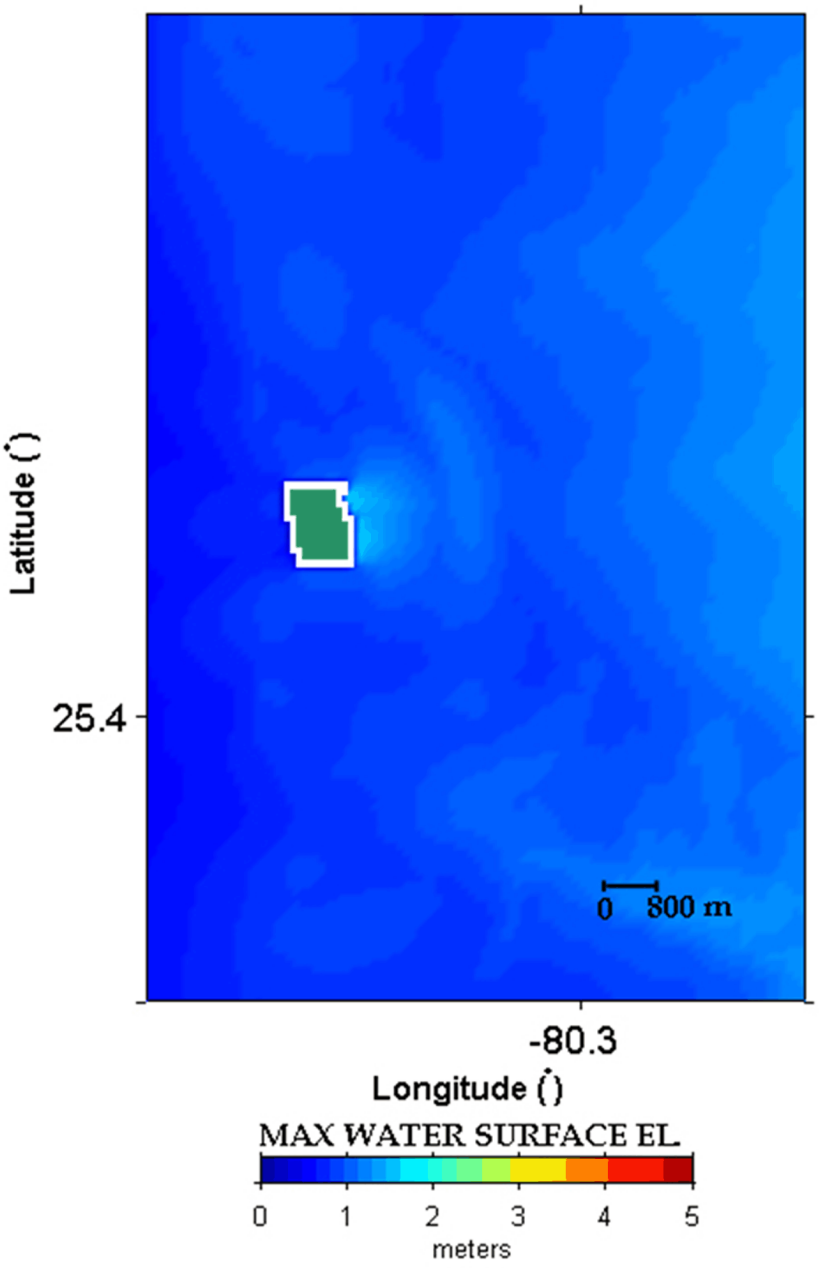

Notes:
1. Water surface elevations presented in the above figure are relative to the initial water surface level in FUNWAVE-TVD.
2. The initial water surface level in FUNWAVE-TVD is 1.68 meters MLW.

Figure 2.4.6-323 Case 3 (Static Source): Simulated Maximum Water Surface Rise, Relative to the Initial Seawater Level, in the Vicinity of the Turkey Point Units 6 & 7 Site during the Propagation of the Tsunami Wave Generated by the Slope Failure

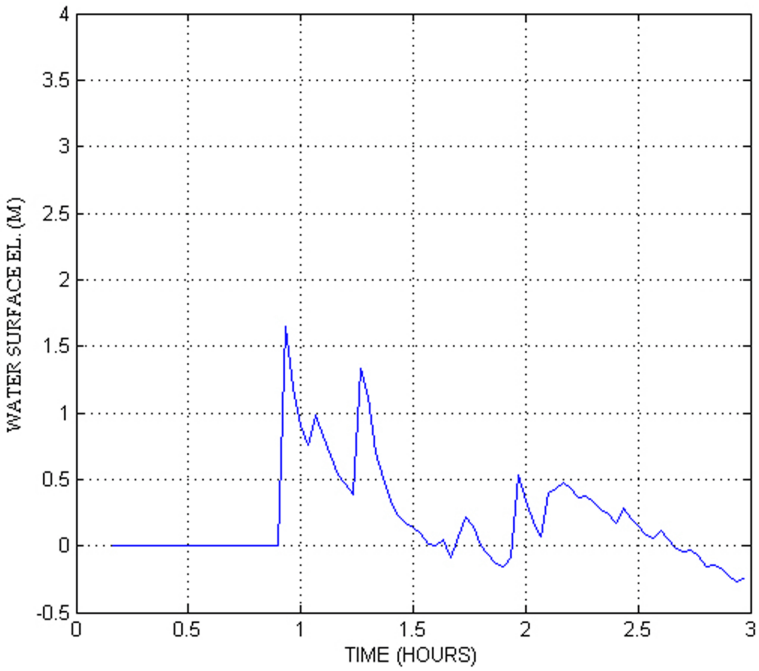

Notes:
1. Water surface elevations presented in the above figure are relative to the initial water surface level in FUNWAVE-TVD.
2. The initial water surface level in FUNWAVE-TVD is 1.68 meters MLW.

Figure 2.4.6-324 Case 3 (Static Source): Water Surface Elevation at the Turkey Point Units 6 & 7 Site as a Function of Time Following the Tsunami Wave Generated by the Slope Failure